Lecture Notes in Production Eng

Ekkard Brinksmeier
Oltmann Riemer
Ralf Gläbe
*Editors*

# Fabricatio
# Complex C

# Lecture Notes in Production Engineering

For further volumes:
http://www.springer.com/series/10642

Ekkard Brinksmeier, Oltmann Riemer,
and Ralf Gläbe (Eds.)

# Fabrication of Complex Optical Components

## From Mold Design to Product

Springer

*Editors*
Ekkard Brinksmeier
Laboratory for Precision
Machining LFM
University of Bremen
Bremen
Germany

Ralf Gläbe
Laboratory for Precision
Machining LFM
University of Bremen
Bremen
Germany

Oltmann Riemer
Laboratory for Precision
Machining LFM
University of Bremen
Bremen
Germany

ISSN 2194-0525 e-ISSN 2194-0533
ISBN 978-3-642-33000-1 e-ISBN 978-3-642-33001-8
DOI 10.1007/978-3-642-33001-8
Springer Heidelberg New York Dordrecht London

Library of Congress Control Number: 2012947589



Printed on acid-free paper

Springer is part of Springer Science+Business Media (www.springer.com)

# Preface

Within the past decades, optics has emerged as a key engineering technology. In the beginning, the development of optics and optical systems was limited to the machining of continuous surfaces. Due to the high demand for components with an extended functionality, over the last years, structured and freeform surfaces have become increasingly important. Their field of application is broad, e.g., reflective or refractive structures are used for automotive illumination systems, light distribution in TFT panels or as reflective foils for traffic signs or safety garments, while diffractive structures are used, for example, for the correction of chromatic aberration or for security applications. Especially in consumer optics, there is a strong demand for large volumes of highly functional but inexpensive components. These parts can only be economically produced by glass or plastic replication. In order to meet the required quality levels though, it is not sufficient to solely optimize the manufacturing processes. It is essential to take into consideration the overall sequence of processes, or in other words, the process chain.

In the late 1990's, this demand was evident to my esteemed colleagues Prof. Manfred Weck from the Technical University of Aachen, Prof. Don A. Lucca from Oklahoma State University in Stillwater and myself. The idea was born to start collaborations between the Universities of Aachen, Bremen and Stillwater. While there had been a frequent exchange of scientific information through the German Academic Society for Production Engineering (WGP) and the International Academy for Production Engineering (CIRP) already, this collaboration was aimed at directly bringing together scientists from the three universities to pursue focused research on the manufacture of complex optics. It was mere coincidence, that the German Research Foundation (DFG) just had released a new type of collaborative research funding: the Transregional Collaborative Research Center (SFB/TR), aiming at funding just this kind of cooperation. On this basis, a proposal was launched by the three universities on the topic of "Process Chains for the Replication of Complex Optical Elements".

The goal was to combine the emerging technologies of optical mold making and glass or plastic replication processes on a broad basis. On the machining side, focus was laid on processes for generating optical freeform surfaces, like diamond

milling, ultraprecision grinding or CNC-controlled polishing. On the other side, replication processes such as blank pressing of glass optics and injection or injection-compression molding were considered. For obtaining a holistic view of the production process, these technologies were connected with an integral optics design and a comprehensive metrology frame and quality management. In total, 16 sub-projects were defined on this basis within the fields of design, hard coatings, mold making, replication and metrology. The initial proposers were Professors Klocke, Michaeli, Pfeifer and Weck from the Technical University of Aachen, Professor Lucca from Oklahoma State University in Stillwater and Professors Brinksmeier, Goch, Mayr and Drs. Mehner, Preuß, Riemer and Stock from the University of Bremen.

After a positive evaluation, we were notified by the DFG in 2001 that the proposal was funded. This research grant became the first engineering SFB/TR in Germany. The research work of the SFB/TR4 finally started on June 1$^{st}$, 2001 with Dr. Oltmann Riemer as the general manager. Later this task was taken over by Dr. Ralf Gläbe, who kept this position until the end of the SFB/TR4 on June 30$^{th}$, 2012.

After eleven years of mutual work, it is safe to say that during this time, the three sites have been connected in a way that would not have been possible by other funding instruments. Furthermore, the SFB/TR4 allowed us to reach profound knowledge in the field of optics that would not have been achieved within individual projects. The various publications, such as dissertations, conference papers and original journal papers originating from the SFB/TR4 have been acknowledged both nationally and internationally by research facilities and industry alike. In total more than ... scientists have worked in the SFB/TR4, and they have written more than 300 publications including 17 dissertations. A detailed overview on the most important publications resulting from the SFB/TR4 is given in the first chapter of this book. Another proof for the success is evident by the seven so-called transfer projects, which were initiated in the final phase of the SFB/TR4 to disseminate the most promising findings into prototype industrial applications.

As the coordinator of the SFB/TR4 I would like to express my sincere gratitude on behalf of all my SFB colleagues and funded staff to the DFG in general, and particularly to Dr. Hollmann for his technical advice, and Dr. Effertz, for her financial advice in the final funding phase. Also I would like to thank the administrations of the involved universities for their ongoing support over the years.

Bremen, August 2012 Prof. Dr.-Ing. habil. Dr.-Ing. E.h. Ekkard Brinksmeier

# Contents

# Introduction

Ekkard Brinksmeier, Oltmann Riemer, and Ralf Gläbe

Photonics is a key enabling technology for a large amount of high-tech products. The largest market volume belongs to consumer products like optics in video projectors, in digital cameras and in illumination optics. Most of these optics are fabricated by replication processes, as this is the most cost-effective way to produce complex optical components in large quantities. Demands for higher precision at lower costs, shorter time to market and finally a hard competition lead to fabrication processes of these components that are even more effective. The fabrication builds on a combination of several process steps, starting with the design and ending with the replication process itself. The development of these processes and, moreover, the interaction of consecutive process steps opens a large potential for industrial improvements, but still require scientific research.

In 2001 the Transregional Collaborative Research Center SFB/TR4 "Process Chains for the Replication of Complex Optical Elements" started with 18 closely cooperating projects aiming at the same goal: to increase the accuracy of replicated complex optical glass and plastic parts and to reduce the number of the required iterations within the applied process chain. The sub-projects were are carried out at eight institutions located at Bremen University, RWTH Aachen at Oklahoma State University in the USA.

In general, this joint research was focused on replicated optics like lenses for digital cameras, laser beam shaping optics, and illumination optics. All these consumer products are fabricated in medium to large series of a few thousand up to millions. It is well known that product costs are decreasing while the demanded performance is increasing. For instance, the performance of mobile phone cameras has increased from less than 1MPixel to more than 5MPixel in less than 5 years whereas at the same time the price went down considerably. In consequence, from year to year the fabrication of such optical components as mass products has to be less expensive and faster at higher precision. Technologies for direct machining of these optical components are well developed; however, they will not always meet the demands for the large series production of complex optics for current consumer products. Thus, for large product numbers replication is inevitable.

In optics fabrication fully automated replication technologies were developed in the 1990ies and are now a key technology for all consumer products. Today the replication of glass and plastic components for imaging and illumination optics is highly developed. Drivers for the current developments are LED illumination, optics for digital cameras with even higher resolution and video projector optics. The challenging demands for these novel optical systems like compact design and reduced weight for enhanced performance have shifted the optical design of lenses from simple spherical geometry to aspherical lenses as well as free form and structured lenses. These types of optical components come up with new challenges in designing and describing optical surfaces, machining of molds, replicating components, metrology and quality chain management.

It is evident that the fabrication of optical components with complex shapes at high quality requires a number of process steps. The sequence of required steps for the deterministic fabrication of optical components is referred to as 'process chain', which is defined as 'The complete series of production steps required to manufacture a component from design to fabrication including all relevant aspects of metrology and quality control.' 'Deterministic fabrication' will imply a holistic view on the complete process chain. Therefore, consecutive process steps have to take into account the deviations of all following and preceding steps. In other words, a number of well developed highly productive process steps in a process chain will not necessarily meet the demands for a highly productive fabrication of high quality optical components. If form accuracy or surface quality suffers from one or more process steps, the replication process and often the complete chain has to be adapted. This iteration is not straightforward and therefore time consuming and expensive. For this reason solutions have to be found to decrease the number of iteration steps. This can be either done by optimizing each step of the process chain separately or by dealing with the deviations and boundary conditions of the complete process chain, or, preferably, by a combination of both.

A standard process chain for replicating optical components typically consists of the following steps: optical design, design of mold and mold insert, mold machining, possibly hard coatings and the replication process itself. Moreover, the metrology of form and roughness of the mold insert and of the replicated component is essential to determine the quality of the whole process chain. In order to reduce the number of iterations it is also necessary to provide an organized communication and data exchange between all steps of the process chain. From a technological as well as a practical point of view glass and plastic replication process chains have to be treated in an entirely different manner, and a distinction between process chains for continuous and structured optics must also be made.

This book is organized according to this framework of process chains, process steps, technologies, and classification of optical surfaces. Since the SFB/TR4 is a highly interdisciplinary research center, most articles are focused on key issues dedicated to plastic and glass replication of continuous and structured optical components. This book presents the major achievements gained within the SFB/TR4 over 11 years. In addition several hundred publications and many doctoral theses where

published, providing the full range of knowledge. The most relevant ones are listed at the end of each chapter. In addition, the results have been presented on numerous national and international conferences, workshops and seminars. For a focused discussion with industry and academia six national and three international conferences have been successfully conducted by the SFB/TR4, all conferences attended by participants from industry and academia.

In 2007 the first findings of the SFB/TR4 found their way from fundamental research to industry. Up to now seven transfer projects in cooperation with industry have emerged from the SFB/TR4. They are dealing with major aspects of the process chain covering mold design, mold making processes, new mold materials and novel metrology devices.

The general mission of all academic research, i.e. transfering new knowledge by teaching and lecturing, also applies for the SFB/TR4. In this context a web-based e-learning lecture has been set up with nine lecturers from all three locations. The lectures were given in English and are accessible via a web-based student portal.

This book covers selected aspects of the process chains. Chapter 2 deals with the question how to organize a process chain for optics replication, especially if located at different sites. The presented solution will combine technological and organizational challenges. The chapters 3 to 7 are dedicated to plastic replication technologies. The focus on mold design that has to consider criteria like temperature management, pressing cycles and the alignment accuracy of the mold inserts. The latter criteria are getting more important for optical components with defined optical axes on front and rear side, where alignment is crucial. For reducing the form deviation caused by shrinkage, intensive research on simulation and experimental investigation has been done. Chapter 4 elucidates the replication process itself including injection molding and injection-compression molding. However, in plastic replication a perfect form of the molded part does not guarantee a high optical quality since a non uniform density of the optical material leads to changes in the refraction index. A detailed investigation of the mold filling process shows the major challenges of plastic molding.

The next chapter covers mold insert manufacturing technologies. Diamond machining is the state-of-the-art process for machining the optical surface of mold inserts for plastic replication. Today optical design often addresses aspherical and free form optical surfaces that are not machinable with traditional turning and milling operation. Customized fly-cutting, ball-end milling and non-circular turning operations like Fast-Tool-Machining processes will be presented for enlarging the spectrum of machinable geometries. This chapter includes material aspects and the selection of machining parameters as well as programming and data handling aspects. These are closely bound to the machining strategy and the achievable surface quality.

While the machining technology described above addresses the manufacturing of continuous surfaces, the generation of structured surfaces has to be handled in a different way. In the beginning of chapter 6 a classification of the most important types of structures is carried out. After that, state-of-the-art and new innovative structuring technologies are discussed. Finally, a new technology called diamond micro

chiseling is presented. It is developed in the SFB/TR4 for machining of arrays of small pyramidal cavities without the need of a galvanic replica. Consequently, it can be used for machining of structures like retroreflective cube corner arrays with a structure size between 50 and 500 $\mu$m.

Diamond machining technologies mentioned above are restricted with respect to the spectrum of materials still limited to aluminum, copper, nickel phosphorus and nickel silver; diamond machining of steel is still a challenge. In the SFB/TR4 a new technology for diamond machining of steel has been developed and is under investigation. Chapter 7 describes the underlying basic idea. The iron of the surface layer of the workpiece is transformed to a nitride in order to get a compound layer which is machinable with diamond tools. By using this technology the chemical reactivity has been reduced by several orders of magnitude. This chapter discusses the requirements in contrast to traditional diamond machining operations.

The following chapters focus on glass replication. In chapter 8 novel processes for the machining of tool inserts for precision molding of optical glass components are addressed in detail. For meeting the demands of glass molding processes the mold insert material is much harder and temperature resistant than for plastic molding processes. These materials are machined by grinding and polishing operations. This chapter presents a novel Wire-EDM process for pre-dressing and profiling grinding wheels that can be used to machine complex shapes like cylindrical lens arrays. However, to achieve a surface roughness of the profiled mold in optical quality a subsequent polishing process is necessary. For this reason, novel profile polishing is introduced. Low surface roughness and high form accuracy can be achieved by this process combination.

In chapter 9 the developed polishing technologies are introduced, focusing on fully automated polishing processes. Despite the fact that steel has been polished for decades, the question how to assess material defects after polishing is still a challenge. Further algorithms for computer controlled polishing of free forms and their implementation into a custom machine tool are discussed. Structuring of discontinuous structures, especially cavities, is typically still a domain of manual polishing. To fully automize this process, customized and adapted tool motions have been developed.

Chapter 10 discusses the major aspects of glass molding with tungsten carbide molds, i.e. mold design, mold manufacturing, mold coating and finally the molding process itself. The chapter will close by proposing a strategy for the reduction of the required iteration steps for the fast fabrication of optical glass components. A major aspect is the introduction of a developed simulation tool.

During the glass and plastic replication process the surface of the mold insert suffers from high mechanical, chemical and thermal load. Some mold materials withstand this load, but hard coatings will help to increase tool life. The development of PVD and sol-gel coating is described in chapter 11. By sol-gel technology thick and crack-free hybrid organic-inorganic coatings are produced, which can be used

with continuous and structured optical mold inserts. Moreover, the coating process can be modified in a way that the sol-gel layers are diamond machinable. These films can be further hardened and provide outstanding mechanical properties by a novel subsequent ion radiation, that has been introduced by the SFB/TR4.

Apart from the design and manufacturing steps in a process chain measuring the geometry and the roughness of the mold insert and the replicated components are essential. In chapter 12 technologies for in-situ and in-process measurement of form and roughness are presented. A newly developed Speckle based roughness measurement system provides fast measurement and distinct robustness. Therefore, it can beneficially be applied for in-process roughness measurement. The precise measurement of the lens shape is typically achieved by interferometry. Accordingly, this chapter demonstrates a setup and custom algorithms for fully automatic interferometric measurement, which can be adapted to a lens replication process for automatic in-situ measurement.

The book ends with contribution provided by Prof. David Whitehouse who was a visiting guest scientist of the SFB. He gives an extensive view on metrology for optical components. He concludes by stating that the greatest potential of metrology can be found in mathematical procedures and algorithms because these will improve the performance of state-of-the-art instruments and will also enable fully automated measurements.

Over a period of eleven years the SFB/TR4 has gathered a large number of leading scientists to perform leading edge research in the challenging and prosperous field of prominent technology in close cooperation with industry.

All sub-projects have been developed new technologies and improved known processes to significant advantage to the state-of-the-art. A super-ordinate coordinated conversation - especially for process chains performed off-site - and a standardized usage of chain relevant data have been developed to encourage an unambiguously process chain wide communication. The SFB/TR4 focused its work on machining of free-form surfaces. This type of optical component fulfils the demands of the current and future market. Moreover, this technology is also evident for the deterministic fabrication of high precision optical components like high precision spherical and aspherical lenses since it allows taking into account the shrinkage during the replication process. In other words, for machining high precision spherical and aspherical lenses free-form mold geometries and/or highly developed technologies for each process step are essential. The final step to a leading-edge process chain is a fast in-process or in-situ measurement of form, roughness, and sub-surface properties. Even here, the SFB/TR4 has developed techniques with industrial significance.

The sum of all developed and investigated methods and processes as well as the holistic view on all process chain relevant impacts provides a fundamental step to a deterministic process chain.

**Acknowledgement**

All authors of this book and all other current and former members and principle investigators want to express their sincere thanks to the German Research Foundation (DFG) for funding the Transregional Collaborative Research Center SFB/TR4 “Process Chains for the Replication of Complex Optical Elements”.

# Total Quality Management in the Replication Process of Sophisticated Optical Elements

Robert Schmitt and Peter Becker

**Abstract.** Total Quality Management (TQM) is a long term business strategy. It is based on the three principles Customer, Associate and Process-Orientation. All activities within TQM focus on the continuous improvement of the company's performance. Such a holistic approach is especially auspicious for cross-sited production chains producing sophisticated components such as highly complex optical elements. Within the sub project M5 Quality Chain Management, the TQM approach was used to develop an internet based software tool. The so called Process Chain Manager (PCM) supports the coordination of the process chains. Especially the aspect of Process-Orientation represents a crucial element within the PCM. The PCM helps to manage the different process steps as well as to coordinate their interfaces within a single process chain. Additionally, it represents the aspects Associates, who are responsible for a smooth process flow as well as Customers, who are located at the end of each process chain and are demanding high quality standards.

## 1 Introduction

Specialization in key competences and decentralization are a major element of competitiveness for manufacturing industries. Fabrication is nowadays an interaction of different suppliers, sub suppliers and the actual manufacturer. Cost and resource efficiency as well as coincidental quality leadership force enterprises to coordinate and manage their cross-sited production chains in a smooth and clever way. Thus, it is very crucial to establish well working cross-sited or cross-enterprise production chains in so called collaborative production networks to combine all necessary technical qualifications for the final products [Sch03].

Such cross-sited collaborations are not easy to handle and likely to fail because of issues such as general misunderstandings, missing respectively not shared information, unprecise specifications as well as cultural differences between the participating companies. Several studies reveal, that between 50 and 90 percent of cross-sited or cross-enterprise cooperation fail or do not meet the expected results

Robert Schmitt · Peter Becker
Fraunhofer Institute for Production Technology IPT, Steinbachstraße 17,
52074, Aachen, Germany

E. Brinksmeier et al. (Eds.): Fabrication of Complex Optical Components, LNPE, pp. 1–11.
springerlink.com 

of the involved enterprises [Fon95]. Furthermore is the complexity of such cross-sited process chains increasing, with an increase of the complexity of the product. This results in highly complex process chains for sophisticated products such as optical free-form components or aspherical lenses as produced in the Transregional Collaborative Research Center SFB/TR4.

In this context, the Total Quality Management idea is a suitable approach for creating a framework around this whole issue by focusing on a continuous improvement of the company's performance as well as by fulfilling customers' expectations [Eng96]. As a long term business strategy, TQM is based on the three principles Customer, Associate and Process-Orientation. Besides the main target to ensure high quality products, TQM helps in addition to improve the whole process quality. This leads to less failures, a reduction of unproductive process steps, less waste production and less rework. All these negative aspects represent costs and waste of time that are of no use for the customer and thus have to be prevented. [Pfe01]

## 2 Total Quality Management

Total Quality Management is based on the Company Wide Quality Control (CWQC) idea by Ishikawa. Because of the remarkable successes mainly Japanese companies achieved with the CWQC, this approach was getting improved and extended by consideration of the companies surroundings and philosophies [Sch10]. Until now, there does not exist a uniform, international agreed on definition of TQM and thus, opinions concerning this term do vary [Zol06]. Nevertheless, the implementation of TQM leads, scientifically proved by various studies, to an improvement of a company's performance. [War04, Exb02, Efq05, Tan05].


**Fig. 1** Total Quality Management

As in Figure 1 visualized, TQM consists of the three main elements: Total, in terms of an holistic company consideration including processes, customers and associates as well as quality and management that are all connected through a continuous improvement process.

Intern and extern customer satisfaction, respectively the ideal compliance of customer preferences can be considered as the main objective of TQM according to the principle: “Quality is represented by a returning customer, not by a returning product”. Hence, for implementing TQM a company has to focus on its customers and their contentment. [Sch10]

As a consequence, TQM cannot be implemented in a single department of a company but has to permeate the whole company from top management to each single associate. For a successful implementation this fact results in two crucial demands. The first demand consists of a systematic enterprise strategy [Seg07; Zol06]. Of course, this strategy has to be enforced by the top management with involvement of all associates. It is of high importance, that the management is aware and convinced of the possibilities and benefits TQM offers. But, TQM may not appear as an ordinary method. Rather needs the top management to establish the basic conditions for TQM and hence promote suitable programs to enforce TQM throughout the company. Besides this strategy aspect, for a complete implementation of TQM, there has to be also a functional implementation. Whereas in the first step, the strategy implementation, mainly the management is involved to appoint a global strategy, the second step, the functional implementation, requires clearly defined measures of qualification for the single specifications within the strategy as well as a regular assessment of the status quo. In this context, it is very crucial, that the employee sees his tasks as a contribution to the overall target. To achieve such an understanding, the company’s overall target and strategy has to be openly communicated to each associate. [Sch10]

Because the process orientation within the TQM concept is, besides the already mentioned aspects of associates and customers, of high importance and additionally combines all three aspects, process orientation will get highlighted in the following.

The reason for stressing process orientation is due to the awareness that organizations work more effectively, if connected activities within such an organization are well understood. This fact demands an overall approach to analyze and to evaluate all relevant process chains.

For a systematic evaluation it is first of all necessary to define a process. Each activity that receives an input and subsequently transforms this input into an output can be considered as a process. A systematic regulation and conduction of such processes as well as their interfaces between the single process steps can be described as process orientation. In this context, intern and extern client specification do play a crucial role. Thus, each downstream process step is considered as client whose wishes, targets and issues have to be taken seriously care of. This leads to the request, that for a profound analysis, a total consideration of the complete process chain has to take place. Commencing at its end, the customer and going, in a so called back flow stream, all the way to the process chains origin. By this, each process step and each associate in charge of one process step is going to be considered. [Sch10]

The major advantage after a successful implementation of process orientation implies a management that can make decisions based on facts and concentrate on targets which are relevant for a surpassing enterprise performance. [Sch10]

In the Transregional Collaborative Research Center SFB/TR4, the end customer is the optical components using industry. This industry sector has a very wide cross section from production technology and metrology, over life science to energy technology and information technology. [May07]

The market for optical components is steadily growing, especially for consumer goods with electro optical systems. This is due to extreme short product cycles, constantly declining prices and coeval growing effectiveness.

Cell phones with integrated cameras represent a vivid example of the application area of optical components and the development of these products are exemplary for the whole sector. There is a constantly high demand of cell phones due to a relatively short service life and a high amount of consumers. The quality of the integrated cameras is a key aspect of the cell phone and thus has to meet the customers expectations. To these belong among others a high image resolution, minimal size of the cell phone and thus of the embedded optical elements, simple and competitive replication as well as highly complex geometries. [Tra07]

For TQM this means, to see to it that these customers' expectations are getting fulfilled. This is a key aspect that leads to enthusiastic customers as shown in Figure 2.

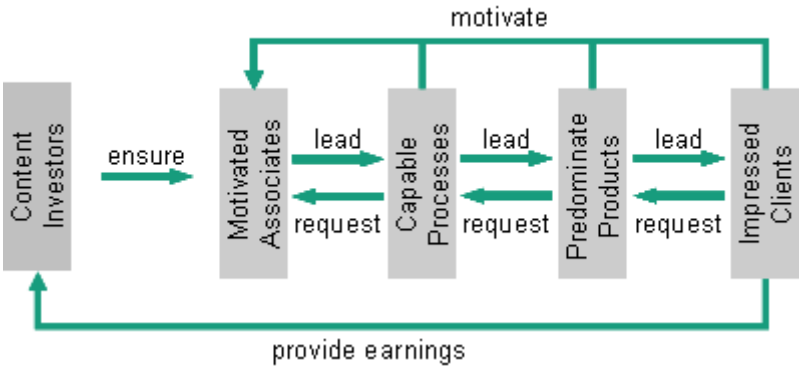


**Fig. 2** Causal connections within TQM

However, predominate products can only be produced if all necessary processes are capable and well working. Therefore are motivated associates inevitable. Figure 2 shows in a well-arranged way all causal connections within the TQM approach and highlights the importance of well working process chains that lead to predominate products.

In the Transregional Collaborative Research Center SFB/TR4, the main target consists of producing highly complex optical components such as aspherical lenses or free-form components. Certainly, process chains for these products are equally complex and their organization a challenging task. To support and facilitate this task the so called Process Chain Manager (PCM) has been developed in the sub project M5 Quality Chain Management. The basic idea of the PCM emanates from the sub domain process orientation of the TQM approach and will be next described in detail.

## 3 Process Chain Manager

In general, collaborative engineering processes can be characterised as unstructured and information centred by nature [Men03]. Thus, a systematic approach is needed to guarantee a smooth work flow.

A process chain usually contains several process steps with extensive dependencies at the organisational as well as technological interfaces between the individual process elements. The real or perceived complexity of a cross-sited process chain can be put in relation to the information that is needed for a successful production as well as to the geographical distance between the single process steps. [Sch08] For this issue, a systematic approach has been developed and can be seen in Figure 3.

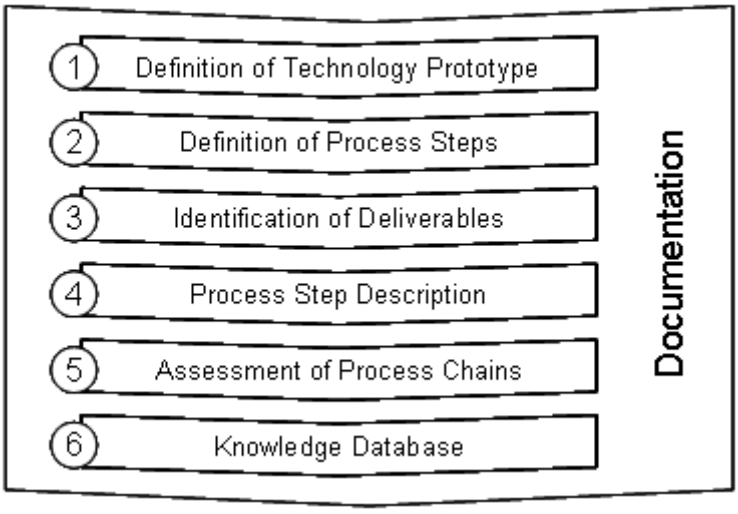


**Fig. 3** Six steps of process chain planning and control

For the production of optical components such an approach means, that in the first step the specifications of a technological prototype in form of a special lens type has to take place. As specifications, aspects such as geometrical dimensions, optical function, surface quality, shape accuracy and the lens material have to be listed. To guarantee that all needed information about the product is mentioned, a generic parameter model is used for the specification set up.

The second step compiles all relevant process steps for the production of the defined lens consecutively, as visualized in Figure 4. In each process step only one technology is described and there has to be one person who is directly in charge of this step.

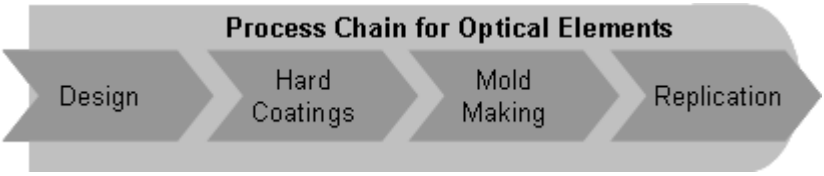


**Fig. 4** Typical Process Chain for Optical Elements

After having visualized the complete process chain in detail, the exchange of deliverables between the single process steps has to be coordinated to prevent that the responsible process step operators are missing information and thus the complete process chain might fail. According to analyses of well established process chains, informational relationships exist not only between sequential process step interfaces, but also within the whole process chain, whether directly linked or not [Pet01]. A visualization of all informational relationships between the single process steps can be seen in Figure 5, the so called Process Structure Matrix (PSM).

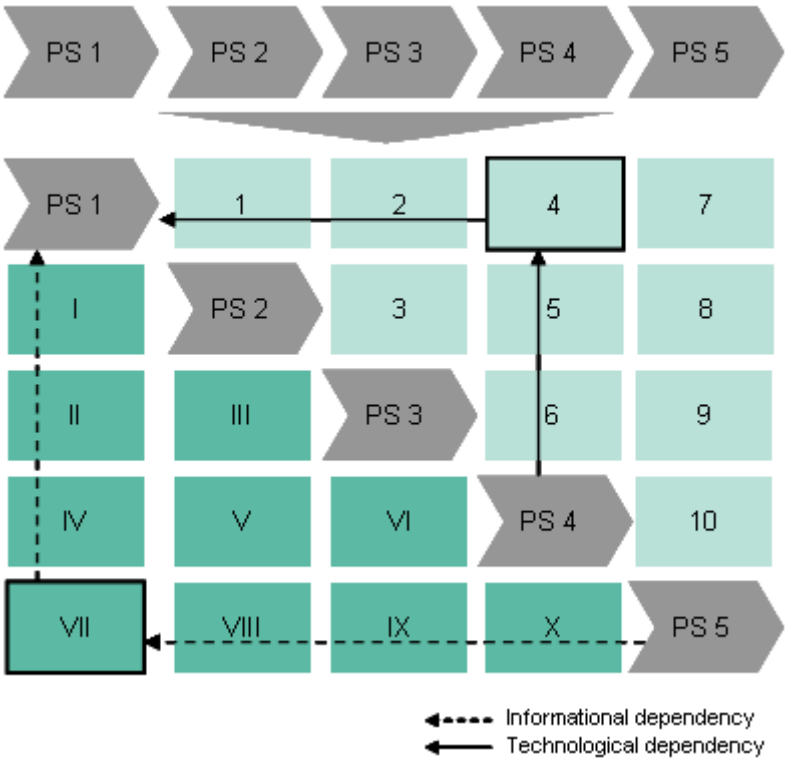


**Fig. 5** Process structure matrix for documentation of dependencies

The third step of the process planning approach consists of the development of a PSM as shown in Figure 5. The initial process steps from Figure 4 will be arranged on the main diagonal of the matrix. Each remaining cell in the matrix illustrates an interface between two process steps where information or materials are exchanged. The required information to previous and following process steps is documented for each interface between the process steps. The deliverables' characteristics and the delivery date are agreed upon in special meetings and transferred into an action list, so that the participants involved in a process chain have every time a clear overview about the whole process.

In step four, the "Process Step Description", each single step has to be described very precisely. The intention of this step is to get a clear idea about where exactly the demanded deliverables will be applied in the process steps and to achieve an output of the process step that meets the requested demands of the respective process steps.

In step five, the evaluation of the complete process chain begins. The process chain participants take part in an assessment workshop to discuss the process chain results. The lens specification will be compared with the actual manufactured lenses and measures to improve the process chain will be derived. These are essential proceedings to improve the process chain and to achieve constantly better results.

The last step is a continuation of step five. Gained experiences are evaluated and afterwards categorized in a database. Thus, information is stored and available for future coordination and improvement of new and already existing process chains. The database is part of the internet based management tool that will be described and introduced in the following.

## 4 Internet Based Process Chain Control

The described method of a systematic approach for coordinating cross-sited or cross-enterprise process chains has to be transformed into an easy to apply tool. Additionally, it is necessary to find a way of managing all customer-supplier-relations in a decentralized way [Lut01]. An internet based and thus location independent management tool seemed for this concern most suitable.

The development of the so called Process Chain Manager (PCM) is the transformation of a theoretical approach into an actual tool. It enables a cross-sited project team to map and coordinate all customer-supplier-dependencies and to control the project progress by generating action lists and time schedules. The software tool is built up on a mySQL data base.

The PCM is a Web 2.0 interactive platform. Each project team member has a private access to this tool. Being logged in, the software automatically recognises the user. Each user has his or her own profile which he or she has to create in order to present other project team members all relevant information about his or her responsibilities concerning different process steps as well as chains. Additionally, individual information such as name, contact address, subproject in charge, institute respectively company and the running as well as finished process chains are listed for each member profile. Besides the member profiles, there is an

e-mail service which enables immediate communication between the members and a general overview of all existing running and finished process chains within the project.

When setting up a new process chain, the product has to be first described in regard of its specifications. These information get listed in a special product template and additionally, documents like technical drawings or photographs can be uploaded. This enables all project member to have direct access to all relevant information concerning the product.

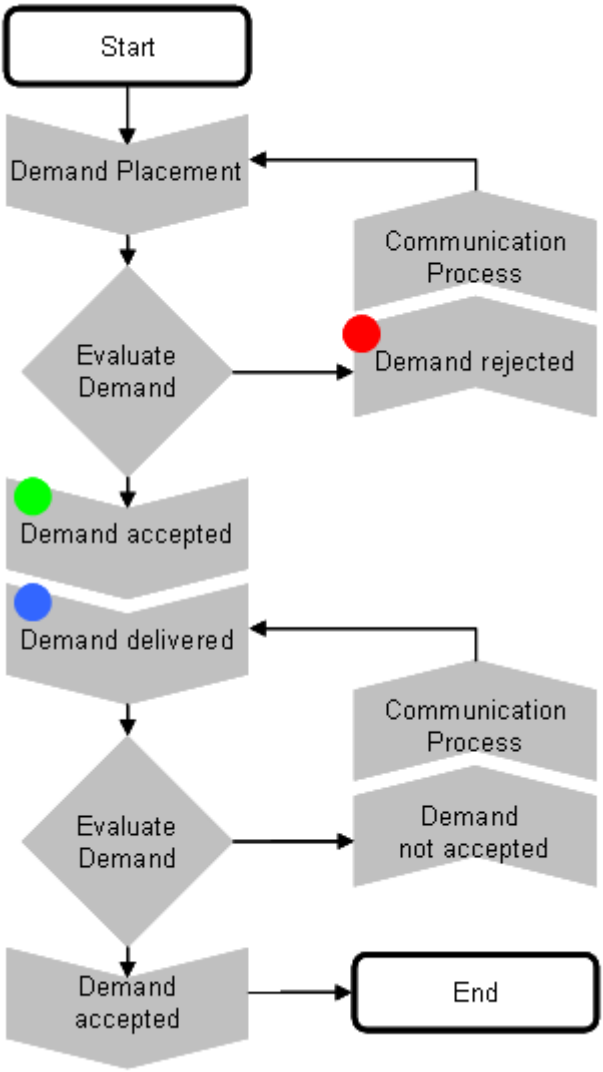


**Fig. 6** A systematic approach for the Process Structure Matrix

However, the major application of the PCM is the usage of the Process Structure Matrix (PSM) for coordinating demands and deliverables between the single process steps. After the definition of the process chain and the single process steps with their technologies and employee in charge of, the PSM has to get filled in with all demands and deliverables. Therefore, a systematic approach was developed as shown in Figure 6.

The software allows each member by means of the assigned access authorisation to place demands only at the interfaces assigned to the process steps he or she is responsible for. After all demands are placed, a process like visualized in the flow chart of Figure 6 follows. The colours used in the flow chart are also used in the PSM with the same meaning so that every project member knows just by seeing the colour of an interface between two steps at which level the process of demand and deliverables negotiation is.

Next, all users are requested to confirm the demands they were asked for. If a demand is accepted (green colour), the supplier of the deliverable must define actions which are suitable to fulfill the requests. Furthermore, the supplier indicates the time needed to carry out the actions. If the demand cannot be fulfilled in the way proposed (red colour), a communication process is launched in which the demands and deliverables between the demanding and the supplying participant are coordinated gradually along the process chain. On the basis of the indicated time needed to carry out the actions, the software generates the target project schedule.

Once all demands are mapped and coordinated, the next phase of the workflow is launched. The project schedule is transferred from the target schedule into the current schedule. The type of representation of the process matrix remains unchanged, the only difference is that the coordinated demands are transferred into deliverables that should be generated. If a deliverable in the form of a defined action is generated, the supplier marks the action as finished (blue colour). The customer is now requested to confirm the correct supply of the demanded deliverable. Only if the deliverable is classified as fulfilled, the entry in the actual project plan is updated. All process participants have full access to the target and current schedule, so that the current process progress is transparent and available at any time.

The last and decisive step is the acquisition of process knowledge. The development of this knowledge is considered highly important [Roz02]. Production processes for optical components are extremely individual and complicated and thus, each process chain has to be used to gain experiences. Using theses experiences as a knowledge base, the quality of future process chains will increase. Each process member is therefore requested to document and assess the experiences made during the cycle of the process chain. The assessment takes place in a workshop with all involved process chain participants. All electronically available documents, such as designs, parts lists, work instructions, metrology records etc. can be listed in the product template which is stored on the server and thus available for all process chain participants. Hereby, time expenditure for searching available information can be reduced immensely.

## 5 Conclusion

Cross-sited or cross-enterprise production chains often fail to achieve the predefined targets due to an insufficient information flow and because of too many undefined interfaces between the single process steps within the whole process chain.

Total Quality Management stands for a holistic approach to coordinate a company always trying to meet customers expectations according to the principle: "Quality is represented by a returning customer, not by a returning product".

The introduced approach, using TQM as basis for developing a software tool for process organization, shows a suitable set of methods for a structured planning and managing of cross-sited production process chains. The key to efficient process chains is the coordination of the relevant customer-supplier-relationships at the process interfaces. This can only be achieved by a very precise definition of the product and all its specifications. Additionally, there has to be a clear and profound analyse of asked and technical possible demands and deliverables at the interfaces in advanced. Thus, the introduced PCM supports cross-sited project teams on the basis of TQM.

**Acknowledgement.** The authors like to thank the German Research Foundation (DFG) for funding this work as a part of the Transregional Collaborative Research Center SFB/TR4 "Process Chains for the Replication of Complex Optical Elements".

## References

[Efq05] EFQM, BQF: Organizational Excellence Strategies & Improved Financial Performance. London BQF (2005)

[Eng96] English, L.P.: Data Quality Improvement: Maximizing Data Value Through Metrics and Management. In: Seminar 3rd Information Impact International, pp. 1–2 (1996)

[Exb02] VDI, forum! GmbH marketing + communications: Excellence Barometer (ExBa) Deutschland (2002), http://www.tqmcenter.com/CFDOCS/cms3/admin/cms/download.cfm?FileID=294&GroupID=91 (visisted on October 3, 2010)

[Fon95] Fontanari, M.-L.: Voraussetzung für den Kooperationserfolg -eine empirische Analyse. In: Schertler, W. (ed.) Management von Unternehmenskooperationen, Ueberreuther, Wien (1995)

[Lut01] Lutters, D., Mentink, R.J., van Houten, F.J.A.M.: Workflow management based on Information Management. Annals of CIRP 50(1), 309–312 (2001)

[May07] Mayer, A.: Optische Technologien. Wirtschaftliche Bedeutung in Deutschland. Bundesministerium für Bildung und Forschung (2007)

[Men03] Mentink, R.J., van Houten, F.J.A.M., Kals, H.J.J.: Dynamic process management for engineering environments. Annals of CIRP 52(1), 351–354 (2003)

[Pet01] Petridis, K.D., Pfeifer, T., Scheermesser, S.: Business Process Improvement: Development of an Quality-Characteristics-Library as Controlling Instrument for Business Processes. In: Proceedings of the 45th EOQ Congress, vol. 45, pp. 313–323 (2001)

[Pfe01] Pfeifer, T.: Qualitätsmanagement Stratgien Methoden Techniken. Hanser (2001)

[Roz02] Rozenfeld, H.: An Architecture for Shared Management of Explicit Knowledge Applied to Development Processes. Annals of CIRP 51(1), 413–416 (2002)

[Sch03] Schuh, G., Bergholz, M.: Collaborative Production on the Basis of Object Oriented Software Engineering Principles. Annals of CIRP 52(1), 393–396 (2003)

[Sch08] Schmitt, R., Scharrenberg, C.: Approach for the Systematic Implementation of Quality Gates for the Planning and Control of Complex Production Chains. Vimation Journal (1), 40–45 (2008)

[Sch10] Schmitt, R., Pfeifer, T.: Qualitätsmanagement Strategien Methoden Techniken. Hanser (2010)

[Seg07] Seghezzi, H.D.: Konzepte – Modelle – Systeme. In: Schmitt, R., Pfeifer, T. (hrsg.) Masing – Handbuch Qualtiätsmanagement, 5th edn., pp. 155–171. Hanser (2007)

[Tan05] Tanner, S.J.: Is Business Excellence of any Value?. West Yorkshire. Oakland Consulting (2005)

[Tra07] Transregionaler Sonderforschungsbereich SFB/TR4. Prozessketten zur Replikation komplexer Optikkomponenten. Finanzierungsantrag, 9–14 (2007)

[War04] Warwood, S.J., Roberts, P.A.B.: A Survey of TQM Success Factors in the UK. Total Qualtiy Management 15(8), 1109–1117 (2004)

[Zol06] Zollondz, H.-D.: Grundlagen Qualitätsmanagement. Einführung in Geschichte, Begriffe, Systeme und Konzepte, 2nd edn., Oldenburg (2006)

# Mold Design for Complex Optical Plastics Components

Walter Michaeli and Maximilian Schöngart

**Abstract.** A key condition for the successful manufacturing of optical plastics parts and a major challenge at the same time is to develop high-performance injection and injection-compression molds. Particularly in the field of optics, the stringent requirements placed on part dimensions and the homogeneity of the internal properties lead to a large number of requirements in terms of the mold concept.

In order to meet these requirements, a modularly-designed injection-compression mold has been developed. The mold features a cone-alignment to ensure a precise centering of the two mold inserts to each other. In injection-compression molding processes, it is necessary to seal the cavity before the polymer is injected. Therefore, a spring-supported sealing ring is implemented that seals the cavity after the two mold inserts are aligned. In this position, the mold is not closed completely and it is possible to mold polymer optics using both injection molding and injection-compression molding.

A second mold has been designed with two cavities to ensure symmetrical forces and hence to increase the reproduction accuracy. Injection-compression molding can be performed either via the closing movement of the injection molding machine or the movement of internal hydraulic pistons. Using this concept it is possible to compare the two compression techniques. During the compression process a gate closure prevents the melt from flowing back into the plasticizing unit. Furthermore, the mold features a parting line locker, which is needed when the compression cores are moved by the machine movement.

## 1 Introduction

Optical systems made of transparent polymers compete economically with glass optics [Cha04]. Technological advantages in polymer processing allow increasing substitution of glass optics. The great freedom of plastics in the design of optical functional surfaces, the integration of several functional parts, the good moldability, a low specific weight and not at least low material costs prove the

Walter Michaeli · Maximilian Schöngart
Institut für Kunststoffverarbeitung IKV, Pontstraße 55, 52062, RWTH Aachen, Germany

E. Brinksmeier et al. (Eds.): Fabrication of Complex Optical Components, LNPE, pp. 13–24.
springerlink.com 

substitution potential. Injection molding and injection-compression molding allow a comparatively cheap one-step-manufacturing of high precision plastics parts [Kun07, May07].

The optical quality of plastic lenses is significantly influenced by both the geometrical accuracy of the optical shape and inner properties. A key condition for the successful manufacturing of optical plastics parts and a major challenge at the same time is to develop high-performance injection and injection-compression molds.

In preliminary investigations it could be shown that injection-compression molding is appropriate for manufacturing thick-walled optical lenses [Böl01, For06]. Therefore, the replication of optical plastics components by injection-compression molding techniques should be further investigated. For this purpose, two injection-compression molds have been designed and built. These molds and their key features are described in this chapter.

## 2 Design Guidelines for Optical Plastics Components

To make successfully use of the advantages of injection and injection-compression molding, some restrictions and boundary conditions have to be taken into account. These rules apply to the design of injection molded plastics parts in general and for optical plastics parts in particular.

Any forms of undercuts in the part geometry have to be avoided, since they work against the demolding of the part and may damage or destroy it. Furthermore, any surfaces parallel to the direction of demolding should be equipped with a draft angle of 1° to 1.5° for an easy demolding process. If possible, any leaps in wall thickness should be avoided or minimized. They lead to a non-uniform filling of the cavity, which may cause an air entrapment in the part. Furthermore, leaps in wall thickness cause a non-uniform cooling of the part resulting in a higher degree of warpage. However, the optical functionality of a lens requires different wall thicknesses across the lens. Therefore, the part has to be designed in a way that a continuous transition of the wall thickness enables a good filling behavior. The gate of injection molded plastics lenses is usually located at the side of the lens, since a gate on the optical surface would cause a mark that cannot be tolerated.

## 3 Development of a One-Cavity Injection-Compression Mold

The first key aspect of the mold design is the modularity of the mold, which means that the investigations are not limited to a fixed lens geometry. A mold base has been designed that can be equipped with interchangeable mold inserts on both mold halves. With this mold, the replication of a variety of different lens geometries can be investigated. Basic conditions are only the diameter of the optical functional area of 50 mm and the thickness of the lens at the edge of 8 mm.

A concave-convex shaped lens, a so called meniscus lens, was chosen as the basic lens geometry. For the convex side, the spherical radius can be varied from 100 mm to 500 mm. On the concave side it can be varied from 100 mm to

150 mm. The resulting minimal thickness of the lens in the center is 4.77 mm, the maximum thickness is 8.23 mm. In addition to spherical shapes, mold inserts with aspherical geometries can also be used.

## *3.1 Filling of the Mold Cavity*

For the rheological design of the mold, the shape of the lens and the geometry of the gate have to be determined and then tested with regard to the filling behavior of the cavity. A focus of the filling simulation is on the edge of the lens. This edge is formed by a ring with a constant thickness of 8 mm and an outer diameter of 80 mm. On the one hand, this ring is required for the demolding of the lens, since the ejector pins cannot be placed on the optical surface of the lens. On the other hand, this ring is used to fix the molded lenses in various optical measuring devices.

For the filling simulation, the injection molding simulation software CADMOULD was used. Figure 1 shows the flow of the melt front during different stages in the filling process. The maximum thickness of the lens is located in the center, so no running ahead of the melt along the edges can be seen. On the other hand, for a lens with the minimum thickness in the center and the maximum thickness at the edge, a more critical filling behavior can be expected. The melt front will run ahead along the edges, so the simulation has to ensure that no binding line will occur. Instead, a continuous melt flow across the optical functional area is preferred.

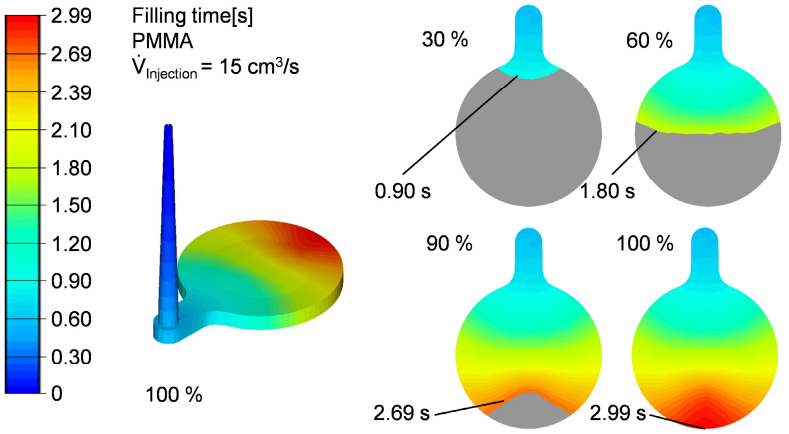


**Fig. 1** Filling simulation of the mould cavity

The gate diameter was designed to have the same dimension as the edge of the lens. With the gate being the last part of the lens to freeze in the injection molding cycle, an effective holding pressure can be applied for a time as long as possible. The gate diameter at the lens was calculated to 10 mm with a draft angle of 1.8°

for easy demolding during the ejection. With the chosen gate geometry and the geometrical boundary conditions of the cavity, a mold filling without binding lines and air entrapment can be expected.

## 3.2 Centering of the Mold Halves

The geometries of the lens and the gate system are important for the filling of the cavity during the injection phase. For the optical performance of the lens, a precise replication of the surface topography is essential. While the surface quality of the lens depends on the surface quality of the mold insert, the contour accuracy of the lens is determined by the mold base. The replication in the injection molding process can only be as precise as the cavity of the closed mold. This requires a precise and reproducible centering of the mold inserts to each other during the closing of the mold.

While the mold inserts are centered and fixed in the mold halves via tapered guides, the mold halves are opened for demolding and afterwards closed again from cycle to cycle. The basic centering of the mold halves during closing is usually performed by pillars on the one mold half that are dipped into the other mold half. For a much more precise centering, a fine centering system after the dipping of the pillars has been designed. With a fine centering of the mold halves via tapered guides, an increased abrasive wear of the tapered surfaces was expected, since the forces occurring during the centering would have been compensated only by the flexibility of the entire mold. For this reason, a new concept using a floating mount was developed. The floating mount is placed between two mold plates on the moving mold half, so a part of the mold can move relatively to the stationary mold half.

## 3.3 Sealing Ring for Injection-Compression Molding

The mold was designed to be used not only in injection molding, but also in injection-compression molding. In this type of process, the mold not entirely closed before the injection of the polymer. Instead, it is opened by the compression gap. After the polymer is injected, the mold is closed, leading to an uniform pressure distribution across the part surface. For injection-compression molding, it is necessary to seal the cavity when the mold is closed to the compression gap. One way to seal the cavity is the integration of shearing edges. A disadvantage of shearing edges is that they would be in contact before the centering took place. This would limit the moving range of the floating mount to the tolerances of the shearing edges (i.e. 0.02 mm). Otherwise, a dipping of the shearing edges would be disturbed and abrasive wear would occur. Moreover, the entire compression period would happen without the centering, since the tapered guides are only functional when the mold is closed completely. For these reasons, a concept was developed that decouples the centering of the mould halves from the sealing of the cavity using to separate elements (Figure 2). The centering ring with tapered surfaces has a resilient mounting in the moving mold half. When the mold is open, the centering ring is pushed forward by springs for the distance of

the compression gap. When the mold is being closed, the centering ring is the first to get in contact with the fixed mold half, positioning itself to the fixed mold half. The prestressed ball bearing without clearance between the centering ring and the mold core with the fixed mold insert causes a centering of the mold insert at the same time. At this point, the two mold halves are already centered to each other, even though the mold is not closed completely yet.

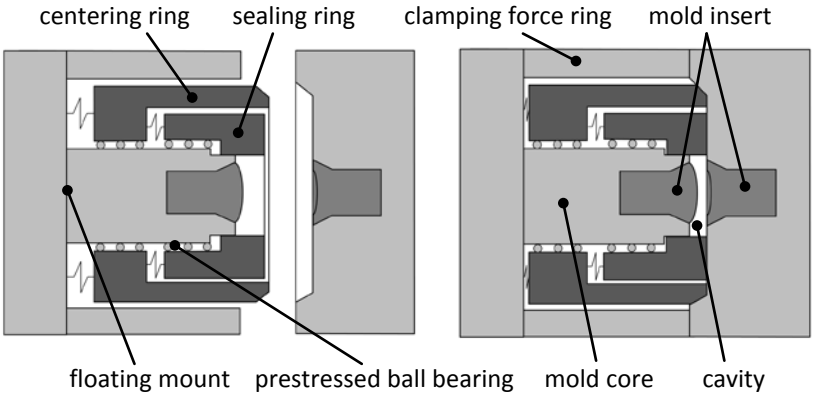


**Fig. 2** Schematic cross section view of the injection-compression-mold

When the mold is further closed, the sealing ring which also has a resilient mounting presses against the fixed mold half and seals the cavity. From now on, the cavity is sealed and a compression gap can be adjusted by the closing movement of the injection molding machine. During the compression period, the radial position of the mold inserts to each other persists, since the mold core and the mold insert are moved within the centering ring via the ball bearing. The compression movement can happen until the so called clamping force ring gets into contact with the fixed mold half. At this point of time, the mold is entirely closed (Figure 2, right). For conventional injection molding, this position is accessed before the injection of the polymer without stopover.

This mold concept has several advantages. It uses a floating mount to allow a lateral moving of the mold halves to each other within a certain range. The shearing edges are integrated into the moving mold half between the sealing ring and the mold core which contains the interchangeable mold insert. Thus, the shearing edges are in permanent contact, which minimizes abrasive wear. Furthermore, the two mold halves are centered to each other even before the sealing ring gets in contact with the opposite mold half, which means that there is now lateral movement between them when the clamping force is applied. Moreover, the centering of the mold halves persists during the entire compression movement.

Even after the molding and cooling of the part this mold design exhibits certain advantages. When the mold is opened, the mold insert on the moving side is

moved back. The lens cannot follow this movement, since it is fixed to the sealing ring by the draft angle on the edge. In the next step, the sealing ring looses contact with the fixed mold half, while the centering of the two halves still persists. Now the contact between centering ring and fixed mold half is loosened and the centering gets lost. These guided movements during the opening and demolding have the advantage, that a lateral movement between the mold insert and the lens can be avoided completely. This is of high interest, especially when lenses with a microstructured surface are molded. The two halves of the open injection-compression mold can be seen in Figure 3. On the fixed half, the interchangeable mold insert and the gate can be seen. Furthermore, the tapered surfaces can be seen that get in contact with the centering ring of the moving mold half when the mold is closed. On the moving mold half, the cavity, the centering ring, and the sealing ring (dark) can be seen.

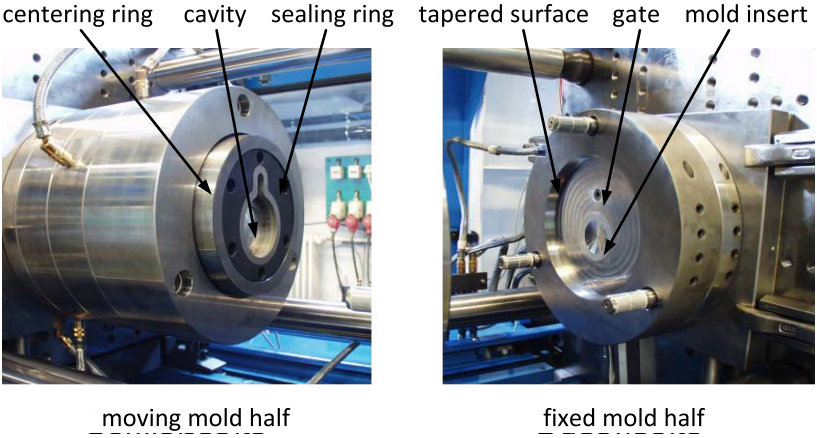


**Fig. 3** Moving mold half (left) and fixed mold half (right)

## 4 Development of a Two-Cavity Injection Compression Mold

The injection-compression mold described before has only one cavity with a gate at the side. This eccentrical position of the cavity leads to an asymmetrical pressure distribution which causes a bend up of the parting plane with high cavity pressures. Furthermore, this mold can only be used for the injection-compression molding variant with a movement via the clamping unit of the injection molding machine, where the force acts on the entire area of the molded part. In order to further increase the replication accuracy and to investigate the different variants of injection-compression molding, a new mold base has been designed [Hes10].

An important aspect of the new mold design is to ensure a symmetrical flow of force. This can be achieved with a two cavity mold where the gate is located between the two cavities. As the first mold, this mold is also modular designed for examinations of different lens geometries.

With the developed mold base lenses with a diameter of 70 mm can be manufactured (Figure 4). The diameter of the compression core on the moving mold half is 60 mm. Inside the compression core it is possible to change mold inserts with different surface geometries with a diameter of 50 mm. On the fixed mold half mold inserts can be changed with a diameter of 56 mm. The ejector pins were integrated in the fixed mold half, due to the complex and modular design of the compression technique in the moving mold half. The lenses have a thickness of 6 mm on the edges.

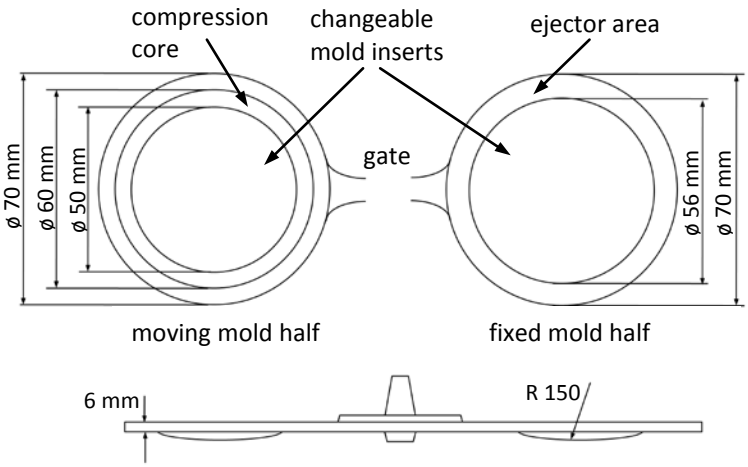


**Fig. 4** Lens geometry of the two-cavity mold

## *4.1 Centering of the Mold Halves*

As described before, the centering of the mold inserts to each other is an important aspect. The rough centering of the two mold halves is realised by a pillar guide. Pillars mounted on the moving side of the mold dip into the fixed mold half while the mold is being closed. Furthermore, a fine centering is necessary for a precise and reproducible positioning of the mold inserts. For this purpose, trapezoidal centering elements next to the mold inserts are used (Figure 5). These elements get in contact just before the mold is entirely closed and precisely centre the mold inserts to each other. Since the compression core with the mold insert has to be moved inside the mold plate, a centering with tapered guides is not possible. Instead, a prestressed ball bearing is used. The mold inserts in the compression core on the moving half of the mold and also the mold inserts in the fixed half are centered using tapered guides.

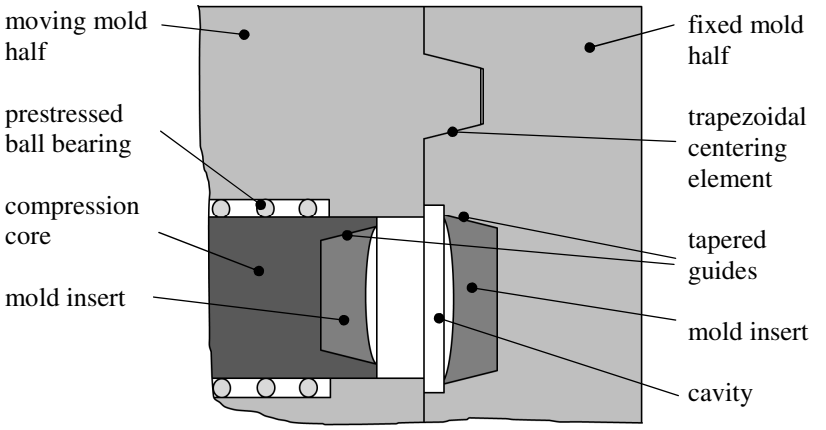


**Fig. 5** Centering with trapezoidal elements and tapered surfaces

## *4.2 Gate Closure for Injection-Compression Molding*

During the compression period, a back flow of the melt into the plasticizing unit of the injection molding machine has to be prevented. This back flow would cause orientations and residual stresses inside the part that negatively affect the optical quality. Usually, needle-valve nozzles are used to close the gate. However, these elements often have dead water (stagnation) zones which lead to extended retention times of the material in the channel. This further on may lead to a thermal degradation of the material. Therefore, needle-valve nozzles are not suitable for optical polymers.

There are two general demands to a gate closure system: First, it should be as close as possible to the cavity to minimize the volume that is being compressed. This automatically reduces the flow of material during the compression. Second, no material should stick to the closure system or retain in the system. This may lead to degradation and a defect on the molded lens.

A plate slider for each cavity, moved by a hydraulic cylinder was chosen. This gate closure can be opened and closed independently of the plasticizing unit. The slider is designed as a plate with a hole in it. Instead of squeezing the material to close the gate, this slider transfers the material completely out of the gate channel. This ensures that no material can stick to the slider or retain inside the channel.

The use of grease lubrication is not possible in molds for the replication of optical components, since the lubricant may contaminate the molded parts. To reduce friction and abrasive wear, a DLC-coating (diamond-like-carbon) was applied to all moving elements of the gate closure.

## *4.3 Injection-Compression Molding via Mold-Integrated Compression Cores*

Figure 6 compares the conventional injection-compression molding (left) to the so called core-compression molding (right). In the conventional process, the compression force acts on the entire area of the part. For the production of plastics lenses it can be advantageous to only compress the optical area of the lens. Therefore, the core-compression molding uses cores that only compress certain areas of the cavity. Already frozen parts of the melt at the edge of the part are not compressed, which significantly decreases the stresses induced in this area.

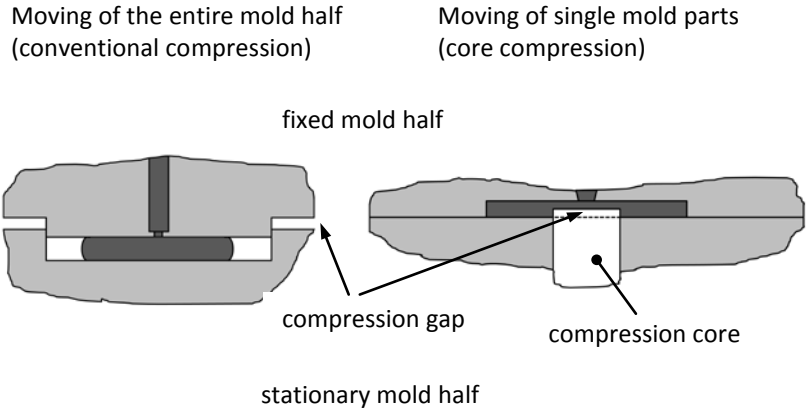


**Fig. 6.** Comparison of different compression techniques

The movement in the compression-phase can be either performed by the clamping unit of the injection molding machine (moving of the entire mold half) or by integrated hydraulic pistons (moving of single mold parts). The use of hydraulic pistons inside the mold has the advantage that less mass has to be moved, which increases the overall accuracy of the movement. The mold base was designed to be used for core-compression molding, either with the moving of the mold half by the injection molding machine or with a movement by integrated hydraulic pistons. This is realized by a change-over of the moving mold half, exchanging the hydraulic pistons and a mold plate. A cross section view of the mold equipped with integrated hydraulic pistons is shown in Figure 7. In the lower half of the picture, the hydraulic piston is moved back, so the compression core is moved back by the amount of the desired compression gap. The upper part of the picture shows the mold at the end of the compression period. The hydraulic piston has pushed the compression core all the way to the front. This position is also used for injection molding without compression.

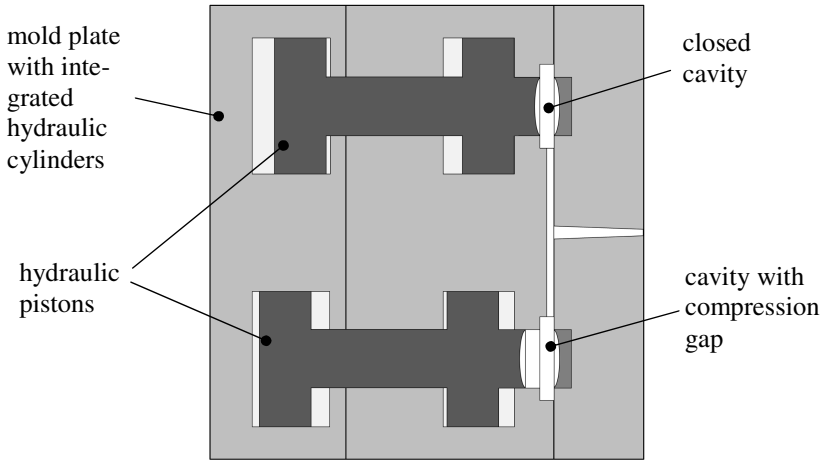


**Fig. 7** Injection mold with integrated hydraulic pistons

To investigate core-compression molding with the movement of the clamping unit of the machine, the back part of the mold base containing the hydraulic pistons is replaced by a simple mold plate (Figure 8). This mold plate is directly connected to the compression cores, leading the compression force from the injection molding machine directly to the cavity.

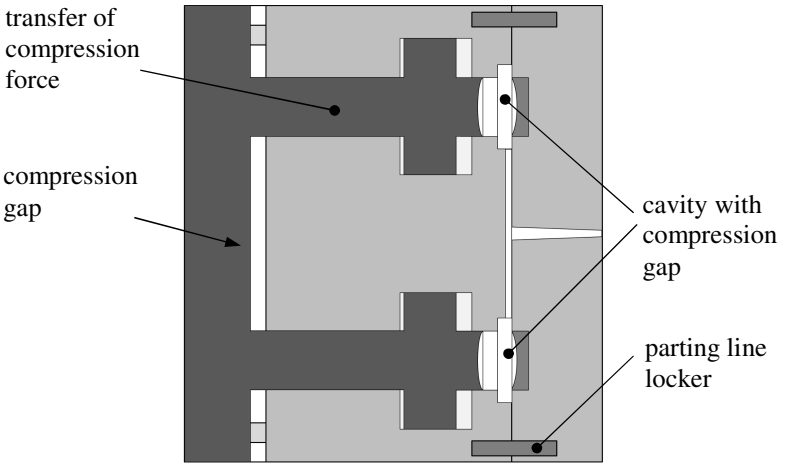


**Fig. 8** Injection mold for compression movement by the injection molding machine

### *4.4 Parting Line Locker*

When the integrated hydraulic pistons are used for compression, the cavity is kept closed by the clamping force of the injection molding machine. In the other case, the clamping unit is being used for the movement of the compression cores. When the inner parts of the lenses are compressed, the melt pressure inside the cavity is also transferred on to the edges of the part. This results in a force trying to open the mold. For this reason, a lock of the parting plane has been integrated into the mold base, to seal the cavities while the compression cores are moved by the clamping unit of the injection molding machine. In this variant of the injection-compression molding process the mold is initially completely closed. Because the lock of the parting plane ensures the force closure, the clamping unit of the injection molding machine can be moved back to the compression gap and apply the compression force after melt injection with the compression cores.

Figure 9 shows the two halves of the two-cavity injection-compression mold. One the moving mold half, the trapezoidal centering elements surrounding the cavities (black color) can be seen. On the fixed mold half, the gate closure (vertical black sliders) and the parting line locker can be seen.

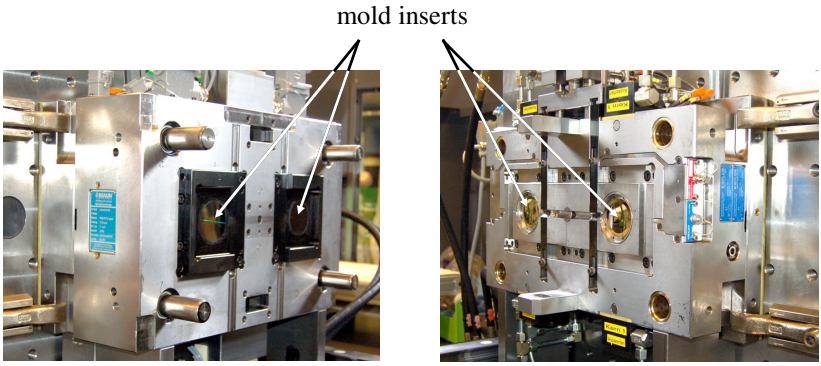


**Fig. 9** Mold halves of the two-cavity injection-compression mold

## 5 Conclusion

Injection molding and injection-compression molding are the primary forming techniques which have a significant potential to produce thick-walled optical parts in mass production. The surface geometry of the optical functional area influences the optical performance substantially as well as internal properties. High requirements concerning the mold design are a result of these demands.

In order to meet these requirements, two modularly-designed injection-compression molds have been developed. Key features of these molds are sophisticated mechanisms for the centering of the mold halves. Both molds can be

used for injection molding as well as for injection-compression molding. Furthermore, they can be equipped with interchangeable mold inserts.

Limitations of the first mold, a one-cavity mold, led to the development of the two-cavity injection-compression mold. This mold allows the investigation of two different injection-compression molding variants, either by integrated hydraulic pistons or by the clamping unit of the injection molding machine. Both molds are successfully being used for detailed replication processes of plastics lenses.

**Acknowledgement.** The authors like to thank the German Research Foundation (DFG) for funding this work as a part of the Transregional Collaborative Research Center SFB/TR4 "Process Chains for the Replication of Complex Optical Elements".

## References

[Böl01] Bölinger, S.: Spritzgießen und Spritzprägen von Kunststoffoptiken. RWTH Aachen, Dissertation (2001) ISBN 3-89653-956-6

[Bro98] Brockmann, C.: Spritzprägen technischer Thermoplastformteile, RWTH Aachen, Dissertation (1998) ISBN 3-89653-423-8

[Cha04] Chada, A.: Prozessorientierte Wirtschaftlichkeitsanalyse zur Herstellung optischer Komponenten aus Glas oder Kunststoff. Institut für Kunststoffverarbeitung, RWTH Aachen, Diploma Thesis (2004); Supervisor: J. Forster, T. Schröder

[For06] Forster, J.: Vergleich der optischen Leistungsfähigkeit spritzgegossener und spritzgeprägter Kunststofflinsen. RWTH Aachen, Dissertation (2006) ISBN 3-86130-846-0

[Hes10] Hessner, S.: Spritzprägen sphärischer und asphärischer Kunststofflinsen. RWTH Aachen, Dissertation (2010) ISBN 3-86130-973-4

[Kun07] Kuntze, T.: Plastic Optics Enable LED Lighting Revolution. Optik & Photonik 2(4), 42–45 (2007)

[May07] Mayer, R.: Precision Injection Moulding. Optik & Photonik 2(4), 46–48 (2007)

# Optical Plastics Components: Replication Processes and Plastic Materials

Walter Michaeli and Paul Walach

**Abstract.** Over the past years, more and more polymers have been applied for manufacturing optical components and have won an increasing market share for spectacle glasses, cameras, or other lens, or light guide applications. The manufacturing of optical components in plastics competes functionally and economically to the material "glass". For optical applications the technological advantages of plastics enable an increasing substitution of glass.

Injection molding and injection-compression molding allow a comparatively cheap one-step-manufacturing of high precision optical plastics components. Both processes are primary forming techniques which have a significant potential to produce optical plastics parts in mass production.

Using injection-compression molding, a combination of the injection molding and pressing process, a high molding accuracy combined with uniform inner properties of the molded parts can be obtained. Excellent process knowledge is a prerequisite to achieve and meet the required tolerances of high-precision plastics parts for imaging optics in the micron range.

## 1 Introduction

Future topical areas of research like information and communication technology, pharmaceutical technology, medical engineering and life science, material engineering but also the automotive industry and the industrial manufacturing as well as measuring technique are affected by optics and laser technology. In all these fields the optical technologies generate new products and processes and contribute increasingly to industry and science as well as to lifestyle of people. Over the past years, more and more polymers have been applied for manufacturing optical components and have won an increasing market share for e. g. glasses or cameras. Up to a resolution of 5 mega pixels of cameras in mobile phones, plastic lenses are used [Alb10]. The wide range of surface design, the integration of several functional components, good moldability, low material costs and low specific weight prove the substitution potential [Alb10, Lan03, Mic05, Pas78].

Walter Michaeli · Paul Walach
Institut für Kunststoffverarbeitung IKV, Pontstraße 55, 52062, RWTH Aachen, Germany

E. Brinksmeier et al. (Eds.): Fabrication of Complex Optical Components, LNPE, pp. 25–40.
springerlink.com 

In the manufacture of optical components plastics compete economically to the material glass [Lan03, Pas78, Zöl08]. For optical applications the technological advantages of plastics enables an increasing substitution of glass. For manufacturing of optical components mainly two processes are suitable. Injection molding and injection-compression molding allow a comparatively cheap one-step-manufacturing of high precision plastics parts [Kun07, May07]. High demands are placed on optical components to achieve the required optical function. Besides these advantages, the disadvantages of this material also have to be considered. Polymer lenses show a significant lower scratch and temperature resistance. The refraction index depends on temperature and on the content of moisture [Mic07]. The obtainable optical part quality is significantly depending on the specific material, the specific production process and the processing parameters. Therefore it is necessary to examine the whole value creation chain for each application to obtain a high precision optical component.

By classifying the optical applications in accordance with its requirements in three quality sections, the largest substitution potential of polymer optical parts is located in the area of low and medium quality requirements for medium and large quantities. To increase the substitution potential in the area of higher demands the cause-effect relationships during the manufacturing process have to be developed by fundamental research work.

The geometry of optical components is often contrary to common design guidelines for the manufacture of plastic parts by injection molding. The potential of shrinkage rises with increasing wall thickness of the molded parts. Especially the geometrical accuracy of thick-walled plastic lenses is negatively influenced during the molding process [Böl01]. The optical quality of plastics lenses is significantly influenced by both the geometrical accuracy of the optical shape and inner properties. Thus, the molding of optical components poses a serious challenge for mould, machine, and process.

## 2 Replication Processes for Optical Components

For the replication of optical plastics components mainly two processes are used. Injection molding and the resultant advancement injection-compression molding can obtain the required high-precision in a fully automated manufacturing [Kun07, May07]. Several studies have shown that in particular injection-compression molding is suitable for the production of thick-walled optical components. By the combination of the injection molding and the pressing process, a high molding accuracy with uniform inner properties can be obtained. The injection-compression molding allows a fully automated production of high precision plastic lenses [Böl01, For06].

### *2.1 Injection Molding Process*

Injection molding, as it is known from the 1950s, is a wide-spread and highly developed manufacturing process paired with many advantages [Joh04]. The main

advantages of the injection molding process are the short cycle time, the possibility of automated mass production and especially for optical components the freedom of design in the layout of the manufactured parts. In contradiction to the manufacturing of glass components it is possible to produce complex geometries like aspheric lenses, light guides or products with free form surfaces. More integrated products can be realised using the multi-component injection molding. Functional components of the optical system that cannot be covered by the optical plastics material, e.g. a mechanical fitting or sealing against surrounding media can be added in an additional shot using an appropriate plastics material.

The short cycle times compared to glass processing and the possibility to realise a highly automated process, make the injection molding process attractive from an economic point of view. To use the plastics optics for a growing number of applications and to replace inorganic glass, it is still necessary to improve the quality of the plastics optics.

The optical properties of a lens depend besides the geometry of the surface on the inner properties. The dimensional accuracy of the surface is depending on the plastics material used, the accuracy of the mold and the injection molding process. This leads to very high requirements on the manufacturing process itself.

At the beginning of the injection molding process a homogeneous melt is provided by the plasticizing unit. Before the plasticizing process, the material conditioning is very important, because foreign particles are the major source of defects while producing optical components. The material for optical application has usually strict restrictions on dust and dirt content. These enclosures lead to black specks and defects and with it to scrap [Böl01]. Black specks are partially degraded material at the screw surface, barrel or back-flow valves that detach from the surface and get into the part. The material and surface choice of screw and barrel are therefore very important.

The used materials have to be dried to avoid streaks because of humidity. Optical materials have the inclination of yellowing when they get overheated, so an overdrying has to be avoided. Besides drying conditions optical materials are thermal and shear sensitive. Therefore the materials are plasticized with a low screw speed and low back pressure.

The properties of the injection molded lenses are mainly influenced by the filling and cooling process. The characteristic factors for the cavity filling are the mold temperature, the melt temperature and the injection speed [Kle87]. For optical components it is very important to obtain very homogeneous inner properties [Böl01].

The packing and cooling phase have besides the injection phase high importance for the quality of the injection molded lenses. Therefore, the main factors are packing pressure and cooling time. In this phase important quality criteria like inner properties and geometrical accuracy are influenced. The cooling time has also an influence on the geometrical accuracy, since uncontrolled shrinkage occurs with too low cooling time [Böl01].

Because of the parameter's choice for obtaining a high part quality when injection molding is used for optical components, longer cycle times than in

common thermoplastic injection molding are the result. In dependency on the part geometry cycle times between 2 and 25 minutes can be necessary.

Using the described injection molding process with long packing pressure times causes highly oriented parts with non-uniform inner properties. A limitation of the optical performance is the result. Therefore the injection-compression molding process can be advantageous.

## *2.2 Injection-Compression Molding Process*

Since the 1960s the injection-compression molding process has been used to achieve high precision plastics parts [Wal61]. Uniform inner properties of the produced parts are the reason why the injection-compression molding process is often used for optical components.

The injection compression molding process can be divided into two separate process steps: melt injection and compression. During the injection phase, a specific volume of polymer melt is injected into the cavity. During this process step, the volume of the cavity is extended by the compression gap. Thus, the melt forms a melt accumulation in front of the gate. A mold design with shear edges avoids a melt flow in to the parting plane. During the compression phase the melt accumulation is compressed and distributed in the cavity. The part geometry is finally molded by the closing movement of the two mold halves. A mechanical or thermal sealing of the gate avoids the backward flow of the melt into the screw antechamber. The application of packing pressure from the plasticizing unit is not necessary in this case [Mic00].

Injection-compression molding as a combination of injection molding and compression molding unifies the advantages of both manufacturing processes. The molded parts stand out due to high geometrical accuracy, narrow tolerances, high class surfaces, low residual stresses and excellent mechanical properties [Hab99, Mic98, Tra73]. The advantages of automation and varied options of intervention result from the injection molding, the advantages of uniform material density and homogeneous pressure distribution result from the compression molding [Ber00].

Derived from these characteristics, the injection-compression molding has two fields of application:

The production of thick-walled parts because of an enhanced shrinkage compensation, a lower distortion and less shrink marks. Mainly for producing optical lenses (viewfinder lens, condenser lens, lenses for imaging optics, magnifiers, lenses, Fresnel lenses and prisms) with very high requirements concerning accuracy the injection-compression molding was established and developed [Wal61, Mat85, Kle87, Böl01].

Another field is the production of thin-walled parts with large dimensions. With the same filling pressure higher flow path/wall-thickness ratios are possible with injection-compression molding than with injection molding [Men68, Mic98]. As an example, a protective cover for a triangle could be realized with a wall-thickness of 0.4 mm and a flow path/wall-thickness ratio of 270 [Bro98]. Further examples of parts are optical storages (DVD) and car glazing [Bür99, Hei00, Mic98].

The injection-compression molding process can be classified in different variants shown in Figure 1. The procedure with partial fill of the cavity and the realization of the movement of the compression core with the moved mould half has the highest relevance [Fri90, Fri93]. This mode of the injection-compression molding process is called “injection-compression molding with the moved mold half” [Kna82, Kna84]. The mold is opened to the compression gap and can be closed either sequentially or simultaneously to the injection process.

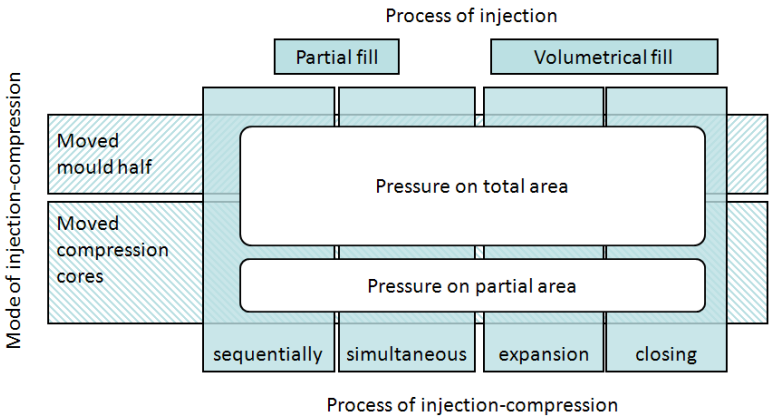


**Fig. 1** Overview of injection-compression molded process variants

While the injection-compression molding with volumetrical fill is used, the movement of the compression core is not used for forming the melt, but for the compensation of the thermal volume shrinkage of the part while cooling. The volume of the cavity is therefore only enlarged by the amount of the volume shrinkage.

Whereas at the common injection-compression molding with partial fill the moving mold half is pulled back to a wider compression gap than used for the compensation of the thermal volume contraction. Furthermore, the compression process can be realized by compression cores, which are moved when the mold is sealed. The compression cores can take effect either on the whole cross-sectional area or only on a partial area [Wal61, Bro98]. This variant of injection-compression molding makes more complex geometries possible than injection-compression molding with the whole mold half [Kud99].

Besides these variants of active compression molding the inactive compression molding represents a process in which the mold is closed with reduced clamping force. While filling the cavity the mold opens because of an adjustable resilience up to the preset compression gap. Due to an increase of the clamping force the compression process takes place afterwards [Kna84]. This so called “expansion compression” process can be combined with a variothermal process control, a heating of the cavity surface by radiation or electromagnetic induction, for the replication of optical components or optical microstructures [Bür01]. This process

control has the advantage that the hot cavity surface is overflowed in the beginning of the injection process, which leads to a good surface replication of the molded parts. The final part thickness is set by the injection-compression phase. The thermal contraction can be controlled by applying a compression pressure.

## 3 Measuring Techniques

Because each individual process and also the process parameters have a high influence on the optical properties of a manufactured lens, a 100 %-quality check is often needed in the production of optical components. To characterize the molded optical plastics parts regarding their quality, several criteria have to be defined. These quality criteria can be classified into the following domains.

First of all the optical function of a lens is depending on the surface geometry. The geometrical accuracy can be determined by tactile or contactless measurement methods. For optical components the contactless method is the common one, a chromatic sensor or an interferometer can be used.

Moreover the quality is also depending on the inner properties. Internal stress and orientations can be detected by polarization optics. The optical properties like distortion and the resolving power can be determined directly by an optical bench or a wavefront-sensor.

For a quality characterisation of a molded plastics lens it is necessary to determine both the geometrical accuracy and the optical performance of the lens.

### *3.1 Geometrical Accuracy*

To determine the geometrical accuracy of the injection-compression molded optical lenses, the surface geometries of both cavity and lens are measured by a chromatic sensor. This so-called MicroGlider, Fries Research & Technology GmbH, Bergisch Gladbach, is based on the chromatic aberration of optical lenses caused by the wave-length dependent refraction index and allows a non-contact and non-destructive measurement.

Focused white light is used to irradiate the lenses surface. Varying focal points of blue and red light are a consequence of the chromatic aberration of the sensor. These focal points are located on different levels. Depending on the surface topography and with it the distance between sensor and surface, the varying focal points are reflected by the surface with different intensity. The measured wave length of the reflected light gives information about the distance between sensor and surface and with it about the surface topography (Figure 2).

In an area of 60 mm x 60 mm 200 lines with 200 measuring points each are acquired. This results in a resolution of one point each 0.3 mm. The test set-up has a measurement uncertainty of 2 µm. The measurement range amounts up to 3000 µm, the accuracy of measurement is down to about 2 µm.

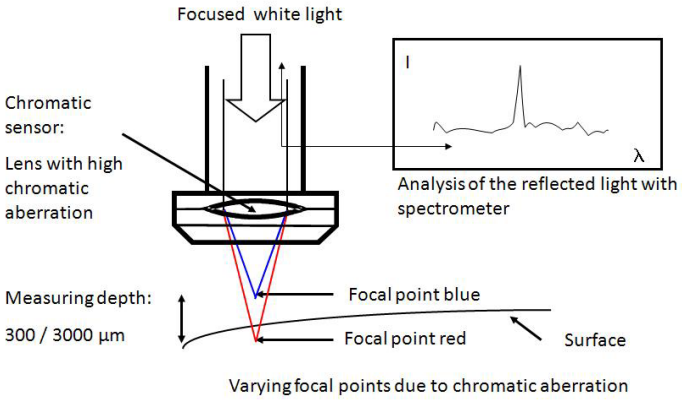


**Fig. 2** Measuring principle of a chromatic sensor

To analyze the surface accuracy, the surface data are passed on to the evaluation program AIX-Comp, which has been developed at IKV Aachen. The three-dimensional surface data of the molded lens and the mold insert are subtracted and the peak-to-valley-value (PV-value) is calculated (Figure 3). With this program a characteristic value for the maximum difference between mold and lens surface can be calculated for both sides of the lens. A high PV-value represents a lower geometrical accuracy because of a high difference between cavity and molded lens, a PV-value at a lower level represents higher geometrical accuracy.

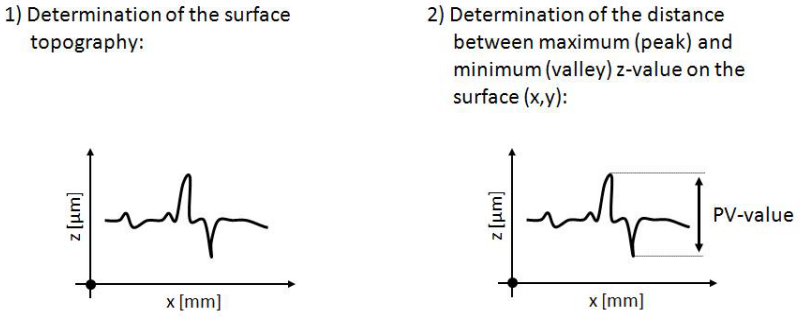


**Fig. 3** Determination of the PV-value

## *3.2 Optical Performance*

A wavefront-sensor, the so-called Shack-Hartmann-sensor (SHS), is an established tool to characterize optical properties of lenses by transmitted light. The SHS determines the local wave front gradient simultaneously at several

positions. It is possible to reconstruct the shape of the wave front by mathematical integration. Further optical quality functions (PSF, MTF) and criterions (Strehl value, Zernike coefficients) can be evaluated by knowing the shape of wave front [Are00].

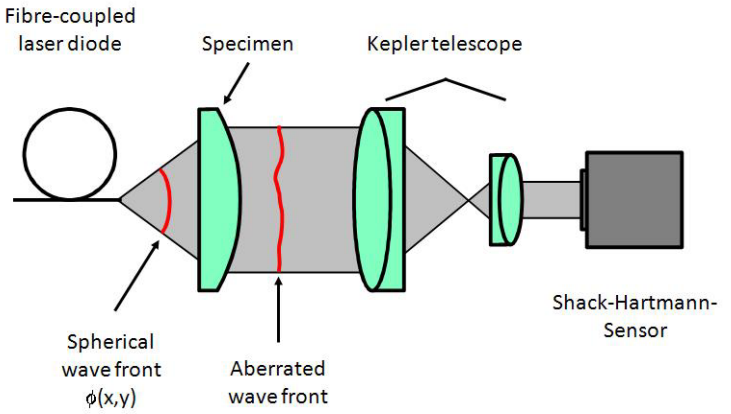


**Fig. 4** Set-up for Shack-Hartmann aberrometry

A SHS is based on a lens array and a CCD chip. The lens array subdivides the optical aperture into subapertures and images the analyzed light beam as focal points onto the CCD chip (Figure 5) [Are00].

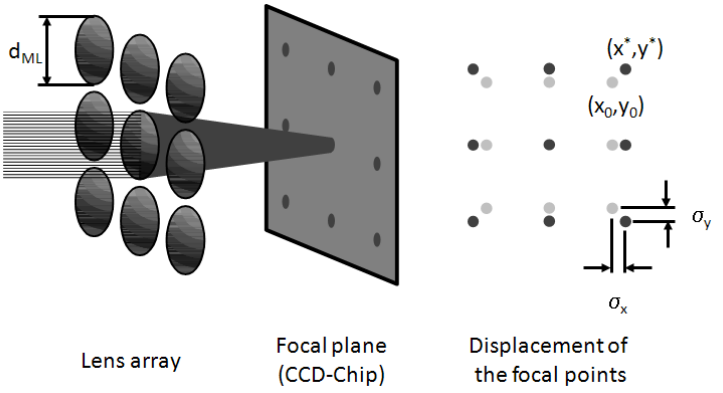


**Fig. 5** Principal of the Shack-Hartmann sensor

Physically the SHS is based on measuring the displacement of the focal points. From the displacement the local inclination of the wave front can be evaluated. The divergent light from a fibre-coupled laser diode (tested wave length $\lambda = 635$

nm) is collimated and imaged onto the SHS which determines the wave front aberration caused by the tested lens.

One determined quality function is the point spread function (PSF), which can be calculated from the wave front aberration. This function describes the luminous intensity distribution in the image plane of an ideal point which is imaged with a lens. With the PSF the Strehl value can be calculated, which is used as a quality criterion for optical lenses. The Strehl value is the ratio of the maximum luminous intensity in the image plane of a tested lens and the image of an ideal diffractively limited lens with the same aperture. The resolving capacity of an optical lens is characterized by the modulation transfer function (MTF). The MTF describes the contrast depending on the spatial frequency.

## 4 Comparison of the Replication Processes

The precision of the molded parts is crucial for a good functionality of the optical components. In order to achieve a distortion-free image, the geometry of the polymer lens has to meet the surface contour given by the optical design as good as possible. On the other hand the sharpness of the image is depending mainly on the surface roughness. While the surface roughness is mainly depending on the manufacturing of the cavity, the geometry of the injection molded part is determined by the molding process itself.

To analyze the inner properties of the plastics parts, a polarizing optical system can be used. The polarizing optics shows the birefringence of light passing through the part. The effect of double refraction results from the molecular orientation inside the part as well as from the state of internal stresses. Using polarized white light, the double refraction effect can be observed as a coloured pattern, with monochromatic light, the polarised image shows dark and bright areas. Figure 6 shows an exemplary monochromatic polarised image of an injection molded and an injection-compression molded polycarbonate lens. It is

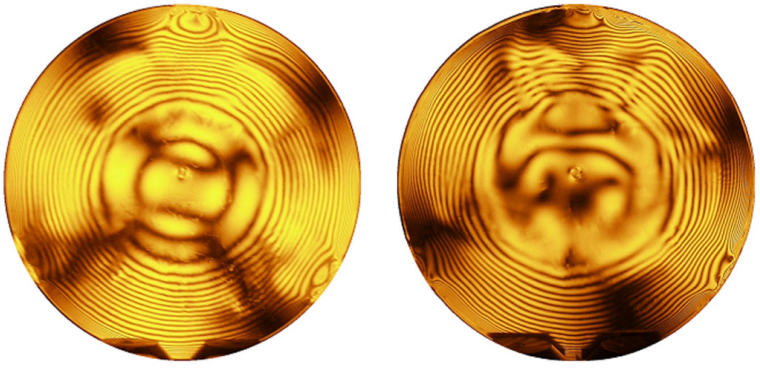

Injection molding Injection-compression molding

**Fig. 6** Birefringences in comparison for different injection molding techniques

obvious, that the manufacturing process has an influence on the inner properties of an optical part, so that the decision for a production method is always depending on the part geometry and the plastics material.

The difference between mold and lens surface is slightly reduced by changing from injection molding to the more complex injection-compression molding (Figure 7). For the function of a lens in an optical system the geometrical accuracy but particularly its optical effect is of importance. The optical effect results of the surface geometry and the internal properties of the lens. Contaminations of the polymer, molecular orientation or internal stresses can reduce the optical performance in spite of best geometrical accuracy.

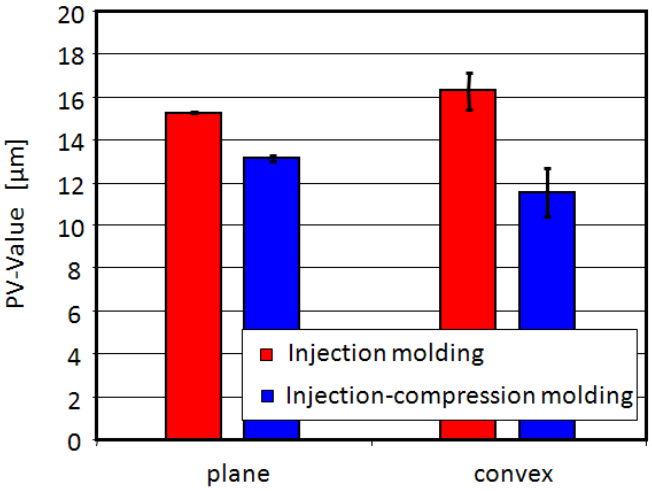


**Fig. 7** Geometrical accuracy of optical lenses

In which way the wave-front aberrometries effect the imaging performance can be seen in the PSF of both specimens, each molded using the best process parameters. In Figure 8 the PSF of the best injection molded and the best injection-compression molded lens are displayed.

It is evident that the intensity ten times higher in the centre results in a clearly better optical performance of the injection-compression molded lens. In the PSF of these lenses only two concentric secondary maximums with lower intensity are visible. The injection molded lenses has several secondary maxima. Its intensity is in the range of the maximum main intensity and deteriorates the contrast.

The results show that the injection-compression molding process is the appropriate process for the production of thick-walled optical components. By the combination of the injection molding and pressing process, a high molding accuracy with uniform inner properties can be obtained. Besides the process the used materials have a high influence on the resulting optical performance of the manufactured parts.

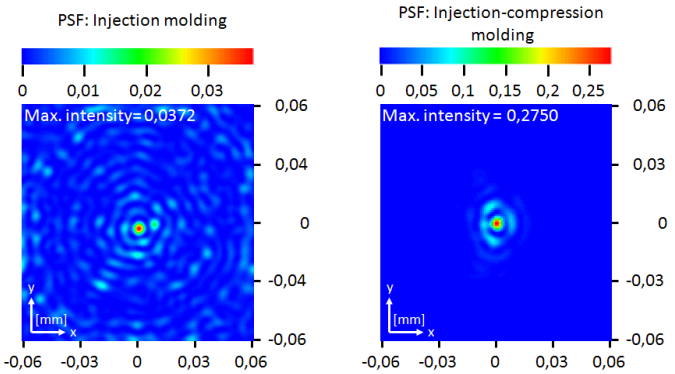


**Fig. 8** Measured point spread functions of injection molded and injection-compression molded lenses

## 5 Plastic Materials for Optical Components

For the replication of plastics components with optical functionality only amorphous thermoplastic polymers can be used. For the right choice of the material a specific list of requirements is needed for each individual application. Criteria can be for example the materials transmittance, the refraction index, the hardness, or heat resistance.

The used plastic material has a high influence on the parts characteristic and processing properties in the injection molding process. For the design of the optical components the optical and thermal properties of the material are important. Table 1 summarizes the most important physical characteristics of seven common materials used for replication of optical components [NN01a, NN01b, NN02, NN04a, NN04b, NN06a, NN06b, NN06c, NN06d, NN09a, NN09b, NN09c, Oen05, OM03, Zöl08].

### *5.1 Polymethylmethacrylat (PMMA)*

PMMA is a very often used acrylate polymer with a high transmittance of 92 % in the range of the visible light. The refraction index has the lowest value of the listed transparent polymers, a low optical refraction power is the result. The most important property for many applications is besides good optical properties a high hardness and with it a good scratch resistance. Because of an easy processability and a relatively low price, the polymer is widely used. PMMA has good flow characteristics and is processed in relative low temperature ranges (220 °C-260 °C). With 100 °C it has a low heat resistance [NN01a, NN04a].

### *5.2 Cycloolefin Copolymere (COC)*

In contrast to polyolefins, which are synthesized of one monomer unit, COC is typically synthesized out of two different units. TOPAS Advanced Polymers

**Table 1.** Properties and processing details of transparent plastics

| Property | PMMA | PC | COC | PA | PMMI | PCC | PES |
|---|---|---|---|---|---|---|---|
| MVR ISO 1133 [cm³/10 min] | 3 - 12 | 6- 12,5 | 4- 48 | 204 | 1,7 | 8 | 70 |
| temperature [°C] | 230 | 300 | 260 | 300 | 260 | 330 | 260 |
| load [kg] | 3,8 | 1,2 | 2,16 | 10 | 10 | 2,16 | 10 |
| Property | PMMA | PC | COC | PA | PMMI | PCC | PES |
| refraction index $n_d$ [-] | 1,49 | 1,587 | 1,533 | 1,51 | 1,53 | 1,566 | 1,65 |
| transmittance [%] | 92 | 88 | 91 | 90 | 91 | 89 | 80 |
| tensile modulus of elasticity [MPa] | 3200 | 2400 | 3000 | 1400 | 4000 | 2400 | 2700 |
| Charpy impact strength-notched (23 °C) [kJ/m²] | 20 | N/A | 13-15 | N/A | 20 | N/A | N/A |
| glass transition temperature (10°C/min) [°C] | 99 - 117 | 145 | 134 - 158 | 140 | 163 | 201 | 225 |
| heat resistance (0,45 MPa) [°C] | 95 - 103 | 136 | 130 - 150 | 135 | 158 | 191 | 218 |
| coefficient of thermal expansion [1/K] | 8·10-5 | 6,5·10-5 | 6·10-5 | 9·10-5 | 4,5·10 -5 | 7·10-5 | 5,2·10-5 |
| density [g/cm3] | 1,19 | 1,2 | 1,02 | 1,02 | 1,21 | 1,14 | 1,37 |
| moisture absorption (23 °C, 50 % rel. h.) [%] | 0,6 | 0,12 | <0,01 | 1,5 | 2,25 | 0,12 | 0,8 |
| heat conductivity of the melt [W/mK] | 0,181 | 0,173 | 0,193 | 0,25 | N/A | 0,165 | 0,18 |
| processing temperature [°C] | 220-260 | 280-310 | 240-310 | 280-300 | 260-290 | 330 | 340-390 |
| mold temperature [°C] | 60-90 | 80-130 | 95-145 | 60-80 | 130 | 100 | 120-170 |

GmbH, Frankfurt, uses therefore the monomers ethylene and norborene. In this combination the typical material properties of COC result.

Although cycloolefin copolymers are build only from olefinic monomer units, they are in contrast to the semi-crystalline polyolefins polyethylene (PE) and polypropylene (PP) amorphous and thereby transparent. Because of the olefinic monomer units the COC-melts have the typical polyolefinic properties like a good acid- and alkali-resistance. While processing COC, an oxidative degradation takes place, which leads to a yellowing of the product. This can be avoided by processing it with inert gas like nitrogen in the material feed. Concerning optical applications the COC-melts have low water absorption, a low density, a high heat resistance with a low double refraction and are therefore a good alternative to polycarbonate [NN06a, NN06b, NN06c, NN06d, Spa05].

## *5.3 Polycarbonate (PC)*

In comparison to PMMA and COC, polycarbonate has a higher impact resistance, so the material is used for applications where higher impact load or shock can

occur. Therefore it is used for example in safety glasses and visors and also for car glazing, where these loads can appear. PC is in contrary to PMMA a material with low flowability, which has to be injected with a high injection speed [NN02].

## 5.4 Polycarbonate Copolymere (PCC)

Using copolymerization, the properties of polycarbonate like heat resistance can be improved and combined with the convenient properties like impact resistance, transparency, light stability and flowability. The material can be used in applications with even higher requirements on the heat resistance than PC [NN09a].

## 5.5 Microcrystalline Polyamide (PA)

Transparent, microcrystalline polyamide 12 combines the optical properties of an amorphous with the mechanical properties of a semi-crystalline polymer. The crystallites are so small that visible light is not scattered so the material is transparent for human eyes. This combination of properties allows producing filigree optical frames as well as lenses for sport- and sunglasses. Furthermore frameless glasses can be produced because the necessary screw caps and bondings do not cause stress cracks. This combination of good optical and outstanding mechanical properties still has a high price [Oen05].

## 5.6 Polymethylmethacrylimide (PMMI)

PMMI are partially imidized methacrylat polymers. Because of the imidization the elastic modulus, the viscosity, the refraction index and the moisture absorption rise to higher values. The imidization takes place when PMMA reacts with methylamine in a dispersion or in melt in a reactor with methanol as a by-product. This leads to structures of imide rings at the branching of the PMMA-molecules, which stiffens the macromolecule. The degree of conversion can be controlled, so that a tailored molding compound will be obtained for each individual application [Buc90].

PMMI is a thermoplastic polymer with a high heat resistance (158 °C). Its very good optical properties remain stable within temperatures up to 150 °C. Therefore, the material can be used in applications with a high thermal load, for example headlight-lenses.

## 5.7 Polyethersulfone (PES)

PES is an amorphous high performance plastic, which has an amber transparency and belongs to the group of polysulphone (PSU). Polyethersulfone is in its chemical and impact resistance superior to polysulphone. PES has an unique heat resistance of 220 °C, so it can be used for applications in the pharmaceutical and food industry with a superheated steam sterilization. PES has a processing

temperature of 390 °C and with it very high requirements concerning the plastification [NN04b].

### *5.8 Liquid Silicone Rubber (LSR)*

Liquid silicone rubber has a high transparency up to 95 %, very low haze-values and a good physical stability. Therefore, the material is used for the production of LED-lenses for the automotive sector. With increasing distribution of so called high performance LED for the automotive sector the requirements concerning the used materials rise. Besides of the high degree of efficiency of these light sources the temperatures rise up to 150 °C together with a high share of ultra-violet radiation because of the compact design. The combination of high temperature with radiation leads to an accelerated aging while using the common optical thermoplastic polymers. LSR is an important alternative for these applications [NN08a].

## 6 Conclusion

Injection molding and injection-compression molding are the primary forming techniques which have a significant potential to produce optical parts in mass production. Especially in the area of imaging optics the geometrical accuracy and optical performance have to fulfil high requirements. Injection-compression molding features technological advantages in producing optical plastics components with uniform inner properties and optimal optical performance.

To achieve high precision optical parts excellent process knowledge is as important as the used material and mold. Therefore, it is necessary to examine the whole value creation chain for each individual application to obtain the required precision. To get the best results when producing plastics optics, they should not be introduced as an afterthought or as a replacement for glass, but just from the beginning for the total design. It is essential to bring the optical designer, the plastics processor and the production engineer together at the concept stage, to ensure that full use is made of the freedom of optical and mechanical design offered by plastics.

**Acknowledgement.** The authors like to thank the German Research Foundation (DFG) for funding this work as a part of the Transregional Collaborative Research Center SFB/TR4 “Process Chains for the Replication of Complex Optical Elements”.

## References

[Alb10] Albrecht, K.: Der Werkstoff PMMA vielseitig und langlebig. Tagungsumdruck Transparente Kunststoffe, SKZ, Würzburg, B1–B30 (2010)

[Are00] Ares, J., Mancebo, T., Bara, S.: Position and displacement sensing with Shack-Hartmann wave-front sensors. Applied Optics 39(10), 1511–1520 (2000)

[Ber00] Berthold, J.: Verarbeitung von duroplastischen Formmassen im Spritzprägeverfahren. RWTH Aachen, Dissertation (2000) ISBN 3-89653-449-1

[Bro98] Brockmann, C.: Spritzprägen technischer Thermoplastformteile. RWTH Aachen, Dissertation (1998) ISBN 3-89653-423-8

[Böl01] Bölinger, S.: Spritzgießen und Spritzprägen von Kunststoffoptiken. RWTH Aachen, Dissertation (2001) ISBN 3-89653-956-6

[Buc90] Buck, M.: Polymethylmethacrylate. Kunststoffe 80(10), 1134 (1990)

[Bür99] Bürkle, E., Wohlrab, W.: Spritzprägen - Präzisionstechnik für Spritzgußteile ohne Eigenspannungen. Kunststoffe 89(9), 64–69 (1999)

[Bür01] Bürkle, E., Klotz, B., Lichtinger, P.: Durchblick im Spritzguss. Das Herstellen hochtransparenter optischer Formteile - eine neue Herausforderung. Kunststoffe 91(11), 54–60 (2001)

[Fri90] Friedrichs, B., Friesenbichler, W., Gissing, K.: Spritzprägen dünnwandiger thermoplastischer Formteile. Kunststoffe 80(5), 583–587 (1990)

[Fri93] Friesenbichler, W., Ebster, M., Langecker, G.: Spritzprägewerkzeuge für dünnwandige Formteile richtig auslegen. Kunststoffe 83(6), 445–448 (1993)

[For06] Forster, J.: Vergleich der optischen Leistungsfähigkeit spritzgegossener und spritzgeprägter Kunststofflinsen. RWTH Aachen, Dissertation (2006) ISBN 3-86130-846-0

[Hab99] Haberstroh, E., Berthold, J., Jüntgen, T.: Spritzprägen mit prägnanten Vorteilen. Spritzprägen von Duroplasten - eine Alternative zum Spritzgießen. Kunststoffberater 44(10), 42–45 (1999)

[Hei00] Auf der Heide, K.: Innovative Spritzprägetechnik am Beispiel der CD-Herstellung. In: Heilbronner Kunststoff-Symposium, Heilbronn (2000)

[Joh04] Johannaber, F., Michaeli, W.: Handbuch Spritzgießen. Carl Hanser Verlag, München (2004)

[Kle87] Klepek, G.: Herstellung optischer Linsen im Spritzprägeverfahren. Kunststoffe 77(11), 1147–1151 (1987)

[Kna82] Knappe, W.: Zum optimalen Zyklusverlauf beim Spritzprägen. Leobener Kunststoff-Kolloquium über Spritzgießen und Spritzprägen, Leoben, Österreich (1982)

[Kna84] Knappe, W., Lampl, A.: Zum optimalen Zyklusverlauf beim Spritzprägen. Kunststoffe 74(2), 79–83 (1984)

[Kud99] Kudlik, N.: Dünnwandtechnik. Spritzgießverfahren für geringe Wanddicken. Kunststoffe 89(9), 92–96 (1999)

[Kun07] Kuntze, T.: Plastic Optics Enable LED Lighting Revolution. Optik & Photonik 2(4), 42–45 (2007)

[Lan03] Landt, A.: Kunststoffoptik: Von der Entwicklung bis zur Serienfertigung. Photonik 35(1) (2003)

[Mat85] Matsuda, S., Tamura, T.: Plastics Lens by Injection & Compression Molding. Japan Plastics Age 1(2), 31–34 (1985)

[May07] Mayer, R.: Precision Injection Moulding. Optik & Photonik 2(4), 46–48 (2007)

[Men68] Menges, G., Jürgens, W.: Spritzgießen und Spritzprägen, Vor- und Nachteile. Plastverarbeiter 19(11), 863–872 (1968)

[Mic98] Michaeli, W., Brockmann, C.: Innovative Werkzeugkonzepte für das Spritzprägeverfahren. Der Stahlformenbauer 15(3), 22–30 (1998)

[Mic00] Michaeli, W., Wielpütz, M.: Optimisation of the optical party quality of polymer glasses in the injection compression moulding process. Macromolecular Material Engenieering, 8–13 (2000)

[Mic05] Michaeli, W., Schröder, T.: Wirtschaftliche Bedeutung des Kunststoffs im Bereich optischer Anwendungen, Tagungsumdruck zum Seminar zur Kunststoffverarbeitung: Optische Bauteile aus Kunststoff, pp. 1–14. IKV, Aachen (2005)

[Mic07] Michaeli, W., Forster, J., Heßner, S., Klaiber, F.: Geometrical Accuracy and Optical Performance of Injection Moulded and Injection-compression Moulded Plastic Parts. Annals of the CIRP 56(1) (2007)

[NN01a] N.N.: Produktinformation Plexiglas Formmasse 6N, Plexiglas Formmasse 7N, Plexiglas Formmasse 8N. Darmstadt: Röhm GmbH & Co. KG (2001)

[NN01b] N.N.: Topas - Cyclic Olefin Copolymers, Optics Applications. Frankfurt a.M.: Ticona GmbH (2001)

[NN02] N.N. Anwendungstechnische Informationen (ATI 8013) Makrolon (PC). Leverkusen: Bayer AG, Geschäftsbereich Kunststoffe (2002)

[NN04a] N.N.: Lieferprogramm Formmassen. Darmstadt: Röhm GmbH & Co. KG (2004)

[NN04b] N.N. Produktinformation Ultrason® E 2010 natur, Ludwigshafen: BASF AG (2004)

[NN06a] N.N.: Processing Conditions for Injection Molding TOPAS® 5013S-04, Frankfurt, Topas Advanced Polymers GmbH (2006)

[NN06b] N.N.: Datenblatt TOPAS® 5013S-04, Frankfurt, Topas Advanced Polymers GmbH (2006)

[NN06c] N.N.: Processing Conditions for Injection Molding TOPAS® 6015S-04, Frankfurt, Topas Advanced Polymers GmbH (2006)

[NN06d] N.N.: Datenblatt TOPAS® 5013S-04, Frankfurt, Topas Advanced Polymers GmbH (2006)

[NN08a] N.N.: Optische Linsen aus LSR. K-Zeitung 39(21) (2008) (November 06, 2008)

[NN09a] N.N.: Datenblatt APEC 2097, Leverkusen, Bayer MaterialScience AG (2009)

[NN09b] N.N.: Produktinformation Pleximid® TT70, Darmstadt, Evonik Röhm GmbH (2009)

[NN09c] N.N.: TROGAMID® CX – Transparente Polyamide mit einer einzigartigen Kombination an Eigenschaften. Marl, Evonik Degussa GmbH (2009)

[Oen05] Oenbrink, G.: Innovative Problemlösungen mit transparenten Polyamiden. Tagungsumdruck Transparente Kunststoffe, SKZ, Würzburg, pp. D1–D17 (2005)

[OM03] Osswald, T.A., Menges, G.: Optical Properties of Polymers. In: Materials Science of Polymers for Engineers, pp. 545–569. Hanser Verlag, Munich

[Pas78] Pasco, I.K., Everest, J.H.: Plastics optics for opto-electronics. Optics & Laser Technology 10(2), 71–76 (1978)

[Spa05] Sparenberg, B.: Cycloolefin-Copolymere (COC). Kunststoffe 95(10), 156–160 (2005)

[Tra73] Trausch, G., Schleith, O.: Spezielle Spritzgießverfahren. Thermoplastschaumgießen - Spritzprägen. Kunststoffe 63(10), 659–662 (1973)

[Wal61] Wallner, J.: Spritz-Prägeverfahren für gleichmäßigen Schwundausgleich. Herstellung starkwandiger oder in der Wandstärke stark unterschiedlicher Spritzgußteile aus Polymethacrylat. Plastverarbeiter 12(6), 229–232 (1961)

[Zöl08] Zöllner, O., Protte, R., Döbler, M.: Machbarkeit bewiesen – LED-Linsen aus Polycarbonat. Plastverarbeiter 59(2), 36–38 (2008)

# Freeform Machining of Molds for Replication of Plastic Optics

Christian Brecher, Dominik Lindemann, Michael Merz,
Christian Wenzel, and Werner Preuß

**Abstract.** The success of plastic optics relies on the availability of molds needed for mass production. This chapter deals with the machining of molds with continuous surfaces exhibiting aspheric and free-form shapes, while the machining of molds with discontinuous surfaces (prisms, facets, Fresnel structures, etc.) will be discussed in Chapter 6. Molds may be classified according to size, shape, and tolerance requirements. As a mold material for replication of plastic optics, a nickel-phosphorous plated steel alloy is frequently chosen, which meets temperature and wear resistance requirements and can be machined with monocrystalline diamond tools. Basically, there are three methods for machining asymmetric shapes: raster milling, ball-end milling, and tool- or slide-servo turning. The discussion of this chapter includes material response to diamond machining, selection of machining parameters, programming and data handling, machining strategy, and achievable surface roughness and figure accuracy. Since the machining of molds is still the most cost-effective factor of the production chain, a reduction of set-up and machining times remains the biggest challenge for future research.

## 1 Introduction

Plastic lenses with aspheric surfaces have conquered a large market. They are found today in video projectors, pocket cameras, mobile phones, computer mice, scanners, LED illumination systems, fingerprint waveguide optics, head-up displays and many other optical devices [Bäu10]. The size of replicated plastic lenses ranges from approx. 1mm diameter (e.g. collimating lenses for DVD players) to approx. 200mm (e.g. head-up displays for automobiles), their shapes

Christian Brecher · Dominik Lindemann · Michael Merz · Christian Wenzel
Laboratory for Machine Tools and Production Engineering WZL, Steinbachstraße 19, 52074, RWTH Aachen, Germany

Werner Preuß
Laboratory for Precision Machining LFM, University of Bremen, Badgasteiner Straße 2, 28359 Bremen, Germany

E. Brinksmeier et al. (Eds.): Fabrication of Complex Optical Components, LNPE, pp. 41–52.
springerlink.com 

vary from mild aspheres (e.g. pocket camera lenses) to freeform surfaces with small local radii of curvature (e.g. f-theta-lenses). Often, datum surfaces defining the position and orientation of a lens in the optical system must be included in the opto-mechanical design. In some cases (e.g. fingerprint scanners) several optical surfaces with well-defined relative orientations are integrated into a single monolithic functional unit which is one of the innovative solutions offered by molded optics but might be a challenge for mold manufacturing.

Thermoplastic materials most commonly used for injection, injection-compression or variothermal molding of plastic lenses are polymethyl-metha crylate (PMMA), polycarbonate (PC), and cyclic olefin polymer or copolymer (COP, COC) with transition temperatures between 105°C (PMMA) and 145°C (PC). The optical mold inserts used for replication must resist process temperatures up to 180°C, i.e. the optical surfaces must not wear or oxidize and must maintain figure and roughness tolerances for thousands of molding cycles. Commonly, the optical surfaces are machined into a steel substrate, which must be ground and polished, or into a nickel-phosphorous layer plated onto a steel substrate, which can be diamond machined [Osm06a]. Although the deposition of a nickel-phosphorous layer introduces additional manufacturing steps (plating and, in case of galvanic deposition, a reworking of the contour), the advantages are obvious, since diamond machining allows the deterministic generation of aspherical surfaces with optical quality.

## 2 Fly-Cutting

The diamond machining process most frequently employed for the generation of freeform surfaces is single-edge circumferential milling, commonly referred to as fly-cutting [Bri02]. A fly-cutter usually consists of a steel disc holding a radius

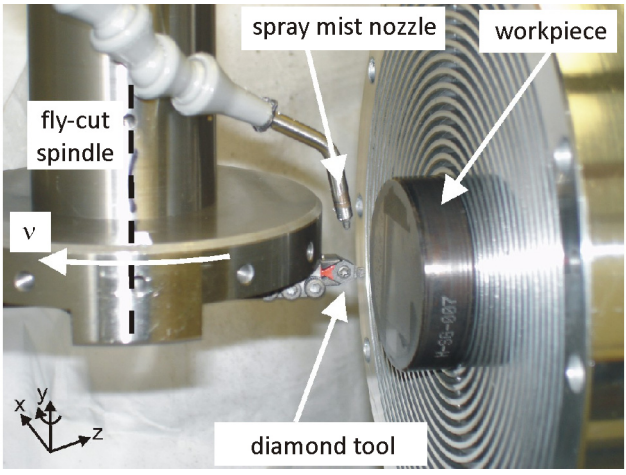


**Fig. 1** Fly-cutting of an electroless nickel plated mold on a Precitech Freeform 3000 ultra-precision machine

tool with nose radius $\rho$ rotating on a fly-cut radius $r$, defined as the distance from the spindle axis to the tip of the diamond tool. Thus, the effective envelope surface described by the rotating circular cutting edge is a toroid. Typically, $\rho$ is about 1mm, while $r$ is between 50mm and 70mm (cf. Figure 1). However, both radii must not exceed the smallest (concave) radius of curvature (along the relevant directions) on the surface to be machined. The spindle speed is usually kept below $4000\text{min}^{-1}$ for easier balancing and for avoiding centrifugal distortions.

There are two different kinematics applied in fly-cutting of freeform surfaces:

(a) In *raster milling* the fly-cutter is moved relative to the workpiece along (more or less) equally spaced raster lines.

(b) In *spiral milling* the fly-cutter is moved relative to the workpiece along a (more or less) equally spaced (Archimedean) spiral.

During machining, cutter normalcy conditions must be maintained (i.e. the toroidal envelope surface of the fly-cutter must always be tangential to the surface). If the contact point on the cutting edge is allowed to shift during machining, the orientation of the fly-cut plane may be kept constant with respect to the machine coordinate system, reducing the number of controllable linear axes to three. In raster milling, one of the three linear axes may be 'frozen' by moving the midpoint of the fly-cutter parallel to a major axis of the machine. (In that case, the raster lines will not be lines of intersection of a plane surfaces with the freeform surface). Likewise, in spiral milling, the number of linear axes may be reduced to two, if the spacing of contact points along the spiral is adjusted (by changing the rotational speed of the workpiece) such that cutter normalcy conditions are maintained.

Neglecting the local curvature of the freeform surface, the texture of a fly-cut surface can be described as a mosaic of tiny rectangular 'scallops' with length $l$, width $w$ and depth

$$R_{kin} = l^2 / (8r) = w^2 / (8\rho) \tag{1}$$

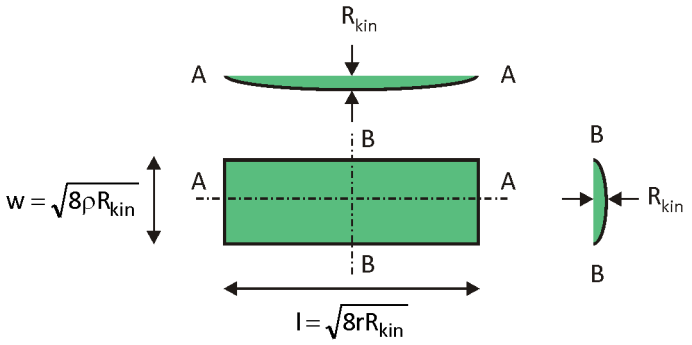


**Fig. 2** Length l, width w and kinematic roughness $R_{kin}$ of a rectangular surface element created in fly-cutting

Thus, the rate of surface generation $s$ in a fly-cutting process is determined by the area $l \cdot w$ of a 'scallop' (depending on the desired kinematic roughness $R_{kin}$, cf. Figure 2) and the rotational frequency $v$ of the spindle (i.e. the rate at which 'scallops' are generated):

$$s = lw \cdot v = 8vR_{kin}\sqrt{\rho r} \tag{2}$$

Typically, for a finish cut ($R_{kin}$ = 10nm, $v$ = 4000min$^{-1}$, $\rho \approx$ 1mm, $r \approx$ 65mm), $s \approx$ 2.5mm$^2$/min, i.e. fly-cutting of a freeform surface may last many hours imposing high demands on the stability of the process and on tool life. As is evident from (2), cutting time cannot be reduced significantly by increasing the tool nose radius or the fly-cut radius (for which there might be geometrical limitations), but only by increasing spindle speed. However, centrifugal forces are scaling with the square of the rotational frequency making balancing increasingly difficult. Hence, high speed diamond milling will only become available, if new balancing concepts and / or new milling tools with multiple cutting edges will be developed.

Unfortunately, there is no generally accepted format in the optics manufacturing community for defining a freeform surface. Sometimes an analytic expression is used (e.g. a polynomial or a modified sag equation), sometimes the surface is expanded in a Fourier or a Zernike series, sometimes a set of surface coordinates (called a 'data cloud') is generated by a ray-tracing program or through the numerical solution of differential or integral equations. However, the density of the grit on which coordinates are calculated must be fine enough so that coordinates and normal vectors (which are needed for cutter compensation and / or for figure evaluation with stylus instruments) at positions between the grit points can be interpolated with sufficient accuracy. In order to reduce the amount of data needed for defining the freeform surface, coordinates may be interpolated by spline functions with common first and second derivatives at the grit points. Within the SFB/TR4 the NURBS (Non-Uniform Rational B-Splines) [Pie97] concept has been implemented as a common description of freeform surfaces throughout the complete production chain from optical design to manufacturing and testing [Bre06a]. When converting a data cloud derived from an analytic expression or from numerical calculations into NURBS, care must be taken to avoid unphysical maxima and minima ('bumbs') between grit points by selecting an appropriate degree of B-splines and suitable knot vectors.

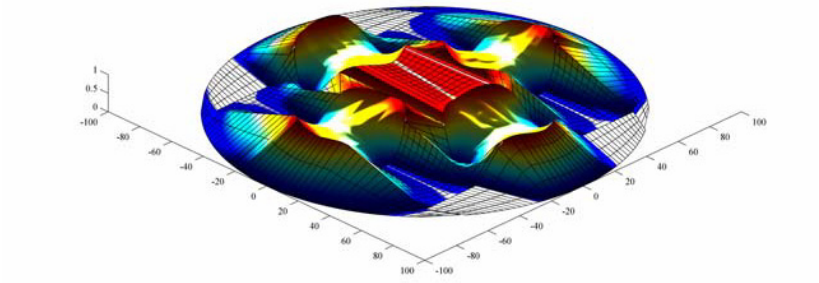

**Fig. 3** Tool path optimized set-point data for off-axis turning of a demonstrator part containing four freeform mirrors

Figure 3 shows the NURBS-based set-point data of four freeform mirrors, optimized with respect to the machining process. Integrated fill surfaces allow for a smooth and efficient tool path generation including critical infeed areas. A data format based on NURBS combines properties which quality its use for highly precise description of freeforms during design, for the calculation of complex tool trajectories, for the calculation of corrective re-machining steps, and for the handling in a machine control system [Osm08].

Usually, the mesh size of the control points used for programming the machine axes must be finer than the grit on which NURBS have been defined, since the numerical control of the machine is interpolating linearly between individual control points. For avoiding figure errors by linear interpolation, the maximum allowed distance $d_c$ between control points can be estimated from the smallest radius of curvature $r_c$ that occurs on the surface and the positional accuracy $\delta$ of the machine:

$$d_c = \sqrt{8\delta r_c} \tag{3}$$

With a positional accuracy of a state-of-the-art ultra-precision machine of $\delta$ = 5nm and a minimum radius of curvature $r_c > r \approx 65$mm, a maximum distance $d_c \approx 50\mu$m is obtained yielding a density of approx. 400 control points / mm$^2$. Since the rate of surface generation is about 2.5mm$^2$/min, about 1000 commands / min have to be processed by the numerical control when machining a freeform surface in optical quality.

Before machining can begin, the workpiece and the fly-cutter have to be aligned with respect to the coordinate frame of the machine. This can only be done, if

(a) there are datum surfaces on the workpiece which can be referenced to the machine coordinate system;

(b) the fly-cut radius, the tool nose radius, the position of the midpoint of the fly-cutter and the orientation of the spindle axis with respect to the machine coordinate system have been verified.

Datum surfaces are also needed when the machined surface is inspected; otherwise the part coordinate frame would be undefined. Likewise, datum surfaces or marks defining the part coordinate frame are needed on the molded optical element (for assembly in an optical system and / or for inspection). The necessity of incorporating datum surfaces into the design of freeform optical elements is obvious when the production chain is seen as a whole.

The figure accuracy obtained in freeform machining of molds mainly depends on the quality of alignment. The volumetric positional accuracy of modern ultra-precision machines is better than 0.5µm over 100mm of travel, provided care is taken to secure safe performance of the machining system. Surface finish, however, depends on many factors: quality of balancing, machining parameters, machining strategy, chatter, sharpness of the cutting edge, and response of the workpiece material to cutting. Due to the importance of surface roughness for the replication process and the quality of the final product, the hierarchy of these effects has been studied in detail within the SFB/TR4.

It has been found that the dominating factor is the quality of balancing of the fly-cut spindle [Bri07]. As can be seen in Figure 4, the selection of machining parameters has a minor influence on surface roughness compared to balancing. Thus, precision balancing of the fly-cut spindle is imperative.

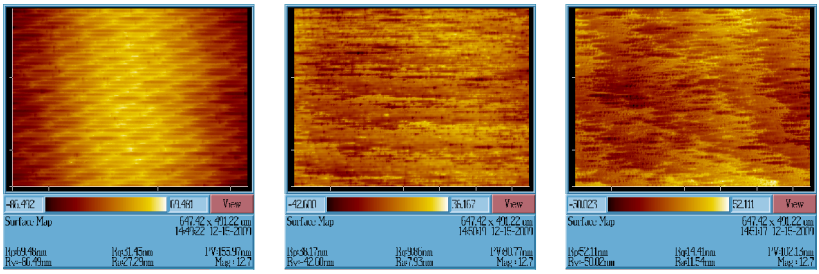

f = 102 µm (rough cut) f = 72 µm (pre-finish) f = 41 µm (finish cut)

| | |
|---|---|
| tool nose radius | ρ = 0.75mm |
| spindle speed | ν = 3000min$^{-1}$ |
| fly-cut radius | r = 66.5mm |
| cutting speed | v = 20.9m/s |
| feed / rev. | f = 102µm , 72µm , 41µm |
| up-milling mode | |

*white-light interferometric images*
*size of pictures: 491µm x 647µm*

**Fig. 4** Surface texture obtained in fly-cutting of electroless nickel with an unbalanced spindle at different feed rates

Once a balancing quality < 0.01gmm has been reached, surface roughness is determined by the kinematic roughness and the response of the material to cutting. This can be demonstrated when cutting an isolated raster line (cylindrical groove) into amorphous electroless nickel where surface roughness is not impaired by a grain structure. As can be seen in Figure 5, the kinematic milling cups are obscured by a number of marks caused by inhomogeneous chip flow within individual sweeps of the cutting edge whose number and amplitude decrease with decreasing feed per revolution, and hence with uncut chip thickness.

Generally, down-milling is recommended, but experiments have shown that in the case of electroless nickel, the milling mode does not affect surface roughness, since nickel-phosphorous alloys are comparatively hard metals. The next important factor influencing surface roughness is chatter which might be caused by high cutting forces compared to the machine's stiffness. Cutting forces also increase with increasing wear (rounding) of the cutting edge. Chatter and vibrations might also be introduced by sudden accelerations, e.g. at turning points or when the cutting direction is reversed. This risk must be considered when designing tool path and cutting strategy for a particular part. Figure 6 shows an example of a state-of-the-art raster fly-cut electroless nickel plated steel mold exhibiting a peak-to-valley contour accuracy of 0.3µm and a surface roughness Sa of 4nm.

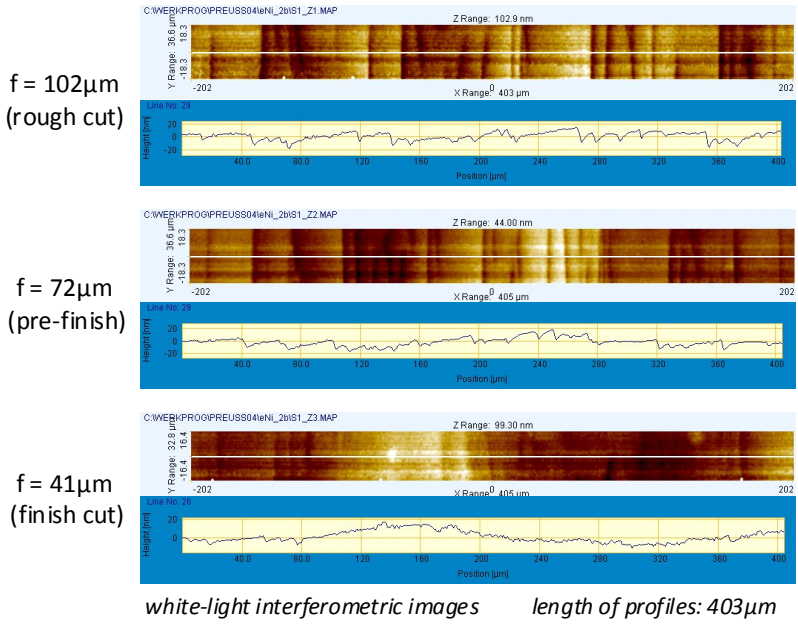


**Fig. 5** Surface texture of grooves obtained in fly-cutting of electroless nickel at different feed rates (machining parameters cf. Fig. 4)

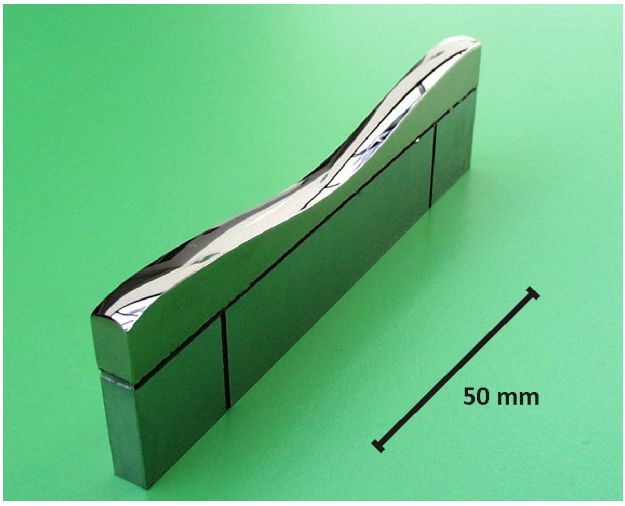


**Fig. 6** Electroless nickel plated mold for an f-theta lens

## 3 Ball-End Milling

Ball-end milling must be used, if the smallest radius of curvature of a convex part along the cutting direction is smaller than about 10mm and / or the shaft of the fly-cutter would collide with the part's contour during machining [Bri04a]. Typically, half arc diamond tools are used for ball-end milling, and the spindle axis is inclined by a certain angle with respect to the surface tangent to avoid cutting with the extreme edge of the half-arc tool (Figure 7) [Bri03]. The disadvantage of ball-end milling is the low rate of surface generation obtained from (2) by substituting r by ρ yielding

$$s = 8v\rho R_{kin} \tag{4}$$

which leads to machining times which are about 10 times longer than in fly-cutting. Moreover, cutting forces may increase, if the local radius of curvature approaches ρ, whereby increasing the risk of chatter [Osm06b].

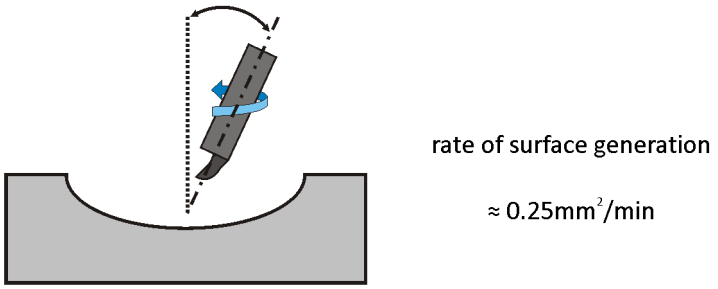


**Fig. 7** Ball-end milling. Spindle axis inclined with respect to the normal of the surface.

## 4 Non-circular Turning

An elegant way of reducing machining time for generating freeform surfaces is substituting fly-cutting or ball-end milling by non-circular turning [Osm07]. This can be accomplished in two ways:

(a) The tool movement is performed with two of the major axes of the machine. This is called 'slow slide servo' (SSS) turning.

(b) The tool movement is performed with two of the major axes of the machine and an additional fast moving axis, either a voice coil with a long (millimetre range) stroke or a piezo actuator with a short (micrometer range) stroke. This is called 'fast tool servo' (FTS) turning.

In both cases the tool movement must be synchronized with the angular position of the rotating workpiece. The rotational frequency ν is limited by the following error of the slides which must not exceed a maximum preset value when oscillating back and forth during machining. Typically, ν is of the order of 1Hz, which yields a rate of surface generation roughly 10 times lower than in circular

turning, but 10 times higher than in raster fly-cutting. Hence, about 1000 commands / s have to be processed by the numerical control in SSS or FTS turning of freeform surfaces [Bre04b]. Since in non-circular turning the slope of the surface with respect to the orientation of the diamond tool is not constant, care must be taken that sufficient clearance exists between the surface and the tool during machining.

Unfortunately, in commercially available FTS or SSS turning systems the direction of the stroke is predefined and usually set to be parallel to the axis of rotation (z-stroke) which imposes a limitation to the surface shapes machinable by non-circular turning. As shown in Figure 8, it is impossible to turn hemispherical

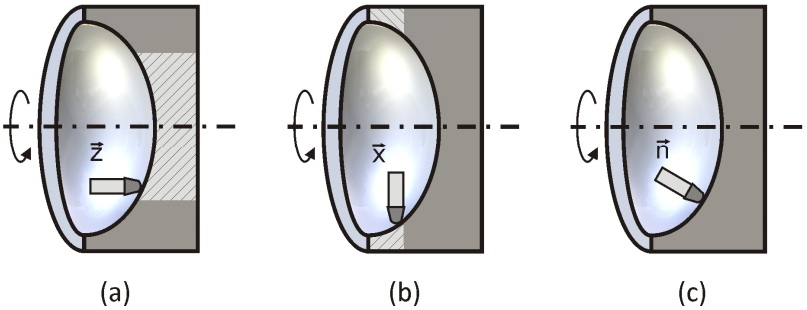


**Fig. 8** Slow slide servo turning modes. (a) Stroke along z-direction. Central area machinable only. (b) Stroke along x-direction. Apex area machinable only. (c) Stroke normal to surface. Full part machinable.

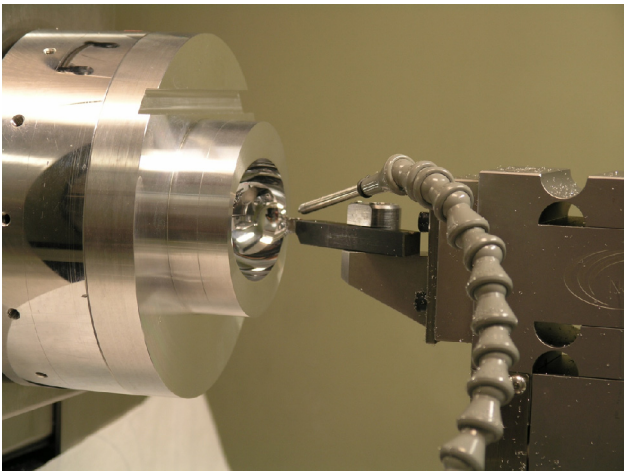

**Fig. 9** Slow slide servo turning of an elliptic half-shell (a = 35mm, b = 25mm)

cavities with a stoke along the z-direction, since the acceleration of the tool would become infinite when the apex of the contour is approached. On the other hand, if the stroke is perpendicular to the axis of rotation (x-stroke), the apex could be machined but the acceleration would become infinite at the center of the part. Within the SFB/TR4 an SSS turning technique with a variable stroke direction has been developed which is always normal to the surface (n-stroke). This SSS technique allows non-circular turning of 180° hemispherical cavities and cups like elliptic half-shells (Figure 9).

## 5 Control System Design for Highly Dynamic Axes

Standardized interfaces become more and more important for effective data processing through the different process steps for easy combination and replacement of algorithms and for providing the data integrity needed for complex machining processes [Bri04b]. Methods of data reduction and encapsulation have been used successfully for establishing interfaces which connect the initial optical design, CAM pre-processes, tool path generation, freeform machining, surface metrology, re-design as well as correction of machining processes. Maintaining a continuous high level of information, various functionalities, for instance points of intersection between rays and the surface, local derivatives or transformations, can be used to allocate the data needed in every step of the process chain. Furthermore, metadata such as type and unit of data, allocated coordinate system or transformation, date and method of compilation, sensor type and principle of measurement etc. become an important element to guaranty deterministic data processing. By using encapsulated data formats containing mathematical descriptions of the designed freeform, set-points for an optimized tool path, point clouds of surface measurements and the respective metadata, the high accuracy essential for manufacturing of ultra-precise optical components can be achieved.

Machine tools designed for ultra-precision machining such as diamond turning are often driven by a very robust servo control to achieve a good disturbance rejection. In contrary, the manufacturing of freeform surfaces requires much more dynamic movements, since no symmetrical elements exist. Hence, control systems have been developed providing fast tool axes with highly dynamic control loops and, at the same time, avoiding filters performing numerical differentiations which are prone to noises. Making use of a NURBS-based surface description, analytical methods of directional derivatives can be designed, allowing for low-noise, model-based feed-forward controls. Thereby, the maximal achievable bandwidth of highly dynamic axes can be enhanced significantly. Additionally, the dynamics of fast tool axes can be further increased by using an FPGA-based control system [Bre10]. The control loops strongly benefit from the achievable control clocks of up to 250 kHz as well as from a very low latency of the signals processed within an FPGA. Due to the possibility of parallelizing algorithms on an FPGA, a very effective design of critical control paths can be realized. Hence, a combination of both the main advantage of analog controls - latency can be reduced by a factor of ten - and the advantages of a digital control system can be implemented. Within the SFB/TR4 a hybrid control system, consisting of an FPGA-based low level part

for the control loops and a microprocessor-based high level part for set-point generation, was developed, enhancing the bandwidth of a piezo driven fast tool axis by a factor of three.

## 6 Conclusion

During the last ten years, three different methods for the generation of freeform surfaces by diamond machining have been developed and investigated in detail within the SFB/TR4, i.e. fly-cutting, ball-end milling and non-circular turning. Fly-cutting is most frequently used but is limited to convex surfaces and concave surfaces with radii of curvature larger than the fly-cut radius. If it is smaller, fly-cutting must be substituted by ball-end milling. Machining time can be reduced by non-circular turning, provided local slopes are moderate so that the surface will not interfere with the geometry of the diamond tool. The n-stroke slow slide servo turning technique, developed within the SFB/TR4, expands the range of surface shapes machinable by non-circular turning. Data handling requires a unique data format across the complete production chain from the design stage through machining to quality control. This has been realized in the SFB/TR4 by using a NURBS description for the freeform surfaces and standardized interfaces. Despite the high standard reached in freeform machining of molds for replication of plastic lenses, a reduction of machining time is an important issue for future research.

**Acknowledgement.** The authors like to thank the German Research Foundation (DFG) for funding this work as a part of the Transregional Collaborative Research Center SFB/TR4 “Process Chains for the Replication of Complex Optical Elements”.

## References

[Bäu10] Bäumer, S. (ed.): Handbook of Plastic Optics. Wiley-VCH Publ. Co. (2010)

[Bre06a] Brecher, C., Lange, S., Merz, M., Niehaus, F., Wenzel, C., Winter-schladen, M., Weck, M.: NURBS Based Ultra-Precision Free-Form Machining. In: Annals of the CIRP 55/1/2006, Kobe, Japan, August 20-26, pp. 547–550 (2006)

[Bre06b] Brecher, C., Lange, S., Merz, M., Niehaus, F., Winterschladen, M.: Off-Axis Machining of NURBS Freeform Surfaces by Fast Tool Servo Systems. In: Proceedings of the 4M 2006 Second International Conference on Multi-Material Micro Manufacture, Grenoble, France, September 20-22, pp. 59–62 (2006)

[Bre10] Brecher, C., Lindemann, D., Merz, M., Wenzel, C.: FPGA-Based Control System for Highly Dynamic Axes in Ultra-Precision Machining. In: Proceedings of the ASPE Spring Topical Meeting, Boston (2010)

[Bri02] Brinksmeier, E., Grimme, D., Preuß, W.: Generation of Freeform Surfaces by Diamond Machining. In: Proc. of the 17th Annual ASPE Meeting, St. Louis, Missouri, USA, October 20-25, pp. 542–545 (2002)

[Bri03] Brinksmeier, E., Gläbe, R., Autschbach, L.: Novel Ultraprecise Tool Alignment Setup for Contour Boring ad Ball-end Milling. In: Proc. of the ASPE s 18th Annual Meeting, Portland, Oregon, October 26-31, pp. 271–274 (2003)

[Bri04a] Brinksmeier, E., Autschbach, L.: Ball-end milling of Free-form Surfaces for Optical Mold Inserts. In: ASPE s 19th Annual Meeting, Orlando, FL, USA, October 24-29, pp. 88–91 (2004)

[Bri04b] Brinksmeier, E., Autschbach, L., Weck, M., Winterschladen, M.: Closed Loop Manufacturing of Optical Molds using an Integrated Simulation Interface. In: Proc. of Euspen International Conference, Glasgow, Scotland, May 30-June 03, pp. 215–217 (2004)

[Bri07] Brinksmeier, E., Gläbe, R., Krause, A.: Precision balancing in ultraprecision diamond machining. In: Laser Metrology and Machine Performance VIII, 8th International Conference and Exhibition on Laser Metrology, Machine Tool, CMM & Robotic Performance, Lamdamap, pp. 262–269 (2007)

[Osm06a] Osmer, J., Autschbach, L., Brinksmeier, E.: Study of different nickel platings in ultra precision diamond turning. In: Proc. of the 6th Euspen International Conference, Baden b. Wien, May 28-June 01, vol. II, pp. 44–47 (2006)

[Osm06b] Osmer, J., Brinksmeier, E., Lünemann, B.: Simulation of surface micro-topography in ultra precision ball-end milling. In: Proc. of the 6th Euspen International Conference, Baden b. Wien, vol. II, May 28-June 01, pp. 40–43 (2006)

[Osm07] Osmer, J., Weingärtner, S., Riemer, O., Brinksmeier, E., Fröhlich, M., Müller, W., Bliedtner, J., Bürger, W.: Diamond Machining of Free-Form Surfaces: A Comparison of Raster Milling and Slow Tool Servo Machining. In: Proceedings of the 7th International Conference and 9th Annual General Meeting of the European Society for Precision Engineering and Nanotechnology, Congress Centre Bremen, Germany, May 20-24, pp. 189–192 (2007)

[Osm08] Osmer, J., Riemer, O., Brinksmeier, E.: Ultra Precision Machining of Free-Form Surfaces and Tool Path Generation. In: Proceedings of the Euspen International Conference, Zürich, vol. 2, pp. 53–56 (May 2008)

[Pie97] Piegl, L., Tiller, W.: The NURBS Book. Springer Publ. Co. (1997)

# Mold Structuring by Diamond Machining

Lars Schönemann and Werner Preuß

**Abstract.** This chapter will discuss the state of the art and advances in the development of dedicated processes for mold structuring by diamond machining with defined cutting edge geometry. The advantages and disadvantages of the individual processes, e.g. the achievable geometry spectrum or the required machining time, will be discussed. Particular attention will be given to the Diamond Micro Chiseling (DMC) process which was developed within the SFB/TR4 for structuring molds with discontinuous prismatic microstructures. Utilizing a novel tool kinematics and custom built V-shaped diamond tools, this process enables the machining and replication of such structures in optical quality.

## 1 Introduction

The demand for the replication of complex optical elements has increased in the past decades. Besides molds with continuous surfaces, as they have been described in the previous chapter, mold structuring technologies have gained great importance for the generation of functional surfaces. They are delimited from continuous surfaces by featuring *"a deterministic pattern of usually high aspect ratio geometric features designed to give a specific function"* [Eva99].

The range of application for optical microstructures is manifold. Perhaps the most important application of structured molds today is the production of retro-reflective tapes used on sign-boards, safety garments, vehicles and many consumer articles [Bri05]. Other examples include optical patterns for the light distribution and homogenization in flat panel displays [Cor08], energy efficient headlights in the automotive industry [Neu07] or large-scale Fresnel lenses for astronomic applications [Ohm02]. Figure 1 shows some exemplary microstructures.

Although such structures can be obtained by various processes, diamond machining utilizing tools with defined geometry serves as a key technology [Rie08]. It offers a high degree of flexibility while allowing the generation of nanometer scale surface roughness and sub-micrometer form accuracy [Dav03]. Therefore, the only machining step within a typical process chain for the replication of optical elements is mold structuring by diamond machining. Additional finishing steps, such as polishing, are not required in this case.

Lars Schönemann · Werner Preuß
Laboratory for Precision Machining LFM, University of Bremen, Badgasteiner Straße 2, 28359 Bremen, Germany

E. Brinksmeier et al. (Eds.): Fabrication of Complex Optical Components, LNPE, pp. 53–66.
springerlink.com 

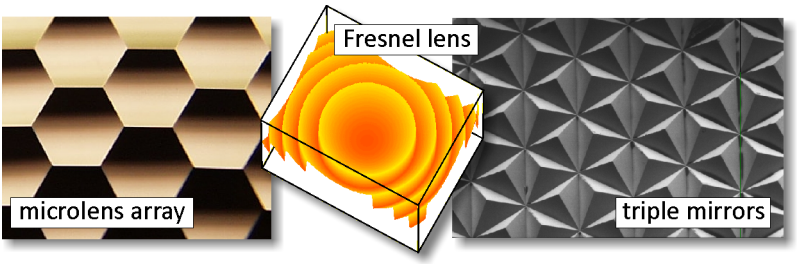


**Fig. 1** Exemplary microstructures generated by diamond machining

Due to its limited spectrum of machinable materials, diamond machining is mainly used for the replication of plastic optics. Optical structures with feature size down to the nanometer level can be replicated using injection or injection-compression molding. Here, it is important that the machined features are replicated without deformations resulting from clogging of the mold, demolding forces or solidification due to high temperature gradients within the mold [Mic08].

## 2 Machining Processes for Mold Structuring

The processes utilized for generating optical microstructures can be categorized according to their cutting motion. These include:

- processes with rotating workpiece, i.e. turning
- processes with rotating tool, i.e. milling
- processes with neither rotating tool nor workpiece, i.e. planing

Additionally, optical structures can be classified from the geometrical point of view according to Figure 2.

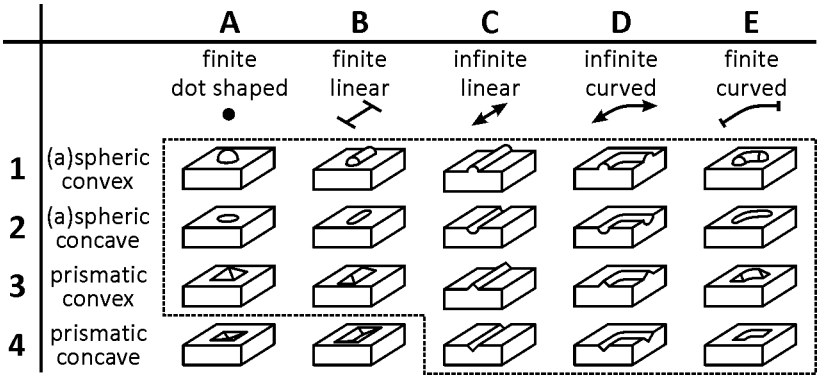


**Fig. 2** Geometric spectrum of machinable geometries

Most structure types can be machined in concave form by applying processes with rotary cutting motion, while their convex counterparts are obtained by replication processes. However, certain restrictions have to be considered with respect to the different processes: Milling processes are basically limited to linear features (grooves), diamond turning is used for generating Fresnel lenses, and micro lens arrays can be machined using contour boring or ball-end milling processes [Dor08]. In the recent past, the introduction of additional high-dynamic machining axes, like fast tool servos, has extended the geometric spectrum of turning processes to certain kinds of non-symmetric structures. Nevertheless, prismatic structures with sharp-edged facets (types A4 and B4), cannot be machined by these "conventional" processes. In this case, processes with dedicated kinematics are required.

In the following, the relevant machining processes for each category will be presented in detail.

## 2.1 Diamond Turning Processes

In turning processes, the main cutting motion is generated by the rotation of the workpiece, while the (fixed) tool is moved along the surface. The application and the possibilities of diamond turning for the generation of microstructures is shown in Figure 3.

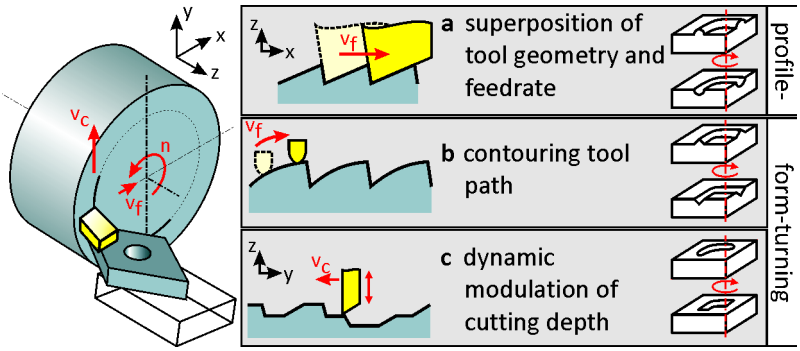


**Fig. 3** Machining of microstructures in a turning process

In a basic turning setup, microstructures can either be generated by applying a feed-rate which is significantly larger than the characteristic dimension of the tool or by modulating the depth of cut according to the radial position on the workpiece. This however, always results in rotational symmetric (or helical) types of structures (type D), such as Fresnel lenses or facetted structures. If finite curved features (type E) are to be machined in a turning process, the depth of cut has to be dynamically modulated using a Fast Tool Servo (FTS) or Slow Slide Servo ($S^3$). While the techniques are mainly intended for the generation of freeform surfaces, they can also be utilized to generate structured surfaces (cf. Figure 3c). Examples include the machining of lens arrays or diffractive gratings.

The achievable aspect ratios, however, are limited, as the slope of the modulated depth of cut has to be smaller than the clearance angle of the tool. Furthermore, the structural density of the microstructures is limited by the bandwidth of the servo system, which implies a decrease in machining speed. Another disadvantage of FTS/S³ turning is the asymmetry of the machined features, which can be explained by the relation between process parameters, bandwidth of the servo and resulting structure size at a specific radial position.

The number of structures *(s)* per revolution depends on spindle speed *(n)* and modulation frequency *(f)*:

$$s = \frac{f}{n} \tag{1}$$

The length of a structure $(l_i)$ can then be calculated by dividing the circumference at the current radial position $(r_i)$ by the number of structures *(s)*:

$$l_i = \frac{2 \cdot \pi \cdot r_i}{s} \tag{2}$$

For example, when machining a workpiece at a spindle speed of $n = 100\ min^{-1}$ utilizing an FTS with a maximal bandwidth of $f = 5\ kHz$, a possible amount of $s = 3000$ structures can be cut in circumferential direction. This means, the individual structures have a minimal size of $l_i = 31.41\ \mu m$ at the radius of $r_i = 15\ mm$. This size is constantly reduced upon moving the tool closer to the center of rotation ($l_i = 20.94\ \mu m$ at $r_i = 10\ mm$, $l_i = 10.47\ \mu m$ at $r_i = 5\ mm$ etc.) until a continuous cut is made and no discrete features are machined anymore.

When mounting the workpiece in an off-axis position, the curvature of the machined features can be reduced. This however, interferes with the use of FTS/S³ systems, as the machining speed (and thereby the required bandwith) is largely increased. In part, this effect can be avoided by applying a multi-pass cutting strategy: In the first cut, a specific amount of structures is omitted, thus reducing the required bandwidth. These structures are then cut in a second (or further) step of the process.

## 2.2 Diamond Milling Processes

In this category, the diamond tool is rotating on the main spindle and moved in relation to a fixed workpiece. According to the configuration of the machine setup, the processes can be sub-divided into peripheral- and face milling (see Figure 4).

In peripheral milling, the tool is rotating around an axis parallel to the machined surface. Thus, the geometry of the cutting tool is directly copied into the workpiece. According to the chosen tool geometry (radius, V-shaped, trapezoidal etc.), different kinds of groove-like structures (type C, cf. Figure 2) are generated this way. By intersecting multiple of these grooves, prismatic features (types A3 and B3), such as triple mirrors, can be realized. Besides the tool geometry, the swing radius of the tool has a large influence on the speed and geometric spectrum

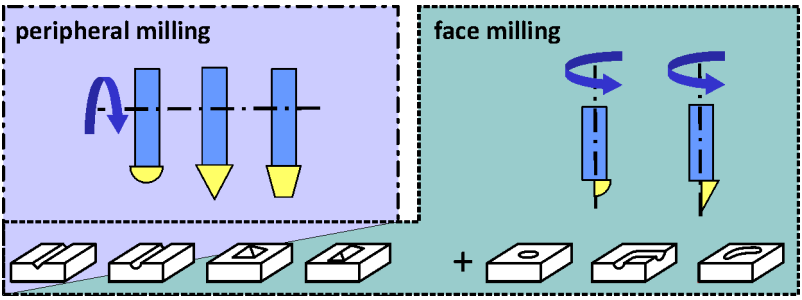


**Fig. 4** Classification of milling processes and possible geometric spectrum (cf. Figure 2)

of the peripheral milling operations. A large swing radius decreases the machining time, as larger feed rates can be applied for achieving an optical surface roughness. However, the minimal dimension of finite concave microstructures is limited, due to the necessary space for tool approach and retraction.

In face milling operations, the diamond tool is rotating around an axis perpendicular to the machined surface. By using half-arc or triangular tools, rotational symmetric cavities (type A2) and groove-like structures (types B2, C2, D2, C4 and D4) can be machined. Due to the primary cutting motion, the geometry of the grooves is limited to rotational symmetric profiles. Prismatic concave structures (A4 and B4) cannot be machined in this way. Compared to peripheral milling, the spectrum of machinable geometry is increased considerably on the one hand, but on the other hand the required machining time is extended as well.

## *2.3 Processes with Neither Rotating Tool Nor Workpiece (Intermittent Cuts)*

Standard milling or turning processes, as they have been described above, are somewhat limited in generating microstructures considering the required process times or the achievable geometric spectrum. To some extent, these limitations can be overcome by processes with non-rotating cutting motion. For example, planing processes can be used to machine large microstructured parts in adequate time [Day02]. On the other hand, the geometric spectrum can be extended using the microgrooving process developed by Takeuchi et al. [Tak09], which allows the generation of V-shaped grooves with flat-ends on one side.

However, the machining of prismatic features with sharp edges on all sides (A4 and B4 in Figure 2), such as pyramidal micro cavities, linear finite V-grooves or corner cube retroreflectors, is not possible with these processes. Thus, the Diamond Micro Chiseling (DMC) process has been developed to overcome these restrictions [Bri08]. It requires the use of an ultraprecision machine tool with at least five numerically controlled axes (see Figure 5): three linear axes (X, Y and Z) are used for positioning the tool relative to the surface of the workpiece and two rotational axes are needed for setting the opening angle of the structure and for rotating the workpiece to the required angular position.

The applied kinematics differs fundamentally from other known manufacturing processes: a V-shaped tool is moved on a triangular or trapezoidal path through the workpiece, forming a single facet with sharp edges. Multiple of these cuts, each with a different angular position of the workpiece, are connected by their start and endpoints in a way, that they form a pyramidal cavity. The number of facets is hereby only limited by the tools' opening angle. The final machining step has to have its endpoint in the starting point of the initial cut, or otherwise the chip cannot be removed.

The cutting steps for machining a three-sided cavity are illustrated in Figure 5.

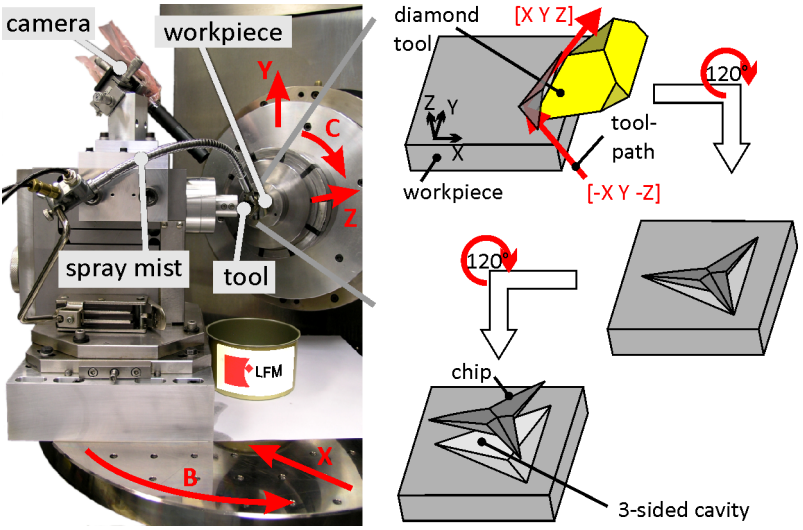


**Fig. 5** DMC machining setup and exemplary steps for generating a three-sided cavity

Such a cavity is typically cut in multiple layers with the aim of limiting the undeformed chip thickness. The cavity is thereby growing in its lateral dimensions, until the nominal geometry is reached. As there is no "feed" in the conventional sense, no kinematic roughness occurs. Thus, the surface quality of the facets is only depending on the workpiece material and the state of the tool during the last cut. Typically a roughness of Ra = 4-8 nm is reached.

Using the DMC process, it is possible to machine prismatic micro cavities with a characteristic dimension of 50 to 500 µm. The individual structures can be aligned systematically, in order to form new types of structures. In this way, it is possible to machine corner cube retroreflectors by overlapping several three-sided cavities in a hexagonal pattern.

## 3 Suitable Materials for Microstructured Molds

Just like for continuous surfaces, nickel phosphorous plated steel is the material of choice for microstructuring of molds in most cases. Its characteristics have been

described in the previous chapter. However, softer materials are preferred in some cases to obtain an extended tool life. While good results have been achieved using aluminum or oxygen-free high-conductivity copper as substrate materials, alloys such as nickel silver have been frequently used as mold material for microstructuring applications. It has been shown, that structures cut into specific nickel silver allows can almost reach [Sch10] or sometime exceed [Bri07] the surface quality of a comparable structures cut into a nickel phosphorous plating. Especially burr-formation is negligible when using nickel silver as workpiece material [Bri10a]. Figure 6 exemplary shows the measured surface roughness of different V-grooves machined by the DMC process in OFHC copper (Cu), nickel silver alloy (N37) and nickel phosphorous (NiP).

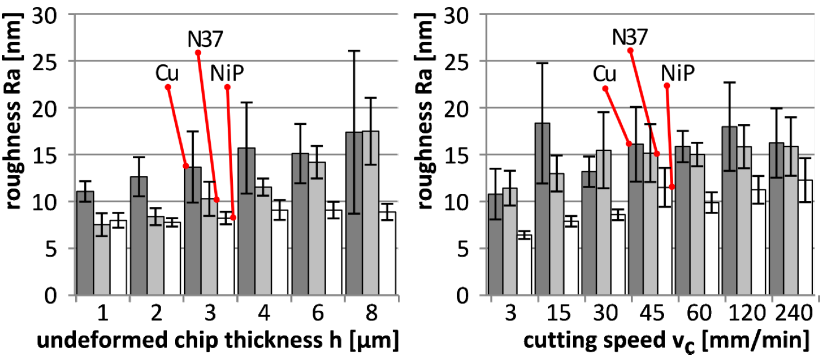


**Fig. 6** Surface roughness Ra against undeformed chip thickness (left) and cutting speed (right) for different workpiece materials machined by DMC [Bri10b]

To ensure sharp-edged machining paths, the cutting speed in DMC is chosen very low in comparison to conventional cutting processes. As in the DMC process the last layer of each facet is machined in a single cut, no kinematic roughness occurs. Thus, the surface quality is depending on the substrate material and the geometry of the cutting edge only. The best surface quality is achieved using NiP plating. However, the N37 alloy yields comparable results with selected parameters. N37 is a nickel silver alloy consisting of 62 % copper, 18 % nickel, 19 % zinc and 1 % lead and is mainly used for manufacturing hinges and joints in the eyewear industry. It has an elastic modulus of $E = 130\ kN/mm^2$ and a melting temperature of $T_S = 1050–1100°C$ (manufacturer's data). Thus, its mechanical properties are similar to those of OFHC-Cu $(E = 125\ kN/mm^2,\ T_S = 1083°C)$, which does not achieve an optical surface finish *(i.e. Ra > 10 nm)*, regardless of the chosen parameters. Compared to NiP, the induced tool wear is greatly reduced.

The machining of microstructures on hard coatings is possible as well. For example Sol-Gel films with a low hardness (<0.5 GPa) can be structured using tools with a small negative rake angle ($\gamma = -10°$). With an ideal set of parameters, a surface roughness of Ra = 5-15 nm can be achieved with almost no burr formation. In any case, the low thickness of the coating is the limiting factor for most microstructuring applications [Meh10]. Detailed information on hard coatings can be found in chapter 11.

The characteristics of the mold materials used for generating optical microstructures are summarized in Table 1.

**Table 1** Properties of mold materials used for microstructuring

| **material** | OFHC-copper | nickel phosphorous | nickel silver | Sol-Gel |
|---|---|---|---|---|
| **composition** | 99.9% Cu | 82-97% Ni, 3-18% P | 62% Cu, 18% Ni, 19% Zn, 1% Pb | $Si(Na_w)O_xC_yH_z$ |
| **Young's-modulus [kN/mm²]** | 110-128 | 120-190 | 130 | 3.8-6.6 |
| **melting temp. $T_s$ [°C]** | 1083 | 860-890 | 1050-1100 | >600 |
| **hardness** | 50-90 HB | 500-700 HV 0.1 | 170 HB | $H_{IT}$ = 1 GPa |
| **structurability** | + | +++ | ++ | ++ |
| **applicability as mold-material** | + | +++ | ++ | + |
| **tool wear** | +++ | + | ++ | + |

## 4 Diamond Tools for Microstructuring

In diamond machining, the tool geometry is directly copied into the surface. Therefore, mainly V-shaped, knife-type or facetted tools are used for microstructuring molds with grooves, blaze gratings or trapezoid structures. Half-arc radius tools are mainly used in contour boring or ball-end milling processes for generating microlens-arrays.

Although the specific requirements are varying, depending on the process kinematics and applied diamond tools, a precise tool alignment is crucial to all microstructuring processes. The errors in tool alignment can be divided into positional and angular errors and can have their source either in the tool or workpiece itself or are the result of a displacement of the tool coordinate system.

In contour boring processes used for the machining of microlens arrays, for example, a misalignment of the tool leads to the formation of artifacts at the bottom of the cavity, or to an ogive-like deviation of the lens' form (see Figure 7). Several attempts have been made in order to compensate the tool alignment in contour boring or ball-end milling, including mechanical [Bri03] and electrically driven [Sch09] tool holders.

Similar demands apply to fly-cutting with V-shaped diamond tools. For example, an angular misalignment of the tool directly leads to a form error of the machined V-grooves. Lateral misalignment of the tool, however, is only relevant if multiple intersecting grooves are generated to form pyramidal structures. If the individual grooves do not meet at the desired point, the optical functionality of the structure is affected.

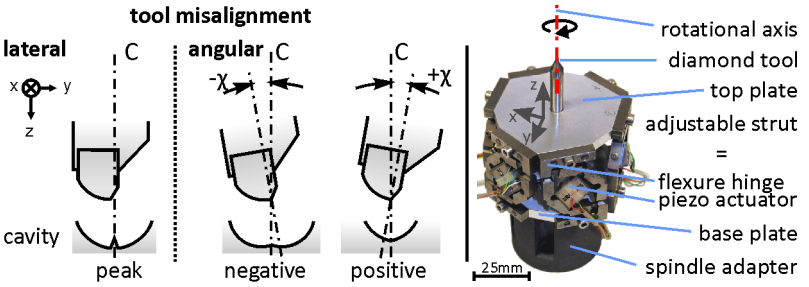


**Fig. 7** Types of tool misalignment in contour boring [Bri03] (left) and tool holder for in-situ tool alignment [Sch09] (right)

## *4.1 Dedicated Tool Design for Diamond Micro Chiseling*

Some processes, such as Diamond Micro Chiseling, require tools with a geometry dedicated to the requirements of the process (Figure 8). The notable difference to standard diamond tools is that the tool is rotated 90° around the shaft axis [Sch10], thus resulting in a switched alignment of rake and flank face.

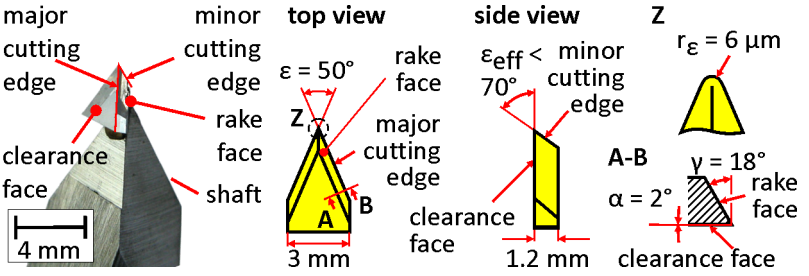


**Fig. 8** Diamond tools used for DMC of molds [Sch10]

The alignment of the diamond tools for Diamond Micro Chiseling is even more complex than the tool-setting for milling or turning processes. The DMC process requires a precise alignment of the diamond tool in all five machining axes in order to work as desired. Therefore, an iterative setup procedure utilizing a calibrated high-resolution video microscope is applied to measure dedicated test structures cut into the surface of the workpiece.

As an example, the vertical and lateral position of the tool tip according to the workpiece coordinate system is determined by cutting a square-type test structure with a defined edge length into the surface. This is done in a two-step process, beginning with the lower left part of the square. After cutting this part, the workpiece is rotated 180° and the tool tip is repositioned to the calculated position of the previously cut structure. In the next step, the remaining part of the square is cut at the calculated position. If a deviation between the calculated and the true

position of the tool occurs, this can be observed and measured from the deformation of the test structure.

Using this tool alignment procedure in combination with other test structures for determining the angular position, the tool tip can be positioned with an accuracy of below 1 µm in all linear axes and below 0.1° in the rotational axes.

## 5 Machining Time

Machining of small-area microstructures is challenging, yet feasible. However, when trying to increase the microstructured area or to decrease the characteristic dimension of the individual features, machining time becomes a critical issue [Flu09]. Depending on the scaled parameter, the effect can be linear (increase of structured area) or potential (decrease of characteristic dimension). Figure 9 shows the magnitude of the scaling effect. All values are estimated for comparable characteristic dimensions, respectively the same amount of structured area.

In the following, the scaling effect for increasing the structured area at a fixed characteristic dimension is examined for the different processes.

In this context, turning processes have the most favorable scaling behavior: the time is merely depending on the workpiece' radius and the applied feed and therefore shows a rather small inclination. When extending a turning process by a slow or fast tool servo system, the maximum applicable cutting speed is restricted by the bandwidth of the system, thereby slightly increasing the inclination.

In milling operations, the machining time is dependent on the length in feed direction and the pitch of the individual features. This has to be multiplied by the number of necessary machining directions (e.g. three, for machining triple-mirror features as shown in Figure 1). The result is an increased machining time for a

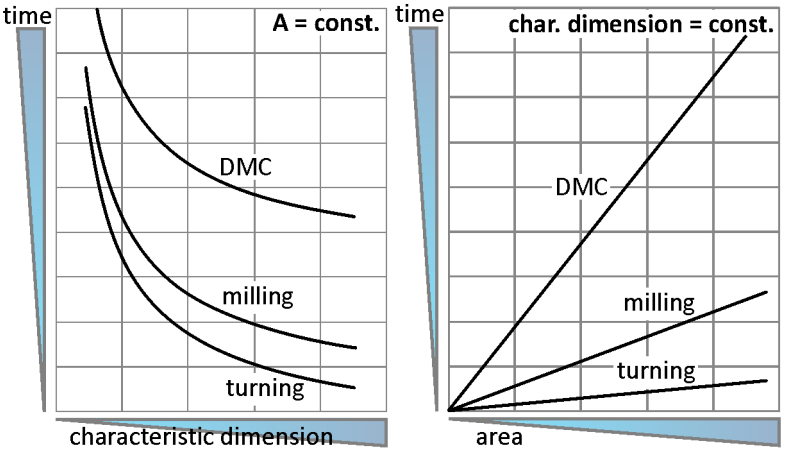


**Fig. 9** Scaling effect of machining time for constant structured area (A) (left) and constant characteristic dimension (right) [Flu09]

similar amount of structured area, compared to a turning process. However, the overall relation between structured area and machining time remains linear.

The calculation of machining time for Diamond Micro Chilseling is even more complex than for the other mentioned processes. As each facet is cut separately and in multiple layers, the machining time depends on a number of factors. Besides the high number of cuts for machining a single cavity, the machine axes have to be moved very slowly in order to achieve the desired sharp-edged corners without inducing vibrations or overshoot of the machining axes.

In typical applications, machining time ranges from a few minutes (turning), over several hours (milling) up to a couple of days (DMC). In this context, machine stability and environmental influences gain importance. In order to reduce these influences to a minimum, microstructuring processes have to be conducted in a controlled environment. This includes temperature-control, humidity-control and decoupled foundations for the machine tools. Nevertheless, innovative procedures for process monitoring and in-situ quality control have to be utilized to detect a critical state of the process at an early stage. As this occurs, dedicated compensation strategies (e.g. correction of tool alignment or change of worn out tools) have to be applied.

## 6 Tool Wear in Microstructuring

Besides the challenges of alignment, temperature and structural stability, tool wear is a critical issue, due to the extremely long machining times. When machining optical V-grooves by fly-cutting, for example, flank wear might degrade the roughness of the grooves' flanks, while wear of the diamond tool tip leads to a rounding of the edges of the prisms. The result is a decrease of brightness of light reflected by the machined structure.

A first attempt to determine tool wear as well as its effect on the machined surface has been made by conducting up- and down-milling experiments of V-shaped grooves on nickel phosphorous plating. For evaluating the surface quality, the flanks of the machined grooves were inspected with a white-light interferometer (cf. Figure 10).

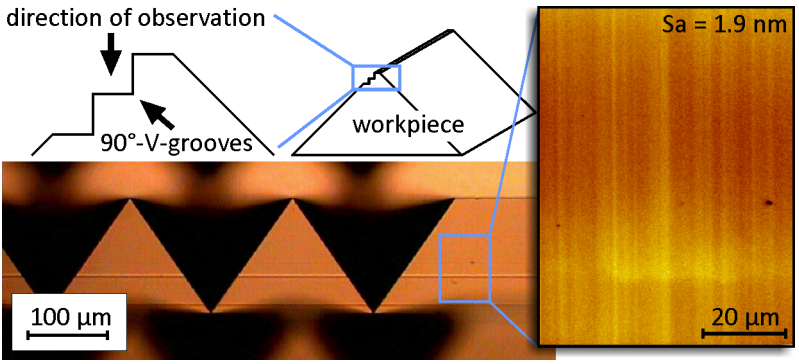


**Fig. 10** 90°-V-grooves cut into nickel phosphorous (left) and white-light interferometric image of one groove flank (right)

There is no significant difference in roughness whether the grooves are cut in the up-milling or down-milling mode. Thus, alternating up- und down-milling may be applied which reduces machining time by a factor of two.

The wear of the diamond tool has been investigated by fly-cutting 70°-V-grooves into a large NiP plate and inspecting the tool after regular intervals (cf. Figure 11). After a total groove length of 400 m (corresponding to a cutting time of 60 hours), a rounding of the tip of the diamond tool of about 2 µm has been observed. Although this observation is based on one single experiment, it may be taken as a guideline to how long a typical V-shaped diamond tool may be engaged, before tool wear starts to degrade geometry and roughness of the grooves.

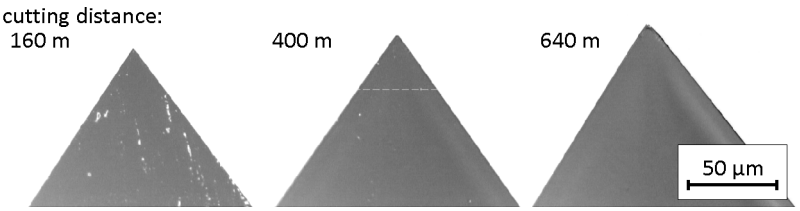


**Fig. 11** Flank faces of diamond tools after cutting distances of 160 m (left), 400 m (center) and 640 m (right)

Machining of structures which exceed the tool life criterion require a tool-change within the process. It has to be ensured, that the second tool can be aligned with a high level of precision with respect to the structure machined by the first tool.

## 7 Conclusion

Diamond machining offers a broad spectrum of processes for fabricating optical structures with varying complexity and characteristic dimensions in the sub-millimeter and down to the nanometer level. The inherent advantage of these processes is the high flexibility while achieving a low surface roughness as well as excellent form accuracy. On the other hand, the choice of workpiece material is limited compared to the machining of freeform surfaces.

Depending on the type of structure, each process has its specific advantages and disadvantages: diamond turning always results in curved structures, but offers a very high machining speed, even on large areas. FTS and $S^3$ are extending the capabilities of turning processes significantly. Milling processes are capable of machining linear features, but require an increased amount of time for comparable structured areas. Other processes, like Diamond Micro Chiseling pose high demands on the required equipment and require extremely long machining times, but allow generating novel types of geometries and therefore open up completely new areas in optical microstructuring.

**Acknowledgement.** The authors like to thank the German Research Foundation (DFG) for funding this work as a part of the Transregional Collaborative Research Center SFB/TR4 "Process Chains for the Replication of Complex Optical Elements".

## References

[Bri03] Brinksmeier, E., Gläbe, R., Autschbach, L.: Novel ultraprecise tool alignment setup for contour boring and ball-end milling. In: Proc. of the ASPE Annual Meeting, Portland, Oregon, October 26-31, pp. 271–274 (2003)

[Bri05] Brinksmeier, E., Autschbach, L., Gubela, H.-E., Ahbe, T.: Herstellung dreidimensionaler mikrooptischer Funktionsflächen. HTM 60(1), 33–39 (2005) (in German)

[Bri07] Brinksmeier, E., Gläbe, R., Lünemann, B.: Diamond machining of diffractive optical patterns by using a nanometer-stroke Fast Tool Servo. In: Proc. of the VII LAMDAMAP Conference, Cardiff, Wales, June 25-28, pp. 232–241 (2007)

[Bri08] Brinksmeier, E., Gläbe, R., Flucke, C.: Manufacturing of molds for replication of micro cube corner retroreflectors. Production Engineering - Research & Development 2(1), 33–38 (2008)

[Bri10a] Brinksmeier, E., Riemer, O., Gläbe, R., et al.: Submicron functional surfaces generated by diamond machining. CIRP Annals – Man. Tech. 59, 535–538 (2010)

[Bri10b] Brinksmeier, E., Schönemann, L., Gläbe, R.: Review on Diamond-Machining Processes for the Generation of Functional Surface Structures. In: Proc. of 4th HPC Conference, Gifu, Japan, October 24-25, pp. 79–84 (2010)

[Cor08] Cornelissen, H.: Polarized-light backlights for liquid-crystal displays. SPIE Newsroom (November 12, 2008), http://dx.doi.org/10.1117/2.1200811.1363 (viewed online October 01, 2010)

[Dav03] Davies, M.A., Evans, C.J., Patterson, R.S., Vohra, V., Bergner, B.C.: Application of precision diamond machining to the manufacture of micro-photonics components. In: Proc. of SPIE, vol. 5183, pp. 94–108 (2003)

[Day02] Day, M., Weck, M.: Ultraprecsion Milling and Planing Machine for large Workpieces. In: Proc. of the 3rd Euspen Conference, Eindhoven, Netherlands, May 26-30, vol. 1, pp. 345–348 (2002)

[Dor08] Dornfeld, D., Lee, D.E.: Precision Manufacturing, Springer Science+ Business Media (2008) ISBN 978 0 387 32467 8

[Eva99] Evans, C.J., Bryan, J.B.: "Structured", "Textured" or "Engineered" Surfaces. CIRP Annals – Man. Tech. 48, 541–556 (1999)

[Flu09] Flucke, C., Schönemann, L., Brinksmeier, E., et al.: Scaling in Machining of Optics from Reflective to Diffractive Function. In: Proc. of the 9th Euspen Conference, San Sebastian, Spain, vol. 1, pp. 17–20 (June 2009)

[Meh10] Mehner, A., Dong, J., Hoja, T., Prenzel, T., Mutlugunes, Y., Brinksmeier, E., Lucca, D.A., Klaiber, F.: Diamond Machinable Sol-Gel Silica Based Hybrid Coatings for High Precision Optical Molds. Key Engineering Materials 438, 65–72 (2010)

[Mic08] Michaeli, W., Klaiber, F., Scholz, S.: Investigations in Variothermal Injection Moulding of Microstructures and Microstructured Surfaces. In: Proceedings of the 4M2008 Conference (2008), http://www.4m-net.org/files/papers/4M2008/06-12/06-12.PDF (viewed online November 19, 2010)

[Neu07] Neumann, C.: Innovative Optical Systems for Automotive Signal Lamps. Presentation at the iMOC 2007, Bremen, Germany (May 24, 2007)

[Ohm02] Ohmori, H., Uehara, Y., Ueno, Y., Suzuki, T., Morita, S.: Ultraprecision Fabrication Process of Large Double-sided Spherical Fresnel Lens. In: Proc. of the 3rd Euspen Conference, Eindhoven, Netherlands, May 26-30, vol. 1, pp. 365–368 (2002)

[Rie08] Riemer, O.: A Review on Machining of Micro-Structured Optical Molds. Key Engineering Materials 364-366, 13–18 (2008)

[Sch09] Schönemann, L., Brinksmeier, E., Osmer, J.: A piezo-driven adaptive tool holder for ultraprecision diamond tool alignment. In: Proc. of the 9th Euspen Conference, San Sebastian, Spain, vol. 1, pp. 398–401 (June 2009)

[Sch10] Schönemann, L., Brinksmeier, E., Flucke, C., Gläbe, R.: Tool Development for Diamond Micro Chiseling. In: Proc. of the 10th Euspen Conference, Delft, Netherlands, May 31-June 04, vol. 2, pp. 86–90 (2010)

[Tak09] Takeuchi, Y., Yoneyama, Y., Ishida, T., Kawai, T.: 6-Axis control ultraprecision microgrooving on sculptured surfaces with non-rotational cutting tool. CIRP Annals - Manufacturing Technology 58-1, 53–56 (2009)

# Diamond Machinable Tool Steels by Novel Nitriding Processes

Ekkard Brinksmeier, Franz Hoffmann, Ralf Gläbe, Juan Dong, and Jens Osmer

**Abstract.** The ultraprecision machining of steel alloys with optical surface finish could not be achieved in the past as catastrophic wear of the mono-crystal diamond tool occurs inevitably. A recently developed solution of this problem is a thermo-chemical treatment of the steel e.g. by custom nitriding or nitrocarburizing. This process leads to a compound layer at the steel surface, in which the iron atoms are bonded to nitride or carbon nitride, a layer which is diamond machinable without significant tool wear. This chapter covers all facts about the thermo-chemical treatment and the subsequent diamond cutting process: different nitriding and nitrocarburizing processes to produce a dense thick compound layer on steel are described. Results from the diamond machining of these layers show that an optical surface quality is achievable and the chemical tool wear can be suppressed. Furthermore, differences between the machining of non-ferrous metals and thermo-chemically treated steel alloys are discussed. Finally, examples for the replication of glass and plastic optics with moulding inserts made of thermo-chemically treated steel are given. Therefore, this chapter gives an overview over the whole process chain for the replication of complex optical parts with nitrided or nitrocarburized steel moulds.

## 1 Introduction

The ultraprecision machining of non-ferrous metals with single crystal diamond tools is state-of-the-art in optics manufacturing. Whereas an optical surface finish machining of steel alloys cannot be achieved as catastrophic wear of the single crystal diamond tool occurs. This is a severe disadvantage. Especially for the manufacture of complex glass or plastic lenses, as for the replication of these optical components moulding inserts made of steel alloys or ceramics have to be applied. So far these moulds are machined with various iterative process steps like

Ekkard Brinksmeier · Ralf Gläbe · Jens Osmer
Laboratory for Precision Machining LFM, University of Bremen, Badgasteiner Straße 2, 28359 Bremen, Germany

Franz Hoffmann · Juan Dong
Institute for Materials Science IWT, Badgasteiner Straße 3, 28359, Bremen, Germany

E. Brinksmeier et al. (Eds.): Fabrication of Complex Optical Components, LNPE, pp. 67–83.
springerlink.com 

grinding, polishing and measuring (cf. Fig. 1). A manufacturing procedure requiring only one single diamond machining process would reduce both machining time and cost.

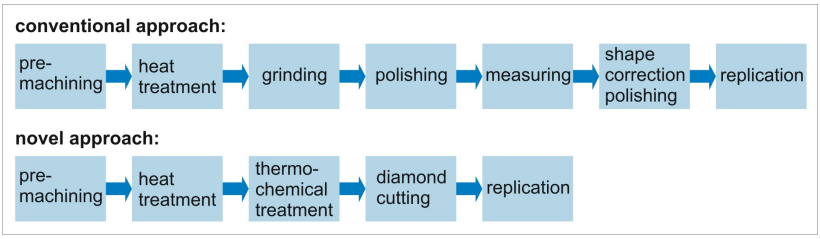


**Fig. 1** Novel approach for optical mould making applying diamond cutting for substituting the conventional approach

Even though the diamond tool wear mechanisms in ultra precision cutting of ferrous metal alloys are not fully understood it is clear that the wear is of chemical-abrasive nature. This is similar to thermo-chemical polishing of diamond with a steel disc [Che07]. Where iron catalysis a $sp^2$-hybridisation of the carbon bonding at the surface of the diamond. This leads to a phase transition of the upper layers of the diamond lattice and the carbon atoms oxidise to CO and $CO_2$ even at room temperature. Another possible removal mechanism is the diffusion of carbon atoms into the steel substrate.

Since the wear mechanism has a chemical component many attempts to reduce the wear rate have been carried out for example by cooling the workpiece [Eva91], machining under carbon saturated atmospheres [Cas83], modifying or coating of the diamond cutting tool [Glä03] or by reducing contact time between workpiece and cutting tool in an ultrasonic assisted turning process [Mor99]. In recent developments the frequency of ultrasonic systems for diamond turning has been increased to 80 kHz, which reduces both contact time between workpiece and cutting tool and the tool wear. With these systems optical surface quality and excellent form accuracy can be achieved [Klo10]. Still one remaining disadvantage of ultrasonic assisted diamond turning is the comparably long machining time, which makes it only applicable for small optical components.

In the research work of the SFB/TR4 a different approach has been undertaken based on a thermo-chemical treatment of the surface layer of the steel. The approach is motivated by the fact that thermo-chemical tool wear is not only a phenomenon in diamond machining of steel alloys, but also in machining of nickel based alloys. In this case the catalytic behaviour of the nickel can be reduced by alloying 10-12 percent phosphorus [Pau96]. Since the electron configuration of nickel (3 un-paired d-shell electrons) and iron (4 un-paired d-shell electrons) are comparable, the same effect can be used for steel alloys by adding nitrogen to the surface boundary layer by gas nitriding or gas nitrocarburising [DON03]. This thermo-chemical treatment leads to a compound layer where the iron atoms are bonded to nitrides or carbon nitrides minimising the catalytic activity of the iron and enabling diamond machining without significant tool wear [Bri06].

## 2 Nitriding and Nitrocarburizing

Nitriding and nitrocarburizing are thermo-chemical surface treatments performed at elevated temperature in a medium with nitrogen- and/or carbon-bearing species. Thereby nitrogen or nitrogen and carbon are diffused into steel surface, leading to formation of a compound layer, consisting of ε-$Fe_{2-3}$(N,C) and/or γ'-$Fe_4$(N,C), and below this a diffusion zone. The compound layer has therefore a distinguished chemical composition, electron configuration, crystal structure and properties in comparison with the steel substrate. A typical compound layer is shown in Figure 2.

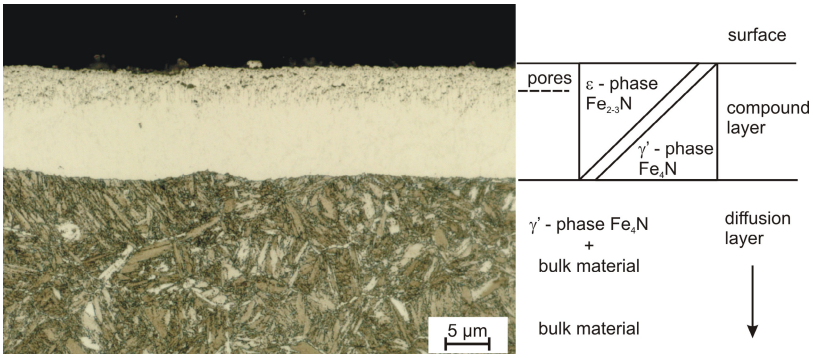


**Fig. 2** Cross section and dominant phases after nitriding a hardened steel (42CrMo4)

Machinability of the nitrided steel compound layer has been proven by diamond machining experiments showing that the diamond tool wear has been largely reduced by at least a factor of 300 [Don03, Bri04]. The success of these experiments leads to the encouraging aspect that the thermo-chemical treatment can enable steel to become diamond machinable. This application, however, demands a thicker and denser compound layer with better machinability and enhanced mechanical properties, and therefore the thermo-chemical treatment needs further development.

The generation of thick compound layers in nitrocarburizing processes can generally be realized by increasing temperature, duration and nitriding potential. But the growth of the compound layer is accompanied by formation of pores leading to a reduction of density, hardness, strength and toughness of the compound layer. Furthermore, the porosity increases with increasing layer thickness [Hof91]. The decomposition of nitrides and the recombination of atomic to molecular nitrogen are regarded as a possible reason for the pore formation [Pre73, Som92, Hof96]. Till now, the knowledge about creating a thick compound layer with low porosity is still insufficient. Therefore, experimental investigations were conducted in the present work. The investigations concerned the influence of essential process parameters on the porosity of the compound layer. These parameters included process temperature, duration, nitriding potential $K_N$,

carburizing potential $K_C^B$ as well as the carbon bearing species used for nitrocarburizing. The important results were selected and presented in the following.

# 3 Process Condition

## *3.1 Equipment*

Low nitriding potential was recognized to be beneficial for the suppression of pore formation on low alloy steels [Pre73, Sly89], while hydrogen with a high partial pressure could favor the pore formation [Gra68, Sch02, Vog02]. This was examined by the present experiments. Two measures were taken to realize a low nitriding potential and a low hydrogen partial pressure. The first was a dilution of the process atmosphere by adding nitrogen and the second was a suppression of

volume: 400 liter
dimension: Ø 600 x 700 mm
max. load weight: 200 kg
$T_{max}$ = 830°C
circulation
retort: steel X15CrNiSi25-21 (1.4841)
sensors: oxygen sensor
$H_2$-sensor
$NH_3$ analyzer,
control: nitriding potential
$K_N = p(NH_3)/p(H_2)^{1/2}$ $bar^{1/2}$
carburizing potential
$K_C^B = p(CO)^2/p(CO_2)$ bar
oxidation potential
$K_O = p(H_2O)/p(H_2)$

**Fig. 3** Retort furnace for thermo-chemical treatment

volume: 5.5 Liter,
dimension: Ø10 × 70 cm
load weight: small work pieces
max. Temp.: ca. 650°C
mass flow controller: $N_2$, $NH_3$, $O_2$, $CO_2$
sensors: $O_2$-sensor,
$H_2$-sensor
no regulation of $K_N$
feature: quartz glass tube (inert)

**Fig. 4** Furnace with quartz glass reactor for thermo-chemical treatment

ammonia decomposition by avoiding unwanted catalytic surfaces. The later can for example be influenced by the steel retort of the nitriding furnace. Therefore, two equipments were introduced in this experimental work. These are a retort furnace and a quartz glass reactor as shown in figure 3 and 4.

## *3.2 Nitriding in a Mixture of Ammonia and Nitrogen*

The first nitriding process (process 1.1N) was carried out in the retort furnace for 6 h at 590 °C with a gas mixture of $NH_3/N_2$ = 5/5 and the nitriding potential $K_N$ = 0.6. The second nitriding process (process 2.1N) was carried out in the quartz reactor for 6 h at 615 °C with a gas mixture of $NH_3/N_2$ = 3/7 and the nitriding potential $K_N$ = 2.0. The hydrogen partial pressures were determined to be about 0.37 and 0.18 bar respectively.

The metallographic microstructures of the steel 42CrMo4 after the two process 1.1N and 2.1N (figure 5) showed the compound layers of about 30 µm and 22 µm respectively. The former had a porous outer zone of about 12 µm, which took about 40% the thickness of the compound layer. The later had a thinner porous zone of about 32% the thickness of the compound layer. The porosity level of the porous zone in the thinner compound layer appeared to be lower. The lower hydrogen partial pressure of process 2.1N was responsible for the lower porosity of the layer, while higher nitriding potential is supposed to favor the pore formation. The growth rate of the compound layer may be related to the porosity.

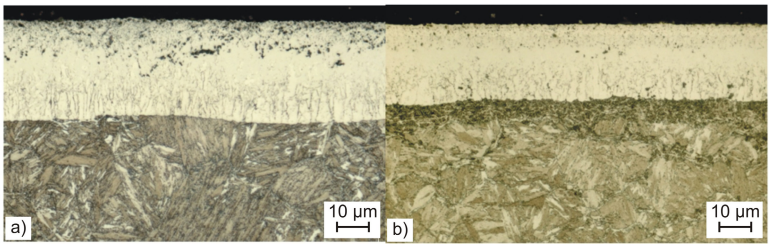


**Fig. 5** Compound (white) layer on 42CrMo4 after
a) Process 1.1N: 6 h at 590 °C, $NH_3/N_2$ = 5/5, $K_N$ = 0.6, and
b) Process 2.1N: 6 h at 615 °C, $NH_3/N_2$ = 3/7, $K_N$ = 2.0.

## *3.3 Nitrocarburizing with Addition of Carbon Monoxide or Carbon Dioxide*

Carbon monoxide (CO) and carbon dioxide ($CO_2$) was used as donator for the nitrocarburizing. The influence of the carbon donator on the pore formation was examined by two experiments. These were carried out in the quartz reactor using the gas mixture of $NH_3/N_2$= 2/8 + 4.8% $CO_2$ (process 2.2NC) and $NH_3/N_2$= 3/7 + 2.0% CO (process 2.3NC) correspondingly.

The microstructures after the nitrocarburizing (figure 6) demonstrate that the compound layer of process 2.2NC is thicker than that of process 2.3NC. The

porous zone takes about 50% of the thickness of the compound layers. The nitrocarburizing combined with high nitriding potential is unfavorable for obtaining a dense compound layer. The carbon content in the compound layers reaches about 1% and 2% correspondingly. The higher carbon content hindered the growth of the compound layer.

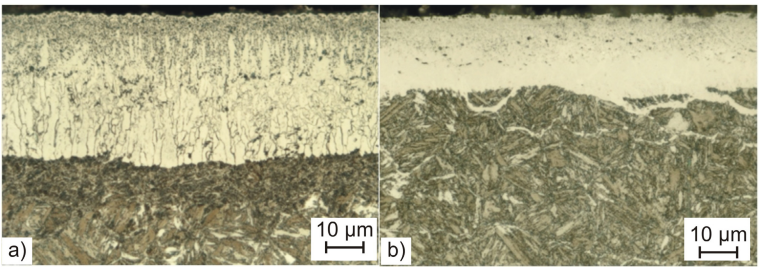


**Fig. 6** Compound layer on 42CrMo4 after
a) process 2.2NC: 6 h at 605 °C, $NH_3/N_2$= 2/8 + 4.8% $CO_2$, $K_N$ = 2.2, and
b) process 2.3NC: 6 h at 590 °C, $NH_3/N_2$= 3/7 + 2.0% CO, $K_N$ = 3.0.

The combination of high hydrogen partial pressure and carbon dioxide in the nitrocarburizing atmosphere (process 1.3NC) also led to the formation of a porous compound layer with lateral cracks as figure 7 showes. Contra wise the nitrocarburizing in the nitrogen diluted gas mixture (process 1.2NC) suppressed the porosity effectively.

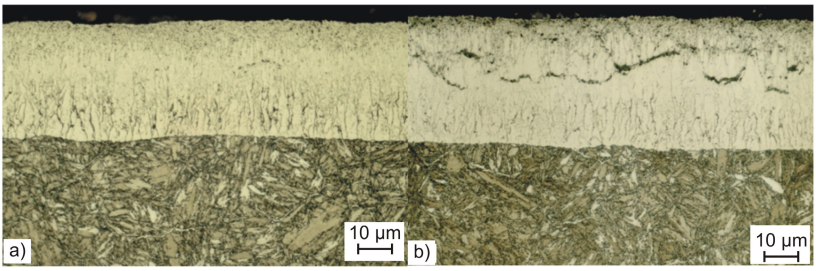


**Fig. 7** Compound layer on 42CrMo4 after nitrocarburizing 10 h at 590 °C
a) process 1.2NC: in $NH_3/N_2$= 4/5 + 2.7% $CO_2$, $K_N$ = 0.8, $P_{H2}$ = 0.30 bar, and
b) process 1.3NC: in $NH_3$ + 2.6% $CO_2$, $K_N$ = 0.6, $K_C^B$ = 0.1, $P_{H2}$ = 0.54 bar.

## *3.4 Two-Step Process*

In contrast to the conventional one-step nitrocarburizing process, a two-steps process was introduced in order to clarify if the porosity of the compound layer could be affected. The two-step process (process 1.4N-NC) involved the nitriding for 6 h at 590 °C in the first step and the nitrocarburizing for 10 h at 480 °C in the

second step. The microstructure of 42CrMo4 (figure 8a) showed that the thickness of the compound layer obtained by the two-step process is comparable to that by the one-step process (figure 5a). The pores seem smaller in figure 8a than in figure 5a. This result indicates that the compound layer did not grow further in the second step at the lower temperature and the pores in the layer increased neither. But the nitrogen and carbon content in the compound layer were determined to be higher in the two-step process compared to the one-step process (figure 8b).

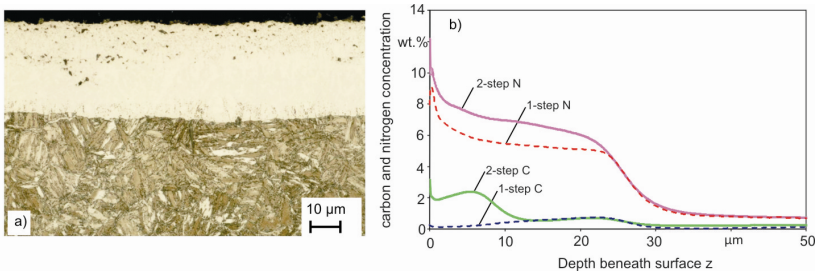


**Fig. 8** a) Compound layer, b) N- and C-profile in the layer (in comparison with that of the one-step process) on 42CrMo4 after the two-step process 1.4N-NC: 6 h at 590 °C, $NH_3/N_2$ = 5/5, $K_N$ = 0.7 in the first step and 10 h at 480 °C, $NH_3/N_2$ = 5/5 + 2.4%CO, $K_N$ > 10, $K_C^B$ = 0.1 in the second step.

It can be derived that the thickness of the compound layer is determined by fast diffusion of nitrogen in the first step at the higher temperature. The porosity of the layer can be reduced slightly in the second step, because pore formation can be suppressed by lowering the temperature and the specific volume of the carbon nitride increases with increasing content of nitrogen and carbon in the compound layer. The two-step process can therefore be used to control the thickness and composition of the compound layer separately.

## *3.5 Alloy Elements in Steel*

Compared to the steel 42CrMo4, two other alloy steels were nitrided or nitrocarburized in the same processes (2.1N in figure 1b and 1.3NC in figure 6b). The microstructures of the alloy steels are shown in figure 9 and 10. The compound layers, consisting of special nitride $Me_XN_Y$ besides ε- and/or γ'-iron nitride, were generally thinner on the high alloy steels (X40CrMoV5-1 and X40Cr13) than those on 42CrMo4 after the same process. The compound layers after the nitriding (process 2.1N) were almost free of pores. In contrast the presence of carbon dioxide together with high hydrogen partial pressure (process 1.3NC) led to the formation of pores and pore chains or cracks in the compound layers. The grain boundaries appeared to be the preferred places for pores to grow.

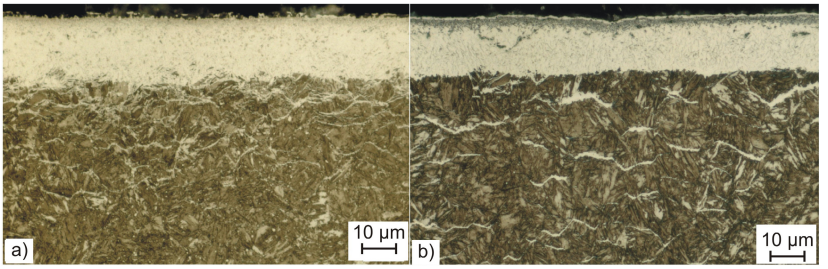


**Fig. 9** Compound layers on X40CrMoV5-1 after a) process 2.1N: 6 h at 615 °C, $NH_3/N_2 = 3/7$, $K_N = 2.0$ and b) process 1.3NC: 10 h at 590 °C in $NH_3$ + 2.6% $CO_2$, $K_N = 0.6$, $K_C^B = 0.1$

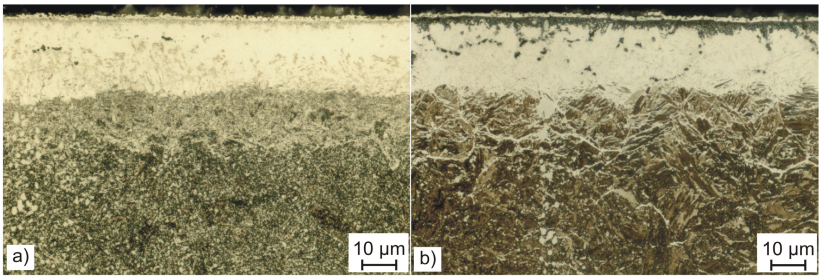


**Fig. 10** Compound layers on X40Cr13 after a) process 2.1N: 6 h at 615 °C, $NH_3/N_2 = 3/7$, $K_N = 2.0$ and b) process 1.3NC: 10 h at 590 °C in $NH_3$ + 2.6% $CO_2$, $K_N = 0.6$, $K_C^B = 0.1$

## 4 Diamond Machining

During the development of the new thermo-chemical workpiece modification, diamond cutting tests were performed by using a diamond face turning process, which enabled a basic evaluation of the wear and machining results. With the consideration of practical needs (e.g. generation of free form surfaces) a raster fly cutting process was also applied. Figure 11 shows the machining set-ups for diamond turning and milling on ultra-precision machine tools. In the diamond turning set-up the cutting tool is fixed on an adjustable tool post and the workpiece is mounted with a vacuum chuck on the air bearing main spindle. For the milling experiments a four axes ultra-precision machine tool is applied. The cutting tool is mounted on a disc and is adapted to an air bearing milling spindle which can be linearly moved in x- and y-direction. The workpiece is mounted with a vacuum chuck on the clamped rotary axis of the machine tool.

Table 1 summarises typical cutting parameters for both machining operations, diamond turning and diamond milling. As cutting tools single crystal diamond tools with nose radii from $r_\varepsilon = 0.76$ mm to $r_\varepsilon = 3$ mm have been applied. The cutting edge sharpness of the tools is in the range of $r_\beta = 20$ nm.

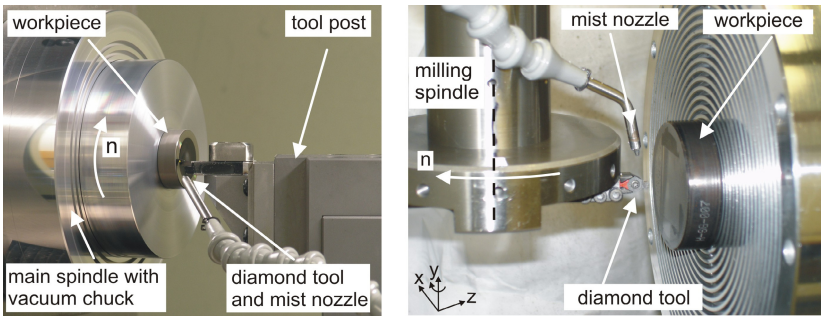


**Fig. 11** Diamond turning (left) and diamond milling (right) set-ups on ultra-precision machine tools

**Table 1** Process parameters for diamond turning and diamond milling of thermo-chemically treated steel alloys

| Cutting parameter | diamond turning | diamond milling |
|---|---|---|
| spindle speed n | 250 - 500 rpm | 3,000 - 10,000 rpm |
| feed rate f | 2 - 10 µm | 8 - 160 µm |
| cutting speed $v_c$ | 20 - 160 m/min | 470 - 4,000 m/min |
| depth of cut $a_p$ | 2 - 10 µm | 2 - 10 µm |
| pitch | --- | 72 µm |
| swing radius | --- | 25 - 65 mm |

To characterize the diamond machining results the cutting tool wear and the surface quality of the workpieces has been investigated. Subsequently detailed results for both, diamond turning and milling are presented.

## 5 Diamond Turning

The turning experiments were initially performed with an untreated steel workpiece as reference to evaluate the wear reduction effect when using nitrocarburized

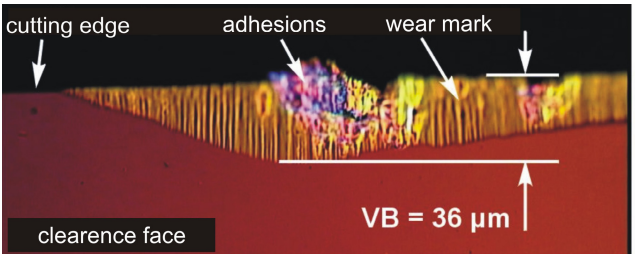


**Fig. 12** Microscopic image of the clearance face of a diamond tool after face turning of untreated carbon steel (0.45% C); cutting distance 500 m

workpieces. The cutting tool wear has been measured with a Nomarski light microscope. Figure 12 shows the flank wear of the applied diamond tool.

In this case the machining yielded a catastrophic wear land width of VB = 36 µm after a comparably low cutting distance of 500 m. This tool wear leads to a non-optical surface finish and therefore the machining of moulding inserts with high requirements concerning surface quality and form accuracy cannot be achieved.

After the basic investigations with carbon steel, further workpiece materials which are more frequently used for optical moulds, were thermo-chemically treated and diamond turned. Several experiments showed that by applying optimized cutting and nitrocarburizing parameters the tool wear can be reduced by three orders of magnitude. Diamond turning of thermo-chemically modified stress relieved and hardened 42CrMo4 tempering steel that exhibits a more homogeneous texture caused a diamond tool wear of less than 2 µm after diamond turning of $l_c$ = 500 m cutting distance. Figure 13 shows exemplarily a cutting edge after diamond turning of a nitrocarburized 42CrMo4 measured with a Nomarksi microscope (cf. figure 13 left). As the tool wear is in the range of the lateral resolution of the Nomarski microscope an atomic force microscope has been applied for a detailed measurement of the cutting edge. The observed tool wear mark is shown on the right in figure 13. It is in the range of 1.5 µm. This wear is slightly higher compared to that occurring in the diamond machining of electroless nickel [Bri10]. The detectable wear is a result of the high hardness of the compound layer. Typical hardness values are about 1000 HV, whereas electroless nickel has a hardness of 550 HV. Further influence on the wear behaviour is the inhomogeneous structure of the workpiece material.

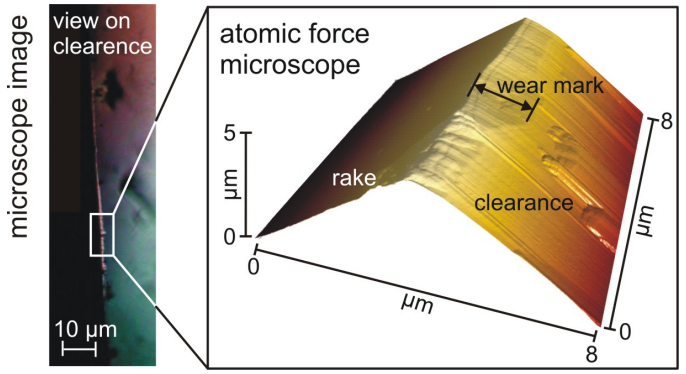


**Fig. 13** Microscope and AFM image of a diamond cutting tool after machining a nitrocarburized steel workpiece

Diamond turning experiments with a hardened thermo-chemically treated high alloyed tool steel resulted in a wear land width of 5 µm after a cutting distance of $l_c$ = 300 m. The detectable wear is a result of the high hardness of 1200 HV which remained unchanged by the thermo-chemical modification process as well as the inhomogeneous structure of the workpiece material.

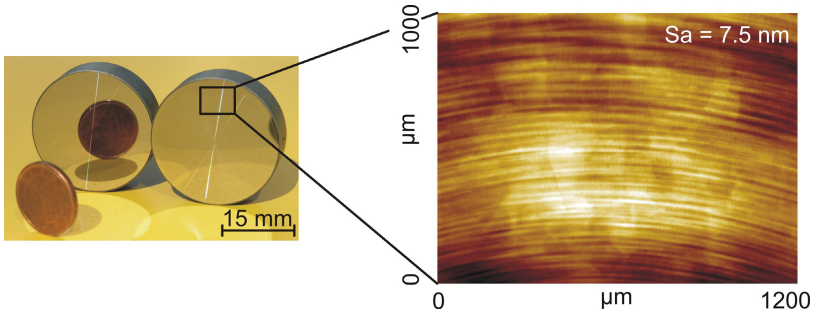


**Fig. 14** Moulding inserts for the replication of glass optics and resulting surface topography measured with a white light interferometer

The surface roughness was measured with a white light interferometer over an area of 1200 x 1000 µm$^2$ at different locations on the surface. The measured roughness values of Ra = 8 - 12 nm did not depend on the cutting distance. The surface roughness could easily be reduced to approx. 4 nm Ra by manual post-polishing. Figure 14 shows two diamond turned moulding inserts made of X40CrMoV5-1 for the replication of glass lenses.

To evaluate the differences in the machining of nitrocarburized steels compared to conventionally applied materials in ultra precision machining diamond turning experiments with five typical non-ferrous metals and nitrocarburized steel have been conducted [Osm10]. The non-ferrous metals were three aluminium alloys which are pure aluminium, AlMg3 and a special fine grained aluminium alloy RSA-905. Moreover, OFHC-copper and an electroless nickel plating have been included. The sixth material was a nitrocarburized tool steel. Table 2 shows the applied process parameter for the diamond turning experiments.

**Table 2** Process parameters for diamond turning of non-ferrous metals and nitrocarburized steel

| Cutting parameter | diamond turning |
|---|---|
| cutting tool | single crystal diamond, $r_\varepsilon$ = 0.76 mm, $\alpha = 6°$, $\gamma = 0°$ |
| feed rate f | 5 / 10 µm |
| cutting speed $v_c$ | 10 / 20 m/min |
| depth of cut $a_p$ | 5 / 10 µm |
| Lubricant | spray mist, mineral oil |

The roughness values have been measured with a white light interferometer on an area of 1200 x 980 µm². Table 3 gives the minimal and maximal average values for the varied parameter combinations. Every value is the average of eight measurements per turning experiment. Slight differences concerning the surface roughness could be found for the different parameter combinations, but none of the variables show a statistically significant influence.

**Table 3** Achieved surface roughness Sa for different diamond turned workpiece materials

| workpiece material | | Al | AlMg3 | RSA-905 | OFHC-copper | NiP-plating | nitro-carburized steel |
|---|---|---|---|---|---|---|---|
| roughness Sa [nm] | min | 6.5 | 6.0 | 7.0 | 6.3 | 6.5 | 9.0 |
| | max | 8.0 | 8.5 | 9.0 | 8.6 | 9.7 | 12.0 |

Hence, the varied process parameters show no significant influence; the dominating factor for the surface roughness seems to be the inner microstructure of the material itself. In case of the pure aluminum and the OFHC-copper the anisotropy of the grain structure leads to unsteady surface topography [Lee00]. The amorphous electroless nickel plating and the fine grained RSA-905 aluminum alloy show a very regular surface topography which is dominated by the kinematics of the face turning process. The same effect can be found for the investigated nitrocarburized steel materials. Figure 15 shows exemplarily three surface topographies for the different steel materials. In all cases the surfaces exhibit a smooth and even surface topography dominated by the kinematics of the face turning process.

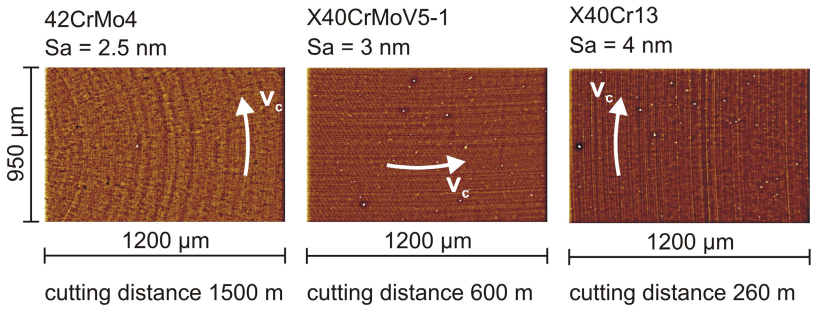


**Fig. 15** Surface topography for diamond turned nitrocarburized steels

## 6 Diamond Milling

For the future generation of moulding inserts with free form surfaces diamond milling experiments were performed. As a first result the preliminary diamond turning experiments showed that there is a strong correlation between cutting in the ε-phase or the γ'-phase of the compound layer and the diamond tool wear.

Therefore, several diamond milling experiments were performed at a depth beneath surface of 3 µm to 20 µm. Figure 16 shows three examples after diamond milling of 30 x 30 $mm^2$ steel surfaces with a 15 µm thick compound layer at different depth of cut.


**Fig. 16** Diamond milled steel workpieces

To characterize the diamond milled surfaces a white light interferometer was used to measure the surface roughness Sa. Therefore, all samples were measured at a size of 1200 x 980 $µm^2$ at 10 different positions. Figure 17 summarizes these measurements. The lowest roughness value of Sa = 6.0 nm can be achieved at a depth beneath surface of 6 µm.

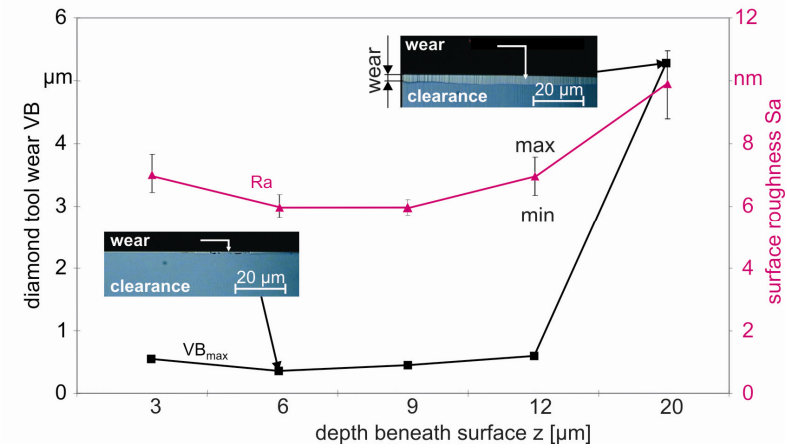


**Fig. 17** Surface roughness and diamond tool wear depending on the depth beneath the surface

Moreover, figure 17 shows the diamond tool wear for the experiments discussed above. The wear is almost independent from the depth beneath surface indicating, that the chemical and mechanical properties in the compound layer are constant. The exceptional measuring point at a depth beneath surface of 20 µm with a width of wear land of approximately 5 µm shows that the diamond tool wear increases if the machining takes place in the diffusion layer beneath the compound layer. Therefore, it is essential for an optical surface finish and less diamond tool wear to machine the moulding inserts within the compound layer.

In addition to the machining of continuous surfaces the micro-structuring of nitrocarburized steels has been investigated. Diamond milling experiments using a V-shaped diamond tool have been carried out. The cone angle of the tool was $\varepsilon = 150°$. Figure 18 shows images of a scanning electron microscope and a white light interferometer measurement of intersecting linear grooves. The measurement shows that the machining of structures in nitrocarburized steels is possible without burr formation. The surface roughness of the flank is Sa = 3 nm on a measurement area of 30 x 60 µm².

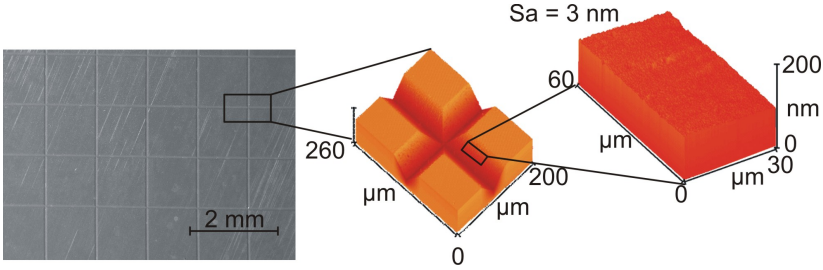


**Fig. 18** Images of SEM- and WLI-measurements of a structured steel mould

## 7 Moulding Inserts for the Replication of Optics

Steels modified by novel nitriding processes become diamond machinable. The possibility to apply this method in practice was inspected by the process chain for manufacturing of moulding inserts (figure 19), which were used for the replication of optics made of plastic or glass.

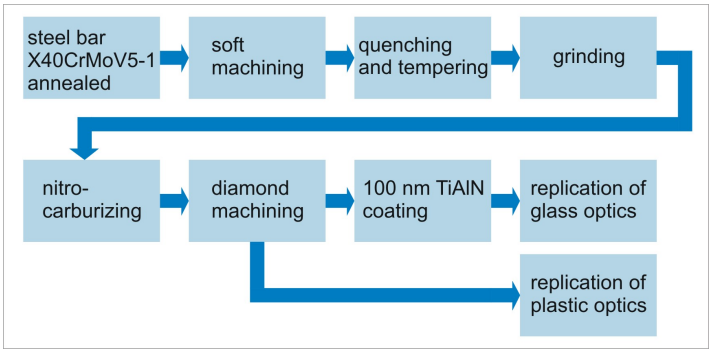


**Fig. 19** Process chain for manufacturing of moulding inserts

The workpieces after grinding were thermo-chemically treated by a two-step process. The first step was nitriding 10 h at 570 °C with $K_N = 1.1$ and the second step nitrocarburizing 10 h at 480 °C with $K_N > 10$, $K_C^B = 0.1$. A compound layer of about 14 µm in thickness was obtained for the steel X40CrMoV5-1. A porous zone of about 4 µm appeared at the outermost range of the layer. The diamond machining had removed a surface layer of about 9 µm. Therefore, a 5 µm compound layer remained on the finished moulding insert. The hardness of the compound layer and the diffusion layer reached about 1300 HV0.025 and 930 HV0.5 respectively. Figure 20a shows the nitrocarburized and diamond machined moulding insert for injection moulding of plastic, figure 20b the nitrocarburized, diamond machined and coated moulding insert for hot pressing of glass. The 100 nm TiAlN coating was needed to prevent oxidation of the steel surface.

The nitrocarburized steel mould (figure 20a) had withstood 50 shoots of injection moulding of PMMA lens without any damage, and the nitrocarburized and coated steel mould (figure 20b) had passed 18 pressings of low-Tg glasses at 375 °C no noticeable change. However, a slight adhesion of plastic or glass at the surfaces of nitrocarburized or the coated steel moulds was observed. Therefore, anti-adhesion will be an issue in the future research work of the SFB/TR4.

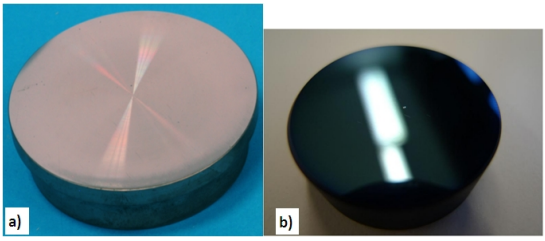


**Fig. 20** a) nitrocarburized moulding insert Ø50 x 15 mm for injection moulding of plastic, and b) nitrocarburized and with 100 nm TiAlN coated moulding insert Ø30 x 10 mm for hot pressing of glass

## 8 Conclusion

The generation of thick and low porosity compound layers can be realized by pure nitriding with optimized process parameters. First of all, nitrogen potential and hydrogen partial pressure of the process atmosphere should be possibly low. The addition of carbon dioxide for nitrocarburizing, however, promotes pore formation. A two-step process is a useful method for controlling the thickness and composition of the compound layer separately. Alloy steel with suitable amount of nitride former shows high resistance against pore formation.

The diamond machining results are a breakthrough in ultra precision turning and milling of steel with optical surface quality. The results prove that ultra precision machining of steel alloys is possible, if the surface zone of the workpieces is thermo-chemically modified in a way that chemical reactions between the carbon atoms of the diamond lattice and the iron atoms of the workpiece material cannot take place,

thus, preventing chemical tool wear. Interestingly, the hardness of the machined compound layer does not affect the diamond tool wear strongly, therefore, a hardened, thermo-chemically modified and diamond machined mould can be used directly for the replication of plastic parts or with a TiAlN coating to prevent oxidation even the hot pressing of low-Tg glasses is possible. Thermo-chemically treated workpieces can be machined by turning and milling, however, milling is more flexible and can be applied to moulds for the replication of optical free form components. First industrial applications have already been realised successfully.

**Acknowledgement.** The authors like to thank the German Research Foundation (DFG) for funding this work as a part of the Transregional Collaborative Research Center SFB/TR4 "Process Chains for the Replication of Complex Optical Elements".

## References

[Bri04] Brinksmeier, E.; Dong, J; Gläbe, R.: Diamond Turning of Steel Moulds for Optical Applications. Proc. of 4th euspen International Conference, Glasgow, Scotland (UK), May-June 2004

[Bri06] Brinksmeier, E; Gläbe, R.; Osmer, J.: „Ultra-precision Diamond Cutting of Steel Moulds". Annals of the CIRP, 55/1, p. 551-554 (2006)

[Bri10] Brinksmeier, E; Gläbe, R.; Osmer, J.: „Diamond Cutting of FeN-Layers on Steel Substrates for Optical Mould Making". Key Engineering Materials Vol. 438, p. 31-34 (2010)

[Cas83] Casstevens, J.: "Diamond Turning of Steel in Carbon Saturated Atmospheres". Precision Engineering 5, p. 9-15 (1983)

[Che07] Chen, Y; Zhang, L.C; Arsecularatne, J.A., Zarudi, I.: "Polishing of polycrystalline diamond by the technique of dynamic friction", Part 3: "Mechanism exploration through debris analysis". International Journal of Machine Tools and Manufacture, 47, p. 2282-2289 (2007)

[Don03] Dong, J.; Gläbe, R.; Mehner, A., Mayr, P.; Brinksmeier, E.: Verfahren zur Mikrozerspanung von metallischen Werkstoffen. German Patent DE 10333860A1, 2003, United States Patent No US7582170B2, 2009

[Eva91] Evans, C.: "Cryogenic Diamond Turning of Stainless Steel", Annals of the CIRP, 40/1, p. 571-575 (1991)

[Glä03] Gläbe, R.: "Prozess- und Schneidstoffentwicklung zur ultrapräzisen Drehbearbeitung von Stahl". Dissertation Universität Bremen, Shaker Verlag (2003)

[Gra68] Grabke, H. J.: Reaktion von Ammoniak, Stickstoff und Wasserstoff an der Oberfläche von Eisen. I. Zur Kinetik der Nitrierung von Eisen mit $NH_3$-$H_2$-Gemischen und der Denitrierung. In: Berichte der Bunsengesellschaft 72 (1968) Nr.4 p. 533-541

[Hof91] Hoffmann, F.; Kunst, H.; Klümper-Westkamp, H.; Liedtke, D.; Mittemeijer E.J.; Rose, E.; Zimmermann, K.: Stand der Kenntnisse über die Porenentstehung beim Nitrieren und Nitrocarburieren. The 1th European conference „Nitriding and Nitrocarburising," 1991, Darmstadt, Proceeding, p. 105-113

[Hof96] Hoffmann, R.; Mittemeijer, E.J.; Somers, M.A.J.: Verbindungsschicht-bildung beim Nitrieren und Nitrocarburieren. In: HTM 51 (1996), Nr. 3, p. 162-169

[Klo10] Klocke, F.; Dambon, O.; Bulla, B.: "Direct Diamond Turning of Aspheric Steel Moulds with Ultra Precise Accuracy". Proc. of the 25th Annual Meeting of the ASPE 2010, Atlanta, USA

[Lee00] Lee, W. B.; To, S.; Cheung, C. F.: “Effect of Crystallographic Orientation in Diamond Turning of Copper Single Crystals”. Scripta Materialia, Volume 42/10 (2000), p. 937-945

[Mor99] Moriwaki, T.; Shamoto, E.: “Ultraprecision Diamond Cutting of Hardened Steel by Applying Elliptical Vibration Cutting”. Annals of the CIRP, 48/1, p. 441-444 (1999)

[Osm10] Osmer, J.; Meier, A.; Gläbe, R.; Riemer, O.; Brinksmeier, E.: “Ultra Precision Machining of Non-Ferrous Metals and Nitrocarburized Tool Steel”. Key Engineerig Materials Volumes 447-448 (2010), p. 46-50

[Pau96] Paul, E.; Evans, C.J.; Mangamelli, A.; Mc Glauflin, M.L.: “Chemical Aspects of Tool Wear in Single Point Diamond Turning”. Precision Engineering 18, p. 4-19 (1996)

[Pre73] Prenosil, B.: Einige neue Erkenntnisse über das Gefüge von um 600 °C in der Gasatmosphäre carbonitrierten Schichten. In: HTM 28 (1973), Nr. 3, p. 157-164

[Sch02] Schröter, W.; Spengler, A.: Beitrag zum Erkenntnisstand der Porenentstehung bei der Schichtbildung durch Stickstoff in Eisenwerkstoffen. ATTT/AWT-Tagung, Aachen, 10.-12. Apr, 2002

[Sly89] Slycke, J.; Sproge, L.: Kinetics of the gaseous nitrocarburising process. In: Surface Engineering 5 (1989) Nr. 2, p. 125-140

[Som92] Somers, M.A.J.; Mittemeijer, E.J.: Verbindungsschichtbildung während des Gasnitrierens und des Gas- und Salzbadnitrocarburierens. In: HTM 47 (1992), Nr. 1, p. 5-13

[Vog02] Vogelsang, K.; Schröter, W.; Hoffmann, R. und Jacobs, H.: Ein Beitrag zum Problem der Porenbildung. In: HTM 57(2002), Nr. 1, p. 42-48

# Novel Processes for the Machining of Tool Inserts for Precision Glass Molding

Fritz Klocke, Ekkard Brinksmeier, Oltmann Riemer, Max Schwade, Heiko Schulte, and Andreas Klink

**Abstract.** In this chapter, two new process chains are introduced using novel processes for the machining of complex molds by diamond grinding and diamond profile grinding in combination with a machine-based abrasive profile polishing. Finest grained diamond grinding wheels with a metal bond provide superior grinding results. But the combination of a metal bond and very fine grains causes great difficulties for the trueing and dressing operation using conventional methods. For the machining of rotational symmetric mold inserts the novel process of electrochemical in-process dressing can be applied to achieve optical surface qualities without a subsequent polishing process.

For more complex shapes a grinding wheel with a micro-profile is needed. The pre-dressing and profiling of the difficult to machine grinding wheels is done by the unconventional Wire-EDM process. To achieve a surface roughness of the profiled mold in optical quality a subsequent polishing process is necessary. Therefore the novel process of diamond profile grinding in combination with a subsequent machine-based profile polishing is introduced.

## 1 Introduction

The optical industry is in need of complex geometries like spheres, aspheres and structured shapes of lenses with very high form accuracies. The mass production of these lenses and lens systems by glass molding is a very high demanding production process. The mold materials need to be very hard and temperature

Fritz Klocke
Fraunhofer Institute for Production Technology IPT,
Steinbachstraße 17, 52074 Aachen, Germany

Ekkard Brinksmeier · Oltmann Riemer · Heiko Schulte
Laboratory for Precision Machining LFM, University of Bremen, Badgasteiner Straße 2,
28359 Bremen, Germany

Max Schwade · Andreas Klink
Laboratory for Machine Tools and Production Engineering WZL,
RWTH Aachen, Steinbachstraße 19, 52074 Aachen, Germany

E. Brinksmeier et al. (Eds.): Fabrication of Complex Optical Components, LNPE, pp. 85–98.
springerlink.com 

resisting like cemented carbides and ceramics. But the machining of these hard and brittle materials is very difficult which makes precision diamond grinding a key technology, confer also [Sha96] and [Bri10]. Using fine grained diamond grinding wheels with a metal bond high profile constancies and wear resistances combined with high material removal rates and optimal surface qualities can be achieved. But the combination of a metal bond and very fine grains causes great difficulties for the trueing and dressing operation using conventional methods.

For the machining of rotational symmetric classical lens mold inserts the novel process of electrochemical in-process dressing for metal-bonded grinding wheels can be applied to create continuous surfaces in optical quality. A subsequent polishing process is not necessary, which reduces time and lowers the manufacturing costs.

More complex mold shapes like cylindrical lens arrays, which are used for the beam collimination of diode lasers, cannot be machined by ultra precision milling in optical quality. In this case diamond profile grinding in combination with a machine-based abrasive profile polishing is the key technology. The profiling of the metal-bonded grinding wheel with a simultaneous dressing operation can be achieved by Wire-EDM. To create a mold surface roughness in optical quality a subsequent profile polishing is necessary.

In comparison to conventional polishing of continuous surface geometries the main challenge for abrasive profile polishing consists in preventing edge rounding, avoiding a non-uniform wear of the polishing tool as well as preventing differences in local material removal. Results from experiments with cemented carbide will show a significant improvement comparing to the pre-ground surface quality. In the following two process chains are introduced using these novel processes and detailed results are presented.

## 2 Process Chain for Rotationally Symmetric Glass Lenses

The initial process chain for the production of rotationally symmetric glass lenses can be seen in Figure 1, using a combination of precision diamond grinding and abrasive polishing for the machining of the molds. The workpiece quality and form accuracy significantly depend on the grinding process and especially the effort of following steps of the process chain depend on the quality of the grinding result. Therefore, the surfaces should possess such a good quality that a subsequent polishing process is unnecessary. This will reduce the needed steps of the manufacturing process, the manufacturing time and the manufacturing costs.

By using metal-bonded grinding wheels a high wear resistance and profile constancy can be achieved during grinding. In combination with fine and ultra fine grains it is possible to create the desired optical surface qualities directly to avoid polishing. Bronze-bonded grinding wheels in particular can be used efficiently, as it is easier to modify their chemical composition – and therefore their bond hardness – to suit the specific grinding tasks. Hence these grinding wheels can be used for the task-specific precision machining of hard and brittle mold materials. But the combination of very small grained diamonds down to the smallest sized grains of only single-digit micrometers and the metal bond cause great difficulties

for conventional dressing. Due to the metal bond composition of the grinding wheel the novel process of electrochemical in-process dressing is a powerful alternative dressing technology.

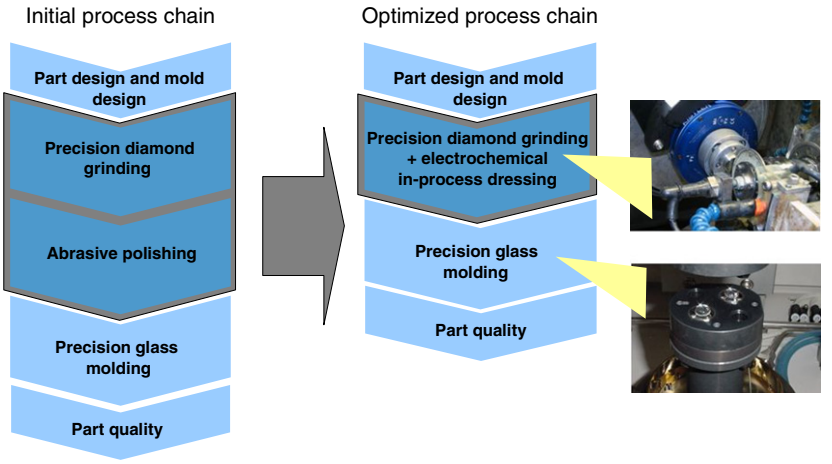


**Fig. 1** Process chains for rotationally symmetric mold inserts

This unconventional dressing process uses the anodic metal dissolution similar to electrochemical machining to set back the metal bond of the grinding wheel. Since the diamond grits are not electrically conductive they are not influenced by the process. It is commonly known that ECM has no thermal effect on the machined surface and thus there is also no indirect effect on the diamond structure. By setting back the bonding material, used diamond grits that have suffered wear by the grinding process are no longer held in place and are removed during grinding. New and sharp diamond grits from deeper layers form the new surface and an optimal grit protrusion can be achieved. The dressing process can be implemented on the actual grinding machine and the dressing operation can be performed in process, in parallel to grinding, as shown in Figure 2. The cooling lubricant used for the grinding process also serves as an electrolyte.

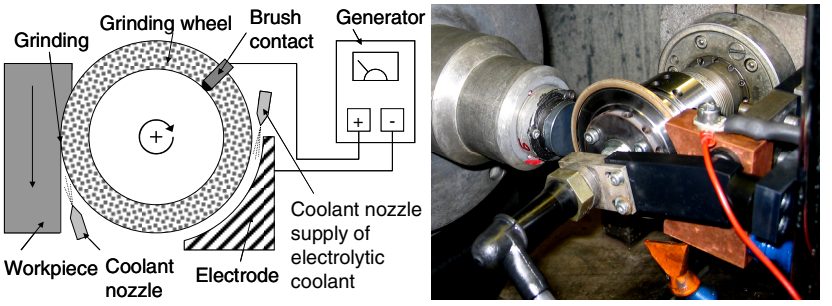


**Fig. 2** Principle of electrochemical in-process dressing

To avoid an excessive wear of the grinding wheel caused by the dressing process the formation of an oxide layer in the passive operating range is used. This layer possesses a high electrical resistance as a function of its thickness which slows down the anodic dissolution until it is stopped altogether (during pre-dressing). The efficiency of this in-process dressing method was already shown by research on the so called ELID-grinding process which also uses an oxide layer formation to restrict the set back of the bonding [Ohm90]. In ELID-grinding primarily cast-iron bonded grinding wheels are used because of their good passivating behaviour. Bronze-bonded grinding wheels are cheaper in production and have as already mentioned the advantage that their chemical composition and therefore their bond hardness can easily be modified to suit a specific grinding task. Therefore basic research on the oxide layer formation on bronze bonds was conducted.

The surface topography of the oxide layers covering the grits of two grinding wheels with different bond material can be seen in Figure 3. The combination of bond material and electrolyte has a great influence on the growth behaviour and composition of the oxide layer which has a major effect on the grinding result.

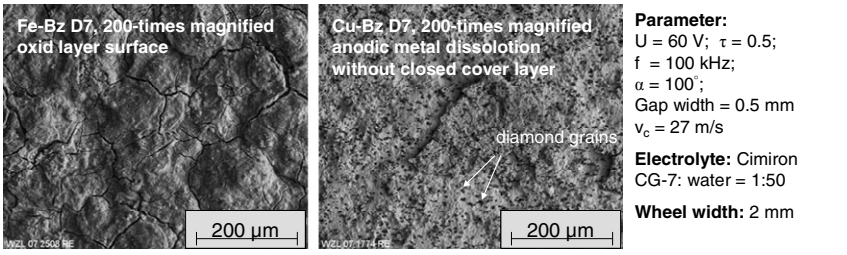


**Fig. 3** Grinding wheel surface after electrochemical pre-dressing, [Kli09]

During grinding, part of the oxide layer is easily mechanically removed which reduces the electrical resistance and thus the dressing operation is resumed. With precise knowledge of all influencing factors for the generation of the oxide layer and the mechanical removal optimal parameters can be found to achieve a dynamic balance by the self regulating process. If only so much of the bonding material is dissolved to remove the used diamond grits and to achieve an ideal grit protrusion with new abrasives, the grinding wheel stays in an optimal sharp condition throughout the grinding process with minimized wear and can produce optimal surface qualities at the same time. The circle of oxide layer growth and mechanical removal is shown in Figure 4 together with a characteristic current-voltage curve. The build-up of the oxide layer is influenced by various factors, obviously by the amount of voltage applied, the gap width between the electrode and the grinding wheel surface and thus the resulting electric current, [Klo08]. Major factors are, as can be seen in Figure 3, the bond-material and electrolyte composition.

Thus it is necessary to choose the correct combination for a specific grinding task. It can be seen that for different compositions of bronze bonds optical surface qualities can be achieved with Ra values of below 10 nm using grit sizes D3 (average grain size from 2 µm to 4 µm) and D7 (average grain size from 5 µm

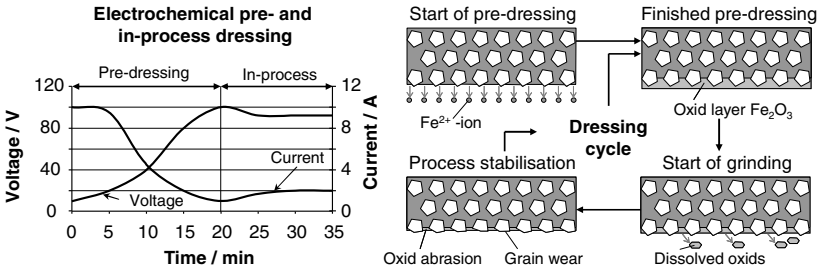


**Fig. 4** Dressing cycle for electrochemical dressing (ELID) after [Ohm90]

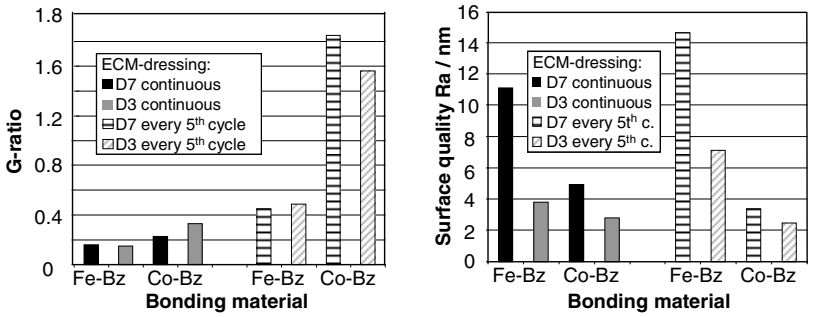


**Process parameters:**

- Grinding wheel: $d_S$ = 75 mm, $b_S$ = 2 mm
- Workpiece: $Si_3N_4$-cylinder D = 25 mm
- Coolant: CIMIRON CG-7; κ = 2 mS/cm
- ECM-parameter: U = 60 V; τ = 0.1; f = 100 kHz
- Kinematics: Rotational peripheral plunge grinding ($v_c$ = 27 m/s; $v_f$ = 5 mm/min; $n_w$ = 100 $min^{-1}$ $a_e$ = 2 µm (D7); 1 µm (D3)

**Fig. 5** G-ratios and surface quality with in process ECM-dressing, [Kli09]

to 10 µm) which fulfils the requirement of surface roughness for the glass molds, as shown in Figure 5.

As workpiece material $Si_3N_4$ was used during testing to maximize the wear of the grinding wheel since this is currently the hardest to machine mold material used and thus less wear can be anticipated during the machining of cemented carbide. To optimize the dressing operation in regard of the wear of the grinding wheel a continuous electrochemical dressing was compared to a duty cycle with a ratio of 1:4 by measuring the G-ratio, which is defined as the ratio of removed material on the workpiece to the removed material on the grinding wheel. More details can be found in [Kli09]. Since the Cu-Bz bond did not form a closed oxide layer covering and thus the dissolution of the bonding material was too fast it was not investigated any further.

Due to the results seen in Figure 5, a spherical cemented carbide mold insert for the precision glass molding operation was manufactured using a bronze-bonded grinding (Co-Bz) wheel with a D7 grit size and a cyclic electrochemical in-process dressing strategy. The mold can be seen in Figure 6 together with the according measurement plot. Using the above mentioned process parameters an optical

surface quality could be achieved with a Ra-value of about 6 nm. The peak-to-valley vertical deviation was 0.53 µm which still can be reduced by further optimization of the electrochemical in-process dressing parameters, [Klo10].

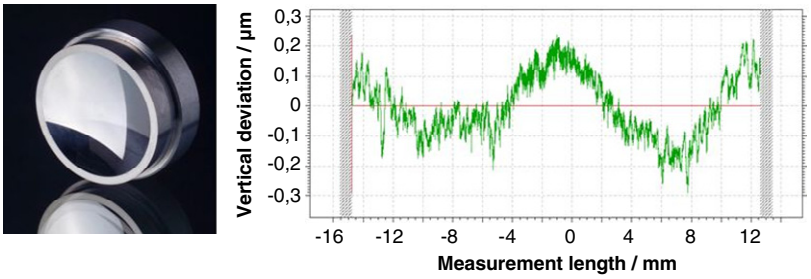


**Fig. 6** Mold insert produced by precision grinding with ECM-dressing

## *2.1 Resume*

Electrochemical in-process dressing of bronze-bonded diamond grinding wheels can be used to reduce the needed steps to manufacture mold inserts for the precision glass molding operation. A subsequent polishing process after precision grinding is unnecessary due to the optical surface quality achieved by grinding.

# 3 Process Chain for Complex Lens Arrays

Collimation lenses for high performance diode lasers show an increasing industrial application with the requirement for micro structured glass optics with cylindrical lens arrays. Insufficient quality of these lenses (e.g. high surface roughness) would lead to minimized power output of the lasers.

As part of the process chain for the replication of complex optical glass parts, which is shown in Figure 7, the machining of structured molds by diamond profile grinding with electro discharge trueing and dressing and machine-based abrasive profile polishing are the key technologies. The subsequent replication is realized by precision glass molding. The quality inspection of mold and glass lenses is realized by white light interferometry for surface quality and by profilometry for shape accuracy.

To machine structured glass molds within the required final quality and to avoid individual post-polishing of the glass lenses itself after the replication, a profile grinding process and an abrasive profile polishing process are well suited. Similar to the first process chain cemented carbides and ceramics are also widely used as mold material for the needed structured tool inserts due to their good performance and long tool life. Therefore metal-bonded grinding wheels with very fine grains in high concentrations are also used for this process chain to achieve best surface qualities and profile constancies. The difficulties in the dressing operation are similar as well. By staying with a metallic bonding material the electrochemical dressing operation described above is applicable, but not practical

since the desired shape of the molds in this case are not rotationally symmetric. By using Wire-EDM instead it is possible to dress the wheel and to create a micro structure on the grinding wheel surface which is transferred to the mold during the profile grinding operation.

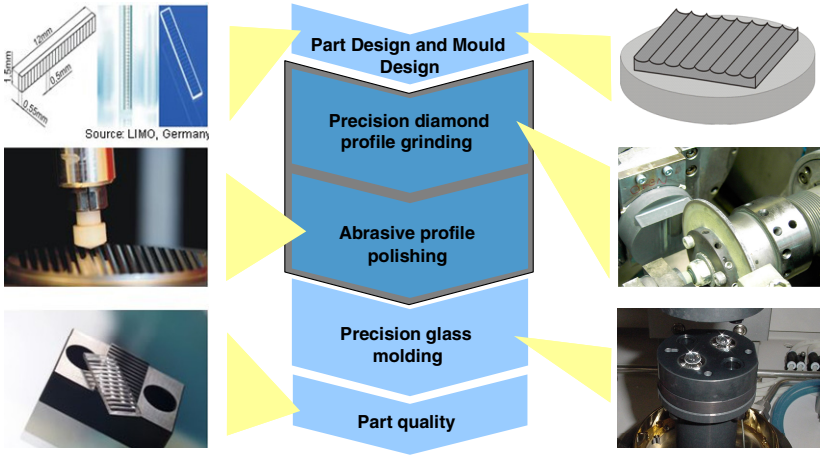


**Fig. 7** Process chain for the replication of complex optical glass parts

The principle of wire electro discharge trueing and dressing is shown in Figure 8. The EDM process with small discharge energies takes place between the electrically conductive metal bond and the wire electrode, separated by a gap filled with a dielectric fluid. Since the diamond grits are not electrically conductive they are not primarily involved in the process and the bond material is set back resulting in the desired grit protrusion. In this way the grinding wheel is dressed and profiled at the same time. The grit protrusion of an eroded grinding wheel surface can be seen in Figure 9.

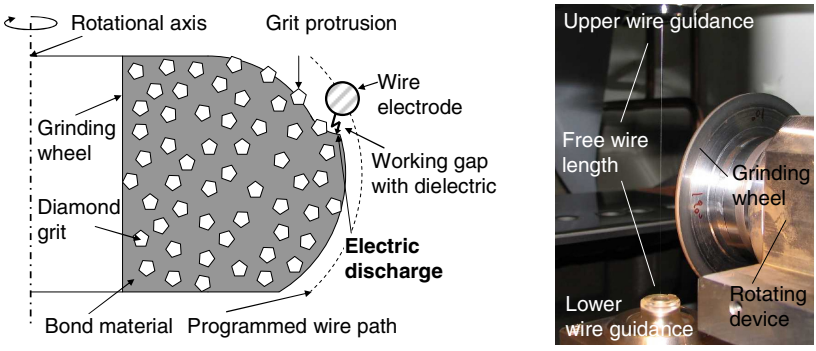


**Fig. 8** Principle of wire electro discharge trueing and dressing

By moving the wire electrode along a predefined contour according to the programmed NC-code, thermal material removal takes place and the rotating grinding wheel is profiled. By using the Wire-EDM process, almost any user-defined profile can flexibly be implemented on the grinding wheel, see also [Uhl08, Mas85]. In contrast to the electrochemical in-process dressing operation the EDM-dressing and profiling is performed before grinding and a precise clamping device is needed to transfer the grinding wheel from the conventional Wire-EDM machine, as shown in Figure 8, to the grinding machine.

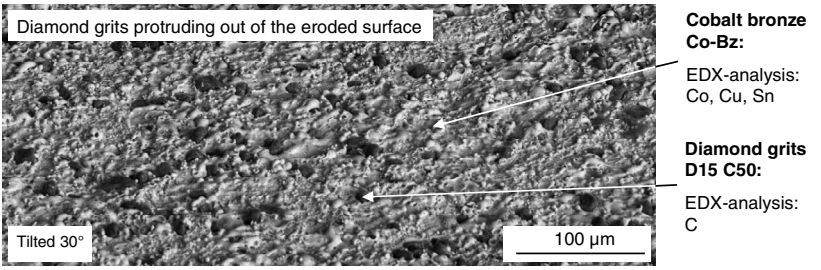


**Fig. 9** Diamond grit protrusion after Wire-EDM processing, [Kli09]

In contrast to the electrochemical removal principle the thermal removal principle of EDM can damage the diamond grits although they are not electrically conductive. The material removal of the EDM process is caused by spark discharges and the formation of plasma channels with very small areas of heat sources on the material surfaces. It is widely believed that the temperature of the plasma channel rises above several thousand K during a discharge, [Klo07a]. At higher temperatures a transformation of diamond to graphite can be observed. The grade of transformation depends on the time and increases exponentially with the given temperature. Even if the heat source is not directly located on the diamond grit, a graphitisation of the diamonds can take place through thermal conduction. The discharges only last in the region of microseconds so the possible graphitisation is highly dependent on the location of the discharges.

To determine the probability of a discharge in a certain location the electrical field between the tool (wire) electrode and the workpiece can be estimated as the electric field within a plate capacitor. The different permittivity characteristics of each material influence the resulting electric field in this region and a discharge will occur at the point with the highest electric field and smallest dielectric strength. FEM simulations have shown that, assuming good grit protrusion, the highest electric force is to be expected at the tips of the diamonds and at the intersection of diamond grit and bonding material using oil-based dielectrics. So discharges are more likely near the diamond grits or, if the diamond surface already shows graphitisation resulting in electric conductivity, on top of the grit itself. Thus the diamond grits can be influenced although they are not electrically conductive before the process.

By adapting the EDM-parameters and special strategies without too many trim cuts (without any additional offset correction) this effect can be limited to the surface of the grits. In this case there still is a diamond structure in the inner volume and the grinding process can still be performed. The wire electro discharge trueing and dressing process achieves very high profile accuracies. For the preparation of defined profiles only the working gap – which is inherent in the EDM process – must be taken into account. Deviation of cyclic running and side run out are below 1 µm after the EDM process, confer also [Kli09].

For machining of the cylindrical grooves a profile grinding process is necessary. Two grinding wheels were trued and dressed by Wire-EDM. The performance of these wheels was tested during grinding of the cylindrical lens array. A rough grinding operation was done with a coarse wheel (average grain size from 15 µm to 30 µm). The following finishing was done with a fine grinding wheel (average grain size from 5 µm to 10 µm). The according fine grinding parameters are shown in Figure 10.

For the evaluation of the grinding process the shape accuracy and surface quality are measured. Therefore, radius RSP of the sphere and surface roughness Ra, on the mold insert were measured. The radius RSP is measured as least square fit radius measuring ± 150 µm from the center of each sphere. The surface roughness is measured perpendicular to the grinding direction. The sphere radius RSP is located within the requested tolerance band of 10 µm. The profile constancy of the fine grinding wheel was verified by a comparison of the graphite clearance grooves before and after the process. The least square fit radii were virtually equal.

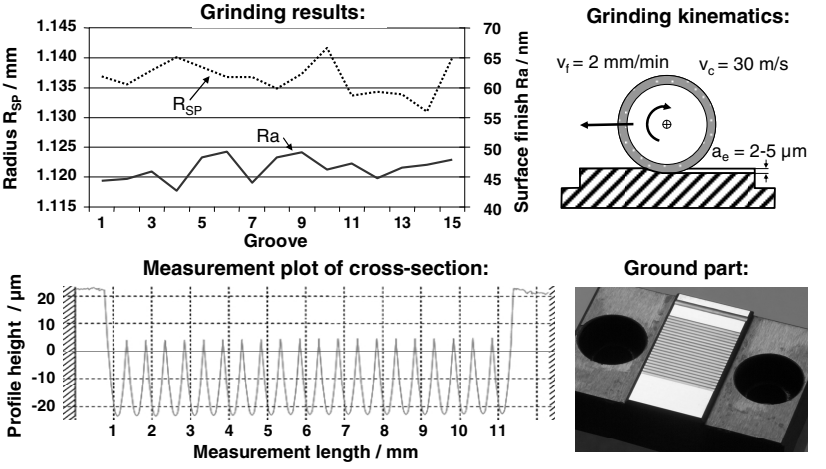


**Fig. 10** Precision grinding of cemented carbide tool insert, [Kli09]

During this process, the micro cross section profile of the circumferential wheel is directly reproduced in the micro geometry of the workpiece. Due to grain size and the grinding kinematics the process has not achieved optical surface quality. The surface roughness Ra is in the range of 38 to 44 nm for all grooves in

comparison to the continuous surface in the first process chain where a much better surface roughness of below 10 nm was directly possible. Thus, a following profile polishing process is needed to reduce surface roughness Ra below 10 nm. In comparison to conventional polishing of continuous surface geometries the main challenge for abrasive profile polishing consists in preventing edge rounding, avoiding a non-uniform wear of the polishing tool as well as preventing differences in local material removal, [Sch07]. Results from experiments with cemented carbide will show a significant improvement comparing to the pre-ground surface quality.

For abrasive polishing of structures an aspheric polishing machine was modified, now incorporating three numerically controlled linear axes (X, Y, Z), a polishing spindle and a workpiece spindle [Bri09], Figure 11a. The polishing spindle mounted on the vertical Z-axis can be tilted by ±90°, Figure 11b. For polishing linear structures the workpiece is aligned to the feed direction by using a manual rotary table. Process forces can be measured by a force transducer placed beneath the workpiece. Furthermore, the polishing tools can be dressed in-situ with a diamond tool to ensure minimal run-out. A camera system with an integrated zoom is used to visualize and control the tool making and the polishing process. The adjustment of a polishing tool above a groove can be controlled by the camera system, Figure 11c. The polishing process can be controlled by monitoring the force components and moving the X-, Y- and Z-axis, in order to guarantee a continuous polishing pressure at the workpiece surface.

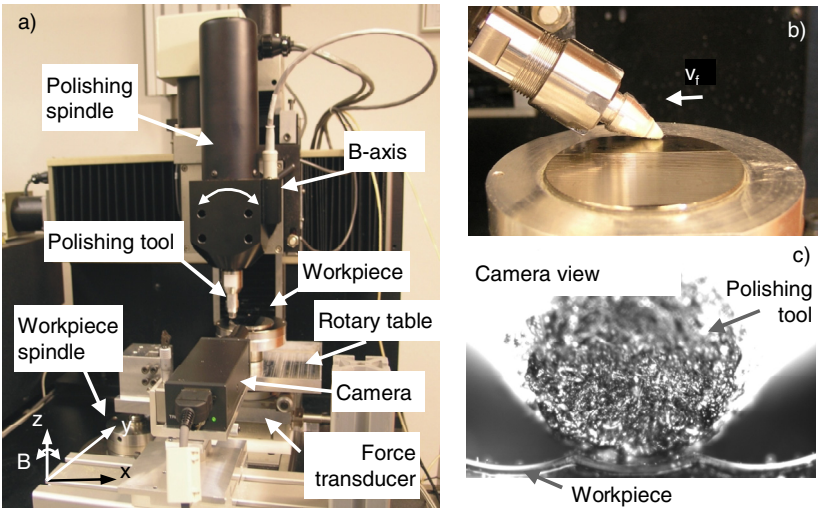


**Fig. 11** Experimental set-up for polishing cylindrical lens arrays [Bri09]

Compared to conventional polishing processes, the polishing tools for structured surfaces are contacting a much smaller area of the workpiece. The tool material must have a high strength of shape but be still soft enough to embed abrasives to ensure the polishing effect [Sch08a]. Preparation of the exact tool

shape is realized by diamond turning in-situ on the polishing machine. Hence, the material must also be machinable by turning operations. The potential of different tool materials was investigated. Organic felt material offers a good polishing effect but a very low strength of shape and no machinability. By impregnating the material to carbonized felt diamond turning of the tool tip becomes possible. But the inhomogeneity of the organic fiber structure and the low wear resistance of the impregnation limit the application of this material. The plastics POM (polyoxymethylen) and PA6 (polyamide) were chosen for polishing experiments because of the very high strength of shape and the good machinability with diamond tools. But a very low polishing effect was achieved with POM/PA6 as only a few abrasives situated in the contact zone between the hard plastic material and the workpiece surface. For the presented experiments laminated pear woods were used. This hard wood has good diamond tool machinability, leads to a good polishing effect and offers a high wear resistance during the polishing process.

The profile polishing of the cylindrical lens array's mold insert was realized by a pin type polishing tool with a planar front side [Sch08b]. The tilt of the planar front side guarantees a constant velocity in the cylindrical groove because of the cylinder edge contact area (linear engagement). By adapting the cylinder diameter of the polishing tool and tilting it the resulting contact ellipse in the workpiece groove ensures a homogeneous polishing pressure. Following polishing parameters were selected:

- Polishing tool: tilted cylindrical pin (inclination: 57°) with planar front side made of laminated hardwood (pear)
- Diamond suspension: oil based (abrasive size: 3 µm)
- Rotation speed: $n = 2500\ min^{-1}$ (relative velocity: $v_r = 4.103$ mm/min)
- Polishing force: $F = 0.2$ N (polishing pressure: $p = 0.8\ N/mm^2$)
- Feed rate: $v_f = 5$ mm/min
- Machining cycles: 2 (± feed direction)

A detailed process analysis is given in Figure 12. It shows the mold insert quality of one single groove. Measurements with white light interferometry show an improvement of the surface quality from $Sa \approx 40$ nm to $Sa < 10$ nm, [Klo07b]. The shape measurement was done by profilometry. Here, a constant shape deviation below 0.5 µm is visible. Only at the groove tips a minimal tool material deformation leads to edge rounding resulting from the compression load during polishing. The tip radius was expanded from 0.005 mm to 0.007 mm.

## *3.1 Resume*

Metal-bonded fine grained diamond grinding wheels can efficiently be used for precision profile grinding of filigree structured mold inserts in highest form accuracy. The resulting surface quality in the range of 40 nm Ra depends on the grit size and on the grinding kinematics. Wire-EDM can successfully be used for trueing and dressing of the grinding wheels. By abrasive profile polishing the roughness of the cylindrical grooves can be improved to optical quality. Therefore, this polishing process is applicable in optical mold making to increase the quality of replicated structured glass lenses.

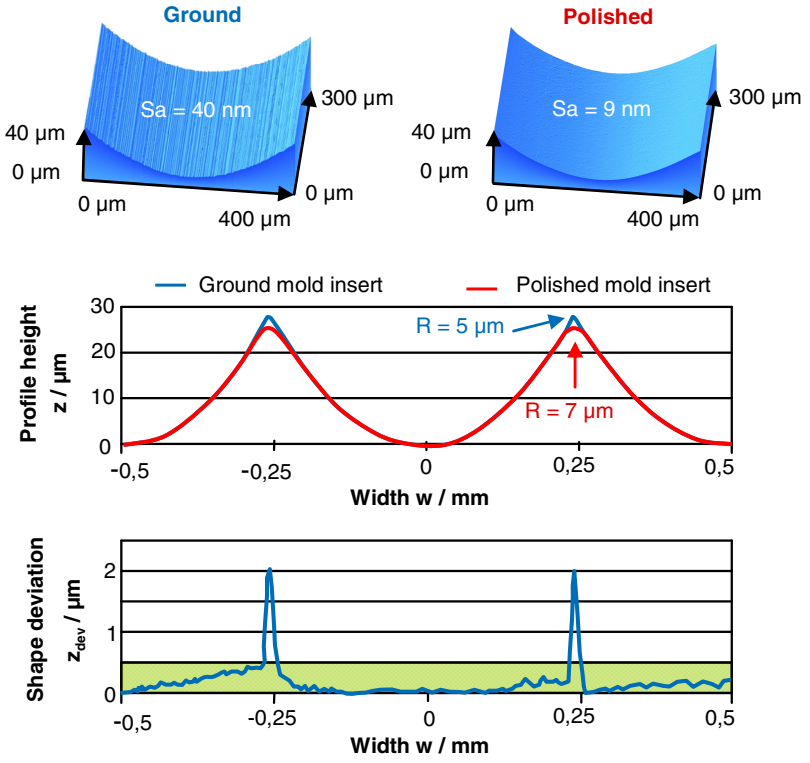


**Fig. 12** Comparison of roughness and profile before and after polishing

## 4 Conclusion

In this chapter, two process chains were presented introducing novel processes for manufacturing of cemented carbide molds with rotationally symmetric and structured surfaces for precision glass molding operations.

It was shown that diamond profile grinding in combination with electrochemical in-process dressing is capable of machining molds with continuous surfaces directly in optical quality. A subsequent polishing process is not necessary and therefore the process chain is condensed which saves time and will lower the manufacturing costs (Figure 13a).

In the second process chain the manufacturing of a mold insert with cylindrical lens array geometry by precision diamond profile grinding and abrasive profile polishing is presented. It was shown that the novel process combination of diamond profile grinding together with Wire-EDM trueing and dressing is capable to create lens arrays with highest profile constancies. By abrasive profile polishing the roughness of the grooves can be improved to optical quality without critical shape deviation. Thus precision glass molding can directly replicate filigree micro structured glass optics, as shown in Figure 13b.

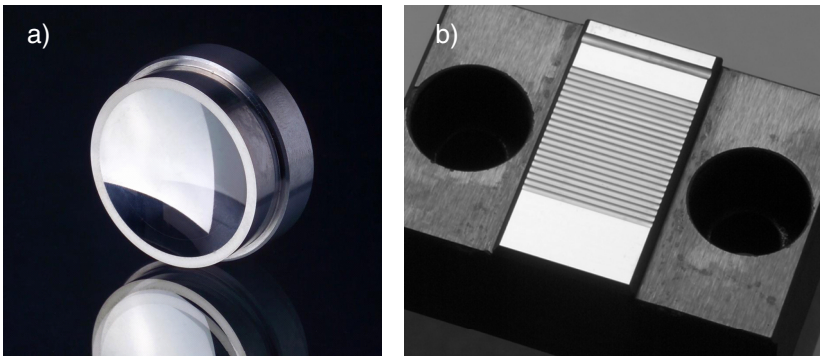


**Fig. 13** Finished cemented carbide glass mold inserts in optical quality

In conclusion the two presented process chains were designed and optimized by applying basic research and development and can now be applied to almost any user defined geometry.

## References

[Bri09] Brinksmeier, E., Riemer, O., Schulte, H.: Mechanisches Polieren linearer und räumlich begrenzter Strukturen. Jahrbuch Schleifen, Honen, Läppen und Polieren, pp. 282–298. Vulkan Verlag, Essen (2009)

[Bri10] Brinksmeier, E., Mutlugünes, Y., Klocke, F., Aurich, J.C., Shore, P., Ohmori, H.: Ultra-precision grinding. Annals of CIRP 59(2), 652–671 (2010)

[Kli09] Klink, A.: Funkenerosives und elektrochemisches Abrichten feinkörniger Schleifwerkzeuge, Dissertation. RWTH Aachen (2009)

[Klo07a] Klocke, F., König, W.: Fertigungsverfahren 3. Abtragen, Generieren und Lasermaterialbearbeitung, pp. 30–37. Springer, Berlin (2007)

[Klo07b] Klocke, F., Brinksmeier, E., Riemer, O., Klink, A., Schulte, H.: Manufacturing structured tool inserts for precision glass moulding with a combination of diamond grinding and abrasive profile polishing. Industrial Diamond Review (4), 64–69 (2007)

[Klo08] Klocke, F., Klink, A., Henerichs, M.: ELID Dressing Behaviour of Fine Grained Bronze-Bonded Diamond Grinding Wheels. In: Proc. of the 1st Int. ELID Grinding Conference, Changsha, pp. 12–18 (2008)

[Klo10] Klocke, F., Schwade, M., Klink, A.: Precision Grinding with In-Process ECM-Dressing. In: Proc. of the 10th Euspen Int. Conf., vol. 2, pp. 339–342 (2010)

[Mas85] Masuzawa, T., Fujino, M., Kobayashi, I.I.S.: Wire Electro-discharge Grin-ding for Micro-Machining. Annals of CIRP 34(1), 431–434 (1985)

[Ohm90] Ohmori, H., Nakagawa, T.: Mirror Surface Grinding of Silicon Wafers with ELID. Annals of CIRP 39(1), 329–332 (1990)

[Sch07] Schulte, H., Riemer, O., Brinksmeier, E.: Surface finishing of ground micro-structured glass molds. In: Proc. of the 7th Euspen Int. Conf., vol. 2, pp. 237–240 (2007)

[Sch08a] Schulte, H., Riemer, O., Gläbe, R., Brinksmeier, E.: Characterization of Pad Materials in Abrasive Profile Polishing. In: Proc. of the ASPE 23th Annual Meeting Portland, Oregon, USA, vol. 43, pp. 428–431 (2008)

[Sch08b] Schulte, H., Riemer, O., Brinksmeier, E.: FEM-based Prevention of Process-related Local Shape Deviation during Polishing of Micro Structures. In: Proc. of the 8th Euspen Int. Conf., vol. 2, pp. 7–10 (2008)

[Sha96] Shaw, M.: Principles of Abrasive Processing. Oxford Uni. Press (1996)

[Uhl08] Uhlmann, E., Piltz, S., Oberschmidt, D.: Machining of micro rotational parts by wire electrical discharge grinding. Prod. Eng. Res. Devel. 2, 227–233 (2008)

# Deterministic Polishing of Smooth and Structured Molds

Fritz Klocke, Christian Brecher, Ekkard Brinksmeier, Barbara Behrens, Olaf Dambon, Oltmann Riemer, Heiko Schulte, Roland Tuecks, Daniel Waechter, Christian Wenzel, and Richard Zunke

**Abstract.** The replication of ultra precise optical components requires molds with an extremely low surface roughness, a minimum of defectivity and high shape accuracy. To meet these demands polishing is essential. In comparison to other fields of application, polishing molds combines high demands and new geometries, e.g. aspherical cavities or structured surfaces for cylindrical lens arrays. Due to a lack of suitable polishing strategies, tools and innovative tool machines, the molds often have to be polished manually. In this chapter the authors discuss the major aspects for deterministic polishing starting from basic investigations on the material removal mechanisms to process strategies, tool development and design of innovative polishing tool machines. The materials dealt with reach from steel to advanced ceramics and tungsten carbide. The addressed geometries are smooth molds with a continuous surface as well as structured surfaces. The discussed issues look at the needs in replication of both plastic and glass optics.

## 1 Introduction

One key to success in the replication of plastic and glass optics represents the mold inserts. Therefore, deterministic, powerful and automated manufacturing processes for the mold making are required. Polishing forms the most frequently

Fritz Klocke · Barbara Behrens · Olaf Dambon · Richard Zunke
Fraunhofer Institute for Production Technology IPT,
Steinbachstraße 17, 52074 Aachen, Germany

Christian Brecher · Roland Tuecks · Daniel Waechter · Christian Wenzel
Laboratory for Machine Tools and Production Engineering WZL, RWTH Aachen,
Steinbachstraße 19, 52074 Aachen, Germany

Ekkard Brinksmeier · Oltmann Riemer · Heiko Schulte
Laboratory for Precision Machining LFM, University of Bremen, Badgasteiner Straße 2,
28359 Bremen, Germany

E. Brinksmeier et al. (Eds.): Fabrication of Complex Optical Components, LNPE, pp. 99–117.
springerlink.com 

used technology if high surface quality in terms of low roughness and high surface integrity is demanded. In many applications polishing secures the functionality of the samples. Due to its position at the end of the manufacturing sequence, it determines the sample quality substantially. For long-time polishing has been established in the conventional manufacturing of optics by grinding and polishing. In the fields of metal sheet forging or plastic injection molding, molds and dies have been polished manually for many years.

The manufacturing of molds for the replication of optics combines the high demands in terms of accuracy of the optics manufacturing with complex geometries, partly dealt with in mold and die making industry.

Within the SFB / TR4 several projects focused on the development of appropriate polishing machines, automated processes and the required fundamental understanding of polishing necessary for finishing mold inserts. Figure 1 provides an overview of the major influences, which determine the polishing result in terms of form accuracy, surface quality, sub-surface condition and efficiency (material removal rate).

Understanding the fundamental mechanisms of the material removal in polishing presents the key for the systematic development of polishing processes and helps to explain the causes of process instabilities and defects on the polished surfaces. This will be presented for the different mold materials in the next section.

In the field of mold and die making industry logical explanatory models are missing for describing defects like pull-outs which are the reason for many judicial issues. Process strategies for manufacturing 'defect free' high gloss polished tool steel surfaces will be shown and a defect chart with advices for avoiding defects will be presented in the second section.

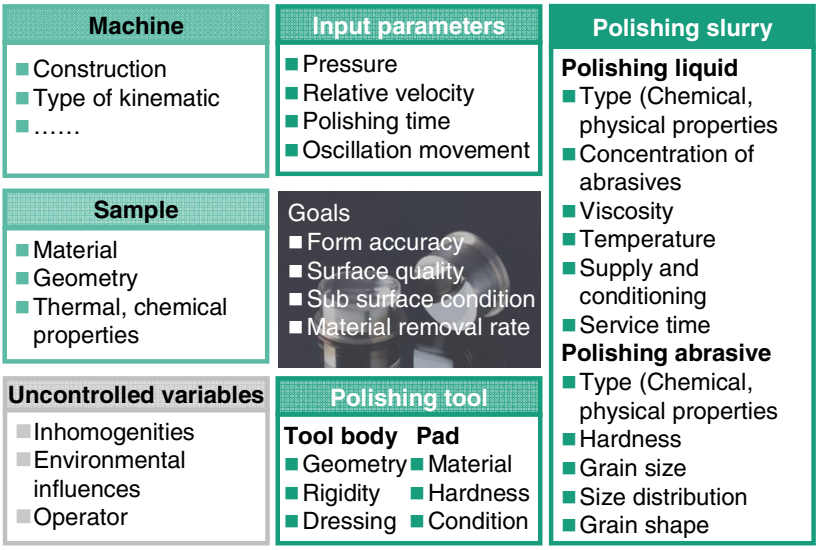


**Fig. 1** Overview of major influences on the polishing results

The following chapter describes an innovative polishing tool machine for local polishing of smooth, free formed surfaces. New membrane based tools are designed and analytical simulations support the choice of the most suitable polishing kinematic in regard to the final surface texture and shape accuracy.

Optical and medical industries are demanding a large variety of optical elements exhibiting complex geometries in the shape of localized cavities or grooves. The authors finally present the development of a new abrasive polishing process for finishing structured molds, which is exclusively realized by vibration motion [Bri09, Schu09, Bri10]. The absence of rotational tools opens up the possibility to machine new types of surface geometries.

## 2 Fundamental Mechanism in Polishing

Four hypotheses about material removal mechanisms in polishing emerged from the investigations on the chemical and physical phenomena in polishing [Ham01, Eva03]. These are the hypothesis of abrasion, the flow hypothesis, the chemical hypothesis and the friction wear hypothesis. Recent research activities focus on the interaction between the system components [Xie96, Kom97, Luo04, Cha08], for example the interaction between an abrasive grain, the sample surface and the polishing pad. *Evans et al.* provide an extensive discussion of the two-component and three-component interactions in the process area [Eva03].

In the following discussion, fundamental differences in material removal mechanisms are expressed by grouping them into two categories: a merely mechanical removal mechanism and a chemical-mechanical one. The mechanical removal mechanism refers particularly to the abrasion and flow hypothesis as well as the abrasive wear theory. *Samuels* stated that the difference between grinding and polishing is only in terms of scratches' and chips' magnitude, but not in terms of removal mechanisms [Agh70, Sam03]. The flow hypothesis, developed by *Beilby*, *Tabor* and *Bowden* [Bei21, Bow50], assumes the occurrence of material displacements and the formation of an modified surface layer.

The chemical-mechanical removal mechanism combines chemical and mechanical effects for explanation of material removal. Examples are the friction wear theory or the developed understanding of chemical-mechanical planarization (CMP) in wafer processing [Kom96, Jia01, Eva03].

Preston's equation represents the basis for modeling the polishing process [Pre27]. It states that the material removal rate dz/dt is proportional to the applied pressure p and to the relative velocity $v_R$ between the sample and the polishing pad:

$$\frac{dz}{dt} = K_P \cdot p \cdot v_R \tag{1}$$

The design of many polishing machines and of nearly all polishing processes is based on Preston's equation. Additionally, more complex predictive models were developed [Xie96, Luo04, Cha08, Wan08], particularly in CMP.

By the design of the polishing system the occurrence of a specific material removal mechanism can be influenced. The polishing system is defined by the sample material, the polishing liquid, the polishing agent and the polishing pad. In

the following, the basic mechanisms and their effects on the surface and sub surface area in polishing steel, advanced ceramics and tungsten carbide are explained when applying one specific material removal mechanism.

## 2.1 Polishing of Steel

Within the SFB / TR4 best results in polishing steel were achieved with diamond slurries. Based on the assumption that the material removal is predominantly of abrasive nature, the chip formation mechanism can be modeled as follows: The polishing grain penetrates the work piece surface and scratches across the surface, embedded in the polishing pad [Dam05, Klo06a]. Both the resulting normal and tangential load generate stresses in the form of pressure, tension and shearing. As soon as the yield strength of the material is exceeded, the stresses lead to plastic deformation [Klo05]. The grooving grain displaces material and, once, the maximum formability is reached, chip formation occurs. A detailed analytical calculation of the penetration depth of a single abrasive grain and the resulting material flow stresses can be found in [Klo08a]. Further chemical aspects in polishing steel are discussed in [Dam05, Klo06b].

In order to draw conclusions on removal mechanisms and chip formation, hardened and unhardened CrMo-steels were investigated [Klo05, Dam05]. One astonishing result is, that hardened steels shows higher material removal rates (MRR) than unhardened ones. The experiments also revealed, that a better surface roughness is reached with hardened steels than with unhardened ones [Klo05].

According to *Zum Gahr*, different chip formation mechanisms can be characterized from the ratio of the displaced volume to the volume of the cutting trace [Gah98]. In the so called micro ploughing only material displacement takes place. In contrast, in micro cutting the removed volume equals the volume of the cutting trace. The findings on the MRR correspond with *Zum Gahr's* wear theory. In polishing ductile, unhardened steel the degree of plastification and material displacement is higher than in polishing brittle, hardened ones. A higher ratio of micro ploughing occurs and the amount of removed material is lower. Contrarily, because of the high dislocation density in hardened steels no significant material displacement appears, but cutting of material occurs instantaneously [Dam05, Klo05].

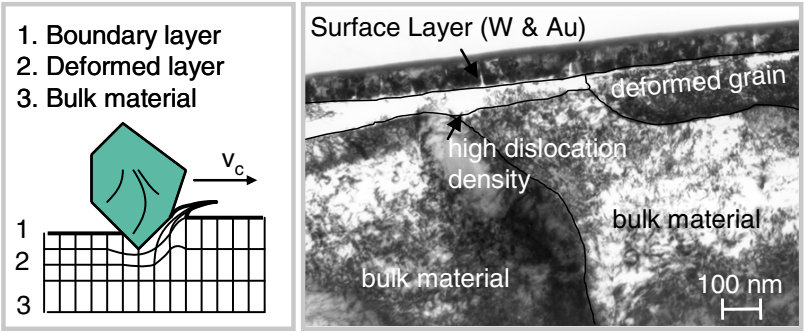


**Fig. 2** Sub surface condition of an unhardened steel after polishing with diamond (TEM, right)

TEM analyses confirm that hardened steel, with its martensitic structure, is less subject to plastic deformation. In terms of unhardened steel a boundary layer close to the surface can be identified with strongly deformed grains and significantly higher dislocation density (Figure 2). In deeper regions, no influence of the polishing process on the lattice structure can be observed. In terms of hardened steel, a boundary layer with a high amount of dislocations can not be identified [Dam05].

## *2.2 Polishing of Advanced Ceramics*

Both silicon carbide and silicon nitride are widely known for superior material properties. In specific applications, for example molds, polishing of these advanced ceramics is required to ensure low surface roughness and damage free subsurface regions.

To clarify the effects of both distinguished material removal mechanisms, investigations on polishing silicon carbide (SIC) and silicon nitride (HIPSN) are summed up [Klo07a, Klo09a]. Three different types of slurries were employed: water-glycol with diamonds (synthetic, 2-4 µm), and two water based slurries with ceria (Opaline by Rhodia) resp. with zirconia (CC10TM by Saint-Gobain). The usage of a diamond slurry results obviously in a mechanically dominated removal mechanism [Kom97, Eva03, Dam05, Klo09a]. Ceria and zirconia slurries feature chemical-mechanical interactions [Kom96, Klo07a]. Due to their lower hardness compared to the ceramics pure abrasion can be excluded.

The occurring material removal mechanism effects the MRR, the surface quality and the influence of machining parameters. Figure 3 indicates the dependency of MRR on material and material removal mechanism, determined by the design of the slurry [Klo09a].

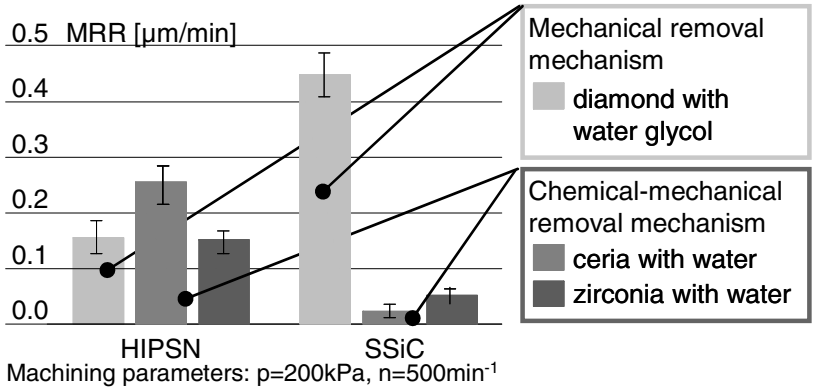


**Fig. 3** Average MRR in polishing silicon based ceramics with various polishing agents

Apparently, employing diamond is the best choice for polishing silicon carbide. In contrary, the usage of the water based ceria slurry was an efficient choice in processing silicon nitride.

An statistical analysis of the influence of pressure and relative velocity on the MRR indicates that they do not show the same effect for all material removal mechanisms. In diamond polishing an increase of both input parameters results in a similar effect on the MRR which correlates with the Preston's equation. Whereas, if using ceria or zirconia, the relative velocity does not effect significantly the MRR in the same manner as the applied pressure. Therefore, the actual removal mechanism has to be considered regarding the choice of machining parameters [Klo09a].

In addition to the empirical investigations, the influence of the material removal mechanism on the surface and sub surface area was investigated by SEM, TEM, and AFM [Klo09a]. After polishing with diamond, the subsurface layer of both ceramics reveals dislocations up to 100 nm. They reach deeper in HIPSN than in SIC. The high toughness of silicon nitride implicates that the applied polishing work is converted to form the dislocations before any micro chipping occurs. In contrary, the high brittleness of silicon carbide leads primarily to micro chipping and cracking [Klo09a].

Following the general argumentation for chemical-mechanical polishing of HIPSN, the silicon nitride surface is worn by hydrolysis with the aid of ceria as a catalyst [Kom96, Jia01, Hah99]. In a second step, ceria removes the formed oxide layer. Own investigations revealed several indicators for the validity of this hypothesis, e.g. an observed increase of pH and a measured amount of ammonia in the slurry [Klo09b]. After chemical-mechanical polishing TEM analyses show a complete absence of any dislocations in the subsurface layer and the surface seems to be free of scratches on AFM images [Klo09a].

## *2.3 Polishing of Tungsten Carbide*

Binder less tungsten carbide represents a common choice of material for the molds and dies in precision glass molding. That is why the previous explained methodology is extended on binderless tungsten carbide. The investigated type shows a ratio of binder below 0.30 % and an ultrafine texture with an average grain size below 200 nm. Due to the high chemical wear resistance of the material, the investigation focuses on a mechanical dominated material removal mechanism.

The effects of the relative velocity and the applied pressure on MRR (Figure 4) show that the Preston's equation can also be applied to describe the material removal when polishing tungsten carbide. But both parameters do not effect the resulting surface quality significantly in terms of roughness parameters. The values of Rms are below 2 nm and the peak to valley roughness below 20 nm (diamond grit size 2-4 µm, polyurethane polishing foil). This result implies that binder less tungsten carbide can be polished with high removal rates without decreasing surface quality, which is not given in polishing steel and advanced ceramics.

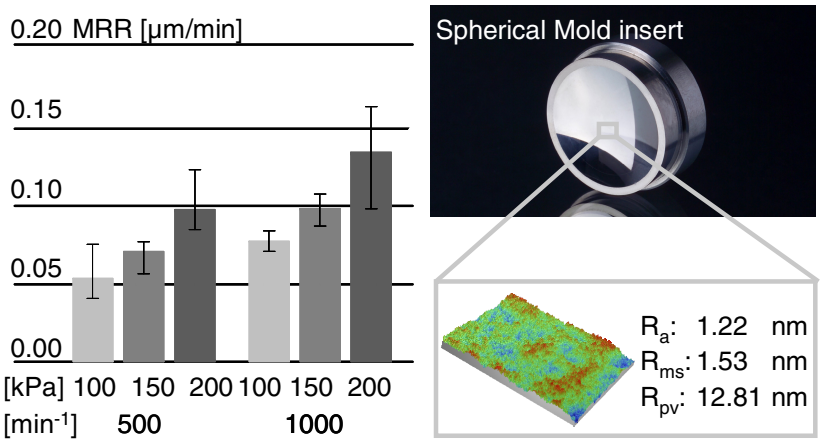


**Fig. 4** Influence of applied pressure and spindle revolution on MRR (left) and average surface roughness (right)

The fundamental investigations were applied on spherical mold inserts, shown on right side of Figure 4, which confirms the feasibility of polishing tungsten carbide in short time with a high surface quality.

## 3 Polishing Processes for the Mold and Die Making Industry

The polishing process in the mold and die making industry is mainly done manually. The quality of a manual polished mold strongly depends on the worker's skill and experience. In order to reduce this dependency, the main goal of the research at Fraunhofer IPT consists in the automation of the polishing process in order to support the worker up to 80% of his manual, monotone work. But previous to the automation a complete understanding of the polishing process and the influencing parameters is essential.

An important aspect is to find logical explanatory models for describing the appearance of imperfections which are a knock-out criterion for the required surface of the final plastic part and the reason for many judicial issues between polisher, steel manufacturer, mold maker and end user.

In the transfer project named SFB/TR4-T3, process strategies for manufacturing of defect free high gloss tool steel surfaces were developed in purpose to get robust strategies for avoiding the imperfections and/or giving advices about what to do when surface imperfections appear.

### *3.1 Polishing Strategies and Influencing Parameters*

To gain a complete understanding of the polishing process, many experiments on different tool steels have been executed in order to analyze the influencing parameters on a polished surface in a scientific manner. The following relevant parameters have been examined during the project:

- steel composition and structure,
- manufacturing process,
- polishing kinematics,
- cleaning strategies and
- polishing systems.

Experiments with different steel compositions gave evidence that small differences in the alloying elements such as manganese, molybdenum and vanadium don't affect the polishing result. Although, differences in microstructure and steel manufacturing show clearly that the number of carbides and non-metallic inclusions are decisive for the quality of the polishing result.

In this context pull-outs might be the most interesting defects, as they appear as peaks on injection molded plastic parts, which therefore are rejected. They occur, as the name indicates, when carbides or non-metallic inclusions breaks out of the steel matrix. Four different scenarios are imaginable for the interaction between a diamond grain and a steel matrix containing carbides (Figure 5, left):

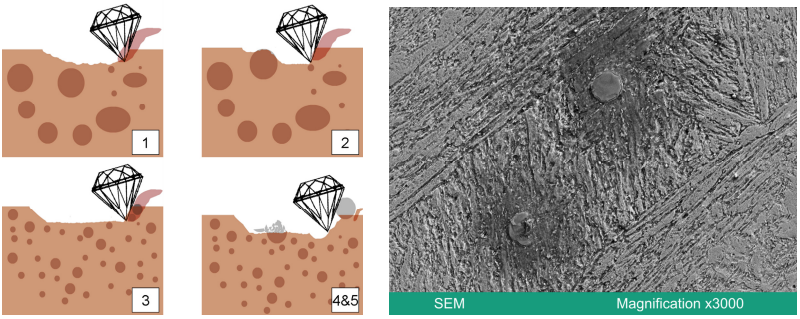


**Fig. 5** Interactions with diamond grain and steel surface (left) [Dam05], Non-metallic inclusion (right)

1. A typical mechanical abrasion of steel caused by a diamond grain (no carbide particles involved),
2. A diamond grain strikes a large primary carbide, which stays in the surface as it is still enclosed by the steel matrix,
3. Secondary carbides, which are smaller than the diamond grain, are removed out of the steel matrix and will not affect the surface quality,
4. Carbides having the same size as the diamond grain, or even larger, are not easily removed out of the steel matrix, but will be cut into pieces/or pulled-out by the diamond grain.

Another reason for the pull-outs are non-metallic inclusions (NMI), e.g. oxidic and/or sulphidic particles occurring as line shaped or globular inclusions. NMI can, as carbides, break out and leave holes or stay in the steel matrix, but in some cases only the softer material around the NMI is removed leaving a "stuffed hole" with the disadvantage that water can enter, leading to corrosions around actual inclusions (see Figure 5 right).

## 3.2 *Defect Chart*

As a first step towards an uniform polishing vocabulary, Fraunhofer IPT has created a defect chart in cooperation with the Swedish University of Halmstad [Reb09] on the basis of the European standard EN ISO 8785 [Eni99].

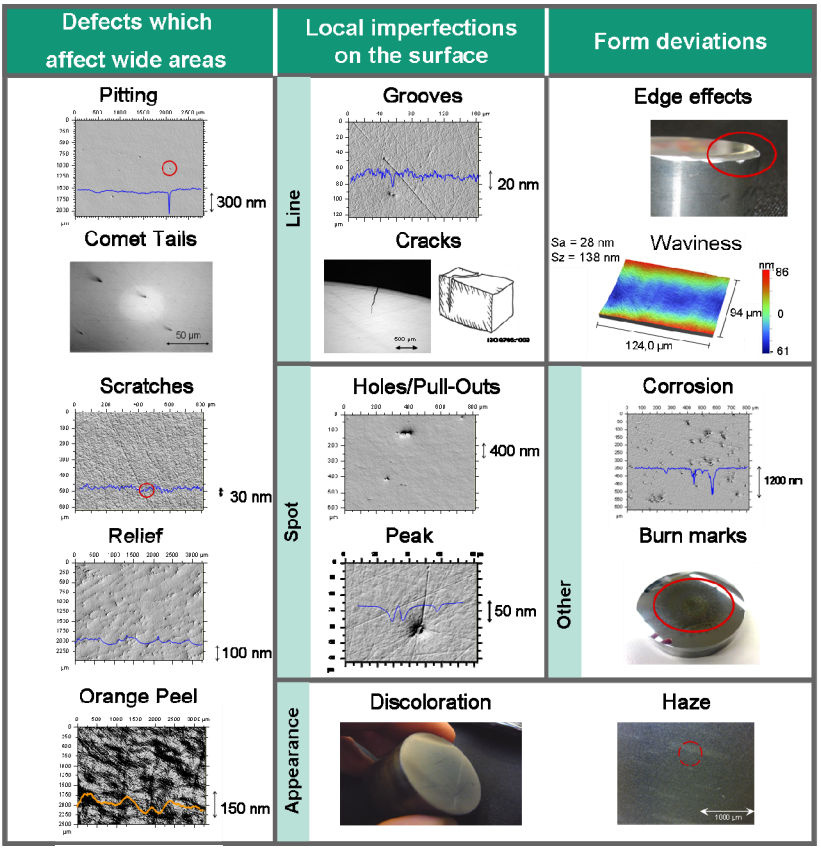


**Fig. 6** Classification of surface imperfections – defect chart

With this table and the according manifold experiments, polishing strategies for various examined steel grades were formulated and are presented on the SFB/TR4 homepage.

On the basis of these results, the aim of further research at Fraunhofer IPT is the development of automated, integrated and robotic polishing systems to compensate the disadvantages of manual processing and to support the manual polisher in his monotone work. The goal is to automate up to 80 percent of the polishing process so that only 20 percent of the work will still be performed manually. This was already shown on parts with freeform surfaces in a robot cell with an integrated force-controlled polishing spindle [Klo10].

# 4 Computer Controlled Polishing of Free Formed Surfaces

Replication technologies, such as the injection molding of plastics or the embossing of glass, bear a very high potential for a cost effective high quality mass production of such complex optical components. The key component within this complex process is the mold insert itself. However, little knowledge about the replication processes and insufficient possibilities of simulating the exact behavior of the deformed material cause a difficult and cost intensive ramp up. Due to the lack in calculation the shrinkage and inner tension related deformations of the replicated optics, the mold inserts has to be tested and iteratively adopted. The form correction machining of the molds for the optimization needs to be able to remove material in a range of a few microns to several tens of Nanometers in order to assure maximum shape deviations below a 100 nm PV. Usually, chemically and mechanically highly withstanding metals or even ceramics are used. A surface finish of down to 2 nm Ra are requested. Conventional path controlled machining such as milling or turning operation does not reach out to this level of accuracy.

## *4.1 Dwell Time Controlled Polishing*

Different from conventional milling or grinding operation, the locally applied polishing is a dwell time controlled process. The material removal is controlled by the feed-rate of the tool on the surface. The more material has to be removed, the slower the feed-rate is adjusted. For little removal the feed-rate is increased. This approach turns the achieved precision on the work piece away from the accuracy of the applied machine tool towards the process stability and a sophisticated pre-calculation of the pursuit polishing strategy. Presupposing the above, defined form corrections in the sub-micron range are possible on materials used in the optical mold making. The pre-calculation is conducted in an off-line mode prior to the actual polishing by an algorithm. As input data, the supposed geometry of the mold insert is needed. This geometry usually differs from the one of the final replicated optic due to the influence of shrinkage and inner tension that needs to be corrected. In addition, a shape measurement of the part taken either interferometrical or tactile is used to determine the local error map of the insert that needs to be corrected. The third requested input is the so called influence function of the locally applied polishing tool, describing the material removal profile in dependence of adjustable process parameters such as pressure and relative velocity. With the above three input variables the subsequent calculation of the polishing algorithm is based on an optimization assisted division of the influence function and the error profile, generating the ultra-precise polishing strategy. Of fundamental importance for the functionality of this machining approach with a pre-calculated dwell time map is a stable, reproducible and deterministically adjustable influence function. For the insurance of the control over the polishing influence function, extensive knowledge about the process itself especially including tribo-mechanical interactions is needed. Beyond this

understanding, a machining system is necessary providing and controlling constant process parameters even on complex form shapes.

## *4.2 Machining System – Adaptive Polishing Head*

At the Fraunhofer IPT a new, adaptable polishing head based on a parallel-kinematic-structure has been developed for the locally applied polishing. The machining system is capable of providing all the relevant kinematics for the polishing tool. The work piece does not have to be driven separately. Due to the kinematic setup of a specially designed Double-V-Parallel-Kinematic-Structure, eccentric movements, angles of precession and dynamic adaptations under consideration of the process relevant eccentricity can be realized. On account of the independence of a work piece rotation or linear movement, the process conditions are ideally stable, also on complex free-form shapes. A more detailed description of the mechanical setup and its control system can be found in [Wec04, Bre05]. Figure 7 shows the final design of the test bench used for the process parameter investigation.

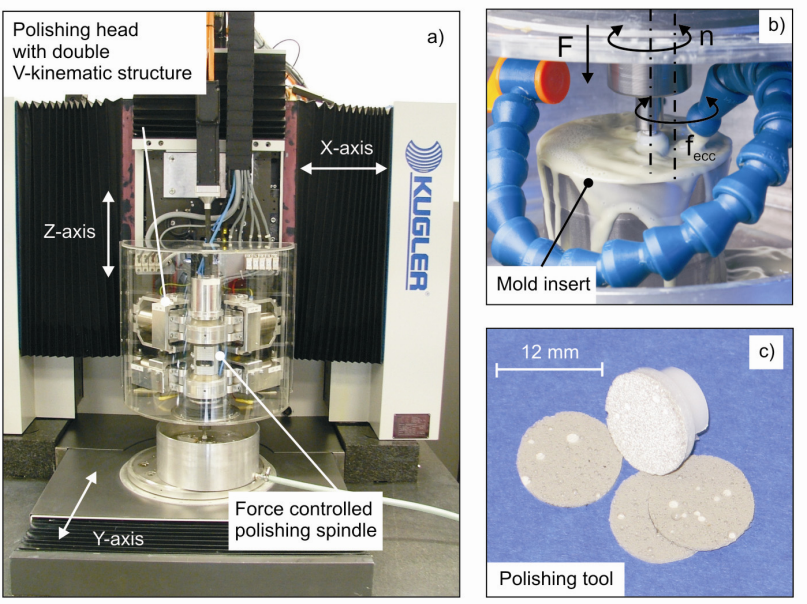


**Fig. 7** a) Machine tool setup used for investigations of the zonal polishing process, b) closer view on the polishing tool and process kinematic, c) polishing pad with polyurethane foil.

The overall machine system consists of a 3-Axis base machine and the attached adaptive polishing head with in addition have 5 DOF. The adjustable parameter ranges are given in table 1.

**Table 1** Parameter range of the polishing head

| | |
|---|---|
| Polishing force F | 0.5 - 20 N |
| Force increment | 0.2 N |
| Eccentric frequency $f_{ecc}$ | 1 - 10 Hz |
| Eccentric radius $r_{ecc}$ | 0.2 - 4 mm |
| Spindle revolutions n | 500 - 5000 $min^{-1}$ |

## *4.3 Process Development for the Zonal Polishing*

Numerous polishing strategies which determine the process conditions and hence the result of the finishing are used for scientific experiments regarding the influence function.

Taking *Preston's* equation for granted (Formula 1), a linear increase of the MRR should be realized starting from the center of the rotating tool. Figure 8 a) shows the accruing characteristic W-profile by the adjusted process parameters pressure p and relative velocity $v_r$ which are based on theoretical conversion of former specified values.

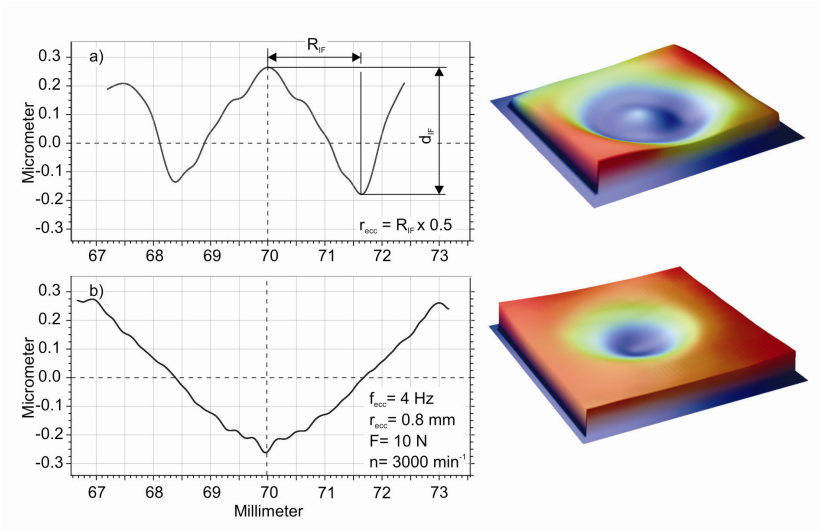


**Fig. 8** Determination of eccentric radius as the main parameter for achieving the required (b) Gaussian profile of the influence function »Footprint« - Process development on a silicon Nitride sample ($Si_3N_4$)

However, the maximum material removal is not found on the outer diameter but at one half to two thirds of the radius of the polishing tool, forming the influence function. Looking further towards the boundary of the influence function, the removal depth declines steadily. This simple trial emphasizes the fact that either an inhomogeneous pressure profile or an influence of the relative velocity in the gap between the tool and the sample is influencing the geometrical formation.

The influence function is characterized by depth $d_{IF}$ and radius $R_{IF}$ which in this case can be identified as 1.6 mm. Preliminary investigations on polishing of steel have shown that this dimension can be used for setting up the eccentricity of the polishing tool movement in order to achieve a Gaussian profile of the influence function [Bre05, Klo08b]. Further investigations lead to a ratio of $R_{IF}$ and eccentric radius $r_{ecc}$ of about 1:2. By using this value and an experimentally identified value for the eccentric frequency $f_{ecc}$ of 4 Hz the required Gaussian profile for the dwell time algorithm can be achieved as shown in figure 7 b). The appropriate volume of removed material $V_{IF}$ was computed by importing the 2D-graph of a Form TalySurf in a specially developed Matlab program and amounts to 0.005 mm³ on average (after polishing time of 240 s).

With the adaptive polishing head, a machine base is given to intensively investigate the formation of the influence function of a locally applied polishing tool. In terms of the machine parameters, the eccentric frequency shows only a small impact for the profile formation. However, the eccentric radius, the applied normal force and the relative velocity do have significant impact on the formation of the influence function determining the process efficiency. This kind of process development is of vital importance in order to conduct form corrections on high precision molds for replication purposes in plastic injection molding or embossing of glass.

## 5 Polishing of Structured Molds

Optical and medical industries are demanding a large variety of optical elements exhibiting complex geometries and multitude opto-functional areas in the range of a few millimeters [Eva99]. Therefore, mold inserts made of steel or carbides must be finished by polishing for the replication of glass and plastic lenses [Klo07b]. For polishing these complex components in the shape of localized cavities or grooves the application of rotating polishing pads is very limited [Bri07]. Established polishing processes are not applicable, so state of the art is a time consuming and therewith expensive polishing procedure by hand. Therefore, a new abrasive polishing process for finishing these complex mold geometries to optical quality was developed. The necessary relative velocity in the contact area between polishing pad and workpiece surface is exclusively realized by vibration motion which is an advantage over vibration assisted rotating polishing processes. The absence of rotation of the pad opens up the possibility to machine new types of surface geometries.

### *5.1 Polishing Machine*

The vibration polishing device is powered by two voice-coil actuators, see figure 9. These two actuators enable frequencies up to f = 150 Hz and amplitudes up to A = 250 µm in two axes and were implemented into a conventional machine tool [Bri10].

During the design process a large area of applicable machining frequencies and amplitudes was considered to achieve a multifunctional and flexible system.

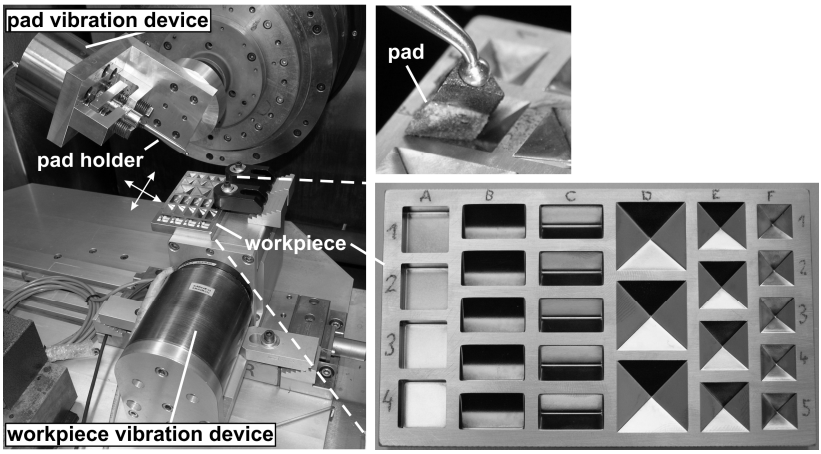


**Fig. 9** Vibration polishing test set up: voice-coil actuators on workpiece side and pad side [Bri10]

On pad side the control is realized open loop with spring return and variable stiffness as this concept enables the maximum vibrational frequency. On work piece side the control is realized closed loop with a position sensor.

## *5.2 Vibration Polishing Material Removal Characterization*

During material removal characterization the polished surface area (material removal function – "footprint") is divided into profile sections. The tip of the profilometer loaded with an adjustable normal force drives along these profiles with continuous speed. The height position of the tip is continuously recorded and with this information the surface contour for each profile section is created. By interpolation between the single profiles the 3D-shape of the measuring area can be evaluated. The data determined with this procedure realizes primarily the material removal calculation. The method for analyzing material removal is described on basis of one single profile section in figure 10 [Bri10]. The workpiece material below the reference height $h_{ref}$ is shown hatched. The remaining areas represent the void volume above and below $h_{ref}$. The distance $l_{tot}$ is the overall length of the measuring profile. The length $l_{ref}$ represents the measuring section, on which no material removal appeared. For calculating the removed material volume the difference from the average void volume of the reference length $V_{void,ref}/l_{ref}$ and the average void volume of the total distance $V_{void,tot}/l_{tot}$ is identified and multiplied with the total distance $l_{tot}$.

The material removal of one single profile is calculated as follows:

$$PMR(\,profile\,material\,removal\,) = \left( \frac{V_{void,tot}}{l_{tot}} - \frac{V_{void,ref}}{l_{ref}} \right) \cdot l_{tot} \tag{2}$$

If this procedure is applied to the entire measured area the material removal is calculated as follows:

$$FMR(\ field\ material\ removal\ ) = \left( \frac{V_{void,tot}}{A_{tot}} - \frac{V_{void,ref}}{A_{ref}} \right) \cdot A_{tot} \tag{3}$$

The process parameters pressure p, polishing time t and relative velocity $v_r$ were characterized regarding their linear dependence on material removal [Scu09], which can be expected according to Preston's equation (Formula 1).

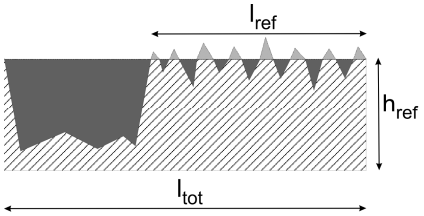


**Fig. 10** Parameter definition for material removal characterization

For validating the linear material removal behavior the parameters were varied on three levels. The polishing system consisted of a synthetic felt pad and an oil-based polishing slurry with diamond abrasives of a size of 1 µm. This system showed a good applicability and low variances. The experiments were accomplished with four repetitions at each level.

Figure 11 (left) shows the linear increase of the material removal dz over polishing time t. The stability index $R^2 = 98{,}6$ % indicates the fit of the measured values to the linear smoothing function. The error bars show the 66,7 % confidence region of the average values of the repetitions. The influence of the polishing time conforms the Preston's equation with variables kp, p and $v_r$ kept constant.

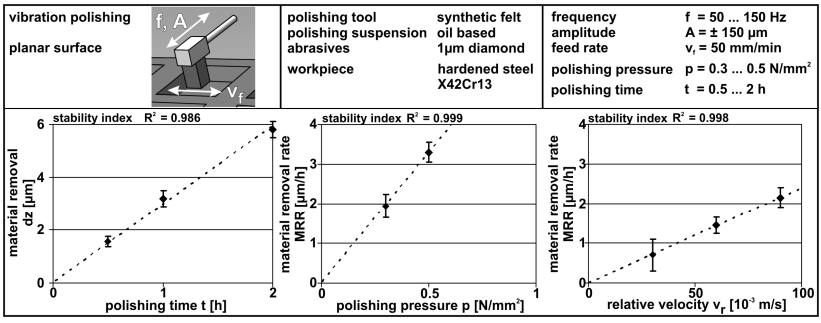


**Fig. 11** Verification of Preston's equation: influence of polishing pressure, relative velocity and polishing time on material removal [Schu09]

The polishing pressure was analyzed at two levels with four repetitions each. A pressure larger than p = 0.5 N/mm² is not practible because of the limited power of the vibration polishing head. A pressure smaller than p = 0.3 N/mm² would lead to very low material removal and therefore non detectible volumes. Figure 11 (center) shows the linear behavior of the polishing pressure within the covered pressure range and confirms also the Preston's equation.

The average relative velocity between polishing pad and workpiece is calculated from the total distance s and time t for one vibration period (1/frequency). The polishing pad covers s = 4 ·A (amplitude) during one period of oscillation. Hence, the value of relative velocity is calculated by

$$v_r = \frac{ds}{dt} = \frac{4 \cdot A}{f^{-1}} = 4 \cdot A \cdot f \tag{4}$$

In order to change the relative velocity both the oscillating amplitude and the oscillating frequency can be varied. The material removal rate was examined in dependence of the frequencies f = 50 Hz, 100 Hz and 150 Hz.

It is evident from figure 11 (right) that a linear dependence of frequency - and thus also the relative velocity - and the material removal rate is applicable. Therefore, Preston's equation can be applied to vibration polishing within the analyzed parameter range without restriction.

Figure 12 shows a polished rectangular slot which was machined to optical quality by vibration polishing [Bri09].

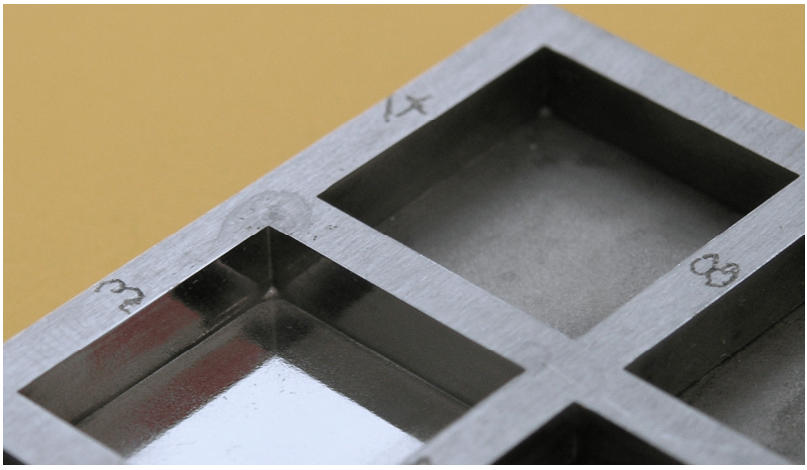

**Fig. 12** Reference workpiece with vibration polished slot [Bri09]

## 6 Conclusion

This chapter started with a fundamental discussion on the material removal mechanisms in polishing with regard to common mold materials. On the one side,

the effects of a mechanical removal mechanism, occurring when using diamond abrasives, on the surface and sub surface were discussed. On the other side, a damage-free chemical-mechanical removal mechanism for polishing silicon nitride was presented. The scientific driven first section was developed to an application ready state for polishing steel molds in the second section. With the explained defect chart and the development of robust process strategies a first step towards a common understanding of the polishing step is made with the goal of an international standardization.

With the adaptive polishing head developed at the Fraunhofer IPT, a machine base is given to intensively investigate the formation of the influence function of a locally applied polishing tool. The machine in combination with the process development enables form corrections on high precision molds, which result in higher accuracies of the molded optics with less iteration in mold making process.

Finally, for finishing complex shaped optical mold inserts a novel polishing process was presented, which operates without the classical rotating motion of the polishing pad and therefore can be used more flexibly at finite-dimensional opto-functional surfaces.

**Acknowledgement.** The authors like to thank the German Research Foundation (DFG) for funding this work as a part of the Transregional Collaborative Research Center SFB/TR4 “Process Chains for the Replication of Complex Optical Elements”.

## References

[Agh70] Aghan, R.L., Samuels, R.L.: Mechanisms of Abrasive Polishing. Wear 16, 293–301 (1970)

[Bre06] Brecher, C., Wenzel, C.: Kinematic Influences on the Formation of the Footprint During Local Polishing of Steel. WGP Annals XIII(1), 23–26 (2006)

[Bri07] Brinksmeier, E., Riemer, O., Schulte, H.: Kinematiken zum Polieren von Mikrostrukturen. Wt Werkstattstechnik Online 97, 431–436 (2007)

[Bri09] Brinksmeier, E., Riemer, O., Schulte, H.: Mechanisches Polieren linearer und räumlich begrenzter Strukturen. Jahrbuch Schleifen, Honen, Läppen und Polieren: Verfahren und Maschinen, pp. 282–298. Vulkan Verlag, Essen (2009)

[Bri10] Brinksmeier, E., Riemer, O., Schulte, H.: Material removal mechanisms in abrasive vibration polishing of complex molds. In: Advanced Optical Manufacturing Technologies, Proceedings of 5th International Symposium on Advanced Optical Manufacturing and Testing Technologies, AOMATT 2010. SPIE, vol. 7655-02 (2010), doi:10.1117/12.864553

[Bei21] Beilby, G.: Aggregation and Flow of Solids. McMillan and Co. Ltd., London (1921)

[Bow50] Bowden, F.P., Tabor, D.: The Friction and Lubrication of Solids. Clarendon Press, Oxford (1950)

[Cha08] Chandra, A., Karra, P., Bastawros, A.F., Biswas, R., Sherman, P.J., Armini, S., Lucca, D.A.: Prediction of scratch generation in chemical mechanical planarization. Annals of the CIRP 57(1), 559–562 (2008)

[Dam05] Dambon, O.: Das Polieren von Stahl für den Werkzeug- und Formenbau, PhD thesis, Shaker, Aachen (2005)

[Eni99] Deutsches Institut für Normung e.V., DIN EN ISO 8785: Geometrische Produktspezifikationen (GPS) – Oberflächenunvollkommenheiten (Oktober 1999)

[Eva99] Evans, C.J., Bryan, J.B.: "Structured", "Textured" or "Engineered" Surfaces. CIRP Annals – Manufacturing Technology 48-2, 541–555 (1999)

[Eva03] Evans, C., Paul, E., Dornfeld, D., Lucca, D., Byrne, G., Tricard, M., Klocke, F., Dambon, O., Mullany, B.: Material Removal Mechanisms in Lapping and Polishing. Annals of the CIRP 52(2), 611–634 (2003)

[Gah98] Zum Gahr, K.-H.: Wear by hard particles. Tribology 31(10), 587–596 (1998)

[Hah99] Hah, S.R., Burk, C.B., Fischer, T.E.: Surface Quality of Tribochemically Polished Silicon Nitride. J. Electrochem. Soc. 146(4), 1505–1509 (1999)

[Ham01] Hambücker, S.: Technologie der Politur sphärischer Optiken mit Hilfe der Synchrospeed-Kinematik, Ph-D-Thesis, University of Technology Aachen (2001)

[Jia01] Jiang, M., Komanduri, R.: Chemical Mechanical Polishing (CMP) in Magnetic Float Polishing (MFP) of Advanced Ceramic (Silicon Nitride) and Glass (Silicon Dioxide). Key Engineering Materials 202-203, 1–14 (2001)

[Klo05] Klocke, F., Dambon, O., Capudi Filho, G.G.: Influence of the polishing process on the near-surface zone of hardened and unhardened steel. Wear 258(11-12), 1794–1803 (2005)

[Klo06a] Dambon, O., Demmer, A., Peters, J.: Surface Interactions in Steel Polishing for the Precision Tool Making. CIRP Annals - Manufacturing Technology 55(1), 609–612 (2006)

[Klo06b] Klocke, F., Dambon, O., Schneider, U.: Removal Mechanisms in the Mechano-chemical Polishing of Steel Using Synchro-Speed Kinematics. In: Production Engineering, WGP (2008)

[Klo07a] Klocke, F., Zunke, R., Dambon, O.: Wirkmechanismen beim Polieren von Keramik. Wt Werkstattstechnik Online 97(6), 437–442 (2007)

[Klo07b] Klocke, F., Brinksmeier, E., Riemer, O., Klink, A., Schulte, H., Sarikaya, H.: Manufacturing structured tool inserts for precision glass moulding with a combination of diamond grinding and abrasive polishing. IDR Industrial Diamond Review 4, 65–69 (2007)

[Klo08a] Klocke, F., Dambon, O., Zunke, R.: Modeling of contact behavior between polishing pad and workpiece surface. In: Production Engineering, WGP (2008)

[Klo08b] Klocke, F., Brecher, C., Zunke, R., Tuecks, R.: Finishing Complex Surfaces with Zonal Polishing Tools. In: 41st CIRP Conference on Manufacturing Systems and Technologies for the New Frontier, Tokyo, Japan, May 26-28, pp. 445–448 (2008)

[Klo09a] Klocke, F., Zunke, R.: Removal mechanisms in polishing of silicon based advanced ceramics. Annals of CIRP 58, 491–494 (2009)

[Klo09b] Klocke, F., Schneider, U., Waechter, D., Zunke, R.: Computer-based monitoring of the polishing processes using LabView. Journal of Material Processing, 6039–6047 (2009)

[Klo10] Klocke, F., Brecher, C., Zunke, R., Tücks, R., Zymla, C., Driemeyer Wilbert, A.: Hochglänzende Freiformflächen aus Stahlwerkzeugen. Wt Werkstattstechnik Online, Jahrgang 100, Heft 6, 480–486 (2010)

[Kom96] Komanduri, R., Umehara, N., Raghunandan, M.: On the Possibility of Chemo-Mechanical Action in Magnetic Float Polishing of Silicon Nitride. J. of Tribology 118(4), 721–727 (1996)

[Kom97] Komanduri, R., Lucca, D.A., Tani, Y.: Technological Advances in Fine Abrasive Processes. Annals of the CIRP 46(2), 545–596 (1997)

[Luo04] Luo, J., Dornfeld, D.: Integrated Modeling of Chemical Mechanical Planarization for Sub-Micron IC Fabrication. Springer, London (2004)

[Pre27] Preston, F.W.: The Theory and Design of Plate Glass Polishing Machines. Journal of the Soc. of Glass Technology 11, 214–256 (1927)

[Reb09] Rebeggiani, S.: Polishability of Tool Steels – Characterisation of High Gloss Polished Tool Steels. Department of Materials and Manufacturing Technology, Chalmers University of Technology, Göteborg (2009)

[Sam03] Samuels, L.E.: Metallographic Polishing by Mechanical Methods. ASM International (2003)

[Scu09] Schulte, H., Riemer, O., Brinksmeier, E.: Finishing complex mold inserts by abrasive vibration polishing. Technical Digest of the SPIE Optifab, TD 06-18, Rochester, New York, USA (2009)

[Wan08] Wang, Y., Zhao, Y., Jiang, J., Li, X., Bai, J.: Modeling effect of chemical-mechanical synergy on material removal at molecular scale in chemical mechanical polishing. Wear 265(5-6), 721–728 (2008)

[Wec04] Weck, M., Wenzel, C.: Adaptable 5-axes Polishing Machine-head. Production Engineering 11(1), 95–98 (2004)

[Xie96] Xie, Y., Bhushan, B.: Effects of particle size, polishing pad and contact pressure in free abrasive polishing. Wear 200(1), 281–295 (1996)

# Process Chain for the Replication of Complex Optical Glass Components

Fritz Klocke, Olaf Dambon, Allen Y. Yi, Fei Wang, Martin Hünten, Kyriakos Georgiadis, Daniel Hollstegge, and Julia Dukwen

**Abstract.** Precision glass molding is becoming a promising technology for fast production of complex optical glass components in high volume. It is a replication process and becomes economical after a few batches. The glass molding process can be holistically described by a process chain which starts with the design of the optical component and modeling of the glass molding process using numerical simulation. An ultraprecision grinding process is applied to manufacturing the molds. Chemically insert coatings are necessary in order to prolong mold life because the mold has to withstand high mechanical and thermal loads. The parameters of the subsequent molding steps such as temperature or pressure depend on the type of glass and the size of the optical component. The last step of the process chain is the qualification of the optical components by measuring their optical properties using precision metrology.

## 1 Introduction

The demand for high-precision, complex-shaped optical components is rapidly growing worldwide. Such components are used in classical metrology applications, such as camera lens modules in mobile phones, optical systems in automobiles or for optical storage media in information technology.

The traditional production method for optical components is grinding, followed by a polishing step. This method is not economical for manufacturing of complex shaped components such as aspheric lenses, free-form lenses or lens arrays in medium to large quantities. The final polishing step is extremely costly and therefore it is only selected for very high-quality components in small volume.

As optical materials, glasses offer many advantages over optical polymers. Glasses have not only higher transparency but also lower susceptibility to

Fritz Klocke · Olaf Dambon · Fei Wang · Martin Hünten · Kyriakos Georgiadis · Daniel Hollstegge · Julia Dukwen
Fraunhofer Institute for Production Technology IPT, Steinbachstraße 17, 52074, Aachen, Germany

Allen Y. Yi
Ohio State University, Ohio, 210 Baker Systems, Columbus, OH 43210, USA

E. Brinksmeier et al. (Eds.): Fabrication of Complex Optical Components, LNPE, pp. 119–132.
springerlink.com 

corrosion and higher strength. Another advantage of glasses is the higher power density they allow. This is necessary for high-energy laser and high power lighting applications. In addition, glasses provide a greater range of refraction indices than optical polymers. On the market different glasses are available. These differences in their composition result in different optical properties.

The precision molding technology is an established technology for fast and economical production of complex optical components in large quantities. A glass preform and the molding tools are heated up to the molding temperature and pressed into the desired shape. In a single step, an optical component with double-sided functional surfaces and high accuracy is produced, without the need for subsequent finishing. Since the mold production by grinding and polishing is costly, and the precision glass molding is a replication process, the entire process chain only becomes economic after a minimum number of batches. By using multi-cavity tools, multiple optical components can be molded in one batch, thus increasing the efficiency of the process.

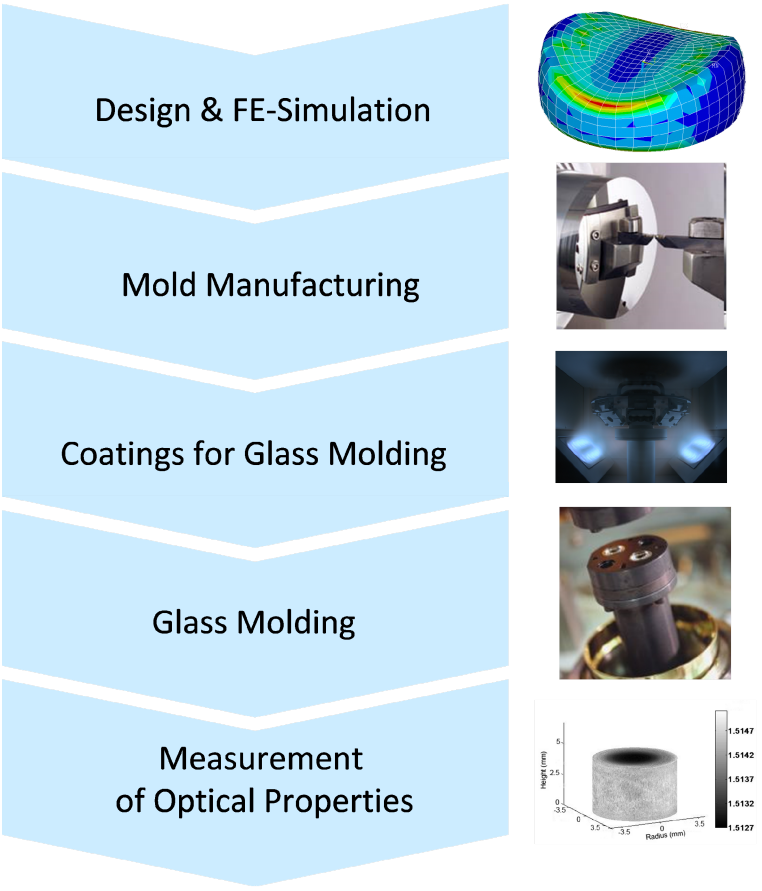


**Fig. 1** Process chain for the replication of glass components

Figure 1 describes the complete glass molding process. In the first step, the optical component is designed and the molding process simulated. Due to the different thermal properties of glass and mold, the lens has a non-negligible deviation from the desired shape after the pressing process because of the shrinkage of the glass during cooling. Using FEM simulation, the shrinkage of glass and changes of its optical properties such as refractive index after molding can be calculated. Taking this into account, the mold is manufactured. High demands are placed in the form accuracy and roughness of the mold, since any form deviations will be transferred to the optical component. To prolong the mold lifetime, protective coatings that prevent wear and thus increase the profitability of the process are deposited on the mold. The parameters of the pressing process such as temperature or pressure depend on the type of glass and the size of the optic. After the molding process, the quality of the lenses is controlled by measuring of their optical properties using precision metrology.

## 2 Design and FE-Simulation

### *2.1 Objective of Simulation*

In precision molding process, glass raw material is first heated to a temperature above its transition temperature (e.g., B270, Tg=533°C, forming temperature 625°C) and subsequently pressed into a lens shape, and then carefully cooled down together with the mold inserts. During pressing and cooling, many factors such as thermal expansion and stress relaxation affect molding process and thus lead to form deviation in final geometry and variation in refractive index. Therefore, by mold design, the surface deviation should be compensated on the mold surface based on the original lens design by adding a slight amount of correction, so that the molded lens matches both the geometrical and optical specifications. Traditionally, the amount of compensation is determined by costly- and time intensive trial and error molding. In recent years, numerical modeling is implemented to assist the mold making process to predict these errors before the actual mold manufacturing.

### *2.2 Thermal and Mechanical Modeling*

The process simulation of precision glass molding is developed based on FE method and consists of a thermal model predicting the actual temperature distribution and a mechanical model to predict the visco-elastic deformation and thermal shrinkage of the molded glass lens.

The thermal model considers all three heat transfer mechanisms occurring in a typical glass molding process (conduction, convection and radiation), in order to determine the temperature distribution and variation rate inside both the glass and mold volumes during the entire molding process. The temperature distribution determines the visco-elastic material behavior of glass material.

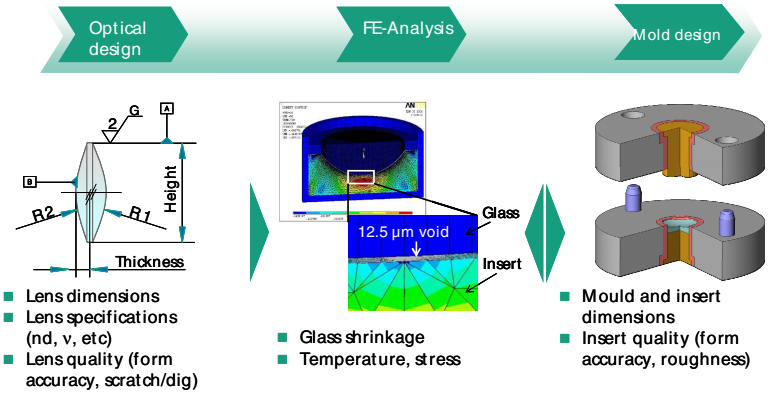


**Fig. 2** Design of molded optical glass components with the assistance of FE-simulation

For a typical visco-elastic material, such as glass at the molding temperature, the application of a constant load will lead to material deformation, which consists of instantaneous deformation (elastic effect) and continuous deformation over time (viscous effect). The visco-elastic property will cause decay of the applied load and this decay is called stress relaxation, which determines the deformation behavior of glass. To describe the visco-elastic behavior, a generalized Maxwell model expressed in Eq. 1:

$$G(t) = 2G\sum_{i=1}^{n} w_i exp(-t/\tau_i) \tag{1}$$

can be used to model the stress relaxation of glass at transition temperature [Dam09, Jai05, Jai06], where G(t) is the stress relaxation module, $\omega_i$ are weighting factor and $\tau_i$ are the corresponding relaxation times under certain temperature.

## 2.3 *Index Variation Modeling*

The refractive index of an optical glass changes after precision compression molding mainly due to structural relaxation in glass. In the past the phenomenon of group index drop has been studied using the Tool-Narayanaswamy-Moynihan (TNM) model for different heat treatment and cooling rates [End99]. Meanwhile inhomogeneous temperature distribution inside the glass during cooling can cause structural distortion and thus refractive index variation after cooling. According to Su et al.'s previous research, the refractive index variation inside the molded glass will also introduce substantial wavefront deviation for precision glass components [Nar71]. This index variation could be modeled by the famous Lorentz-Lorenz equation [Rit55]:

$$\frac{n^2-1}{n^2+2}=\frac{4\pi}{3}\frac{N_A\rho}{M}\alpha \tag{2}$$

where M is molar weight, $N_A$ is Avogadro number, ρ is density and α is mean polarization. Using this equation, refractive index distribution of a molded glass lens could be determined by calculating the density change. This prediction of index variation during molding is especially necessary for precision imaging optics, so that the variation can be compensated during the optical design stage.

### *2.4 Mold Design and Manufacturing*

After the process simulation in the FEM code like ANSYS, ABAQUS or MSC MARC, the calculated glass lens shape after shrinkage is compared to the desired form, which shows a maximum deviation of about several up to a hundred micrometer depending on different lens surface shape and diameter. For efficient compensation, the simulation result of shape deviation will be combined with the compensation value of the index drop and then fitted into standard non-spherical equation. The amount of deviation is directly mirrored on the mold surface as the compensation value. Based on this compensation, the mold inserts made of alloys and ceramics will be manufactured on precision grinding machine (e.g. Toshiba ULG-100D SH3), thus the molded glass lenses match the specification directly without any finishing steps.

## 3 Mold Manufacturing

Optical glass is molded between 350 and more than 800 °C depending on the glass type and its chemical composition. While so called low-Tg glasses can be molded using nickel plated mold materials, ceramic molds are used for the majority of optical glasses. In order to guarantee the highest accuracies and a long mold lifetime ceramics are most suitable to be used as mold materials. Their hardness, chemical resistance, thermal stability and low coefficient of thermal expansion qualify them as the forming tools for the glass molding process. On the other side, those properties make it hard to machine these materials.

While in the past molds made of silicon carbide and other ceramics were used, today a binderless tungsten carbide with fine grains is the first material of choice. In comparison to conventional hard metals those special grades contain just a very small amount of nickel or cobalt, which is used as a metallic binder. Thus, very dense (15,57 g/cm³), hard (2825 HV10) and materials can be produced with the proper properties a glass molding tool needs.

Due to its hardness, tungsten carbide can only be machined by grinding and polishing [Mei09, Bri07, Bri09]. Here, diamonds are typically used as abrasives.

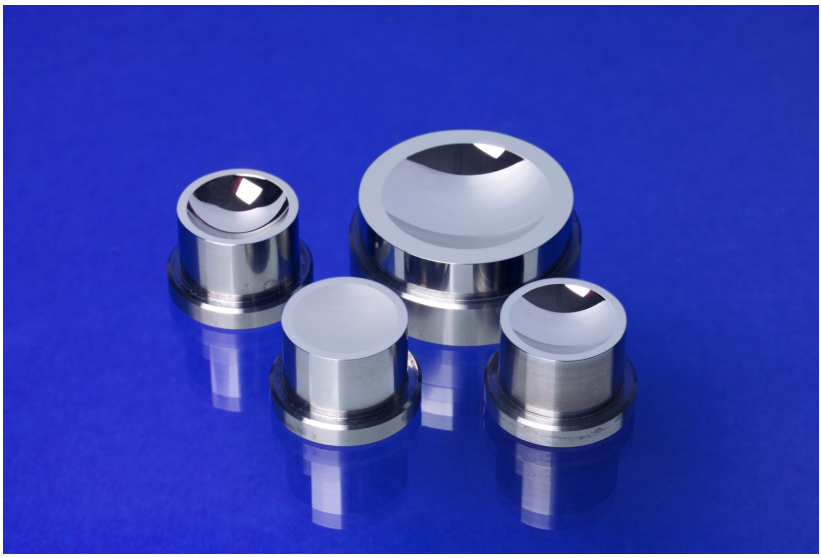

**Fig. 3** Ground tungsten carbide molds for precision glass molding

Since the molds need to be very accurate with optical surface finish, a ductile machining process as described by Bifano [Bif88], Grimme [Gri07] and others [Liu03, Liu01] is necessary. In ductile mode cutting the process parameters are chosen in a way to enable plastically deformation of the material. Thus, cracking of the surface is avoided and a very smooth and shiny surface finish is obtained. Characteristics of ductile mode cutting processes are very small depth of cut and feed rates as well as round instead of sharp cutting edges. Thus, the chip thickness is smaller than the so called critical chip thickness, which is an indicator for ductile mode cutting and depends on the mechanical properties of the material. In addition to the abovementioned process parameters compressive stresses and high temperatures in the cutting zone have positive effects on ductile machining.

To manufacture the molds, an ultraprecision grinding process [Bri10, Che03] is applied. Therefore, ultraprecision machines with highly accurate guideways and air bearing spindles are needed. For the machining of the tungsten carbide materials, resin bonded grinding wheels are used. Typically, the abrasives in the bonding are 3 to 5 µm in diameter. The concentration of diamonds is usually rather high, so high number of cutting edges can machine the material and therefore guarantee a small chip thickness. Thus, a mirror finish can be generated on the tungsten carbide surface showing less than 10 nm roughness (Ra).

Since a grinding wheel is continuously effected by wear, the mold manufacturing process usually needs several iterations to reach the final form accuracies. Typically, the mold is ground and then the form of the mold is measured. Based on this metrology data and their characteristics of the machine setup, the grinding wheel position e.g. can be determined. In the final steps the metrology data is also used to generate the tool path with compensation of the

existing errors on the mold [Luo97, Che10, Mei10]. Thus, form accuracies of up to 150 nm (PV) and irregularities of less than 100 nm can be achieved.

After grinding, the mold surface already shows an optical finish but there are still some regular structures on the mold caused by the grinding process characteristics. These regular structures can effect the quality of the optic. To eliminate them a subsequent polishing process is needed. Since the large number of the molds are rather small or steep, there is no automated polishing process capable to machine the molds. Therefore, the majority of the molds are polished by hand.

Based on the current state of the art, a large spectrum of mold geometries of different sizes can be machined including rotationally symmetric molds with spherical and aspherical shapes, cylindrical shapes, either spherical or aspherical, and freeforms such as non rotationally symmetric parts and arrays.

## 4 Coatings for Glass Molding

A crucial requirement for the successful application of the precision glass molding technology in practice is the protection of the optical surfaces of the molds through the application of suitable coatings [Ma08]. The production of the molds in the extreme form accuracy required for optical applications is technically difficult and therefore expensive. Protective coatings that can withstand the high mechanical, thermal and chemical stresses during the molding process are essential.

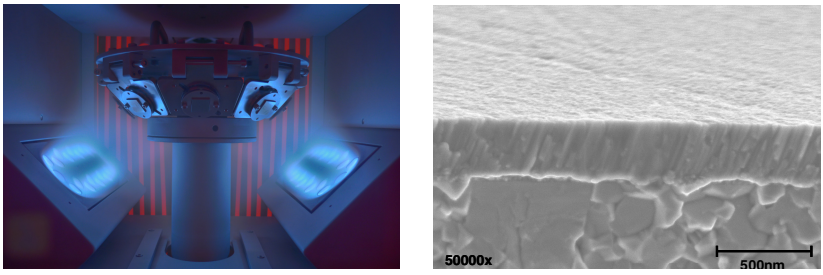


**Fig. 4** Coating process (left); PtIr coating (right)

There are two main failure modes of the molding tools that need to be addressed by coatings:

The first one is glass adhesion on the tool surface. Due to the high temperature and the long contact time between molding tool and glass, sometimes glass sticks to the mold surface. This phenomenon is the result of chemical interactions between the glass and the mold surface. These chemical interactions are accelerated by diffusion processes between glass, coating and substrate that take place near the surface during multiple pressing cycles. Therefore, coatings with the least possible chemical reactivity towards glass, like noble metal coatings, are preferred [Fis10]. Alloys of Platinum and Iridium are being successfully used in

this application [Pat87]. Furthermore, substrates don't contain elements that diffuse easily, like binderless tungsten carbide, are also preferred. Since different glasses can have significantly different compositions, each coating should ideally be optimized for a specific glass type.

The second failure mode is the deterioration of the surface quality of the molding tool (increased roughness, cracks, scratches etc.). The coatings applied should be hard enough to prevent scratching during handling and resilient against mechanical and thermal cyclic loads in order to prevent such defects.

For the deposition of suitable protective coatings, there is a multitude of technologies that could be used. There are however several necessary characteristics that the selected coating technology should exhibit:

- During cooling, there is usually a difference in the shrink rate of the glass and the mold, due to different coefficients of thermal expansion. The adhesion of the coating to the substrate should be higher than the adhesion of the coating to the glass, in order to avoid coating delamination in this situation. Parameters that affect the adhesion are the cleanliness and activation method of the substrate prior to coating, as well as the deposition parameters [Mat10].
- The coating should not increase the surface roughness. This depends on the deposition technology and parameters, as well as the coating thickness [Mat10].
- The coating should be as defect-free as possible. Especially in-situ coating defects (droplets, clusters, pinholes etc.) should be minimized in order to meet the defect density specifications of the optical component.
- The coating thickness should not have large variation across the molding tool surface. A lot of effort is required to produce molding tools with form accuracies down to 150nm (PV or peak to valley). A coating thickness variation of a few hundred nm would derail this effort. Low coating thicknesses (well below 1µm) and suitable substrate rotation during coating can be used to prevent this problem.

By using the above mentioned characteristics as selection criteria, the most suited coating technology is sputtering. This PVD (physical vapor deposition) process is able to provide smooth, defect-free coatings with low coating thickness variation and is extremely flexible regarding possible coatings and substrates [Mat10].

## 5 Glass Molding

Several hot forming technologies for glass products have been developed during the last decades. The most precise of them is called precision glass molding, or precision pressing and was originally developed in Asia and the United States approximately at the same time [Yi07, Klo04].

Sometimes the process is described as 'isothermal' process. This refers to the fact that the molding tools and glass have the same temperature throughout the process. The system itself is exposed to a heat cycle from room temperature to 700° in some cases and is therefore not strictly isothermal. The material input for

the precision glass molding process consists of a glass preform with polished or fire-polished surface quality. As a general rule, the surface quality of the final molded product cannot be better than the preform or the mold surface. Drops of glass can be formed directly from the melt or glass can be cut, ground and polished into balls, disks or spherical lenses. The molding tools with the preform in between are heated up to pressing temperature by infrared radiation in a process chamber. The process chamber is first evacuated and then purged with nitrogen to prevent oxidation on the tools. The pressing temperature is chosen in the range between the yield point and the softening point so that the viscosity of the glass is between 1010 and 107 dPa s. After reaching the pressing temperature a homogenizing phase is added to achieve a uniform temperature distribution within the molds and the glass. The glass does not absorb much of the infrared light and is mainly heated by thermal conduction over the contact area or convection by the nitrogen flow. Thereafter the glass is pressed between the molds. The pressing cycle is mainly force controlled, in combination with the glass viscosity this leads to strain rates of a few mm/ minute. To achieve the desired center thickness of the lens, several end conditions are used. As the temperature control is very exact, a defined pressing time can be used to achieve a defined strain. Alternatively, position control can be employed and an end position for pressing can be defined. When the molding tools engage during pressing in a way that a closed cavity is formed, the center thickness is defined to a large amount by the preform volume.

After the pressing phase, the tools are cooled by nitrogen gas flow. A holding force is applied and the glass is cooled via the heat transfer over the molds. The holding force compensates the shrinkage of the glass when in viscoelastic regime and suppresses deformation due to internal stresses when approaching the elastic regime. The cooling phase is divided in two steps. A first step with a slow, controlled cooling rate and a second step of fast cooling once the glass has been cooled down under the transition temperature. The process ends at approximately 200 °C, the process chamber opens, the molded glass part is removed from the molds and a new preform is put in. The overall cycle time is around 15 to 25 min depending on the size and geometry of the product. To increase throughput, several molding tools can be used in one process. The advantages of this specific glass molding technology is the ability to mold double-sided parts with a lateral alignment of 5 µm and angular alignment of 50 arcseconds using many types of optical glasses.

## 6 Measurement of Optical Properties

Structural relaxation is the non-linear time dependent response of glass material properties (e.g., volume, density and enthalpy) to temperature change [Sch86]. The structural response depends on the thermal history, current temperature and the direction of the temperature change. The optical properties such as refractive index of an optical glass will change after molding due to structural relaxation in glass [Su10]. This requires appropriate process conditions in manufacturing to minimize the impact due to refractive index change. Figure 3 illustrates a three dimensional (3D) measurement setup [Zha09].

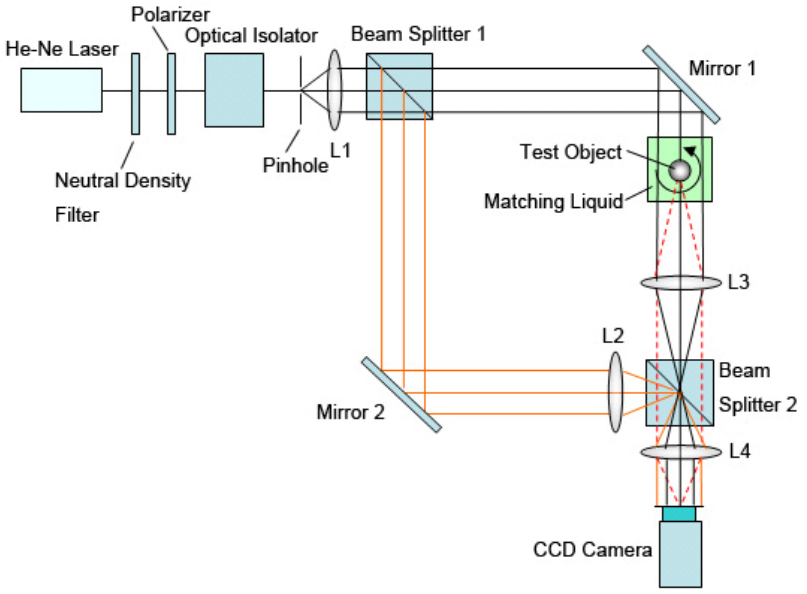


**Fig. 5** Optical setup for 3D refractive index distribution measurement [Zha09]

The 3D measurement shown here is based on computed tomography, a nondestructive method that is widely used to generate 3D images of a specific property inside of an object from a series of two dimensional (2D) projections taken around a single axis of rotation. Details of computed tomography used in glass molding study can be found in [Zha09]. Using this setup, refractive index change down to $10^{-4}$ can be precisely measured.

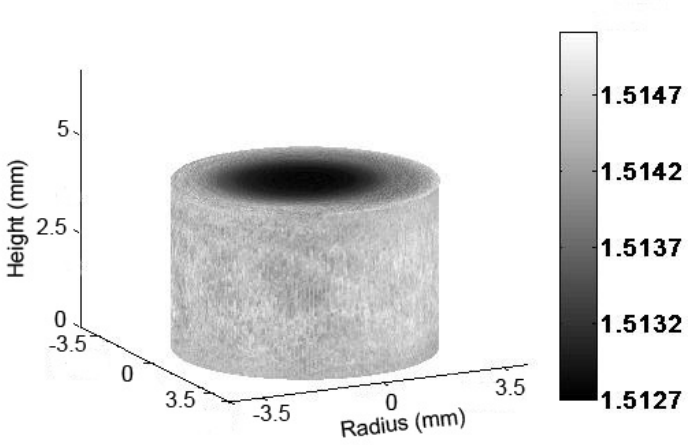


**Fig. 6** 3D refractive index map of a molded BK-7 lens [Zha09]

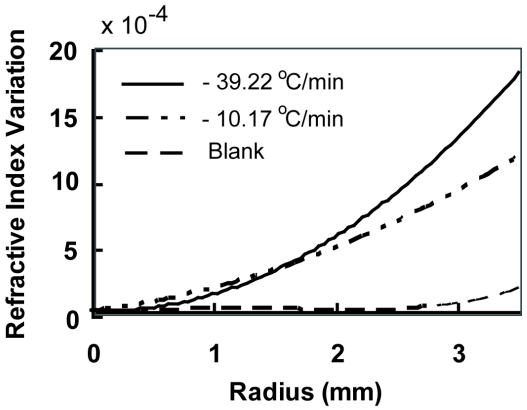


**Fig. 7** Refractive index variation of molded glass lens under different cooling rate [Zha09]

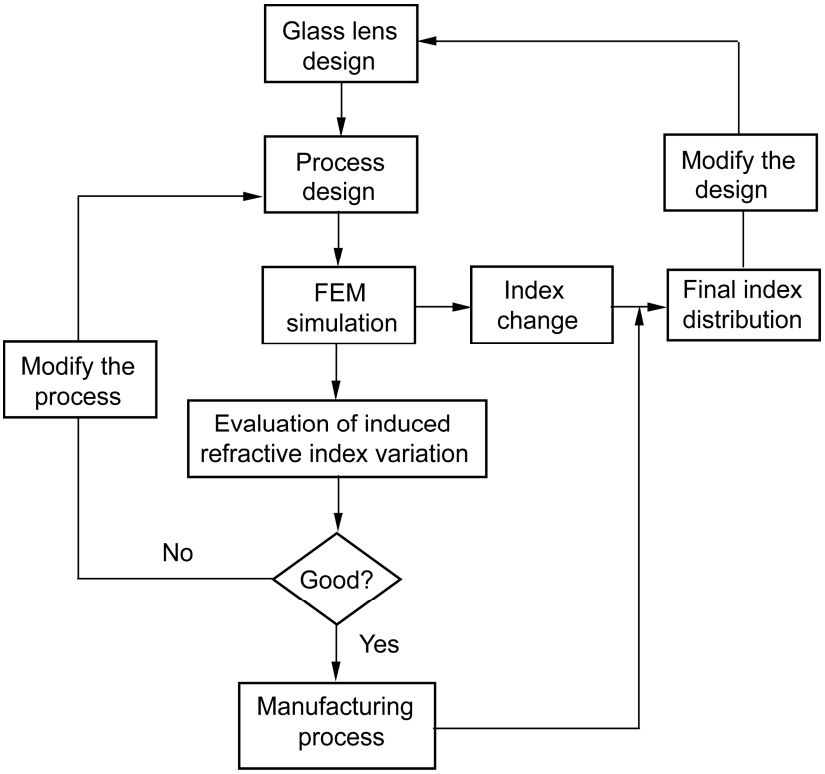


**Fig. 8** Flow chart of FEM assisted glass molding process optimization [Su10]

Figure 4 shows a 3D refractive index distribution map of a molded BK-7 glass lens. The cooling rate for this lens was -39.22 °C/min. The 3D computed tomography shows that the refractive index distribution of the thermally treated glass is no longer uniform. The index variation could be as large as $2x10^{-3}$.

As a comparison, a second BK-7 glass sample was thermally treated with a cooling rate of -10.17 °C/min, and its refractive index distribution was also reconstructed by use of 3D computed tomography, shown in Figure 5 with an untreated glass blank. The refractive index variation under -10.17°C/min cooling was about 1.3 x $10^{-4}$, smaller than the variation for the higher cooling rate (=-39.22°C/min) but still much larger than that of a blank, shown in the dashed line in the same figure, indicating that refractive index variation in a molded glass lens depends on cooling rate and geometry of the lens.

The optical property change is crucial for process compensation in designing glass molding process. Figure 6 is the process flowchart showing how the index variation information can be utilized. Specifically, finite element method (FEM) assisted numerical simulation is adopted to calculate the refractive index changes [Su10]. This information is then incorporated into the optical lens design so the optical lens geometry can be modified to compensate for the index variation due to cooling. This arrangement allows high volume, low cost and high precision optical lenses to be manufactured by eliminating the need for the costly trial and error approach. Similarly, other optical properties such as stress induced birefringence and dispersion also experience different degree of change during cooling thus can be measured and potentially compensated for in manufacturing process using similar strategy.

## 7 Conclusion

Driven by demand for high-precision and low cost optical glass components the precision glass molding technology offers a good possibility for fast production of precision optical glass components in medium and high volumes. The manufacturing process is holistically described by the process chain for replication of complex optical glass components. Each of the process steps has a crucial impact on the final result.

**Acknowledgement.** The authors like to thank the German Research Foundation (DFG) for funding this work as a part of the Transregional Collaborative Re-search Center SFB/TR4 “Process Chains for the Replication of Complex Optical Elements”.

## References

[Bif88] Bifano, T.G.: Ductile regime grinding of brittle materials. PhD Thesis, North Carolina State University (1988)

[Bri07] Brinksmeier, E., Riemer, O., Schulte, H.: Kinematiken zum Polieren von Mikrostrukturen. Werkstattstechnik Online 97(6), 431–436 (2007)

[Bri09] Brinksmeier, E., Riemer, O., Schulte, H.: Mechanisches Polieren linearer und räumlich begrenzter Strukturen. In: Jahrbuch Schleifen, Honen, Läppen und Polieren. Ausgabe, vol. 64, pp. 280–296. Vulkan Verlag, Essen (2009)

[Bri10] Brinksmeier, E., Mutlugünes, Y., Klocke, F., Aurich, J.C., Shore, P., Ohmori, H.: Ultra-precision grinding. CIRP Annals-Manufacturing Technology, 652–671 (2010)

[Che03] Chen, W.K., Huang, H.: Ultra precision grinding of spherical convex surfaces on combination brittle materials using resin and metal bond cup wheels. Journal of Materials Processing Technology, 217–223 (2003)

[Che10] Chen, F.J., Yin, S.H., Huang, H., Ohmori, H., Wang, Y., Fan, Y.F., Zhu, Y.J.: Profile error compensation in ultra-precision grinding of aspheric surfaces with on-machine measurement. International Journal of Machine Tools and Manufacture, 480–486 (2010)

[Dam09] Dambon, O., Wang, F., Chen, Y., Yi, A.Y., Klocke, F., Pongs, G.: Efficient Mold Manufacturing for Precision Glass Molding. Journal of Vacuum Science & Technology B 27(3), 1445–1449 (2009)

[End99] Endrys, J.: Measurement of radiative and effective thermal conductivity of glass. In: Proceedings of the 5th ESG Conference A5, pp. 10–17 (1999)

[Fis10] Fischbach, K.D., Georgiadis, K., Wang, F., Dambon, O., Klocke, F., Chen, Y., Yi, A.Y.: Investigation of the effects of process parameters on the glass-to-mold sticking force during precision glass molding. Surface and Coatings Technology 205, 312–319 (2010)

[Gri07] Grimme, D., Rickens, K., Zhao, Q., Heinzel, C.: Dressing of Coarse-Grained Diamond Wheels for Ductile Machining of Brittle Materials. In: Towards Synthesis of Micro-/Nano-Systems, pp. 305–307 (2007)

[Jai05] Jain, A., Yi, A.Y.: Numerical modeling of viscoelastic stress relaxation during glass lens forming process. Journal of the American Ceramic Society 88(3), 530–535 (2005)

[Jai06] Jain, A., Yi, A.Y., Xie, X., Sooryakumar, R.: Finite Element Modeling of Stress Relaxation in Glass Lens Molding Using Measured, Temperature-Dependent Elastic Modulus and Viscosity Data of Glass. Modelling Simulation in Material Science and Engineering 14(3), 465–477 (2006)

[Klo04] Klocke, F., Pongs, G., Heselhaus, M.: Komplexe Optiken aus der Presse. Photonik, 70–72 (2004)

[Liu01] Liu, K., Li, X.P.: Ductile cutting of tungsten carbide. Journal of Materials Processing Technology 113, 348–354 (2001)

[Liu03] Liu, K., Li, X.P., Rahman, M., Liu, X.D.: CBN tool wear in ductile cutting of tungsten carbide. Wear 255, 1344–1351 (2003)

[Luo97] Luo, S.Y., Liao, Y.S., Chou, C.C., Chen, J.P.: Analysis of the wear of a resin-bonded diamond wheel In the grinding of tungsten carbide. Journal of Materials Processing Technology, 289–296 (1997)

[Ma08] Ma, K.J., Chien, H.H., Chuan, W.H., Chao, C.L., Hwang, K.C.: Design of Protective Coatings for Glass Lens Molding. Key Engineering Materials 366, 655–661 (2008)

[Mat10] Mattox, D.M.: Handbook of physical vapor deposition (PVD) processing, 2nd edn. William Andrew (2010)

[Mei09] Meiners, K., Rickens, K., Riemer, O., Brinksmeier, E.: Ultraprecision grinding of tungsten carbide moulds for hot pressing glasses. In: Proceedings of the Euspen International Conference, vol. I, pp. 146–149 (2009)

[Mei10] Meiners, K., Rickens, K., Riemer, O., Brinksmeier, E.: Investigation on resulting form errors of precision ground optical moulds with respect to tool path compensation. In: Proceedings of the Euspen International Conference 2010, vol. II, pp. 144–147 (2010)

[Nar71] Narayanaswamy, O.S.: A model of structural relaxation in glass. Journal of the American Ceramic Society 54, 491–498 (1971)

[Pat87] Patent US4685948: Mold for press-molding glass optical elements and a molding method using the same. Matsushita Electric Industrial Co. Ltd. (1987)

[Rit55] Ritland, H.N.: Relation between refractive index and density of a glass at a constant temperature. Journal of the American Ceramic Society 38, 86–88 (1955)

[Sch86] Scherer, G.W.: Relaxation in Glass and Composites. John Wiley & Sons, Inc., New York (1986)

[Su10] Su, L.J.: Experimental and Numerical Analysis of Thermal Forming Processes for Precision Optics. PhD Thesis, The Ohio State University (2010)

[Yi07] Yi, A.Y.: Optical Fabrication. The Optics Encyclopedia (2007)

[Zha09] Zhao, W., Chen, Y., Shen, L.G., Yi, A.Y.: Investigation of refractive index distribution in precision compression glass molding by use of 3D tomography. Measurement Science and Technology 20, 055109 (2009)

# Deposition, Machining and Measuring of Novel Hard Coatings

Gert Goch, Don Lucca, Andreas Mehner, Helmut Prekel,
Heinz-Rolf Stock, and Hans-Werner Zoch

**Abstract.** Optical molds for precision glass pressing are frequently coated to improve their wear and oxidation resistance, and to reduce sticking of the hot glass to the mold surface during the glass pressing process. Currently PVD (Ti,Al)N, CrN, ZrN and PtIr coatings are used as protective coatings for these molds. Novel nano crystalline PVD Ti-Ni-N and Ti-Cu-N coatings and thin sol-gel $ZrO_2$ coatings were developed and tested as new protective coatings for glass pressing molds. Optical molds for injection molding of plastic lenses are frequently coated with thick diamond machinable electroless nickel coatings since steel cannot be machined with diamond tools. These nickel coatings have several drawbacks such as residual porosity, limited hardness and temperature resistance. Therefore, thick sol-gel silica based coatings were developed and tested as an alternative for the electroless nickel coatings.

## 1 Introduction

### *1.1 Protective Coatings for Precision Glass Pressing Molds*

Replication of glass lenses for optical applications is performed by precision glass pressing of polished glass balls or glass disks of suited dimensions. Precision glass pressing is carried out at temperatures up to 800 °C with maximum loads up to 6 kN, depending on the type of glass. One pressing cycle takes about 10 min.

Gert Goch · Helmut Prekel
Bremen Institute for Metrology, Automation and Quality Science BIMAQ,
University of Bremen, Linzer Straße 13, 28359 Bremen,Germany

Don Lucca
Oklahoma State University, OK, 218 Engineering North, Stillwater,
Oklahoma 74078-5016, USA

Andreas Mehner · Heinz-Rolf Stock · Hans-Werner Zoch
Institute for Materials Science IWT, Badgasteiner Straße 3, 28359, Bremen, Germany

E. Brinksmeier et al. (Eds.): Fabrication of Complex Optical Components, LNPE, pp. 133–160.
springerlink.com 

Thus, the mechanical, chemical and thermal strain on the mold material is very high. Only a few materials, such as hard ceramics (especially $Si_3N_4$) or cemented tungsten carbide (WC/Co) can withstand these severe conditions during the glass pressing process. As a result of long contact times, there is often sticking between the hot glass and the mold. Thin and hard PVD coatings as TiN, TiAlN, CrN, ZrN or PtIr are known to reduce sticking between the glass and the mold material. These coatings also increase the oxidation resistance of the molds [Rie05]. Novel PVD Ti-Cu-N and Ti-Ni-N coatings and thin sol-gel $ZrO_2$ coatings were developed, characterized and tested as alternative protective coatings for precision glass pressing molds.

## *1.2 Diamond Machinable Coatings for Injection Molding of Plastics*

For mass production of plastic optical elements by injection molding, molten plastics (especially PMMA) with temperatures up to 250 °C are injected into optical mold cavities with pressures up to 1400 bar. Generally the mold cavities are manufactured from hardened stainless steel such as X40Cr13 (AISI 420, WKN 1.2083). Pre-machined steel molds are frequently coated with thick electroless nickel coatings. The nickel coatings allow for the manufacturing of complex aspheric or micro-structured surfaces by high precision machining with diamond tools. Generally, the mechanical and chemical properties of electroless nickel coatings are sufficient for injection molding of plastics, but not for precision glass pressing. Some drawbacks of electroless nickel coatings include residual porosity, limited hardness and temperature resistance, as well as a high heat conductivity which has some negative effects on the injection molding process. Therefore, thick sol-gel silica hybrid coatings were investigated and tested as novel diamond machinable coatings for injection molding.

## *1.3 Demands on the Coating Properties*

The demands on the mechanical, physical and chemical properties of coatings for precision glass pressing and for injection molding are different and in some cases even contrary. The thickness of protective coatings for glass pressing molds should be less than 1 µm, since thicker coatings would change the final shape and surface roughness of the molds. However, diamond machinable coatings for injection molding should have a coating thickness of at least 30 µm to insure a sufficient thickness for the high precision machining process with diamond tools. Also, the demands on the hardness for both types of coatings are different. The hardness of the protective coatings for precision glass pressing should have indentation hardnesses $H_{IT}$ above 7 GPa (≈ 700 HV1) to ensure high wear resistance. For the diamond machinable coatings the hardness should be less than 7 GPa to guarantee good machinability without abrasive wear of the diamond tool. Table 1 shows a summary of coating properties required for protective

**Table 1** Demands on the mechanical, physical and chemical properties of coatings for precision glass pressing and injection molding and the types of PVD and sol-gel coatings investigated

| **Application** | **Precision Glass Pressing** | **Injection Molding** |
|---|---|---|
| **Type of Coating:** | **Protective Coatings** | **Diamond Machinable Coatings** |
| **Thickness (µm)** | **< 1** | **> 30** |
| **Indentation hardness (GPa)**<br>**Hardness (HV 1)**<br>**Hardness (HRC)** | **> 7**<br>**> 700**<br>**> 60** | **< 7**<br>**< 700**<br>**< 60** |
| **Temperature resistance (°C)**<br>**Oxidation resistance** | **> 800** | **> 600** |
| **Diamond machinability** | **--** | **Yes** |
| **Adhesion to the substrate (Rockwell class [DIN39])** | **1** | **1 or 2** |
| **Adhesion to glass or plastics** | **Low** | **Low** |
| **Microstructure (morphology)** | **Amorphous or Nanocrystalline** | **Amorphous or Nanocrystalline** |
| **Porosity (Vol. %)** | **< 1** | **< 1** |
| **Heat conductivity** | **--** | **Low** |
| **Investigated PVD Coatings** | **Ti-Cu-N;**<br>**Ti-Ni-N** | **Ti-Cu-N;**<br>**Ti-Ni-N** |
| **Investigated Sol-Gel Coatings** | **$ZrO_2$** | **$SiO_xC_yH_z$**<br>**$SiNa_uO_xC_yH_z$** |

coatings for glass pressing and for diamond machinable coatings for injection molding of plastics.

## 2 Deposition and Characterization of PVD Coatings

### *2.1 The Magnetron Sputtering Process*

The PVD (physical vapor deposition) coatings investigated in the collaborative research center were deposited by reactive magnetron sputtering using a commercial magnetron sputterer (Fa. Cemecon, CC800/9), shown schematically in Fig. 1.

Novel nanocrystalline Ti-Cu-N and Ti-Ni-N coatings were deposited using titanium targets with integrated copper or nickel blanks. The aim of the research was to deposit and characterize Ti-Ni-N and Ti-Cu-N coatings with thicknesses of at least 30 µm to allow for precision machining and structuring of these coatings by grinding and polishing.

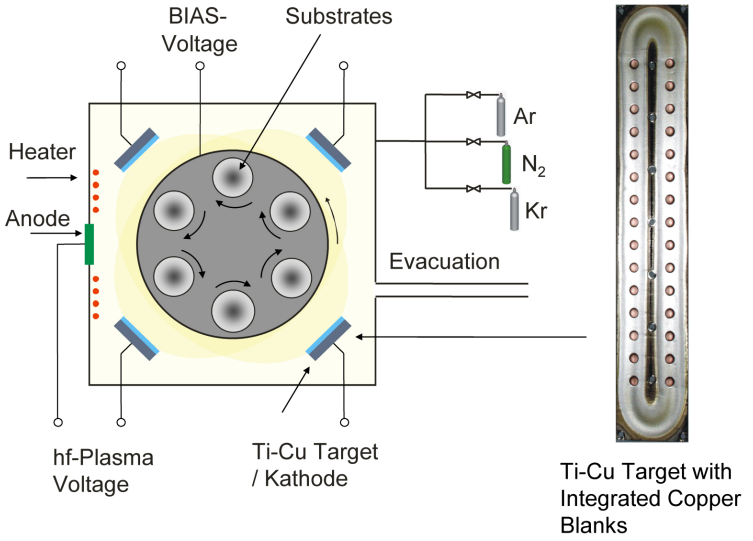


**Fig. 1** Experimental setup of a PVD magnetron sputterer with titanium targets and integrated Cu or Ni blanks

Hardened and polished stainless steel disks (AISI 420, X42Cr13) with a hardness of 53 HRC were used as substrates for the coating experiments. The magnetron chamber was evacuated to a residual pressure of 5 mPa. Argon was added at 200 $ml_n$/min and the bias voltage of the substrates was -650 V for sputter cleaning and activation of the stainless steel surface. The coating process started by igniting a 4 kW pulsed plasma in front of the titanium targets and reducing the bias voltage of the substrates to -60 V. After 10 to 20 s, a Ti-Ni layer several nanometers thick was deposited onto the substrates to improve the adhesion of the following nitride layers. The deposition of the Ti-Ni-N nitride layers by reactive sputtering started after the addition of nitrogen gas to the atmosphere at a rate of 10 to 50 $ml_n$/min. Micro-crystalline and homogenous growth of the coatings was achieved by periodically interrupting the deposition process with a pulsed bias voltage. DC bias voltages result in columnar coating morphologies and pulsed bias voltages result in micro- or even nanocrystalline coating morphologies, as shown in Fig. 2. Pulsing of the bias voltage also prevents the formation of inhomogeneities such as hillocks.

## *2.2 Results for PVD Ti-Ni-N Coatings*

Figure 3 shows a ternary diagram of the chemical composition of PVD Ti-Ni-N coatings deposited onto stainless steel disks (AISI 420, X42Cr13). The nickel content of the coatings was controlled using different titanium targets having 10, 20, 30 or 40 integrated nickel blanks. The nitrogen content was controlled by varying the nitrogen gas flow from 10 to 50 $ml_n$/min. The chemical composition of

the coatings was measured by GDOES (glow discharge optical emission spectroscopy) and nickel contents of approx. 8, 18, 23 or 32 at.% were measured for coatings deposited using titanium targets with 10, 20, 30 or 40 nickel blanks.

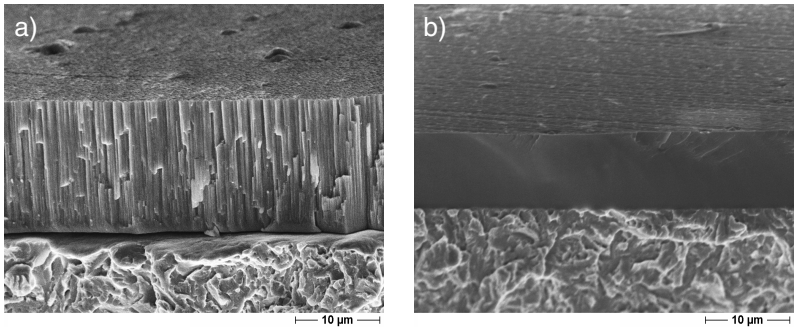


**Fig. 2** Coating morphology of PVD $TiN_x$ coatings deposited with DC bias voltage (a) and with pulsed bias voltage (b)

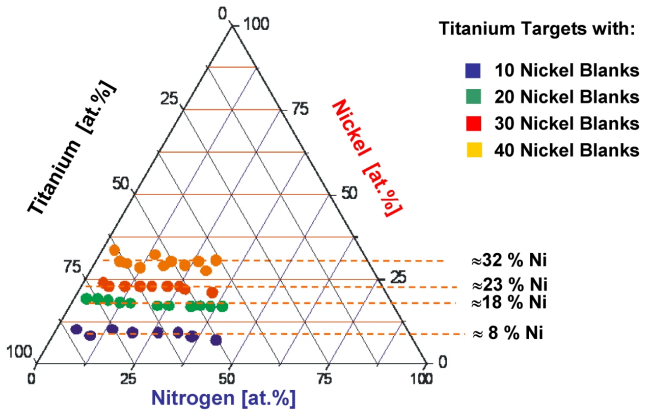


**Fig. 3** Ternary diagram of the chemical composition of Ti-Ni-N coatings measured by GDOES (glow discharge optical emission spectroscopy). The coatings were deposited using different titanium targets that had 10, 20, 30 and 40 Ni blanks.

The coating hardness was measured by micro-indentation using a commercial micro-indenter (Fisherscope 100) with a Vickers diamond indenter and a maximum load of 20 mN. The hardness $HU_{plast}$ increased with the nitrogen content for almost all coatings, as shown in Fig. 4. A maximum hardness $HU_{plast}$ of 22 GPa was measured for Ti-Ni-N coatings with 18 at.% nickel and a N/Ti ratio of 0.9. For stoichiometric TiN coatings $HU_{plast}$ is about 27 GPa, indicating that the addition of nickel does not increase the hardness as observed for Ti-Cu-N [He01, Myu03].

The microstructure of the Ti-Ni-N coatings showed a transition from an amorphous state for low N/Ti ratios, to a columnar microstructure for N/Ti ratios above 0.5. Detailed results for the Ti-Ni-N coatings were previously published [Ben04, Gri04].

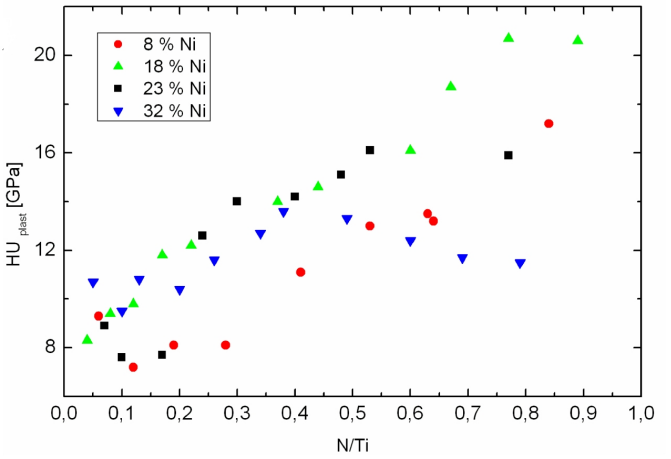


**Fig. 4** Measured indentation hardness $HU_{plast}$ vs. the atomic N/Ti ratio for coatings with nickel contents of 8, 18, 23 and 32 at.%

Figure 5a shows a PVD Ti-Ni-N coated mold which was successfully tested by replicating 500 PMMA disks by injection molding. The surface topography of the coatings as measured by FE-SEM (field emission scanning electron microscopy) and shown in Figs. 5b and 5c did not change after the replication. The visual differences between Figs. 5b and 5c are due to different electric charging of the surface.

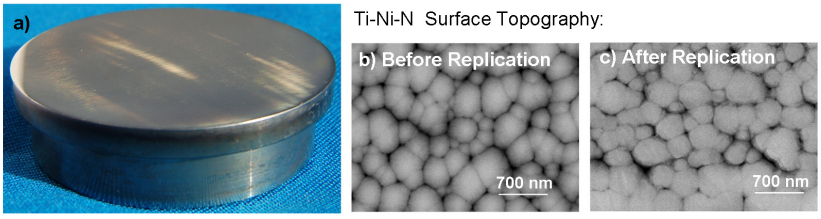


**Fig. 5.** PVD Ti-Ni-N coated mold for injection molding (a). Surface topography measured by FE-SEM (field emission scanning electron microscopy) before (b) and after (c) replication of 500 PMMA disks.

# 3 Sol-Gel Coatings

## *3.1 The Sol-Gel Coating Process*

The sol-gel coating process is based on liquid sols containing metal organic polymers dispersed in organic solvents [Bri90]. The silica hybrid coating ($SiO_xC_yH_z$) sols were deposited onto the substrates by the dip or spin coating process, followed by a heat treatment at 300 °C for 30 min. Figure 6a shows the dip coating process where the substrate is immersed into the sol and withdrawn at constant velocity. These coatings were derived from silica based sols with different molar ratios of ethanol to $SiO_2$. The resulting coating thickness for both sols increased with the withdrawal speed as shown in Fig. 6c. For the spin coating process, which is illustrated in Fig. 6b, the sol was dripped onto the rotating substrate. The resulting coating thickness decreased with increasing spin frequency (Fig. 6d). The coating thickness was measured by the ball grinding method [Meh05].

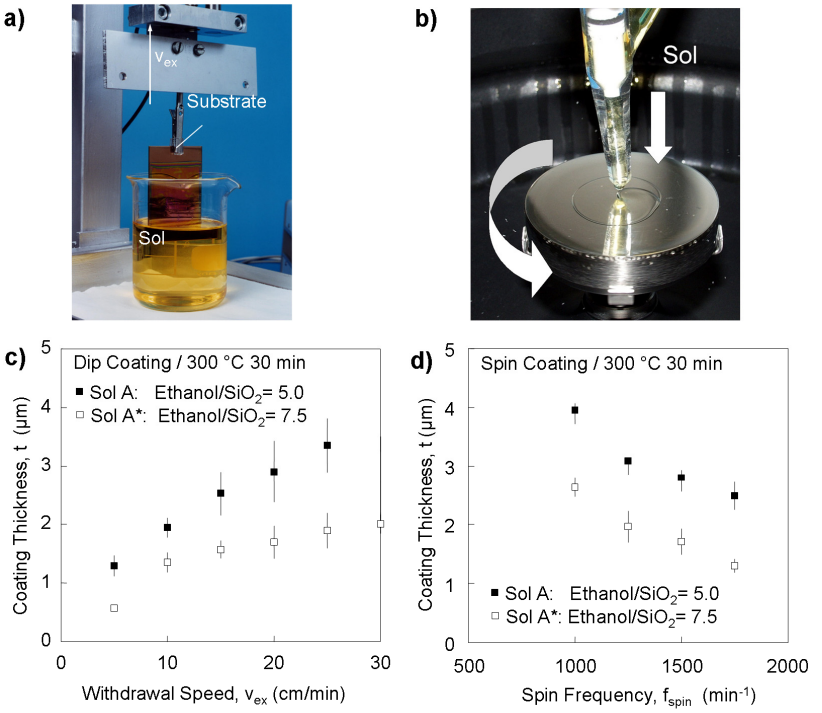


**Fig. 6** Dip coating process (a) and spin coating process (b). Coating thickness of silica hybrid coatings after heat treatment at 300 °C for 30 min as a function of the withdrawal speed for dip coating (c) and as a function of the spin frequency for the spin coating process (d). The results for 2 silica based sols (A and A*) with different molar ratios of the solvent ethanol to $SiO_2$ are shown.

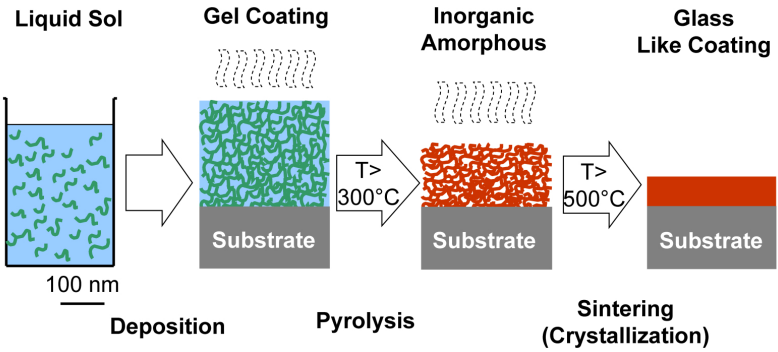


**Fig. 7** The sol-gel coating process illustrated schematically

After depositing the sol, the liquid sol films rapidly transform into solid gel films by the evaporation of the solvent as illustrated schematically in Fig. 7. Above 300 °C the gel converts into an inorganic amorphous xerogel with high residual porosity due to pyrolysis of the organic groups. Above 500 °C the inorganic porous coatings convert into dense glass-like coatings by sintering. Silica based coatings ($SiO_2$) remain amorphous even at higher temperatures. Other metal oxide coatings, such as sol-gel zirconia ($ZrO_2$) or alumina coatings ($Al_2O_3$), crystallize at temperatures above 500 °C and convert into nanocrystalline ceramics [Bri90].

Hardening of the sol-gel coatings by thermal treatment in ambient air frequently induces crack formation due to shrinkage of the coatings during the heat treatment and differences between the thermal expansion coefficients of the coating and substrate. For sol-gel metal oxide coatings such as $ZrO_2$ or $Al_2O_3$, the maximum coating thickness which can be deposited without cracks is limited to about 0.5 µm per layer [Meh05]. For silica based hybrid coatings the maximum thickness was about 5 µm per layer. Thicker coatings were produced by multilayer deposition.

To overcome the problems associated with thermal treatment, hardening by ion irradiation using 125 keV $H^+$, 250 keV $N^{2+}$ and 2 MeV $Cu^{2+}$ was investigated [Luc07, Ghi07].

## *3.2 The Sol Synthesis*

Precursors for the sol synthesis are alkoxides such as TEOS (tetra-ethoxy-ortho-silicate) $Si(OC_2H_5)_4$ and ZTP (zirconium tetra-n-propoxide) $Zr(O^nC_3H_7)_4$ [Bra01]. The general chemical formula of metal alkoxides for a *n*-valent metal M is $M(OR)_n$, where R represents alkyl groups such as methyl ($-CH_3$), ethyl ($-C_2H_5$), propyl ($-C_3H_7$) or butyl ($-C_4H_9$). For the sol synthesis these alkoxides are dissolved in organic solvents such as ethanol, 1- or 2-propanol. Cross-linking of the alkoxides is accomplished by the addition of a small amount of water. The hydrolysis reaction (1) is followed by condensation reactions (2a) and (2b) resulting in the formation of cross linked metal organic polymers [Bri90].

$$(RO)_{n-1}M\text{-}OR + H_2O \rightarrow (RO)_{n-1}M\text{-}OH + ROH \quad (1)$$

$$(RO)_{n-1}M\text{-}OR + HO\text{-}M(OR)_{n-1} \rightarrow (RO)_{n-1}M\text{-}O\text{-}M(OR)_{n-1} + ROH \quad (2a)$$

$$(RO)_{n-1}M\text{-}OH + HO\text{-}M(OR)_{n-1} \rightarrow (RO)_{n-1}M\text{-}O\text{-}M(OR)_{n-1} + H_2O \quad (2b)$$

## *3.3 Thin Sol-Gel $ZrO_2$ Coatings for Glass Pressing Molds*

The precursor for the sol synthesis for the deposition of the $ZrO_2$ coatings was zirconium tetra n-propoxide (ZTP: $Zr(O^nC_3H_7)_4$). In addition to ZTP, the sol consisted of acetylacetone ($CH_3COCH_2COCH_3$), 2-propanol, water and polyethylene glycol (PEG400) with a molar weight of 400 g/mol. The molar ratios of 2-propanol, $H_2O$ and acetylacetone to ZTP were 15, 3 and 1, respectively. To adjust the sol viscosity and prevent film cracking, 5 wt.% PEG 400 was added. More details of the sol synthesis were published previously [Izu89, Pat97].

Hardness measurements were performed on 5-layer sol-gel $ZrO_2$ coatings with total thicknesses of 600 to 800 nm which were deposited onto polished AISI 304 stainless steel substrates, 40 x 20 x 1 $mm^3$ in dimension. Nanoindentation was performed using a load-controlled commercial nanoindenter in conjunction with an atomic force microscopy (AFM) system and a Berkovich diamond indenter. The instrument and sample were allowed to thermally equilibrate for 10 h inside a thermal enclosure before measurements were performed. A single indentation sequence consisted of loading and unloading at 50 µN/sec for 10 sec with a 5 sec hold at the maximum load to allow time dependent effects to diminish. The maximum load ranged from 100-3000 µN which corresponded to indentation depths from 10 to 180 nm. Before each indentation, the local surface topography was measured by AFM. Typical surface roughness was <2 nm rms over a 1 $\mu m^2$ scan area.

Figure 8 shows the measured hardness $H$ and the reduced elastic modulus $E_r$ for 5-layer $ZrO_2$ coatings heat treated for 10 min at temperatures from 400 to 700 °C [Luc04]. The reduced elastic modulus is shown instead of the elastic modulus, since it eliminated the need to assume a value for the Poisson's ratio of the coating. Indentations were performed at normalized contact depths of 7-10% of the total coating thickness. The error bars denote the maximum and minimum values for 5-7 indentations. Both hardness and reduced elastic modulus exhibit a monotonic increase over the temperature range from 450 to 700 °C. X-ray diffraction on coatings from the same sol system indicated a transition of the $ZrO_2$ structure from amorphous, to cubic, to a combination of cubic and monoclinic over this temperature range [Meh97]. The upper part of Fig. 8 shows a plot of the coating density determined from weight gain and coating dimensions. The density is seen to exhibit a modest increase up to 500 °C, and then a significant decrease as the heat treatment temperature is increased further. The increase in density might contribute to the observed increase in hardness at lower temperatures. However, it cannot explain the increase in hardness at higher temperatures. Significant compressive residual stresses measured by x-ray diffraction for similar films heat treated above 600 °C [Meh97] may counter the effects of reduced density at higher temperatures. More details on the crystallographic phase transitions, the evolution of residual stress, hardness and reduced elastic modulus of the $ZrO_2$ coatings were published elsewhere [Pat98, Meh99].

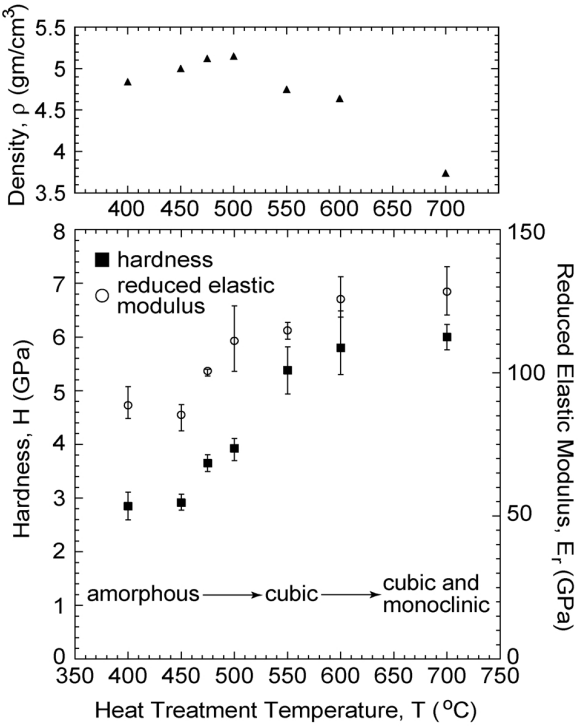


**Fig. 8** Hardness and reduced elastic modulus for various heat treatment temperatures of 5-layer sol-gel $ZrO_2$ coatings [Luc04]. Estimated coating density is shown above

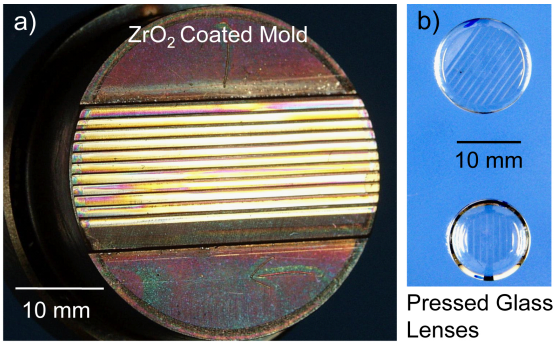


**Fig. 9** $ZrO_2$ coated steel mold with a cylindrical lens array (a) and glass lenses pressed with the coated steel mold (b)

Pre-machined and polished precision glass pressing molds (∅ 25 mm) made of hardened martensitic steel (AISI 420) with 13 wt.% Cr were coated with $ZrO_2$ by spin coating at 2500 rpm, followed by a heat treatment at 600 °C for 30 min in

ambient air. The coating thickness was 120±20 nm, as measured by step height measurements using AFM. The glass pressing process was performed at 570 °C with a load of 4 kN. The pressing cycle for one lens took about 15 min. Figure 9 shows a $ZrO_2$ sol-gel coated mold with a cylindrical lens array structure and glass lenses which were pressed with this mold. No sticking between the coated mold surface and the glass was observed, indicating that the $ZrO_2$ sol-gel coatings successfully prevented the sticking between the glass and the steel mold which occurs for uncoated molds [Meh06].

## *3.4 Silica Based Sol-Gel Coatings for Injection Molding*

Silica based hybrid coatings from sols based on tetraethyl orthosilicate (TEOS: $Si(OC_2H_5)_4$) and methyltriethoxysilane (MTES: $Si(CH_3)(OC_2H_5)_3$) were characterized and tested for manufacturing of micro-structured optical molds [Dat05 Meh06, Meh07, Meh10b].

Sols based on TEOS and MTES precursors must be catalyzed by acids or bases since the chemical reactivity of these molecules is very low. For the acid catalyzed sols, acetic acid ($CH_3COOH$), water and ethanol ($C_2H_5OH$) were used and polyvinyl pyrrolidone (PVP: $(C_6H_9NO)_n$) was added to reduce crack formation during the heat treatment. The typical molar composition for an acid catalyzed sol was TEOS : MTES : $CH_3COOH$ : $H_2O$ : PVP : $C_2H_5OH$ = 0.4 : 0.6 : 1 : 1 : 0.25 : 5 (sol A). Sodium hydroxide (NaOH) was used as a catalyst for the base catalyzed sols having a typical molar composition of TEOS : MTES : NaOH : $H_2O$ : $C_2H_5OH$ = 0.2 : 0.8 : 0.2 : 1.1 : 0.2 (sol B). More details on the sol synthesis of acid and base catalyzed sols were published previously [Meh10a].

The type of catalyst used has significant impact on the growth mechanism of the polysilicates. In acid catalyzed sols the growth of the polysilicates occurs by cluster-cluster aggregation resulting in weakly branched polymers (Fig. 10). For pH < 6 only a few silanol groups (≡Si-OH) are deprotonated and deprotonation preferentially occurs at the ends of the polysilicates [Bri90, Ile79]. In base catalyzed sols the growth of the polysilicates occurs by monomer-cluster aggregation resulting in highly branched, compact polymer clusters (Fig. 10). For pH > 8 the polysilicates exhibit a high degree of deprotonation of the silanol groups (≡Si-$O^-$). The electric repulsion of the negatively charged polysilicates prevents cluster-cluster aggregation and the polysilicates preferentially condensate with neutral monomers by monomer-cluster aggregation [Bri90, Ile79].

The difference in the microstructure of the polysilicates in acid and base catalyzed sols has a direct impact on the mechanical and chemical properties of the resulting coatings.

In the following, coatings from the acetic acid catalyzed sol (sol A) will be denoted as A-coatings ($SiO_xC_yH_z$). Coatings derived from the sodium hydroxide catalyzed sol (sol B) will be denoted as B-coatings ($SiNa_uO_xC_yH_z$). The B-coatings contain sodium due to the sodium hydroxide (NaOH) in the B-sol. The exact chemical composition of these coatings depends on the heat treatment temperature.

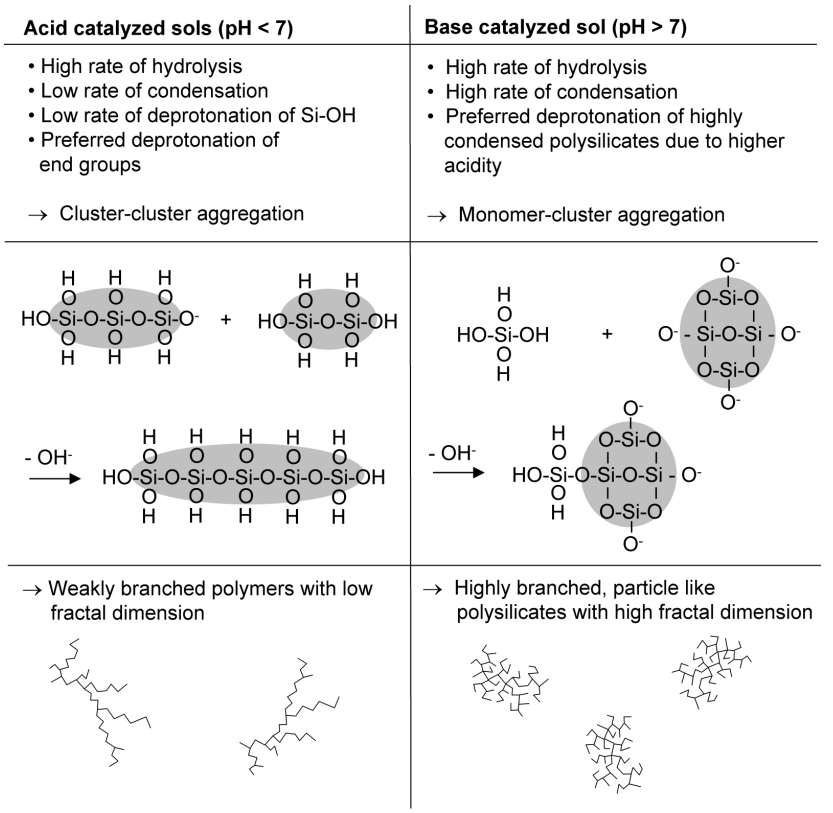


**Fig. 10** The polymer growth mechanisms of acid and base catalyzed silica sols

## *3.5 Mechanical Properties of Silica Hybrid Coatings*

Thickness and hardness of A- and B-coatings were measured as a function of the heat treatment temperature. The thickness was measured by step height measurements of scratched coatings using AFM. The hardness was measured by nanoindentation experiments using a Berkovich diamond indenter with a maximum load resulting in indentation depths of 10% of the coating thickness.

Figure 11 shows the measured thickness and hardness *H* versus heat treatment temperature for A- and B-coatings. The thickness decreased and the hardness increased with increasing heat treatment temperature for both types of coatings. The hardness of the B-coatings exceeded that of the A-coatings for all heat treatment temperatures. A maximum hardness of approximately 3.4 GPa was achieved for the B-coatings ($SiNa_uO_xC_yH_z$) after heat treatment at 600 °C, which is approximately 3-times the measured hardness for A-coatings ($SiO_xC_yH_z$). This indicates that the type of catalyst has an impact on the hardening behavior.

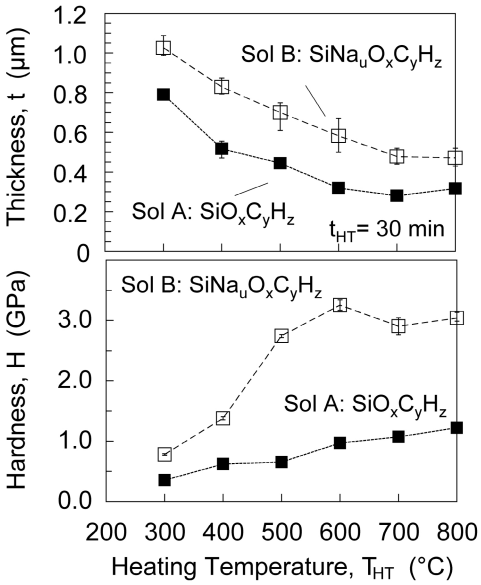


**Fig. 11** Thickness and hardness of A- and B-coatings vs. heat treatment temperature $T_{HT}$. The heat treatment time for the A- and B- coatings was 10 and 30 min, respectively.

The observed decrease of the coating thickness for both types of coatings is due to compaction of the porous coatings by viscous sintering and also due to the evaporation of residual organic and inorganic compounds in the xerogel during heat treatment. Three reasons were proposed to explain the higher hardness of the B-coatings. Firstly, the glass transition temperature $T_g$ of silica glasses decreases with increasing sodium content. For pure silica $T_g$ is 1200 °C, which decreases to 545 °C for a soda-lime glass with 14% sodium [Mar82]. The sodium to silicon ratio Na/Si of the B-coatings was in a range from 0.2 to 0.9, as shown in Fig. 14b [Meh10a]. These ratios correspond to sodium contents of 7.1 to 28%. Therefore, it is expected that the B-coatings have a significantly increased viscous sintering activity compared to the A-coatings which do not contain any sodium [Meh10a]. Secondly, base catalyzed silica sols contain highly condensed particle-like polymers (see Fig. 10) resulting in a higher xerogel density and thus a higher hardness compared to acid catalyzed sols, which contain less branched polymers [Meh10a]. Thirdly, the polymers of acid catalyzed sols are less condensed and therefore contain more organic residuals. These groups are known to constrain the densification processes [Sch97]. All three effects should increase the viscous sintering activity of the B-coatings compared to the A-coatings.

Soda lime glass, which has a similar chemical composition as the B-coatings, has a hardness of 5.5 GPa and an elastic modulus of 70 GPa [Mar82]. Thus, the measured maximum hardness of 3.4 GPa for the B-coatings indicates that the hardening due to sintering is not complete after heat treating for 30 min. This conclusion is supported by long term heat treatment times up to 4 h where a maximum hardness of 6.5 GPa was measured for the coatings [Meh10a].

### 3.6 *Crack Formation of Silica Hybrid Coatings*

A major drawback of the sol-gel coating technology is the limitation of the coating thickness for a single layer due to crack formation [Meh05]. Crack formation, or even delamination, occurs if a critical coating thickness is exceeded. The deposition of crack-free silica hybrid coatings thicker than 5 µm was only achieved by multi-layer deposition which is laborious and time-consuming because each layer needs a complete heat treatment to prevent crack formation. Tensile experiments with coated specimens were carried out in order to characterize the brittleness of the coatings as a function of the sol-gel processing parameters. Figures 12a and 12b show the tensile testing machine which was equipped with a USB microscope for in-situ monitoring of crack formation during the tensile test. The strain of the tensile specimens was measured with a clip gauge mounted on the specimens. Figure 12d shows the typical parallel cracks of a silica coated specimen during the tensile test.

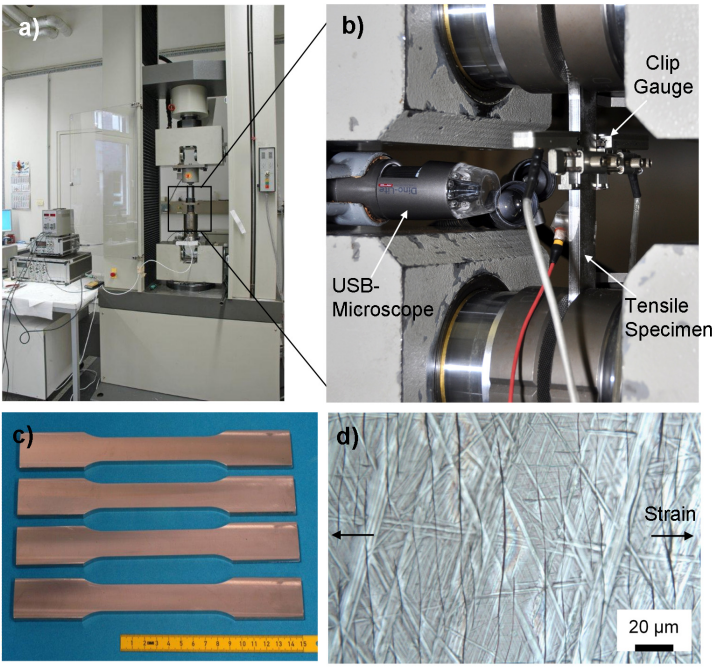


**Fig. 12** Tensile testing machine (a), equipped with an USB-microscope for in-situ monitoring of the crack formation during tensile testing. Sol-gel coated tensile specimens (c). Formation of parallel cracks on the coated specimens during the tensile test (d).

The results in Fig. 13 show that the critical strain for crack formation $\varepsilon_{crit.}$ of A- and B-coatings increased significantly with decreasing coating thickness. This is consistent with the general observation that thin coatings have fewer cracks than thick coatings. Theoretical models to describe this effect are based on an energy

balance analysis of the elastic energy stored in tensile stressed coatings and the energy needed for crack growth [Hut92, Beu96]. The energy needed for crack growth $\Delta E_{Crack}$ is directly proportional to the new area created by the crack $\Delta A_{crack} = \Delta l \cdot t$. ($\Delta l$: increase of the crack length, $t$: coating thickness). Therefore, $\Delta E_{Crack}/\Delta A_{Crack}$ is a constant $R$ ($R$ : crack resistance). Hutchinson and Beuth showed that the released specific elastic energy due to crack growth in a coating $\Delta E_{elast}/\Delta A_{Crack}$ is directly proportional to $\sigma^2/E \cdot t$ ($\sigma$: tensile stress in the coating, $E$: elastic modulus of the coating). Therefore, in thin coatings less elastic energy is released than in thick coatings. Crack growth only occurs if the released elastic energy $\Delta E_{elast}$ /$\Delta A_{Crack}$ is high enough to overcome the crack resistance $R$. Therefore a critical coating thickness exists, below which no crack growth occurs.

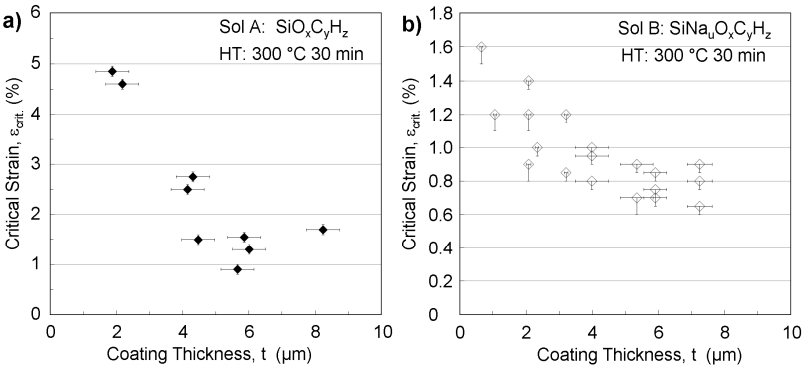


**Fig. 13** Critical strain of silica hybrid coatings from acid (a) and base (b) catalyzed TEOS-MTES sols as a function of the coating thickness

## *3.7 Chemical Properties of Silica Hybrid Coatings*

Several spectroscopic measurements (XPS, Raman, FT-IR) were performed for a more detailed study of the chemical effects during the heat treatment of the B-coatings. The chemical composition of the coatings was analyzed by x-ray photoelectron spectroscopy (XPS), infrared spectroscopy (FT-IR) and Raman spectroscopy. The hydrogen content of the coatings was determined by elastic recoil detection (ERD). Figures 14a and 14b show the chemical composition of A- and B-coatings versus the heat treatment temperature, measured by XPS and ERD.

For the B-coatings the measured atomic ratios of oxygen to silicon (O/Si) increased up to 2.8. Oxygen to silicon ratios above 2 indicate the formation of oxygen containing compounds in addition to silicon dioxide ($SiO_2$). According to the XP-spectra (not shown) sodium bicarbonate ($NaHCO_3$), sodium carbonate ($Na_2CO_3$) or sodium carboxylates (such as NaOOCH) come into consideration as additional oxygen containing compounds. These results were confirmed by FTIR and Raman spectroscopic measurements [Meh10a].

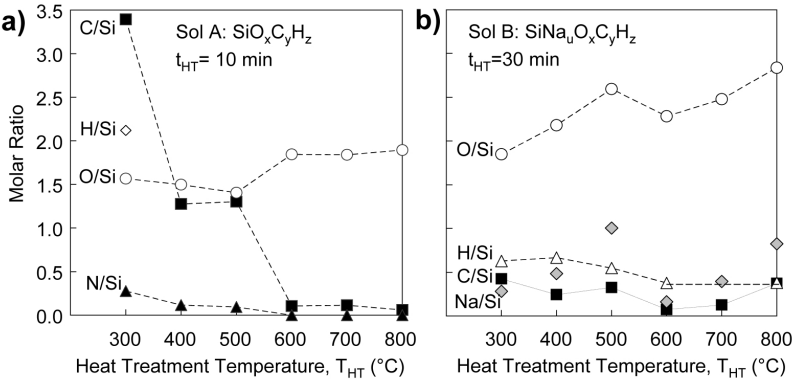


**Fig. 14** Molar ratios of A- and B-coatings as a function of the heat treatment temperature

### 3.7.1 Ion Irradiation of Silica Based Sol-Gel Coatings

Ion irradiation is an alternative to heat treatment for converting the sol-gel films to the ceramic state. In contrast to heat treatment at high temperature, which leads to high levels of carbon loss and film cracking, crack-free films having a high concentration of carbon with the selective release of hydrogen are formed after ion irradiation [Piv97]. Incident ions are decelerated while passing through the film, during which time the energy is transferred to atoms in the films either by collision with target atoms of the film (nuclear stopping) or by excitation of electrons and subsequent ionization (electron stopping) [Tra99].

The ion irradiated films were prepared by diluting the acid and base catalyzed sols and performing an initial heat treatment at 300 °C for 10 and 30 min, respectively. Base catalyzed films had thicknesses ranging from 950 to 1025 nm [Qi10], while acid catalyzed films were about 600 to 650 nm in thickness [Luc08], as determined by step height measurements using AFM. The film density was estimated to be 1.3 g/cm$^3$ based on the measured film thickness, the coated area of the film, and the measured weight gain after coating and heat treatment. Ion irradiation was carried out at room temperature using 125 keV $H^+$ and 250 keV $N^{2+}$ at fluences ranging from $1 \times 10^{14}$ to $2.5 \times 10^{16}$ ions/cm$^2$. To measure the hydrogen concentration of the films, elastic recoil detection (ERD) was performed using 3 MeV $^4He^+$ and a detection angle of 30° with respect to the incident beam. ERD and X-ray photoelectron spectroscopy (XPS) identified the chemical composition of the unirradiated acid catalyzed films as 20 at. % O, 14 at. % Si, 34 at. % H, and 32 at. % C and the unirradiated base catalyzed films as 44.2 at. % O, 22.1 at. % Si, 20.3 at. % H, 10.7 at. % C and 2.7 at. % Na.

Mechanical properties of the resulting thin films were investigated through nanoindentation experiments performed using a load-controlled commercial nanoindenter in conjunction with an AFM. A Berkovich diamond indenter was used for all indentations. Hardness and reduced elastic modulus were measured over a range of contact depths, from a maximum of 20% of the film thickness to a minimum of either 5% of the film thickness or 20-times the rms surface

roughness, whichever was largest. Prior to nanoindentation surface roughness was measured by AFM. The surface roughness of all films, before and after ion irradiation, was approximately 1 nm rms over a scan area of 1 $\mu m^2$.

Figure 15 shows the nanoindentation hardness evaluated at 10% of the film thickness as a function of fluence. The observed hardness increase with increasing ion fluence is consistent with previous studies of the acid catalyzed films [Ghi08]. Irradiation with $N^{2+}$ was found to be more effective than with $H^+$ in converting the sol-gel films to their ceramic state for both the acid and base catalyzed films [Luc10]. For the acid catalyzed films, the irradiating ion species played a greater role in the final achieved hardness than for the base catalyzed system. At the highest fluence investigated for both ions, the hardness of $N^{2+}$ irradiated acid catalyzed film was 270% greater than the hardness of $H^+$ irradiated film. Whereas for the base catalyzed films, only a 30% difference in hardness was observed. In addition, at the highest fluence, $N^{2+}$ irradiation of the acid catalyzed films resulted in higher hardness than for that of the base catalyzed films, 7.4 GPa compared to 4.7 GPa. This is in contrast to $H^+$ irradiation in which the results showed a somewhat higher hardness for the base catalyzed films. For the base catalyzed films, the reduced elastic modulus showed no dependence on ion species.

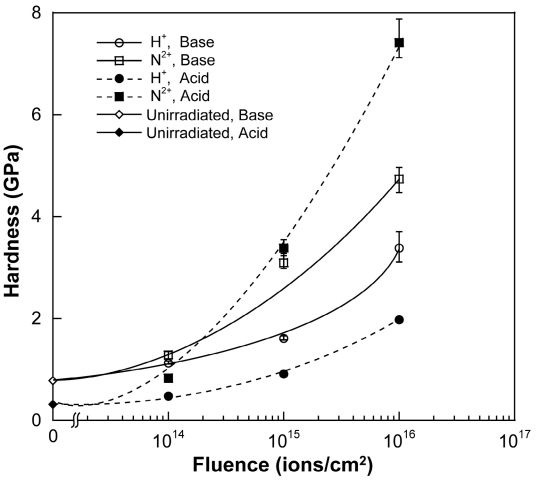


**Fig. 15** Nanoindentation hardness evaluated at 10% of the film thickness as a function of fluence for irradiations with 125 keV $H^+$ and 250 keV $N^{2+}$ [Luc10]

Film thickness of the base catalysed films was observed to decrease with increasing fluence as shown in Fig. 16. Hardness increases with increasing film shrinkage when the films are subjected to ion irradiation, consistent with heat treatment. However hardness is not simply a result of film shrinkage as shown in Fig. 17, where ion irradiation resulted in films with a higher hardness compared to heat treated films with a comparable amount of shrinkage.

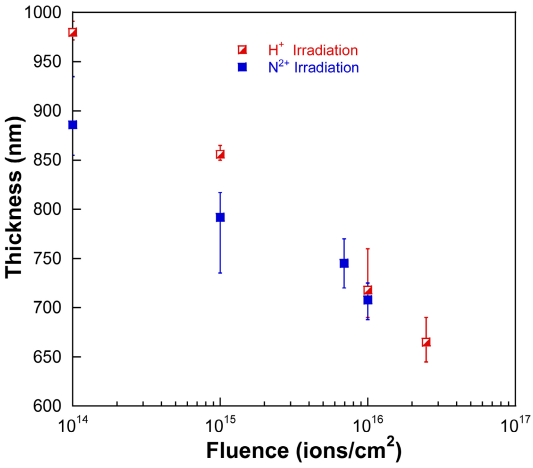


**Fig. 16** Film thickness of the base catalyzed films as a function of fluence for irradiations with 125 keV $H^+$ and 250 keV $N^{2+}$

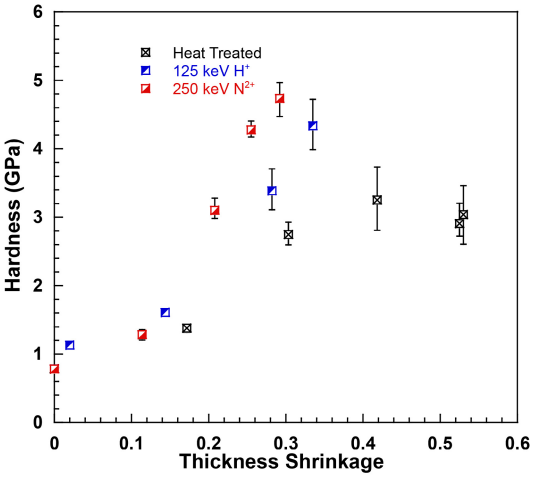


**Fig. 17** Nanoindentation hardness of the base catalyzed films as a function of film shrinkage

The effect of ion irradiation on hardness and hydrogen concentration as a function of fluence is shown in Fig. 18. Compared to the acid catalyzed films, the unirradiated base catalyzed films had a somewhat higher hardness, 0.78 GPa compared to 0.32 GPa. Hardness was observed to increase with fluence, while hydrogen concentration decreased, for both the acid and base catalyzed films. The observed decrease in hydrogen concentration with increasing fluence is consistent with previously reported observations of inorganic polymer films [Tan02, Piv03]. As produced, the acid catalyzed films had a higher concentration of hydrogen than

that for the base catalyzed films, which could be attributed to the addition of polyvinylpyrrolidone (PVP) in the acid catalyzed sols. The films exhibited a different hardening response, as well as hydrogen release process, to irradiation with $H^+$ or $N^{2+}$ based on sol composition.

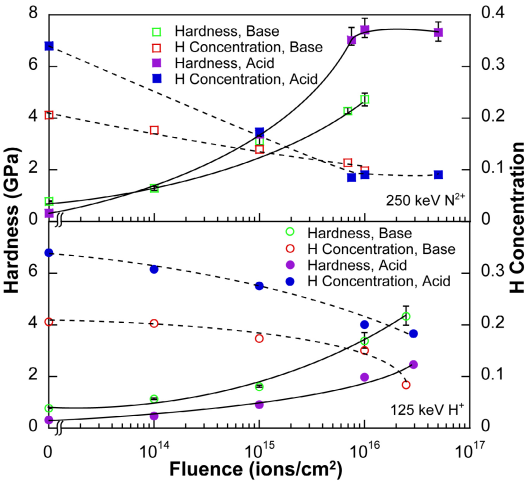


**Fig. 18** Nanoindentation hardness and hydrogen concentration as a function of ion fluence for $H^+$ and $N^{2+}$ [Qi10]

The FT-IR spectra obtained for the unirradiated base catalyzed film and for films irradiated with $H^+$ and $N^{2+}$ over a range of fluences are shown in Figs. 19a and 19b. The FT-IR spectrum of the unirradiated film exhibits three distinct peaks centered near 1060, 1165, and 1275 $cm^{-1}$. The 1060 $cm^{-1}$ peak is associated with the transverse optical (TO) mode of Si-O-Si anti-symmetric stretching and the 1165 $cm^{-1}$ peak has been reported to be related to the longitudinal optical (LO) mode of strained Si-O-Si anti-symmetric stretching in porous silica [Gal02, Alm90]. The peak near 1275 $cm^{-1}$ is attributed to the C-H bending mode of $Si-CH_3$ groups. With increasing fluence, the C-H peak gradually decreases in intensity and is no longer observed at the higher fluences, suggesting a reduction of C-H bonds in $Si-CH_3$ groups due to irradiation. The continuous decrease of the C-H peak intensity is consistent with the decreasing hydrogen concentration observed with increasing fluence shown in Fig. 18.

With increasing fluence, changes in the relative intensity of the TO and LO modes of Si-O-Si bridging bonds are observed. These peaks transition from two distinct peaks into one broad peak, indicating a widening range of Si-O-Si related species. The increase in intensity of the TO mode with increasing fluence, relative to the LO mode suggests a more polymerized network [Gal02]. The decrease in relative intensity of the LO mode also suggests a decrease in film porosity with increasing fluence since the LO mode at 1165 $cm^{-1}$ has been shown to be related to strained Si-O-Si bonds that are present at the surface of gel pores [Gal02].

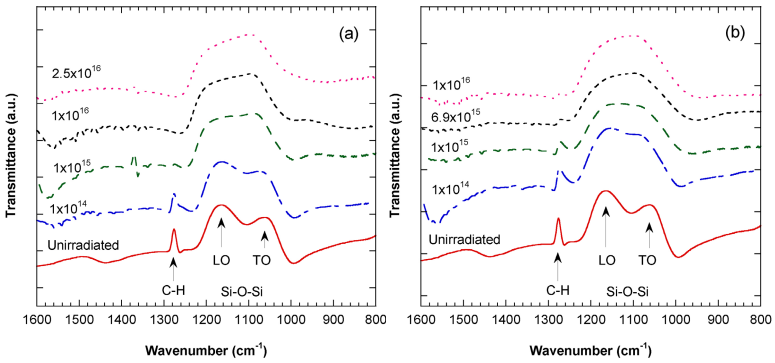


**Fig. 19** FT-IR spectra of base catalyzed films irradiated with (a) 125 keV $H^+$ and (b) 250 keV $N^{2+}$ at various fluences. For comparison the FT-IR spectra for an unirradiated film is also shown [Qi10].

An increase in the network polymerization and a decrease in film porosity may partially account for the increasing hardness that was observed with increasing ion fluence.

## *3.8 Machining of Silica Based Sol-Gel Coatings*

Micro-structured molds for injection molding of optical elements were manufactured by micromachining. Hardened steel disks (Ø 50 mm, *t*: 15 mm, AISI 420: X40Cr13, 55 HRC) were ground and polished to an optical surface quality. The base catalyzed sol B was deposited on the steel disks by spin coating at 500 rpm followed by a heat treatment at 300 °C for 120 min. The spin coating and heat treatment process was repeated 4 times. The resulting 4-layered coatings had a total thickness of ≈ 17 µm. The coatings were structured by fly-cutting using a diamond cutting tool with a negative rake angle $\gamma = -20°$ and a cutting edge radius of $r_\varepsilon = 3$ mm. Diamond machining of the coated molds was performed on an ultra-precision machine tool. The milling process is illustrated in Fig. 20a. Figures 20b and 20c show the structured coating with the micromachined channels [Meh10b]. The surfaces of the machined channels were smooth and the edges were sharp, showing no defects or burr formation. The measured roughness *R*a was about 15 nm. Injection molding of PMMA optical elements was accomplished with sol-gel coated and structured molds using a commercial injection molding machine (backpressure: 1300 bar, PMMA temperature: 230 °C, mold temperature: 80 °C and injection velocity: 20 $cm^3s^{-1}$). Figure 20d shows an example of an optical element replicated by injection molding using the sol-gel coated and micro-structured mold in Fig. 20b. No adhesion or sticking between the PMMA and the coated molds occurred and the replicated elements showed an almost optical surface quality with a surface roughness *R*a of 21 nm. Microscopic examination of non-structured coatings after injection molding of 1000 lenses revealed no visible changes. Thus, corrosion and wear resistance of these

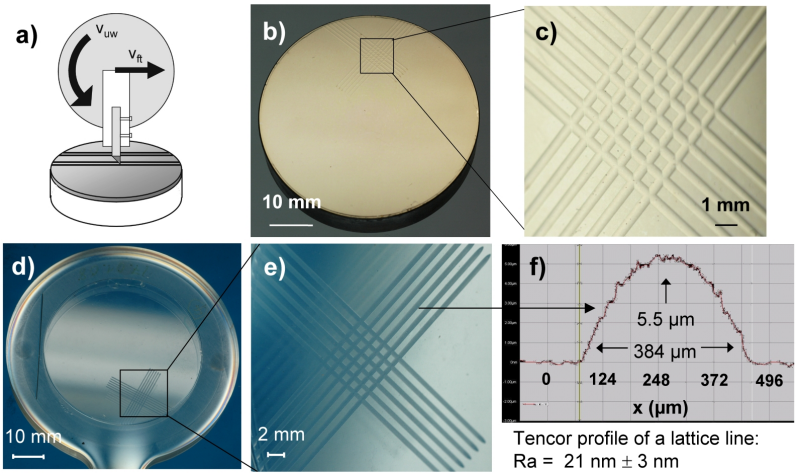


**Fig. 20** Schematic of the diamond milling process (a). Steel mold with a micro-structured B-coating (b) and (c). PMMA optical element replicated by injection molding with the micro-structured mold (d) and (e). Profile of a lattice line (f).

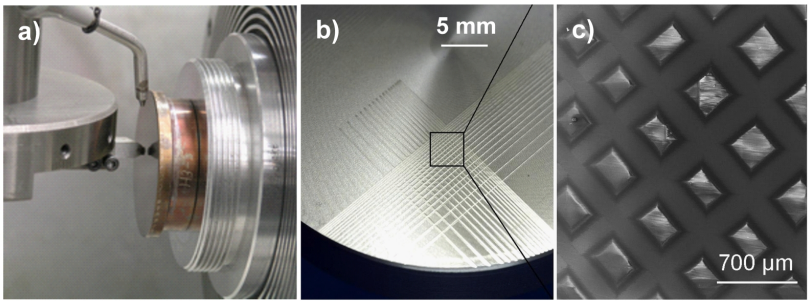


**Fig. 21** Diamond milling of a sol-gel coated steel mold (a). Steel mold with a micro-structured A-coating (b). SEM image of the micromachined coating surface (c).

coatings are sufficient for injection molding of PMMA optical components. Figure 21 shows the micromachining of a 4-layer A-coating and the resulting microstructures.

## 4 Coating Characterization by Photothermal Methods

In addition to mechanical and chemical properties, mold coatings also provide a thermal barrier, which help to control the cooling rates of the injected plastic material. The effectiveness of this thermal barrier depends on its design, mainly the coating thickness and thermal properties (thermal conductivity and heat

capacity) of the material. Photothermal measurement techniques have the ability to measure both the thickness and thermal properties of the coatings.

Different photothermal techniques exist, but in most cases an intensity modulated laser beam will thermally excite the specimen surface as shown in Fig. 22. Thermal waves are created and propagate to the layer/substrate interface [Ros76], where they are reflected back to the surface. Depending on the thermal diffusion length $\mu$, the layer thickness $d$ and the thermal reflection coefficient $R$, multiple thermal wave reflections can occur. These multiple waves result in an oscillating temperature, defined by a temperature amplitude $T_0$ and a phase difference $\Delta\varphi$ (with respect to the exciting thermal wave). This behavior resembles optical thin film interferometry, thus it is often referred to as thermal wave interferometry [Ben82]. The temperature is usually measured by infrared detection and contributions to the phase difference from electronic components are corrected by normalization procedures.

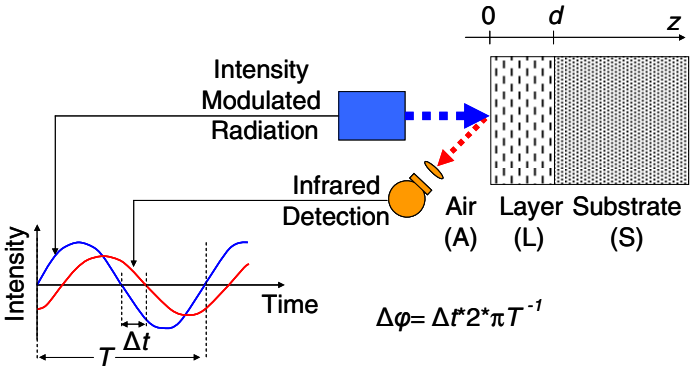


**Fig. 22** Experimental setup of a photothermal measurement and the definition of the measured phase difference $\Delta\varphi$

For a one-dimensional geometry and optically opaque coatings, mathematical equations exist that describe the thermal wave behavior. For instance, at the coating surface ($z$=0) the complex temperature amplitude $T_L$ is given by

$$T_L(z=0) = \frac{I_0}{2\kappa_L \sigma_L} \frac{1+R\cdot\exp(-2\sigma_L d)}{1-R\cdot\exp(-2\sigma_L d)} \tag{1}$$

where $I_0$, $d$, $\kappa_L$ denote the excitation intensity, the layer thickness and the thermal conductivity of the coating layer, respectively. The complex parameter $\sigma_L$ is given by

$$\sigma_L = (1+\mathrm{i})/\mu_L \tag{2}$$

The reflection coefficient for thermal waves, $R$, depends on the thermal contrast between the coating (subscript L) and the substrate (subscript S):

$$R = \frac{1 - \frac{e_S}{e_L}}{1 + \frac{e_S}{e_L}} \tag{3}$$

with

$$e_j = \sqrt{\kappa_j \rho_j c_j} \tag{4}$$

Here, $\rho$ and $c$ are the mass density and the heat capacity, respectively.

The thermal diffusion length $\mu_L$ is finally calculated by

$$\mu_L = \frac{\lambda_L}{2\pi} = \sqrt{\frac{2\alpha_L}{\omega}} = \sqrt{\frac{2\kappa_L}{\rho_L c_L \omega}} \tag{5}$$

The magnitude of the thermal diffusion length, which can be interpreted as the thermal wave propagation range, is smaller than the thermal wavelength $\lambda$ and decreases with increasing modulation frequencies ($f=\omega/2\pi$) of the excitation radiation. Figure 23 shows the calculated phase difference $\Delta\varphi$ of the complex temperature amplitude (Eq. (1)) with respect to the coating thickness $d$, normalized to the thermal diffusion length $\mu_L$. The phase difference varies with the thermal reflection coefficient $R$.

As indicated by the straight line superimposed over the $R$=-0.9 curve, within a limited range the phase difference depends almost linearly on the layer thickness.

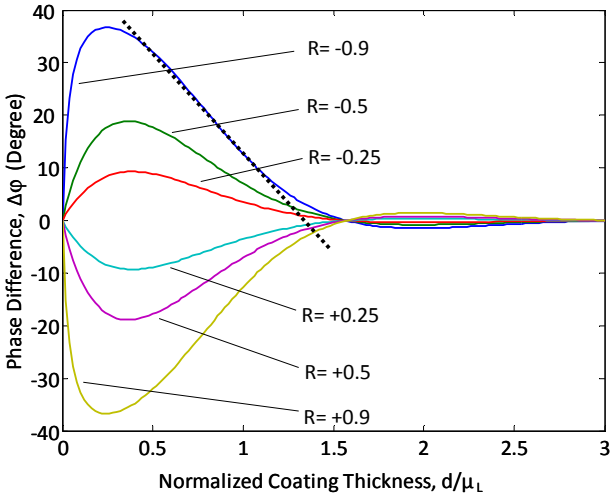


**Fig. 23** Normalized phase difference for different reflection coefficients

Within this nearly linear region, the coating thicknesses can be measured if the thermal parameters of the substrate and the coating are known. (Alternatively, the correlation between $\Delta\varphi$ and $d$ can be determined by calibration.)

It must be noted that in Fig. 23 the layer thickness has no effect on the maximum phase value, which is influenced exclusively by the reflection coefficient $R$.

Figure 23 reveals that the phase curves at constant frequency and varying layer thicknesses $d$ have the same shape as those at constant layer thickness and varying frequencies. In order to determine the coating thermal properties, the phase $\Delta\varphi$ has to be measured for different modulation frequencies and plotted as a function of $f^{1/2}$ (Fig. 24). Then the maximum phase value and the thermal reflection coefficient $R$ can be estimated. Equations (3) and (4) then yield the product $\kappa_L\rho_L c_L$. Afterwards, a normalization factor $s$ for the abscissa in Fig. 24 must be determined by approximation. The correct value of $s$ is found when the maximum of the measured phase is located at the same position as the maximum of the phase curve in Fig. 23 (calculated for the same value of $R$).

$$s = \frac{\sqrt{\dfrac{\kappa_L}{\pi\rho_L c_L}}}{d} \tag{6}$$

Now, the thermal diffusivity $\kappa_L/\rho_L c_L$ can be calculated using the relationship (6). Combining the thermal diffusivity and the product $\kappa_L\rho_L c_L$ will finally yield the thermal conductivity $\kappa_L$ of the coating. Figure 24 shows phase curves as measured for five specimens of PVD TiCuN coatings on steel substrates.

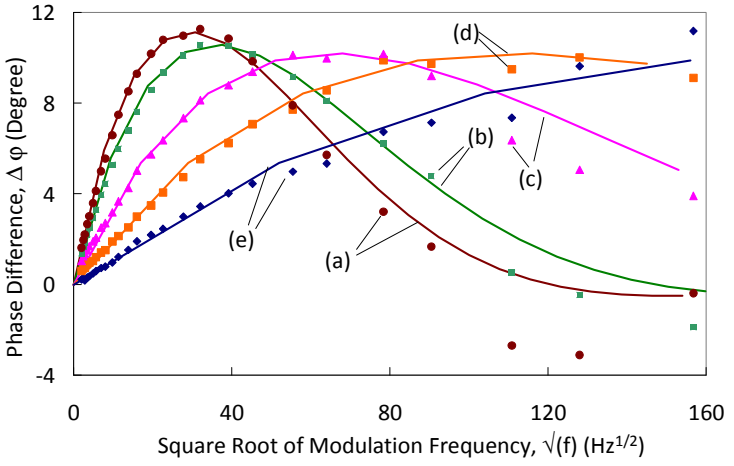


**Fig. 24** Measured phase curves for PVD TiCuN coatings on steel disks with thicknesses of 11.7 µm (a), 10.0 µm (b), 5.3 µm (c), 3.2 µm (d), and 1.8 µm (e)

The coating composition was determined by GDOES analysis as Ti: 84–89%, Cu: 0.4-1.0%, N: 8-13%. The coating thicknesses *d* were measured by ball cratering and the numerical results from the photothermal analysis are summarized in Table 2. More details of sample preparation and analysis were published elsewhere [Goc04].

**Table 2** Numerical results from a photothermal analysis of PVD TiCuN coatings

| | d (μm) | | | | |
|---|---|---|---|---|---|
| | 11.7 | 10.0 | 5.3 | 3.2 | 1.8 |
| R | -0.3 | -0.28 | -0.275 | -0.275 | -0.275 |
| $\alpha$ ($m^2\ s^{-1}$) | 2.55 | 2.77 | 2.55 | 2.79 | 2.54 |
| $e_L$ ($W\ s^{½}\ m^{-2}\ K^{-1}$) | 7135 | 7370 | 7540 | 7540 | 7540 |
| $\kappa$ ($W\ m^{-1}\ K^{-1}$) | 11.4 | 12.3 | 12.0 | 12.6 | 12.0 |

For the above method of determining the coating thermal parameters, the substrate's thermal parameters and the layer thickness must be known. The method is applicable only for one-dimensional thermal wave propagation. Furthermore, the coatings must be opaque to the excitation and detection wavelengths. Another assumption about the coating-substrate interface is that the heat flow and the temperature must be continuous, otherwise a thermal contact resistance arises and the thermal reflection coefficient will become complex [Pre06]. A thermal contact resistance, which is detectable by significant deviations from typical phase curves, indicates a possible layer delamination.

## 5 Summary

The Collaborative Research Center SFB-TR4 has pursued the development of novel hard films to be used as coatings for molds for the replication of complex optics. Coatings for use in the precision pressing of glass and the injection molding of plastics were developed. Nanocrystalline PVD Ti-Ni-N and Ti-Cu-N coatings and thin sol-gel $ZrO_2$ coatings were developed and tested as new protective coatings for glass pressing molds. For mold coatings to be employed in the injection molding of plastics, thick sol-gel silica based coatings were developed and tested as an alternative for traditional electroless nickel coatings. By using hybrid organic-inorganic sol-gels, thick, crack-free coatings could be produced. Micromachining with diamond tools was used to create complex geometries in the coatings while in their pre-ceramic state. Conversion of the sol-gel films to their final ceramic state was achieved by heat treatment and ion irradiation.

**Acknowledgement.** The authors like to thank the German Research Foundation (DFG) for funding this work as a part of the Transregional Collaborative Research Center SFB/TR4 "Process Chains for the Replication of Complex Optical Elements". Funding from the National Science Foundation through Grant Nos. OISE-0352377 and OISE-0128050 is gratefully acknowledged. Portions of this work were performed at the Center for Integrated Nanotechnologies, a US Department of Energy, Office of Basic Energy Sciences, Nanoscale Science Research Center operated jointly by Los Alamos and Sandia National Laboratories.

## References

[Alm90] Almeida, R.M., Pantano, C.G.: Structural investigation of silica gel films by infrared spectroscopy. J. Appl. Phys. 68, 4225–4232 (1990)

[Bra01] Bradley, D.C., Mehrotra, R.C., Rothwell, I.P., Singh, A.A.: Alkoxo and Aryloxo Derivatives of Metals. Academic Press, Boston (2001)

[Ben04] Bengelsdorff, S., Stock, H.-R., Zoch, H.-W., Grimme, D., Preuß, W., Brinksmeier, E.: Abscheidung von diamantbearbeitbaren Titan-Nickel-Nitrid-Schichten für Abformwerkzeuge. Tagungsband zum 7. Werkstofftechnischen Kolloquium in Chemnitz, Schriftenreihe Werkstoffe und werkstofftechnische Anwendungen. Band 18, 256–262 (2004) ISBN 3-00-013553-7, ISSN 1439-1597

[Ben82] Bennett, C.A., Patty, R.R.: Thermal wave interferometry: A potential application of the photoacoustic effect. Appl. Optics 21(1), 49–54 (1982)

[Beu96] Beuth, J.L., Klingbeil, N.W.: Cracking of thin films bonded to elastic-plastic substrates. J. Mech. Phys. Solids 44(9), 1411–1428 (1996)

[Bri90] Brinker, C.J., Scherer, G.W.: Sol-Gel Science: The Physics and Chemistry of Sol-Gel Processing, ch. 3. Academic Press, Boston (1990)

[Dat05] Datchary, W., Mehner, A., Zoch, H.-W., Lucca, D.A., Klopfstein, M.J., Ghisleni, R., Grimme, D., Brinksmeier, E.: High precision diamond machining of hybrid sol-gel coatings. J. Sol-Gel Sci. Technol. 35, 245–251 (2005)

[Gal02] Gallardo, J., Durán, A., Di Martino, D., Almeida, R.M.: Structure of inorganic and hybrid $SiO_2$ sol-gel coatings studied by variable incidence infrared spectroscopy. J. Non-cryst. Solids 298, 219–225 (2002)

[Ghi07] Ghisleni, R., Lucca, D.A., Nastasi, M., Shao, L., Wang, Y.Q., Dong, J., Mehner, A.: Effects of electronic stopping on the irradiation-induced changes in hybrid modified silicate thin films. Nucl. Instrum. Meth. B 257, 581–584 (2007)

[Ghi08] Ghisleni, R., Lucca, D.A., Wang, Y.Q., Lee, J.-K., Nastasi, M., Dong, J., Mehner, A.: Ion irradiation effects on surface mechanical behavior and shrinkage of hybrid sol-gel derived silicate thin films. Nucl. Instrum. Meth. B 266, 2453–2456 (2008)

[Gri04] Grimme, D., Preuß, W., Brinksmeier, E., Bengelsdorff, S., Stock, H.-R., Mayr, P.: Technologische Grundlagenuntersuchungen zur Bearbeitung neuartiger schleif- und polierbarer PVD-Hartstoffschichten. HTM 59, 291–297 (2004)

[Goc04] Goch, G., Prekel, H., Patzelt, S., Ströbel, G., Lucca, D.A., Stock, H.R., Mehner, A.: Non-destructive and non-contact determination of layer thickness and thermal properties of PVD and sol-gel layers by photothermal methods. CIRP Ann.-Manuf. Techn. 53, 471–474 (2004)

[He01] He, J.L., Setsuhara, Y., Shimizu, I., Miyake, S.: Structure refinement and hardness enhancement of titanium nitride films by addition of copper. Surf. Coat. Technol. 137, 38–42 (2001)

[Hut92] Hutchinson, J.W., Suo, Z.: Mixed Mode Cracking in Layered Materials. Chapter V. Cracking of Pre-tensioned Films. In: Advances in Applied Mechanics, vol. 29, pp. 132–137. Academic Press, Boston (1992)

[Ile79] Ller, R.K.: The Chemistry of Silica. Wiley, New York (1979)

[Izu89] Izumi, K., Murakami, M., Deguchi, T., Morita, A., Tohge, N., Minami, T.: Zirconia coatings on stainless-steel sheets from organozirconium compounds. J. American Ceramic Soc. 72, 1465–1468 (1989)

[Luc04] Lucca, D.A., Klopfstein, M.J., Ghisleni, R., Gude, A., Mehner, A., Datchary, W.: Investigation of sol-gel derived $ZrO_2$ thin films by nanoindentation. CIRP Ann.-Manuf. Techn. 53, 475–478 (2004)

[Luc07] Lucca, D.A., Ghisleni, R., Nastasi, M., Shao, L., Wang, Y.Q., Dong, J., Mehner, A.: Effects of ion implantation on surface mechanical properties of sol-gel derived TEOS/MTES thin films. Nucl. Instrum. Meth. B 257, 577–580 (2007)

[Luc08] Lucca, D.A., Ghisleni, R., Lee, J.-K., Wang, Y.Q., Nastasi, M., Dong, J., Mehner, A.: Effects of ion irradiation on the structural transformation of sol-gel derived TEOS/MTES thin films. Nucl. Instrum. Meth. B 266, 2457–2460 (2008)

[Luc10] Lucca, D.A., Qi, Y., Harriman, T.A., Prenzel, T., Wang, Y.Q., Nastasi, M., Dong, J., Mehner, A.: Effects of ion irradiation on the mechanical properties of $SiNa_wO_xC_yH_z$ sol-gel derived thin films. Nucl. Instrum. Meth. B 268, 2926–2929 (2010)

[Mar82] Marschall, D.B., Noma, T., Evans, A.G.: A simple method for determining elastic-modulus-to-hardness ratios using Knoop indentation measurements. J. Am. Ceram. Soc. 65(10), 175–176 (1982)

[Meh97] Mehner, A., Klümper-Westkamp, H., Hoffmann, F., Mayr, P.: Crystallization and residual stress formation of sol-gel-derived zirconia films. Thin Solid Films 308-309, 363–368 (1997)

[Meh99] Mehner, A.: Sinterung und Kristallisation nasschemisch abgeschiedener $ZrO_2$-Filme. Dissertation. Shaker-Verlag, Aachen (1999)

[Meh05] Mehner, A., Datchary, W., Bleil, N., Zoch, H.-W., Klopfstein, M.J., Lucca, D.A.: The influence of sol-gel processing parameters on crack formation, microstructure, density and hardness of sol-gel derived zirconia films. J. Sol-Gel Sci. Technol. 36, 25–32 (2005)

[Meh06] Mehner, A., Zoch, H.-W., Datchary, W., Pongs, G., Kunzmann, H.: Sol-gel coatings for high precision optical molds. CIRP Ann.-Manuf. Techn. 56, 589–592 (2006)

[Meh07] Mehner, A., Dong, J., Zoch, H.-W., Brinksmeier, E., Grimme, D., Lucca, D., Ghisleni, R., Michaeli, W., Kleiber, F.: Diamond Machinable Sol-Gel $SiO_xC_y$-Coatings for High Precision Optical Molds. In: Proceedings of the 6th International Conference THE Coatings in Manufacturing Engineering 2007, Hannover, May 25-26, pp. 55–64 (2007); Berichte aus dem IFW Band 10/2007

[Meh10a] Mehner, A., Dong, J., Prenzel, T., Datchary, W., Lucca, D.A.: Mechanical and chemical properties of thick hybrid sol-gel silica coatings from acid and base catalyzed sols. J. Sol-Gel Sci. Technol. 54, 355–362 (2010)

[Meh10b] Mehner, A., Dong, J., Hoja, T., Prenzel, T., Mutlugünes, Y., Brinksmeier, E., Lucca, D.A., Klaiber, F.: Diamond machinable sol-gel silica based hybrid coatings for high precision optical molds. Key Eng. Mat. 438, 65–72 (2010)

[Myu03] Myung, H.S., Lee, H.M., Shaginyan, L.R., Han, J.G.: Microstructure and mechanical properties of Cu doped TiN superhard nanocomposite coatings. Surf. Coat. Technol. 163-164, 591–596 (2003)

[Pat98] Paterson, M.J., Paterson, P.J.K., Ben-Nissan, B.: The dependence of structural and mechanical properties on film thickness in sol-gel zirconia films. J. Mater. Res. 13, 388–395 (1998)

[Piv97] Pivin, J.C., Colombo, P.: Ceramic coatings by ion irradiation of polycarbosilanes and polysioxanes: Part I conversion mechanism. J. Mater. Sci. 32, 6163–6173 (1997)

[Piv03] Pivin, J.C., Colombo, P., Martucci, A., Sorarù, G.D., Pippel, E., Sendova-Vassileva, M.: Ion beam induced conversion of Si-based polymers and gels layers into ceramics coatings. J. Sol-Gel Sci. Technol. 26, 251–255 (2003)

[Pre06] Prekel, H., Klopfstein, M.J., Giesselbach, M., Patzelt, S., Ghisleni, R., Lucca, D.A., Goch, G., Stock, H.R.: Photothermal investigation of Ti-Cu-N and T Ni N PVD Films. CIRP Ann.-Manuf. Techn. 55, 585–588 (2006)

[Qi10] Qi, Y., Prenzel, T., Harriman, T.A., Wang, Y.Q., Lucca, D.A., Williams, D., Nastasi, M., Dong, J., Mehner, A.: Investigation of hydrogen concentration and hardness of ion irradiated organically modified silicate thin films. Nucl. Instrum. Meth. B 268, 1997–2000 (1999)

[Ros76] Rosencwaig, A., Gersho, A.: Theory of the photoacoustic effect with solids. J. Appl. Phys. 47, 64–69 (1976)

[Rie05] Rieser, D., Spieß, G., Manns, P.: Untersuchungen zum Klebe- und Abriebverhalten von Formenwerkstoffen und Beschichtungen für die Glasheißverarbeitung (AiF-Nr. 13508N). In: Deutsche Glastechnische Gesellschaft -DGG-, Frankfurt/Main: 79. Glastechnische Tagung. Programm und Referate. CD-ROM: Würzburg, Mai 23-25. DGG, Offenbach (2005) ISBN: 3-921089-43-3

[Sch97] Scherer, G.W.: Sintering of sol-gel films. J. Sol.-Gel. Sci. Technol. 8, 353–363 (1997)

[Tan02] Taniike, A., Kubota, N., Takeuchi, M., Furuyama, Y., Kitamura, A.: Ion-irradiation induced hydrogen loss from polyethylene film. J. Appl. Phys. 92, 6489–6495 (2002)

[Tra99] Trakhtenber, L.S., Rubshtein, A.P., Levin, A.D.: Radiation-induced release of hydrogen from C:H films: basic regularities and mechanism. Diam. Relat. Mater. 8, 2164–2168 (1999)

# In-situ and In-process Metrology for Optical Surfaces

Gert Goch, Robert Schmitt, Stefan Patzelt, Stephan Stürwald,
and Andreas Tausendfreund

**Abstract.** Measurements of the form and the roughness during the machining process or the replication process with molds is still difficult and highly inaccurate. An adequate roughness measuring system is based on the analysis of the scattered speckle intensity distribution, emerging from the workpiece surface. This contribution covers the theoretical description of the scattered light measuring process, which is based on the scalar Kirchhoff theory and a ray tracing model of the light propagation in an optical fiber considering physical optics.

Highest accuracy in optical, non tactile measurement of form deviations of molds or the molded optics in the machine is achieved by interferometry. A phase shifting digital holographic measurement method is described in more detail. This comprises an automated alignment set-up including the features of auto focusing and subsequent refocusing, the use of computer generated holograms (CGHs) as well as different approaches for a systematic determination and evaluation of form deviations.

## 1 Introduction

The geometrical form and the surface roughness mainly characterize the quality of ultra-precision machined, optical molds and optical parts. Until today it is often difficult and highly inaccurate to measure the form and the roughness during the ultra-precision machining process or the replication process with molds. The workpiece has to be measured outside the machine tool with an external measuring system. Tool wear during machining increases the roughness, and finally leads to a poor surface quality. A second machining process with a new diamond cutting tool is required. In the case of a post-process measurement the workpiece has to be aligned exactly at the same position as during the first

Gert Goch · Stefan Patzelt · Andreas Tausendfreund
Bremen Institute for Metrology, Automation and Quality Science BIMAQ,
University of Bremen, Linzer Straße 13, 28359 Bremen, Germany

Robert Schmitt · Stephan Stürwald
Fraunhofer Institute for Production Technology IPT, Steinbachstraße 17, 52074,
Aachen, Germany

E. Brinksmeier et al. (Eds.): Fabrication of Complex Optical Components, LNPE, pp. 161–178.
springerlink.com 

machining process, which is at least time-consuming or even impossible. This results in a strong demand for measuring systems that allow form and roughness characterization while the workpiece is still clamped inside the machine tool, either in a process discrete manner (in-situ) or during the machining operation itself (in-process).

An adequate roughness measuring system is based on the analysis of the scattered speckle intensity distribution, emerging from the workpiece surface. It operates fast and contact-free at a working distance of at least some centimeters with a measuring range from $Sq = 1$ nm to $Sq = 150$ nm. It preferably characterizes specularly reflecting surfaces with possibly anisotropic topography in an in-process operation mode. This contribution covers the theoretical description of the scattered light measuring process, which is based on the scalar Kirchhoff theory, and a ray tracing model of the light propagation in an optical fiber considering physical optics.

Form testing interferometry permits fast, non-tactile and full-field quantitative phase imaging for testing optical components in manufacturing. To reduce the influence of vibrations under manufacturing conditions, it is most common to use the FT-based spatial carrier phase measurement technique (SCPM) which requires only a single interferogram recording. The utilization of digital holographic interferometry with relatively new spatial phase-shifting methods operating in the position space offers higher robustness under production conditions. Therefore, phase-shifting digital holography is applied in machine integrated interferometric form testing of optical lenses. Digital holographic interferometry (DHI) allows altering the focus numerically by propagating the complex wave. Especially for compensation of deformations or displacements and for long-term investigations in a machine, a reliable numerical readjustment of the focus is of particular interest in digital holographic microscopy. The concept of numerical parametric lenses is another key feature in DHI and used to correct aberrations in the reconstructed wave front caused by the set-up to measure form deviations of reflective, optical surfaces.

## 2 Roughness Measurement

In contrast to topographic methods for surface roughness measurement (e. g. stylus and autofocusing profilometers, white light interferometers), light scattering techniques show real in-process capabilities. Early investigations resulted in a measuring device based on the measurement of the specularly reflected and the diffusely scattered light component, detected under a certain angle in order to monitor the roughness changes during grinding [Pet65]. The major problem of this device is the dependence of the measuring result on maladjustment, emerging from the waviness of the surface, for example. In-process measuring methods based on the diffuseness of scattered light are less sensitive to maladjustment [Bro84, Lee87]. They assume a strong correlation between the surface height and the surface slope distribution. This is usually correct for specific manufacturing processes [Pet79], but leads to difficulties when a comparative characterization of surfaces produced by different processes is required. The power spectrum of a rough surface can be obtained from the angular distribution of scattered light

[Thw80]. With respect to in-process applications, this ARS-method (ARS = angle resolved scattering) requires a very high dynamic range of the detector, and it is limited to rather smooth optical surfaces (root mean square of the surface heights Sq << light wavelength λ). A survey of state-of-the-art light scattering techniques for a roughness characterization can be found in [Vor81, Whi94, Ben99]. However, all of them are additionally influenced by the correlation length and the shape of the autocorrelation function of the surface [Bro84].

The theoretical analysis of the speckle methods shows that only the root mean square (rms) of the surface heights influences the measuring results [Leh99]. Furthermore, speckle measuring techniques enable large and varying working distances up to 100 mm. The following describes the latest approach of a measuring technique, which is based on roughness dependent partially developed speckle patterns [Leh00].

## *2.1 Roughness Measuring System*

A smooth surface (Sq < λ/4) is illuminated with a fully developed static speckle pattern of a few millimeters in diameter. The statistical properties of the reflected and scattered speckle intensities contain essential informations about the surface roughness. The measuring principle results in a roughness-dependent spatial intensity modulation of the scattered speckle field. This principle has been introduced theoretically and was validated experimentally for transmitting isotropic surfaces [Yos90, Bas95]. A theoretical extension of the method to reflecting and possibly anisotropic surfaces can be found in [Leh99]. A diffuser plate and a spatial filter optic generate the static illumination speckle pattern, which results in a quite expanded set-up of about 30 cm. The demand for a compact and robust measuring device required further investigation concerning the miniaturized generation of a static, fully developed illumination speckle pattern.

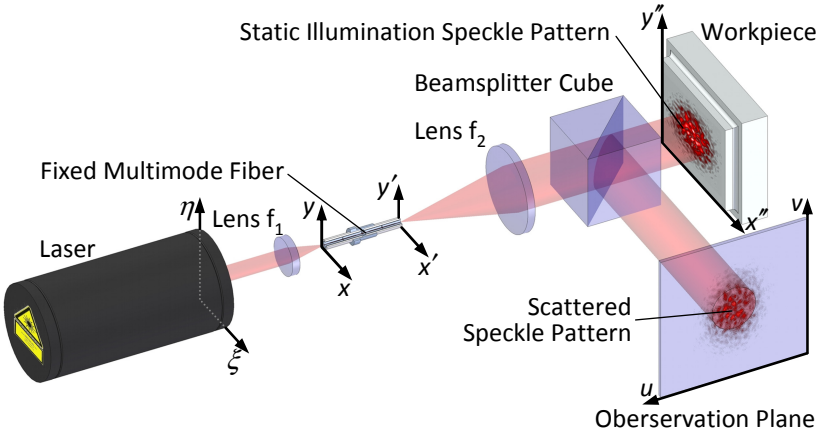


**Fig. 1** Roughness measuring set-up

With the latest approach [Pat10] an optical multimode step-index fiber fixed in a small ceramic tube replaces the diffuser plate and the spatial filter. Mode dispersion within the optical fiber leads to a speckled intensity distribution, which illuminates the workpiece (Figure 1). The biased wave front is very sensitive to surface irregularities in the nanometer range, which results in a roughness dependent speckle intensity modulation in the $u$ - $v$ -observation plane. The fiber optical measuring set-up consists of only a few low-cost components and expands only about 10 cm. The resulting illumination speckle pattern cannot be distinguished from a speckle pattern produced by a diffuser plate and is fully compatible for roughness measurements. A software design tool based on different mathematical models of the light propagation and light scattering processes simulates the measuring process. This enables a fast and cost effective tuning and optimization of the optical measuring process parameters, e.g. light wavelength, optical fiber specifications, focal lengths of the lenses, optical path lengths, surface roughness and lateral correlation length.

## 2.2 Simulation of the Scattered Light Measuring Process

The numerical model of the fiber optical roughness measuring process separates the light path into three sections [Pat10]. The calculation of the light propagation from the laser ( $\xi$ - $\eta$ -plane) to the optical fiber front ( $x$ - $y$ -plane) and from the fiber end ( $x'$ - $y'$ -plane) via the workpiece surface to the detector ( $u$ - $v$ -plane) is based on the scalar Kirchhoff theory [Goo96]. The scalar electrical field distribution of the collimated laser beam is

$$E(\xi,\eta,z) = E_0(\xi,\eta)\cdot e^{ikz}, \qquad \text{with} \quad E_0(\xi,\eta) = E_0\cdot e^{\left(-\frac{\xi^2+\eta^2}{R_L^2}\right)}, \tag{1}$$

where $E_0(\xi,\eta)$ is the Gaussian amplitude distribution of the beam cross section with the radius $R_L$. According to the scalar Kirchhoff theory the lens with the focal length $f_1$ performs a Fourier transformation of the incident light, which leads to the electrical field

$$E_1(x,y,z=0) = \int E(\xi,\eta,z)\cdot e^{-i\frac{2\pi}{\lambda f_1}(\xi\cdot x+\eta\cdot y)}\, d\xi d\eta \tag{2}$$

in the back focal plane or at the optical fiber front face, respectively. The focused beam with the wavelength $\lambda$ and the beam waist radius $r_w = (\lambda\cdot f_1)/(\pi\cdot R_L)$ enters the optical fiber according to Snell's law $\sin\alpha_0 = n\cdot\sin\alpha_0'$, with the fiber core refractive index $n$.

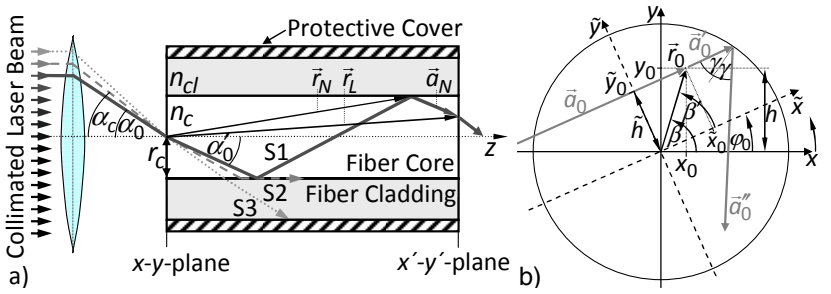


**Fig. 2** Laser beam coupling into an optical fiber a) axial section and b) transverse section

The light propagation within the waveguide and the electrical field distribution at the optical fiber end face follow ray tracing methods and wave optics. Depending on the entrance position of a light beam at the fiber front face, the incidence angle and the physical properties of the optical fiber ray tracing enables to calculate the light path length within the fiber and the exit position of a light beam in the $x'$-$y'$-plane (Figure 2.a). The fiber core guides light beams due to internal total reflections at the core-cladding interface, if the incidence angle is less than a critical angle $\alpha_c$ (S1, S2 and S3 in Figure 2.a). The following considers a beam that enters an optical fiber of the length $L$, the core radius $r_c$ and the refractive index $n_c$ at the position $\vec{r}_0 = (\tilde{x}_0, \tilde{y}_0 = \tilde{h}, z = 0)$ with the incidence angle $\alpha_0 \le \alpha_c$ and the azimuth angle $\varphi_0$ between the incidence plane and the $x$-$z$-plane (Figure 2.b). According to Snell's law the refracted beam includes the angle $\alpha'_0 = \sin^{-1}(\sin\alpha_0 / n_c)$ with the optical $z$-axis and the angle $\gamma = \sin^{-1}\left(\tilde{h}/r_c\right)$ with the surface normal of the core-cladding boundary. The beam undergoes

$$N = \text{ceil}\left\{\frac{L \cdot \tan\alpha'_0 - r_c \cdot \cos\gamma + \tilde{x}_0}{2 \cdot r_c \cdot \cos\gamma}\right\} \tag{3}$$

internal total reflections at the core-cladding interface, where „ceil" denotes that the computational result of the expression within curved brackets must be rounded up to the nearest integer. Finally, a beam propagates in the direction

$$\vec{a}_N = \begin{pmatrix} \sin\alpha'_0 \cdot \cos(\varphi_0 + N \cdot \Delta\varphi) \\ \sin\alpha'_0 \cdot \sin(\varphi_0 + N \cdot \Delta\varphi) \\ \cos\alpha'_0 \end{pmatrix}, \quad \text{with } \Delta\varphi = 180° - 2\gamma, \tag{4}$$

towards the optical fiber end face. To calculate the position of the beam exit $\vec{r}_L = (x_L, y_L, z_L = L)$ at the optical fiber end face, it is necessary to know the position

vector $\vec{r}_N = (x_N, y_N, z_N)$ of the last internal reflection point at the boundary surface:

$$x_N = r_c \cdot \cos\varphi_N,\ y_N = r_c \cdot \sin\varphi_N,\ z_N = \frac{(2 \cdot N - 1) \cdot r_c \cdot \cos\gamma - \tilde{x}_0}{\tan\alpha_0'}, \tag{5}$$

with $\varphi_N = (\gamma + \varphi_0) + (N-1) \cdot \Delta\varphi$. The coordinates of the beam exit point result from a vector addition of Eq.(4) and Eq.(5):

$$\vec{r}_L = \vec{r}_N + c_N \cdot \vec{a}_N = \begin{pmatrix} x_N + c_N \cdot \sin\alpha_0' \cdot \cos(\varphi_0 + N \cdot \Delta\varphi) \\ y_N + c_N \cdot \sin\alpha_0' \cdot \sin(\varphi_0 + N \cdot \Delta\varphi) \\ L \end{pmatrix}, \text{ with } c_N = \frac{(L - z_N)}{\cos\alpha_0'}. \tag{6}$$

The electrical field distribution $E_2(x', y', z = L)$ in the $x'$-$y'$-plane follows from the in-phase superposition of all wavelet amplitudes with the same exit coordinates $\vec{r}_L$ with respect to the geometric optical path lengths. The calculations of the electrical field distributions at the workpiece surface and in the observation plane are based on the scalar Kirchhoff theory. The second lens with the focal length $f_2$ (Figure 1) performs an inverse Fourier transformation of $E_2$:

$$E_3(x'', y'') = \int E_2(x', y') \cdot e^{i\frac{2\pi}{\lambda f_2}(x' \cdot x'' + y' \cdot y'')}\, dx'dy', \tag{7}$$

which describes a static illumination speckle pattern with both a well defined diameter and a well defined mean speckle size. The interaction of this biased wave front with the surface height distribution $h_w(x'', y'')$ of the reflecting workpiece topography leads to a phase modulation $\phi(x'', y'')$ of the incident field $E_3$:

$$E_4(x'', y'') = E_3(x'', y'') \cdot e^{i\phi(x'', y'')}, \text{ with } \phi(x'', y'') = -\frac{4\pi}{\lambda} \cdot h_w(x'', y''). \tag{8}$$

Finally, the electrical field in the $u$-$v$-observation plane at a distance $a$ from the workpiece (Figure ) follows from Eq.(8) and the Fresnel diffraction integral [Goo96]:

$$E_5(u, v) = \frac{-ike^{ika}}{2\pi a} \iint_{S_0} E_4(x'', y'') \cdot e^{\frac{ik}{2a}\left[(u - x'')^2 + (v - y'')^2\right]}\, dx''dy''. \tag{9}$$

$E_5$ describes the same static speckle patter as $E_3$ according to Eq.(7) with an additional intensity modulation of the single speckles depending on the rms of the surface heights $h_w(x'', y'')$. According to the convolution theorem, the convolution integral Eq.(9) can easily be implemented in Matlab by applying fast Fourier transform algorithms.

## 2.3 *Results of Simulations and Measurements*

Figure 3 shows calculated scattered intensity distributions for three different smooth objects as a result of the simulations described above. As readily can be seen, the illumination speckle pattern is the same for all measuring process simulations. However, the speckle intensity modulation increases with the surface roughness.

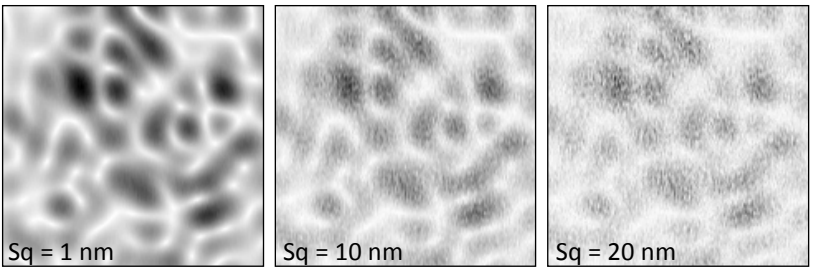


**Fig. 3** Calculated scattered speckle patterns for three different smooth objects

An appropriate optical roughness parameter Ropt characterizes the mean speckle size within scattered light intensity distributions according to Figure 3. The determination of such a parameter is based on the calculation of a two-dimensional discrete speckle intensity autocorrelation function (ACF) [Pat06]. The ACF gradient near to the ACF maximum increases as the speckle intensities become more modulated. Figure 4 presents the connection of the optical roughness parameter Ropt with the Sq-roughness of different isotropic rough model surfaces in the range between Sq = 1 nm and Sq = 100 nm (squares in Figure 4).

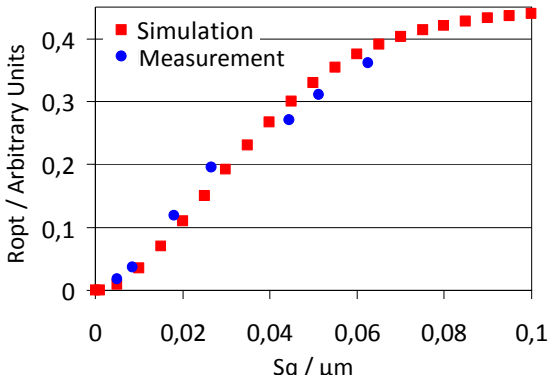


**Fig. 4** Optical roughness values Ropt as a result of measuring process simulations and measurements

Measured Ropt values (circles) from an experimental set-up according to Figure 1 and the parameter values of the measuring process simulation are in a good agreement with the calculated Ropt values. This encourages to design and assemble a corresponding, compact measuring device (Figure 5.a), which has been integrated into an ultra-precision machine tool to perform in-situ roughness measurements (Figure 5.b).

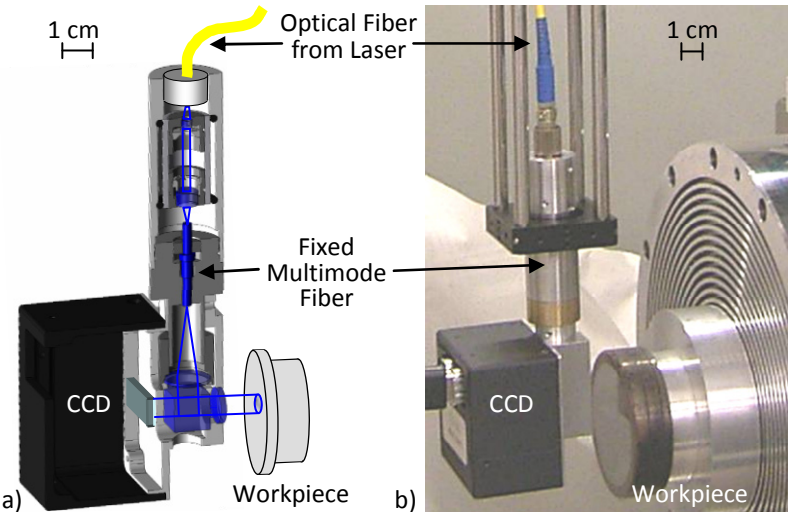


**Fig. 5** Compact measuring device for in-situ roughness measurements a) as a sketch and b) integrated into a machine tool

## 3 Interferometrical Form Measurements

Phase shifting techniques find widespread application to interferometric form testing in ultra precise manufacturing of spherical and aspherical lenses as the accuracy is in the nanometer range. Up to the present a variety of systems and algorithms for phase-shifting methods have been developed for non-destructive testing and quality control of optically smooth and both reflective and transparent samples ([Mal07], [Rob93], [Kre05]). Quality inspection of ultra precise mould inserts and manufactured optics is performed outside the manufacturing machine using phase-shifting methods. The correction of local form deviations is imprecise as the manufactured optics or the mould inserts have to be repositioned in the machine tool. A promising way to overcome this problem is a machine integrated measurement system (Figure 12). Thus for the manufacturing of mould inserts in optical quality as well as for machine-integrated measurements for quality control of optics a closed loop process chain allows a faster manufacturing process and less iterative reworking. The direct integration of phase shifting interferometers into the production environment is difficult because of their sensitivity to external influences. One major disturbing influence is caused by vibrations [Dro95]. The algorithms given here are primarily intended to be used in a machine environment

where vibrations, acoustic noise and air turbulences are unavoidable. Thus different spatial phase-shifting techniques which require only one off-axis interferogram are considered. For a sustainable application of the measurement technology in production the minimization of investment costs is also an important challenge. Thus a cost intensive actuated mirror to perform temporal phase shifting is then not required. Furthermore, by applying a numerical readjustment of the focus, no mechanical focus adjustment is needed and the effective axial resolution can be enhanced numerically by post processing of complex wave fronts without narrowing the field of view leading to a loss of information around the focus plane by blurring.

## *3.1 Set-Up of Measurement System*

For DHI, a variety of different set-ups can be realized. Figure 6 illustrates the schematic set-up for digital holographic quantitative phase contrast intererometry for transmission (Figure 6.a) and incident imaging mode (Figure 6.b). In incident light mode, the investigated reflective surface is illuminated through the measurement objective with the light of a coherent light source (HeNe laser, $\lambda = 632.8$ nm). In combination with a tube lens the same measurement objective images the object onto an image capturing device (CCD sensor).

Here, the object wave is superimposed with a coherent "reference wave" that is slightly tilted by a beam splitter to generate digital "off-axis" holograms [Kre05]. The reference wave is formed by a collimated wave which passes an identical tube lens in order to generate equally shaped wave fronts (Linnik arrangement). Due to geometrical restrictions, a Linnik set-up is realized without a second tube lens as the slightly tilted incoupling beam splitter is located between the objective lens and the imaging tube lens. For both arrangements, the holograms which are formed by the superposition of the object and reference wave are captured by the CCD image sensor and transferred to an image processing system for the numerical reconstruction of the digital holograms.

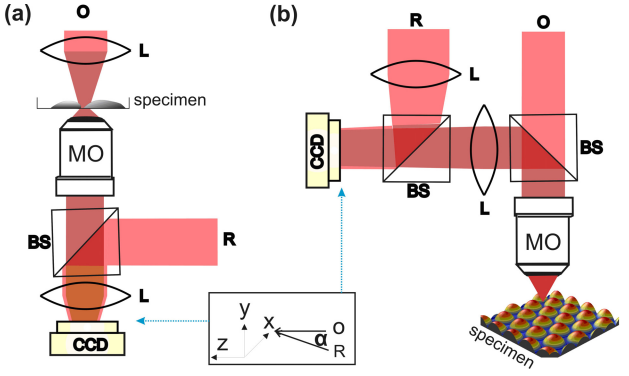


**Fig. 6** Digital holographic imaging modes: a) transmission light arrangement, b) incident light arrangement; O: object wave, R: reference wave, MO: microscope objective, BS: beam splitter, L: lens, CCD: digital image sensor.

## 3.2 Spatial Phase Shifting Techniques Operating in the Position Space

In an interferometer set-up as depicted in Figure 6, a reference wave R(x,y) and an object wave O(x,y) are superimposed in the plane (x,y) of the image recording device, which leads to the interferogram equation [Mal07]:

$$I_k(x,y) = \left|O(x,y) + R(x,y)\right|^2 = \left(I_O(x,y) + I_R(x,y)\right) \cdot \left(1 + \gamma(x,y)\cos\left(\phi_{R,k}(x,y) - \phi_O(x,y)\right)\right) \quad (10)$$

*With* $I_O(x,y)=|O(x,y)|^2$ and $I_R(x,y)=|R(x,y)|^2$ denoting the intensities of the two waves and $\gamma(x,y)$ the interferogram modulation. In presence of a sample in the optical path of O, the phase distribution represents the sum $\phi_O(x,y)= \phi_{O_0}(x,y)+\varphi_S(x,y)$ where $\phi_{O_0}$ designates the pure object wave phase and $\varphi_S$ the optical path length induced by the sample.

### 3.2.1 Spatial Phase Shifting

In case of spatial phase shifting the reference plane wave and the object wave are in off-axis geometry. This latter terminology refers to the fact that the reference wave arrives at the camera with a slight angle in relation to the object wave (Figure 7.a). The resulting carrier fringes of the reference wave can be described as $\phi_R(x,y)=x\beta_x(x,y)+y\beta_y(x,y)+C$. The parameters $\beta_x$ and $\beta_y$ denote the spatial gradient of the phase difference between *O* and *R*. *C* represents a constant phase offset. In this way a spatial carrier fringe pattern is generated. For the reconstruction of the object wave phase from the spatial phase shifted interferograms a method is applied which has been developed for digital holographic microscopy [Lie04]. The principle is based on utilization of intensities of adjacent pixels within a region of interest (ROI, Figure 7.b) around an interferogram pixel to solve an equation system from which the complex object wave can be obtained including phase and amplitude. The utilized algorithm is based on the assumption that only the phase difference $\Delta\varphi_I(x,y)=\phi_{R,k}(x,y)-\phi_O(x,y)$ between the object and reference wave varies rapidly spatially in the interferogram. Additionally, because of the spatial phase-shifting algorithm, the object wave must be assumed to be constant within an area of approximately 5×5 pixels around a given point of interest in the interferogram. These requirements can be fulfilled by a specimen with a smooth surface or an adequate relation between the magnification of the used optical system and the image recording device. Therefore, the magnification has to be chosen in such a way that the smallest imaged structures of the sample, which are restricted by the resolution of the optical imaging system because of the Abbe criterion, are oversampled by the CCD sensor. In this way the lateral resolution of the reconstructed holographic phase contrast images is not decreased by the spatial phase-shifting algorithm.

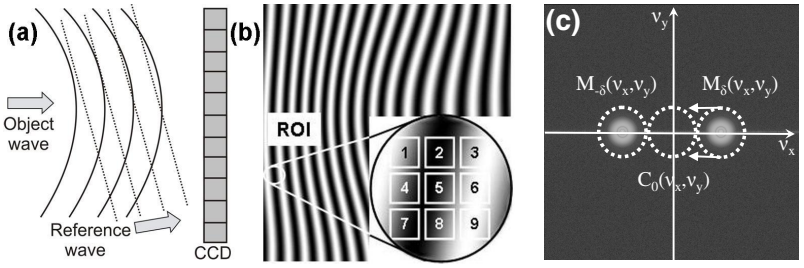


**Fig. 7** a) Formation of an interferogram on a CCD-camera and b) zoom of an interferogram with a ROI of 3×3 pixels. c): Fourier transform of an off-axis interferogram (b) with characteristic, indicated components.

For areas without a sample, $\Delta\varphi_I(x,y)$ can be approximated by a mathematical model [Lie04]:

$$\Delta\varphi_I(x,y) = \phi_{R,k}(x,y) - \phi_O(x,y) = 2\pi(K_x x^2 + K_y y^2 + L_x x + L_y y) \quad (11)$$

The parameters $K_x$, $K_y$ in Eq.(11) describe the divergence of the object wave and the properties of the microscope lens normally applied in digital holographic microscopy. The factors $L_x$, $L_y$ describe the linear phase difference between $O$ and $R$ that is due to the off-axis geometry of the experimental set-up. For quantitative phase measurements from $I_k(x,y)$ the complex object wave $O(x,y)= |O(x,y)| \, exp(i\cdot\Delta\varphi_S(x,y))$ can be calculated for each pixel by solving a set of equations that is obtained by inserting Eq.(11) into Equation (10) (for details see [Lie04]). The parameters $K_x$, $K_y$, $L_x$, $L_y$ in Eq.(11) cannot be obtained directly from the geometry of the set-up in Figure 6 with adequate accuracy. Thus they are fitted in an area of the hologram without a sample by an iterative fitting process [Car04].

### 3.2.2 FT-Based Algorithm

The Fourier transform (FT) based spatial phase-shifting algorithm, also known as SCPM-method, is a widely known and robust method for phase retrieval and described in ([Kre05], [Kre86], [Bon86]). Applying a Hann window function $h_1(x,y)$ and the Fourier transform to a spatial phase shifted interferogram $I(x,y)$ with carrier fringes in x-direction, the partitions in the frequency domain can be written as:

$$\begin{aligned} &\mathrm{FT}[\mathrm{h}_1(\mathrm{x},\mathrm{y})\cdot \mathrm{I}(\mathrm{x},\mathrm{y})] = \mathrm{FT}[\mathrm{h}_1(\mathrm{x},\mathrm{y})] * \mathrm{FT}[\mathrm{I}(\mathrm{x},\mathrm{y})] = \\ &\mathrm{C}_0(\nu_\mathrm{x},\nu_\mathrm{y}) + \mathrm{M}_\delta(\nu_\mathrm{x},\nu_\mathrm{y}) + \mathrm{M}_{-\delta}(\nu_\mathrm{x},\nu_\mathrm{y}) + \mathrm{B}(\nu_\mathrm{x},\nu_\mathrm{y}) \end{aligned} \quad (12)$$

Here, * is the symbol for convolution and $C_0$ denotes the zero order in the Fourier domain which is located in the center (Figure 7.c). The parameters $M_\delta$ and $M_{-\delta}$ indicate the information of the structure shifted with the carrier fringe frequency $\delta$ and $-\delta$ from the zero order. The component $B$ represents the background. The algorithm locates the identical and symmetric components $M_\delta$ and $M_{-\delta}$, eliminates $M_{-\delta}$ and shifts $M_\delta$ to the origin. Afterwards the inverse Fourier transform is applied

to the modified Fourier transform (Figure 7.c) and the phase (modulo 2π) is obtained by

$$\varphi_O(x,y) = \arctan\left(\mathrm{Im}\left[\ \mathrm{FT}^{-1}\left(M_\delta\right)\right] / \mathrm{Re}\left[\ \mathrm{FT}^{-1}\left(M_\delta\right)\right]\right). \tag{13}$$

## 3.3 Phase Retrieval and Interpretation

After determining the phase difference $\Delta\varphi_S(x,y)$ induced by the specimen, the $2\pi$ ambiguity is removed by a line by line phase unwrapping process [Kre05] in case of the algorithms operating in the position space. For the FT-based algorithm a phase unwrapping algorithm operating in the frequency domain is often utilized [Sch03]. The unwrapped phase distributions represent a quantitative phase contrast image. For incident light mode as depicted in Figure 6.b the topography of a reflective specimen $z_s$ can be calculated from the phase distribution $\Delta\varphi_S(x,y)$:

$$z_S(x,y) = \frac{\lambda}{4\pi}\Delta\varphi_S(x,y). \tag{14}$$

For quantitative determination of the form errors, Zernike polynoms are usually utilized [Mal07]. A recently introduced alternative for aspheres with little dynamic are Forbes-polynoms [For07]. Since a Zernike representation needs a relatively long computation time and is relatively complex in higher orders, we propose the application of the more intuitive Forbes polynomial basis. These are generated by normalizing the transverse variable in the standardized representation of aspheres to u=r/rmax

## 3.4 Propagation of the Complex Object Wave

Although the presented reconstruction methods permit a sharply focused object wave during the recording of the hologram, which facilitates the experimental alignment, subsequent propagation and thus focusing is of particular interest. The previously mentioned diffraction-based propagation methods can be applied on the reconstructed complex object wave. The reconstruction of the digital hologram in a plane different to the hologram plane is realized by utilizing the Fresnel diffraction integral. In the case of defocused imaging of the sample, the reconstructed object wave in the hologram plane $O(x,y,z_0)$ is propagated for the distance $d$ to the focused image plane that is located at the autofocus position $d=d_{AF}$ by a convolution-based method [Sch02]:

$$O(X,Y,z=d) = \Gamma^I(X,Y)A\times FFT^{-1}\left\{\begin{matrix} FFT\left[\Gamma^H(x_0,y_0)\ \ O(x_0,y_0,z_0)\right] \\ \times\exp\left(i\pi d\left(\xi^2+\eta^2\right)\right)\end{matrix}\right\} \tag{15}$$

where $\Gamma^I$ and $\Gamma^H$ denote a wavefront and $A(d)$ a constant complex function. The notation *FFT* denotes a Fourier transform operation. Fourier transform, x and y represent the spatial and ξ and η the spectral coordinates. The algorithm preserves a constant image scale, and therefore it is particularly suitable for the determination of the image definition. The reconstructed object wave in the

hologram plane O(x,y,z0) is often distorted by aberrations in the optical system. The concept of numerical parametric lenses (NPL) is a common feature in DHM to achieve optimized wavefront reconstruction by introducing the factors $\Gamma^{I}$ and $\Gamma^{H}$ [Col06].

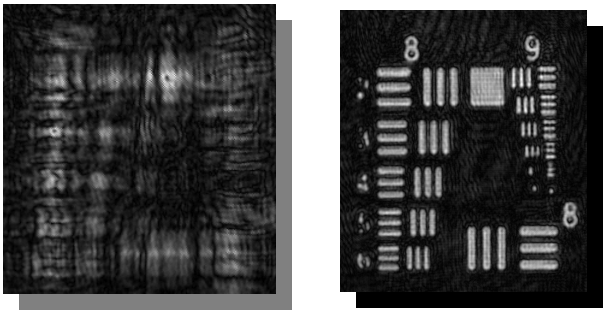


**Fig. 8** Left: recorded hologram. Right: propagated complex wave to sharp image plane

## *3.5 Autofocus Algorithms*

For evaluation and quantification of image sharpness, various methods and applications exist. Common passive optical autofocusing techniques, which are applied e.g. in compact camera photography and bright field microscopy, perform a determination and maximisation of the image sharpness while scanning the imaging system or the stage mechanically [Geu00]. In subsequent digital holographic autofocusing, instead of mechanical scanning this procedure is done numerically by the variation of the distance $z$ in Eq.(15) for the propagation of the reconstructed complex object wave $O$ (Figure 8).

Analogous to common autofocusing techniques, the determination of the autofocus position requires a robust algorithm for the determination of the image definition. Particularly suitable algorithms for the determination of the image sharpness of the reconstructed amplitude distributions are given by the determination of the logarithmically weighted cumulated Fourier spectra (logarithmic power spectrum). The focus value $f_{PS}(z)$ in dependence on the propagation distance $z$ is calculated with Eq. (16), where x' and y' denote the position in the fourier domain:

$$f_{PS}(z) = \sum_{x',y'} \log\left[1 + \left|FFT\left[\left|O(x,y,z)\right|\right]\right|\right]. \tag{16}$$

Another approach is the SMD-method (Sum Modulus Difference):

$$f_{SMD}(z) = \sum_{x=0}^{n-1} \sum_{y=0}^{m-1} \sqrt{\left(\frac{\partial\left|O(x,y,z)\right|}{\partial x}\right)^2 + \left(\frac{\partial\left|O(x,y,z)\right|}{\partial y}\right)^2}\,. \tag{17}$$

A further alternative is given by the Laplace operator:

$$f_{LP}(z) = \sum_{x=0}^{n-1} \sum_{x=0}^{m-1} \left( \nabla^2 \left| O(x, y, z) \right| \right)^2 . \tag{18}$$

As a last method to compare the image focus (Figure 9), we introduce the variance of the pixel values of the reconstructed and propagated wave as a metric:

$$f_{Var}(z) = Var\left[ \left| O(x, y, z) \right| \right]. \tag{19}$$

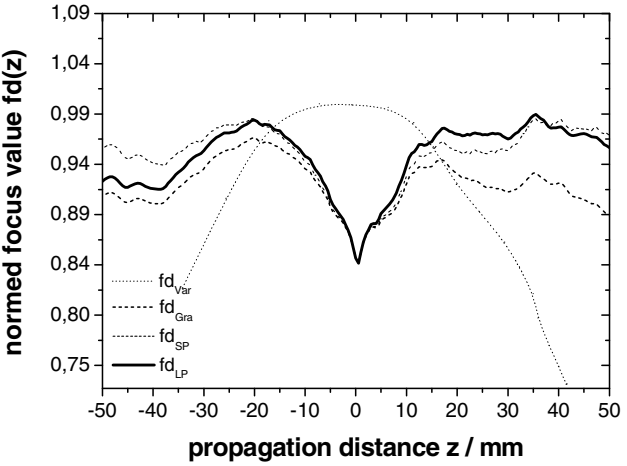


**Fig. 9** Focus values of unwrapped phase distributions of the specimen in Figure 11: A clear dip in the center demonstrates the global minimum of the focus algorithms except the variance $fd_{Var}$ .

### 3.5.1 Strategy for Search of Focus Plane

The determination of the extrema in the focus value curves within the full propagation interval $Az$ = [-10 cm, 10 cm] is very inefficient. In order to speed up the process of locating the extrema without loosing accuracy, a climbing-search strategy [He03] is implemented. In a first step, the whole propagation range is scanned with a large step size for a rough determination of the location of the extremum. In the second step, the interval between the nearest neighbours to the detected extremum is scanned with the smallest step size chosen with respect to the depth of field of the imaging system. This process is illustrated in Figure 10. The thin solid graph represents the schematically normalized focus value function of a pure phase object obtained by scanning the full interval. First, the climbing-search-strategy scans the full interval with a large step size (dashed vertical lines). The neighbouring positions to the minimal focus value define the scan range for the second scanning with the smallest step size available (solid vertical lines, see also Figure 11 for demonstration).

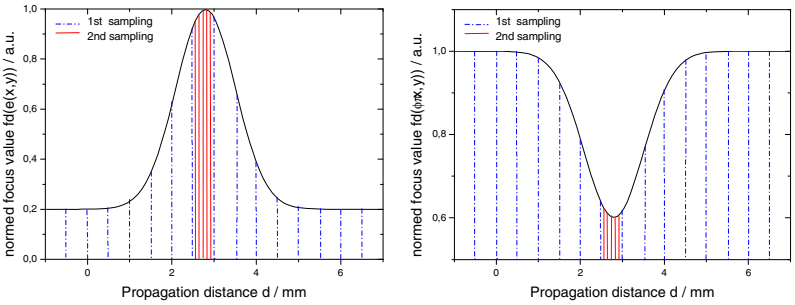


**Fig. 10** Schematic illustration of the "Climbing-Search" iteration strategy

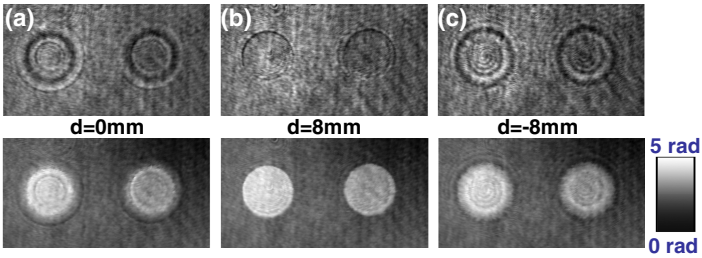


**Fig. 11** Amplitude and phase distribution of structures on a reflective optical surface with a height of 50 nm: Reconstructed wave front in the hologram plane (a), propagated wave to a plane with maximum image sharpness (b) and backward propagated image (c).

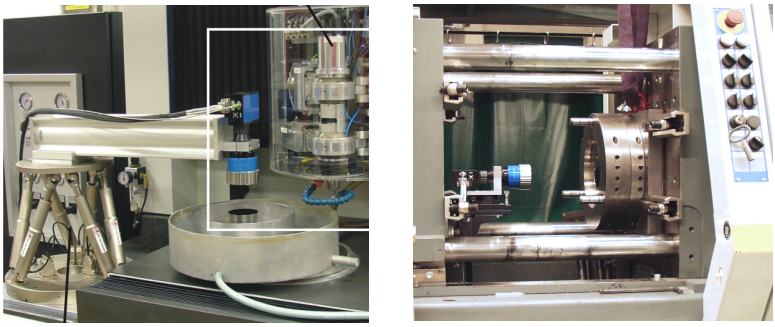

**Fig. 12** Machine integrated interferometric measurement of an optical surface in a polishing machine (left) and integrated mold testing for replication of plastic optics (right)

## *3.6 Automated Adjustment of Set-Up*

For automation of an interferometric measurement system, a hexapod with it's 6 degrees of freedom in positioning is also suitable for set-ups with an integrated CGH (Computer Generated Hologram), that allow the measurement of aspheres

and even freeform surfaces. By applying the two-dimensional FFT of an interferogram, a fine adjustment of the set-up can easily be realised by determining the center of mass of the first order. Common strategies for an automated aligning are univariate and multivariate optimisation methods like simplex optimisation, statistical optimisation, simulated annealing and neural networks [Mis00].

## 4 Conclusion

A combination of mathematical formalisms from the scalar Kirchhoff theory and from ray tracing methods describes optical wavelet propagations in free space and within an optical fiber. The implementation of the corresponding algorithms in Matlab results in a design tool for a scattered light roughness measuring process. Simulations already lead to improvements of the integral roughness measuring method. The resolution concerning the roughness measurement within a range from Rq = 1 nm to Rq = 50 nm was significantly enhanced due to a short laser wavelength of $\lambda = 405$ nm. Furthermore, it is possible to estimate the smallest illumination spot diameter as a function of the lateral correlation length of the rough surface that enables both a sufficient roughness characterization and a high lateral resolution. The simulations result in a compact measuring system according to the fiber optical set-up design. The overall length of about 100 mm enables the device to be integrated into ultra-precision machine tools and to perform in-situ or in-process roughness measurements.

The utilization of digital holographic interferometry in combination with new spatial phase-shifting methods allows higher robustness. The feature of numerical refocusing in a post-processing step permits faster measurements without need of mechanical focusing. The polynomial basis of Forbes enables a more intuitively interpretation of form errors for aspheres.

**Acknowledgement.** The authors like to thank the German Research Foundation (DFG) for funding this work as a part of the Transregional Collaborative Research Center SFB/TR4 “Process Chains for the Replication of Complex Optical Elements”.

## References

[Bas95] Basano, L., Leporatti, S., Ottonello, P., Palestini, V., Rolandi, R.: Measurements of Surface Roughness: Use of a CCD Camera to Correlate Doubly Scattered Speckle Patterns. Applied Optics 34, 7286–7290 (1995)

[Ben99] Bennett, J.M., Mattsson, L.: Introduction to Surface Roughness and Scattering. Optical Society of America, 2nd edn., Washington (1999)

[Bon86] Bone, D.J., Bachor, H.-A., Sandeman, R.J.: Fringe-pattern analysis using a 2-D Fourier transform. Appl. Opt. 25, 1653–1660 (1986)

[Bro84] Brodmann, R., Gast, T., Thurn, G.: An Optical Instrument for Measuring the Surface Roughness in Production Control. Annals of the CIRP 33(1), 403–406 (1984)

[Car04] Carl, D., Kemper, B., Wernicke, G., von Bally, G.: Parameter-optimized digital holographic microscope for high resolution living-cell analysis. Appl. Opt. 43, 6536–6544 (2004)

[Col06] Colomb, T., Montfort, F., Kühn, J., Aspert, N., Cuche, E., Marian, A., Charrière, F., Bourquin, S., Marquet, P., Depeursinge, C.: Numerical parametric lens for shifting, magnification, and complete aberration compensation in digital holographic microscopy. JOSA A 23(12), 3177–3190 (2006)

[Dro95] de Droot, P.J.: Vibration in phase shifting interferometry. J. Opt. Soc. Am. 12(2), 354–365 (1995)

[For07] Forbes, G.W.: Shape specification for axially symmetric optical surfaces. Optics Express 15(8), 5218–5226 (2007)

[Geu00] Geusebroek, J.-M., Cornelissen, F., Smeulders, A.W.M., Geerts, H.: Robust autofocusing in microscopy. Cytometry 39, 1 (2000)

[Goo96] Goodman, J.W.: Introduction to Fourier Optics, 2nd edn. McGraw-Hill, New York (1996)

[He03] He, J., Zhou, R., Hong, Z.: Modified fast climbing search auto-focus algorithm with adaptive step size searching technique for digital camera. IEEE Transactions on Consumer Electronics 49, 257 (2003)

[Kre05] Kreis, T.: Handbook of Holographic Interferometry: Optical and Digital Methods. Akademie Verlag, Berlin (2005)

[Kre86] Kreis, T.: Digital holographic interference-phase measurement using the fouriertransform method. J. Opt. Soc. Am., A 3, 847–855 (1986)

[Lee87] Lee, C.S., Kim, S.W., Yim, D.Y.: An In-Process Measurement Technique Using Laser for Non-Contact Monitoring of Surface Roughness and Form Accuracy of Ground Surfaces. Annals of the CIRP 36(1), 425–428 (1987)

[Leh00] Lehmann, P., Goch, G.: Comparison of Conventional Light Scattering and Speckle Techniques Concerning an In-Process Characterization of Engineered Surfaces. Annals of the CIRP 49(1), 419–422 (2000)

[Leh99] Lehmann, P.: Surface-Roughness Measurement Based on the Intensity Correlation Function of Scattered Light under Speckle-Pattern Illumination. Applied Optics 38(7), 1144–1152 (1999)

[Lie04] Liebling, M., Blu, T., Unser, M.: Complex-Wave Retrieval from a Single Off-Axis Hologram. J. Opt. Soc. Am., A 21(3), 367–377 (2004)

[Mal07] Malacara, D.: Optical shop testing, pp. 547–655. Wiley, New Jersey (2007)

[Mis00] Mischo, H., Bitte, F., Pfeifer, T.: Model-based optimization of interferometers for testing aspherical surfaces. Accepted as Oral Presentation for Laser Interferometry X: Applications at the SPIE 2000 Annual Meeting, San Diego, USA (2000)

[Pat10] Patzelt, S.: Simulation und experimentelle Erprobung parametrisch-optischer Rauheitsmessprozesse auf der Basis von kohärentem Streulicht und Speckle-Korrelationsverfahren, Dissertation Universität Bremen, Prof. Dr.-Ing. G. Goch Forschungsberichte über Messtechnik, Automatisierung, Qualitätswissenschaft und Energiesysteme, vol. 4. Mainz-Verlag, Aachen (2010)

[Pat06] Patzelt, S., Horn, F., Goch, G.: Fast Integral Optical Roughness Measurement of Specular Reflecting Surfaces in the Nanometer Range. In: XVIII IMEKO World Congress, Metrology for a Sustainable Development, Rio de Janeiro (2006); CD-ROM: TC2-4

[Pet79] Peters, J., Vanherck, P., Sastrodinoto, M.: Assessment of Surface Topology Analysis Techniques. Annals of the CIRP 28(2), 539–554 (1979)

[Pet65] Peters, J.: Messung des Mittenrauhwertes zylindrischer Teile. VDI-Berichte 90, 27–31 (1965)

[Rob93] Robinson, D.W., Reid, G.T.: Interferogram Analysis. IOP Publishing, Philadelphia (1993)

[Sch02] Schnars, U., Jüptner, W.: Digital recording and numerical reconstruction of holograms. Meas. Sci. Technol. 13, R85–R101 (2002)

[Sch03] Schofield, M.A., Zhu, Y.: Fast phase unwrapping algorithm for interferometric applications. Optical Letters 28(14) (2003)

[Thw80] Thwaite, E.G.: Power Spectra of Rough Surfaces Obtained by Optical Fourier Transformation. Annals of the CIRP 29(1), 419–422 (1980)

[Vor81] Vorburger, T.V., Teague, E.C.: Optical Techniques for On-Line Measurement of Surface Topography. Precision Engineering 3, 61–83 (1981)

[Whi94] Whitehouse, D.J., Bowen, D.K., Venkatesh, V.C., Lonardo, P., Brown, C.A.: Gloss and Surface Topography. Annals of the CIRP 43(2), 541–549 (1994)

[Yos90] Yoshimura, T., Kazuo, K., Nakagawa, K.: Surface Roughness Dependence of the Intensity Correlation Function under Speckle Pattern Illumination. Journal of the Optical Society of America 7(12), 2254–2259 (1990)

# Metrology Past, Present and Future with Reference to Optics and Manufacture

David Whitehouse

**Abstract.** Aspects of the measurement and manufacture of mainly optical components from early times, the present and the future are described. Two instrumental types having the best pedigree and most potential are singled out namely the stylus method and optical methods with, in the latter case, scanning white light interferometry. Critical issues are highlighted and some examples of future requirements and possible developments are given.

## 1 Introduction

This chapter is concerned with the development of the metrology aspects of manufacture with reference to optics and to the geometry and how the geometry affects the performance. The investigation of surfaces is an old technology Leonardo da Vinci, Amonton and Coulomb all delved into surface behaviour before this century. However, their investigations were largely subjective and not much use quantitatively. Polishing is the foundation of optical functionality and this forms the background to the early part of the chapter.

### *1.1 Early Reference to the Manufacture*

According to Scott [1] and Singer [2] the earliest reference to the polishing of glass is from 782 B.C. from Nimrud in Assyria in the form of a small vessel and the first reference to a polished lens is in a play by Aristophanes in 434 BC. However the art of cutting and polishing natural crystal for jewellery, seals and burning glasses goes back much further probably as far back as 4000 BC.

The changing of shape by rubbing two surfaces together to make a sharp edge tool probably led to the art of polishing. An adjunct to this which may be even earlier is that of engraving or the marking of objects by scratching a soft material by one which is harder which predates any form of painting [3] mainly because of the availability of the implement: a hard object is much more available than paint. One early mention of 'graving' or engraving is in the Book of Exodus where

David Whitehouse
University of Warwick, 171, Cromwell Lane, Burton Green, Coventry, CV4 8AN, England

E. Brinksmeier et al. (Eds.): Fabrication of Complex Optical Components, LNPE, pp. 179–206.
springerlink.com 

Moses says: [4] ‘Take two onyx stones and grave on them the names of the children of Israel‘. So the interaction of two objects for the benefit of mankind in survival as well as cosmetics and beauty has played an important role in human development.

### *1.2 Materials*

Glass has long been the preferred material in optical applications because of its transparency. It is however not as easy to work as metals because of the fact that at normal temperatures and on the usual scale of size it does not yield but obeys Hooke’s Law until it fails. Glass is also difficult to handle because it cannot be clamped in the way of metals and it is not magnetic, so it is usually held by a wax of some sort. There are also constraints when using glass for optical purposes as distinct from purely ornamental because the geometric form has to be largely preserved at the same time as the smoothness is generated.

## 2 Manufacture

The generation of a curved surface on a piece of glass to make a lens or a mirror blank is different. Grinding causes the tool to wear as well as the workpiece so that the tool has continuously to be renewed. There is a way of generating a curve on glass without the use of a tool but just some abrasive. Just rubbing two pieces of material together invokes the ‘Central Limit Theorem‘ of statistics which basically says that if the generation mechanism is sufficiently random then Gaussian statistics will describe the geometry produced. Thus in three dimensions the random abrasion of grains between two contacting bodies will produce a curve on both one positive and the other negative i.e. one concave and one convex and both spherical. This is because the law describing the position of the coordinates x, y, z on the component is Gaussian.

Thus

$$\mathbf{f(x,y,z)} = \mathbf{Const} \times \mathbf{exp}\left(-\frac{\mathbf{x^2+y^2+z^2}}{\mathbf{2\sigma^2}}\right) \tag{1}$$

from which it will be observed that the argument describing the spatial phase i.e. the position, is the formula for a sphere.

Rubbing two pieces of glass together always produces a concave surface and a convex surface of the same curvature but opposite sign. Whitworth (see [5]) developed a technique which avoided this seemingly impossible phenomenon and in the process provided a method for generating optical flat surfaces. This he achieved by using three pieces of glass rather than the two mentioned above. By sequentially rubbing the three pieces in pairs it was easily possible to cancel out the tendency to produce curves. The result of the exercise is that three flat pieces emerge rather than two curved ones: an example of really clever, yet simple, thinking.

### *2.1 Requirements of Manufacture*

While it is obvious that curved surfaces are a prerequisite for producing an optical system it is also a requirement that the surfaces so produced are smooth so that there is no light scatter. For this reason polishing is used but there is another requirement that is not so obvious which is that the actual lens has to be circular so that it can be properly fitted into the body of the instrument. This requirement was one of the reasons for the development of instruments for measuring roundness in the early 1950s by R. E. Reason of Taylor Hobson.

## 3 Instrumentation

### *3.1 Subjective Early Methods*

The obvious methods are the eye and the fingernail: the former for optical assessment and the latter mainly for the assessment of roughness for applications involving mechanical action as in gears and cams.

### *3.2 Early Optical Methods of Measuring Roughness*

The simplest method is Lambert's method [6] in which the polished object is tilted at an acute angle until the reflection appears to be specular i.e. the source of light can be seen in the surface. This is the effect seen in the distance on a road which has a slight convex curvature. When the light scattered from the peaks of the road roughness has a path difference from those in the valleys of about λ/4, where λ is the wavelength of light then effective reflection occurs.

This angle

$$\theta_L \approx \arcsin\left(\frac{\lambda}{8R_t}\right) \tag{2}$$

can be estimated by eye from which some idea of $R_t$ the peak to valley roughness of the surface i.e. the road, can be found. View 2 in the top two parts of figure 1 are the plan view of the profiles shown above.

Another early method relies on gathering all the scattered light called the 'Total Integrated Scatter' (TIS) where

$$TIS \approx \left(\frac{4\pi R_q}{\lambda}\right)^2 \tag{3}$$

The schematic diagram of this is shown in Figure 1. From this TIS value the root mean square roughness $R_q$ can be estimated. A purely comparative method based on gloss is shown in Figure 2 in which the scattered light from a source is picked up by two or more detectors at different angles one being the specular angle and the other being at some arbitrary angle to it.

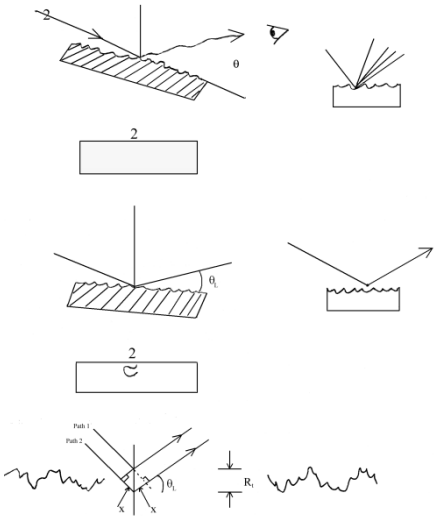

**Fig. 1** Lambert's law

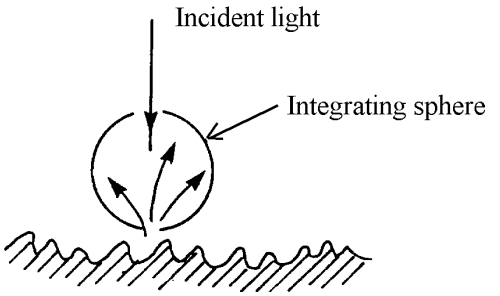


**Fig. 2** The Total Integrated Scattering of an Integrating sphere; See for example [6]

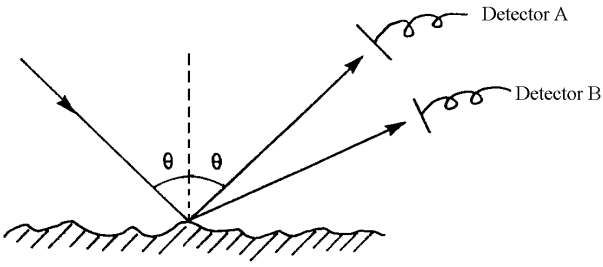


**Fig. 3** The Basis of the Gloss meter; See for example [6]

The surface quality is estimated by taking the ratio

$$\textbf{ratio} = \frac{\mathbf{A-B}}{\mathbf{A+B}} \tag{4}$$

When the surface is perfectly smooth all the light gets reflected into A and the ratio is unity whereas if the surface is rough then the light scattered into A is the same as B and the ratio is zero. This method is simple and cheap but it is a comparator and is useful therefore only for progressing the quality of the surface as it is being finished.

## *3.3 Early Stylus Methods of Measuring Roughness*

In the current century perhaps the first attempt to make an instrument was Tomlinson's in 1919 [7] at the NPL He devised a crude lever system which magnified the surface profile mechanically by a factor of about 20:1. This gave him just enough magnification to be able to see the surface detail but nothing big enough to work on.

The man who really started surface instrumentation was Schmaltz who in 1929 developed the first stylus instrument and began experimenting with optical methods.

His philosophy was very simple. He had seen men in the production departments of some large firms e.g. General Motors and Ford, scratching surfaces with the fingernail to assess the toughness and sometimes viewing the surface obliquely under strip lighting. Schmaltz's idea was to replace the fingernail with the stylus and the eye by imaging optics [8].

Neither instrument was practical but nevertheless they stimulated Dr. Abbott of General Motors in 1936 [9] to advance the technology by making the output from the probe electrical so that substantial magnifications could be achieved. This output was put on a meter for all to see. It still lacked a permanent record for use on the shop floor. It was Mr. R. E. Reason of Taylor Hobson in 1939 who completed the jigsaw by adding on a chart recorder: hence the birth of the profile graph which was enabled by having a tracking mechanism to move the stylus across the surface. He also wrote the first book on the design of stylus instruments [10].

Figure 4 gives the basic instrument:

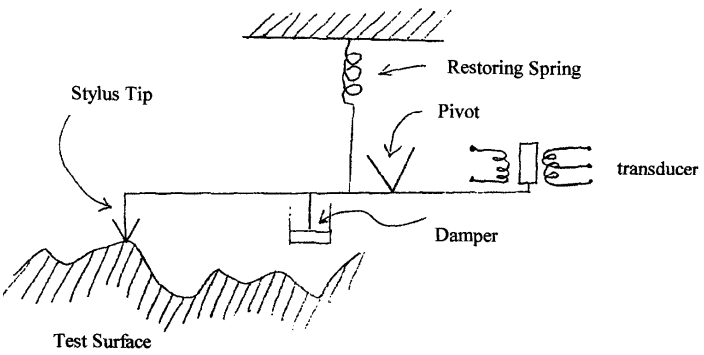


**Fig. 4** Side Acting Gauge

## 3.4 Early Optical Methods of Measuring Form

Placing the test surface on a flat reference surface and illuminating this by a collimated beam of monochromatic light produces Newton's rings (actually Hooke's). The sagital drop h corresponding to the radius of ring 'r' is

$$\mathbf{h} = \frac{\mathbf{r^2}}{\mathbf{2R-h}} \approx \frac{\mathbf{r^2}}{\mathbf{2R}} = \frac{\mathbf{m\lambda}}{\mathbf{2n}} \tag{5}$$

From which R can be estimated although it has to be said that this method is sometimes used to find the wavelength of the source rather than the radius of the curved part.

## 3.5 Early Methods of Measuring Curvature by Contact Methods: Spherometer Method

In this method a three footed frame is rested on a flat surface and a probe situated in the centre of the frame is zeroed. The frame is then put onto the test surface and the probe adjusted until it makes contact with the test surface upon which the amount by which it has been adjusted is recorded. See Figure 6. If this is 'h' and the distance from the probe to the feet is 'r' then the estimate of the radius of curvature of the test piece is given by

$$\mathbf{R} \approx \frac{\mathbf{r^2}}{\mathbf{2h}} \tag{6}$$

Notice that this is the same basic technique as the Newton's ring method:

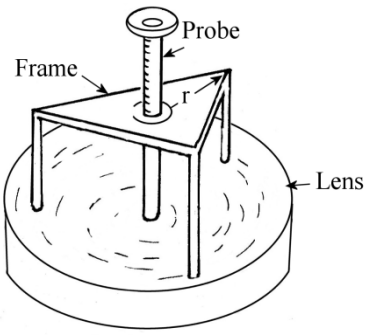


**Fig. 5** Spherometer for measuring curvature

# 4 Present and Future Surfaces and Methods

There are a number of aspects to this discussion which make it difficult to single out individual developments. There are for example improvements in existing methods, new methods of measurement, new ideas about what to measure, analytical methods which improve the capability of existing methods, the changes brought about by developments in conditions such as miniaturization etc. It is not possible to deal with every aspect of improvement or change for example in detectors or sources of energy such as in optics so trends only will be considered. Also, the question of timescale needs to be clarified because the subject of engineering metrology with respect to surfaces is basically only about 75 years old so the concept of 'past' and 'present' is somewhat arbitrary: many basic requirements such as characterization and filtering were implicit at the start and are still developing. Only major shifts can be discussed. Central to this section is the realization that one of the main problems is that there has been a great increase in the number and types of surface which now need to be measured when compared with earlier times and the need to deal with much smaller scales of size. For example structured, patterned and free form surfaces, which require new ways of characterizing, processing, as well as measurement. Not the least of the problems has been the need to develop new manufacturing techniques which have been addressed very successfully in the research project reported above. All of these considerations have meant a rethink in the way surface metrology is approached. However, despite all the changes, the basic types of instrument still preferred are the stylus method and various forms of the optical method. Why not just one method?

## *4.1 Stylus versus Optical Instruments*

The question is often asked why the stylus method is used at all when excellent non contact optical methods are now available. The first reason is obvious which is that if the function of the part is mechanical then ideally the method of measurement should also be mechanical so measuring gears and cams for example should be with a stylus. By the same token optical applications should use optical means of measurement. These are demonstrations of a rule of metrology which says that to get optimum results i.e. high fidelity, the metrology should wherever possible match the function. There is a case when this rule appears to be violated in optical applications which is when the angles of the profile of the component to be measured are very high. In these instances optically focused spots onto the surface from the instrument tend to dissipate light away from the normal if the surface is tilted at the point of incidence so that fidelity of the measurement is impaired. This is an optical consequence of the laws of physics and has nothing to do with the instrument. Figure 11 shows regions 1, 2 and 3 of high slope on an aspheric mould which require a stylus method: here slopes of 80 degrees can be found and would be unsuitable for measurement optically.

Damaging the component by the stylus, which can be a potential problem in cosmetic applications in optics or when measuring delicate thin films, can be mainly avoided by consideration of the forces involved and knowledge of the material properties of the component. As a general rule to decide whether a mark caused by the stylus is possible use can be made of the 'Stylus Damage Prevention Index' ψ devised by Whitehouse.

$$\psi = \frac{1}{\pi}\left(\frac{W}{H^3}\right)^{\frac{1}{3}} \times \left(\frac{E}{R}\right)^{\frac{2}{3}} \frac{1}{1.11^2} \tag{7}$$

It emerges that the damage index so defined ψ has to lie between acceptable limits if no damage is to be done. This criterion is derived in reference [11].

In this formula W is the load, H is the hardness of the material being measured and can be seen from the formula that it is the dominant factor, R is the radius of the tip of the stylus and E is the elastic modulus.

For $\psi > 1$ there can be damage because the elastic pressure is greater than the hardness.

For $\psi < 1$ there is no damage.

In fact the difficult parameters above are W and H. W is the effective mass of the pick-up as it traverses the surface. The problem is that it should include the dynamic forces as well as static imposed on the surface by the stylus. The maximum value of the dynamic force is 2 W where W is the rest weight. This force acts in the valleys so damage, if any, is due to the stylus will be a maximum in the valleys – not the peaks.

**Table 1** Stylus instrument versus optical instrument

| Stylus method | Optical method |
|---|---|
| Possible damage | No damage √ |
| Measures geometry √ | Measures optical path |
| Tip dimension and angle independent √ | Tip resolution and angle dependent |
| Stylus can break | Probe cannot be broken √ |
| Insensitive to tilt of workpiece √ | Limited tilt only allowed |
| Relatively slow speed | Can be very fast scan √ |
| Removes unwanted debris and coolant √ | Measures everything good and bad |
| Can be used to measure physical parameters | Only optical path as well as geometry for example hardness and friction√ |
| Roughness calibration accepted at all scales √ | Difficult to calibrate by standards |
| Temporal and spatial influence/dynamic | Spatial influence/geometric effects |

The other difficult parameter is the value of H. Unfortunately most people think that the bulk value of H should be used in calculations like this i.e. that value of hardness obtained when the surface is indented by tens of micrometers. This value of hardness is incorrect. The value of hardness should be the skin hardness. This is the value obtained when the indentation is fractions of a micrometre. In such cases the effective hardness is two or three times the bulk value. For copper for example it could easily be 300 VPN rather than the bulk value of 100 VPN, where VPN is the Vickers Hardness Number.

Taking these factors into account and bearing in mind the sometimes improper use of a skid it is found that the stylus rarely causes damage. If there is any doubt then one preventative measure which can always be made is to lower the dynamic force by reducing the speed of traverse of the system. A comparison of the two basic methods is given in Table 1 below in which a tick √ indicates the advantage. On balance it is seen that they are about equal in usefulness: which is good or bad depends on the application as will be seen. For a good explanation of optical behaviour at a surface see Ogilvy [12].

## *4.2 Texture and Form*

Traditionally the texture has been measured separately from the form, usually two instruments are used, one for the form and one for the texture, the problem being that the form is invariably of much greater size so that getting a probe to encompass the one invariably means that the much finer detail of the texture is lost and if the texture is measured the extent of the form which can be covered is much too small to be useful. A useful instrument which involved using some of the best features of stylus methods as well as optics has been developed called the Form Talysurf. This uses a straight line datum to measure the form and the texture at the same time as shown in Figure 6.

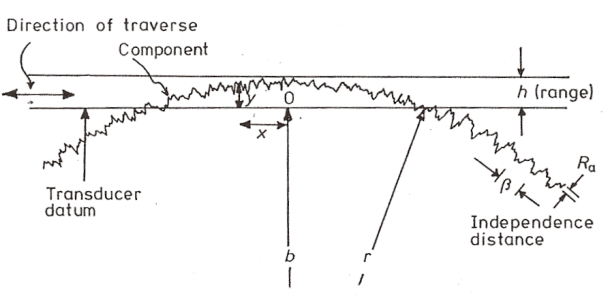


**Fig. 6** Form Talysurf showing the principle of using one measurement for form and texture

It can be seen that the traverse allows the roughness and a portion of the form in this case an arc of a circle to be measured. The key to the technique is to have a mechanical pick up and an optical transducer. In figure 7 the key optical element

is a cylindrical grating which rotates about a precision pivot and is illuminated by means of a collimated laser beam from a low power laser diode. Specially designed optics interrogates the diffraction patterns generated. The arcuate movement is detected and also the changes from normal incidence of the probe on the surface compensated for. This arrangement allows a very high resolution and a wide range probe movement to be achieved.

To be useful a range to resolution of 106 is considered to be a minimum requirement. Such a system has the considerable advantage of not only measuring two features simultaneously but the instrument only has to be calibrated once rather than having two calibration procedures when two separate instruments are used. This is the basis of an 'integrated' measurement system.

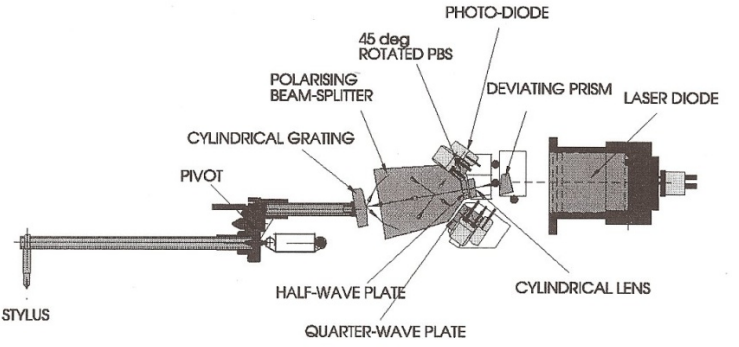


**Fig. 7** Wide range stylus system with high resolution (Taylor Hobson PGI system)

There are various types of stylus which can be used to measure the form of optical components. Two materials are common, one, traditionally, is a jewel such as ruby or sapphire and the other is silicon nitride. For small moulds and concave optics a 300 μm ruby ball is often used. Silicon nitride balls of typically 800 μm radius can be used for measuring diamond turned materials such as germanium. This has the added advantage that it attenuates incipient resonances sometimes generated when measuring certain plastics. For texture as well as form a conisphere shape stylus is now often used. This has a spherical tip merging into a cone and is often made of diamond. The tip can have a radius of 1 μm, 2 μm or 5 μm radius and the choice of a cone angle. Typical of these are 30°, 40° or 90° angle depending upon the application. It should be remembered that the angle of the cone shoulder can integrate out detail as well as the tip itself so for fine texture measurement a 30 degree angle of cone should be used in addition to a 1 or 2 μm tip radius. Acute angle styli are suitable for measuring optical parts with high angles such as micro-lens arrays and small aspheric moulds. However, this type of stylus should be used with care because it is fragile. The 40 degree stylus is more robust. See figure 8.

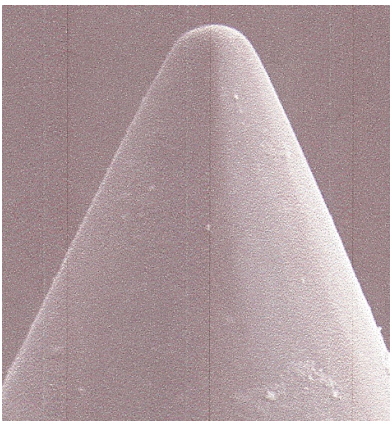

**Fig. 8** A 2 µm tip 40 ° angle diamond stylus

The vertical range of measurement can always be increased simply by lengthening the stylus arm. A maximum length of no more than about 240 mm is recommended.

## *4.3 High Slope Surfaces*

This facility extends to the modern and future in the measurement of high performance optics which require large range measurements as well as high resolution. One example is the measurement of aspheric lens moulds which are used in a variety of consumer applications such as cell phone camera lenses and optical storage devices. These are typically between 1 to 5 mm in diameter and have very high angle sides and require non spherical geometry in the most inaccessible places. Angles of up to about 80° can be accommodated thereby enabling 'blu-ray' i.e. short wave optics and their moulds to be measured. Examples are given in Figures 9, 10 and 11 of form and texture.

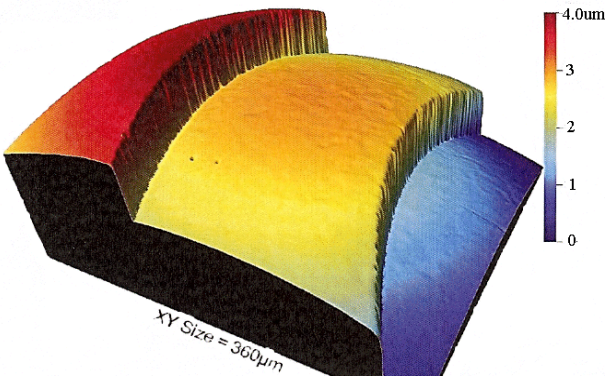


**Fig. 9** Typical area of a diffractive lens measured using stylus instrument

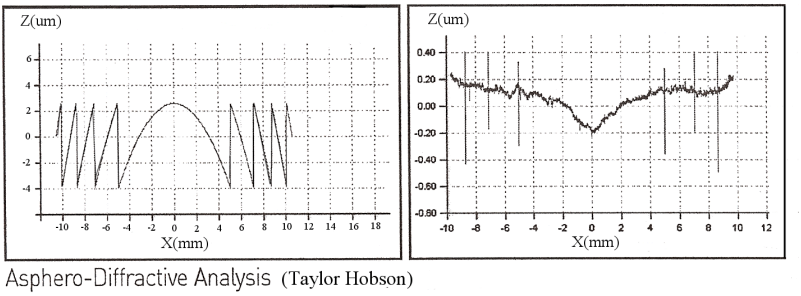


**Fig. 10** Form and texture on an Asphero-Diffractive element

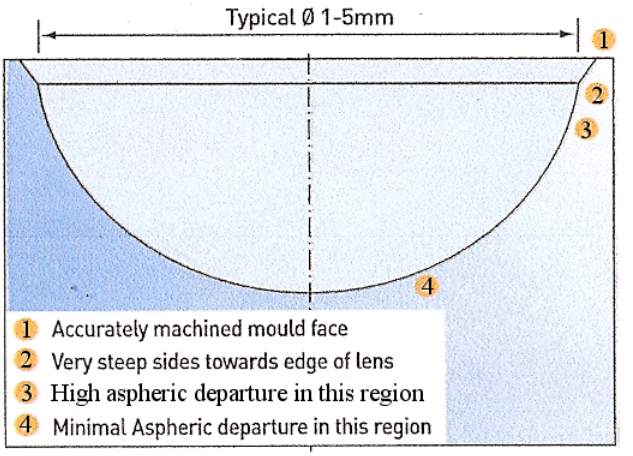


**Fig. 11** Regions on an aspheric mould most suited to being assessed using stylus methods

## *4.4 New Surfaces – New Challenges*

Figure 12 shows three new types of surface which have to be measured today which are being investigated and controlled by stylus and optical methods. These are structured, patterned and freeform surfaces.

Structured and patterned surfaces such as Fresnel lens, retro-reflectors, micro abrasive surfaces etc. are well known. Two of these are shown in figure 12 (a) and (b).

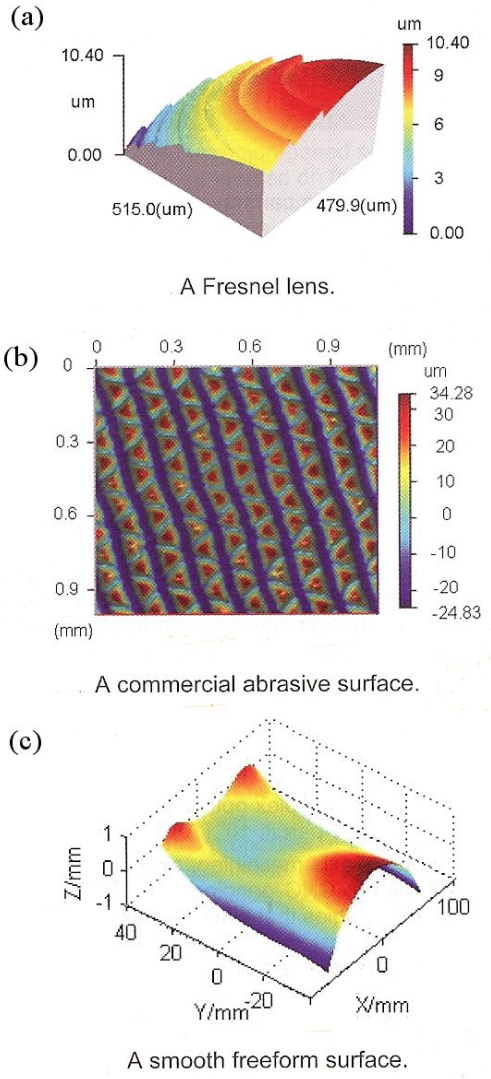


**Fig. 12** New surface challenges (a) structured surfaces, (b) patterned surfaces and (c) free form surfaces

## *4.5 Free Form Surfaces*

Figure 13 shows one of the basic philosophies behind using free form optical systems. Rather than using a complex system of simple elements to achieve an optical wavefront it is possible, at least in principle, to replace them with fewer or even just one complex element calculated to give the same result. These surfaces

are usually described as free form and are non Euclidean in the sense that there is no deterministic formula with which to descibe them: the curvatures vary from point to point. Some complicated shapes are shown in figure 14. Providing the slopes are not severe these surfaces can be measured using optical methods such as the white lght interfermeter as will be seen, but for large slope surfaces the stylus method is used. One example of a freeform mirror is shown in Figure 15. It is used in the head-up display in which a thin film transistor generates a pattern which is projected onto the windshield of a car or aircraft.

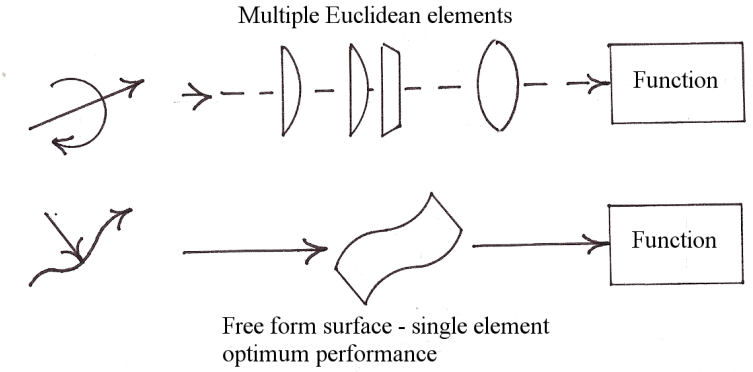


**Fig. 13** Optical free form surfaces concept of use

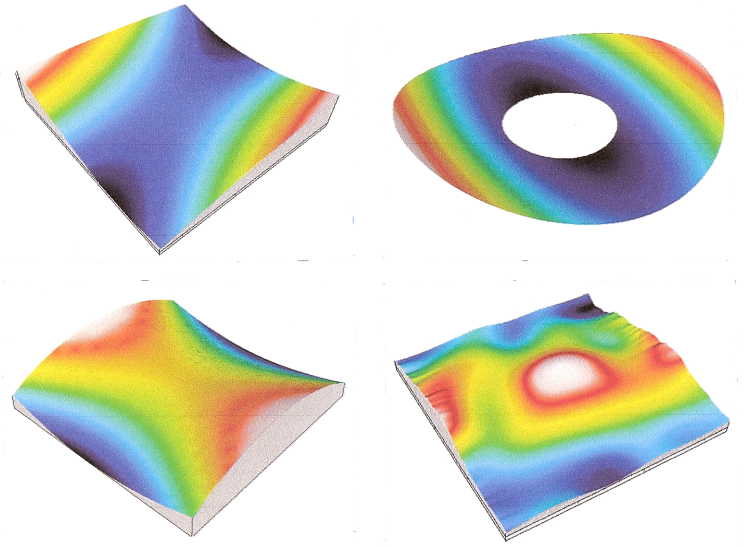

**Fig. 14** Some complex shapes of mirrors

Often free form optics combine with conformal optical systems which are used in missile and aicraft systems. In these an optical sensor has to look through a surface skin which has to have a shape which conforms to a specific external requirement such as minimum aerodynamic drag. The very fact that the window shape is determined by factors which are not optical means that there are serious aberations at the detector which have to be remedied by another optical element having a complex freeform shape or by software modification of the signal after being received.

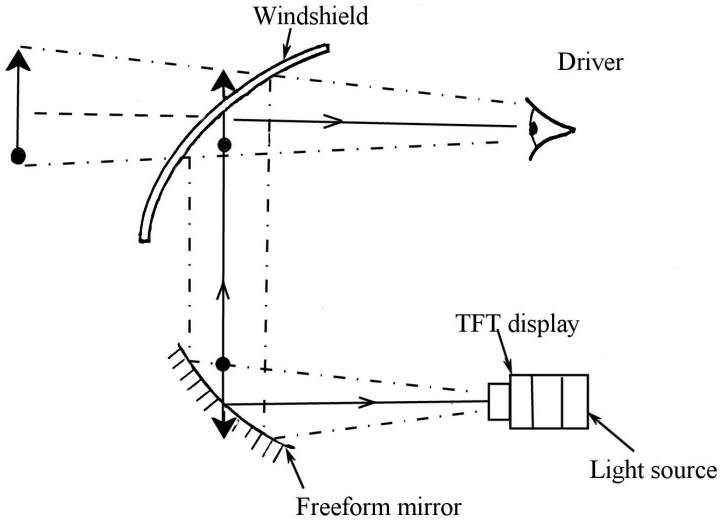


**Fig. 15** Head-up display using a freeform mirror

## *4.6 Optical Trends*

Whereas stylus methods are robust they tend to be slow but optical methods, on the other hand, are fast but are much more sensitive to extraneous effects. They have therefore preferred applications of useage. Optical methods have more options for improvement of performance. Amongst these are confocal methods and white light interferometry which will be descibed briefly below. There are, of course, many other possibilities.

## *4.7 Confocal Optics*

A confocal optical system is one which has a pinhole positioned near to the specimen under test such that it restricts the light, which is not exactly in focus on the object, from hitting the detector and thereby increases the signal to noise ratio of the system. It is a very simple but elegant way of making images clear and well contrasted. Figure 16 shows two embodiments of the principle. Figure 16 (a) illustrates the configuration for viewing an opaque surface and Figure 16 (b)

shows the corresponding configuration for a partly transparent surface. It is clear from this figure where the term confocal comes from: it derives from the symmetry between the optical systems to the right and to the left of the object.

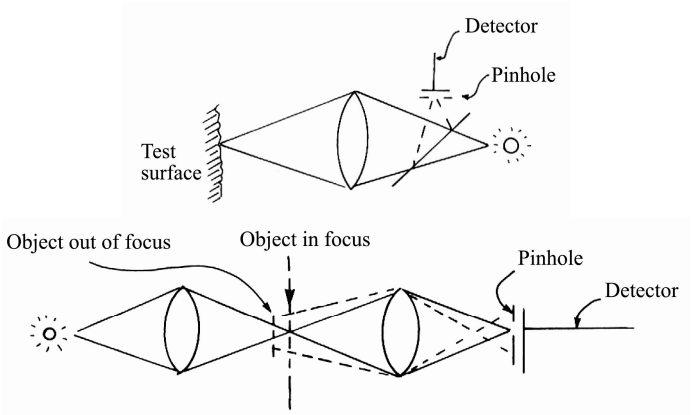


**Fig. 16** Confocal optical system (a) for opaque object (b) for a semi transparent or phase object

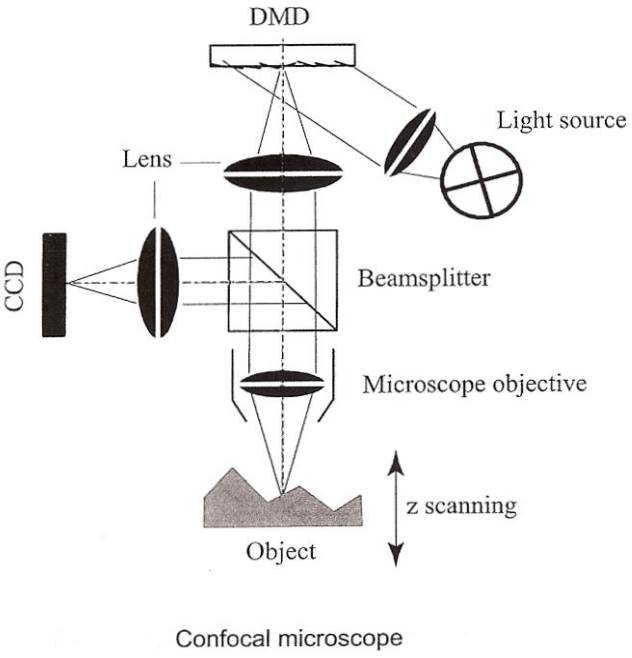


**Fig. 17** Digital confocal microscope based on micro mirrors [13]

An interesting variant on the basic confocal instrument has been proposed by Tiftikci in Holland who has designed what is in effect a digital confocal microscope. See Figure 17.

Tiftikci uses a DMDTM (Digital micro-mirror device) as a virtual illumination pinhole array and a CCD as a virtual detector pinhole array. The point illumination and point detection are enabled by controlling precisely the DMD and CCD pixel scans. The use of the micro-mirror makes the mechanical movements of the x, y scanning unnecessary thereby reducing possible sources of vibration [13]. Confocal methods are widely used in biology and engineering because of the very high clarity of the image produced but as the lateral range is increased the resolution tends to decrease, a factor which does not occur significantly when using interferometric methods. This is just one reason for the dramatic increase in the use of the scanning white light interferometer which is singled out below as probably the most useful optical instrument at present in use for measuring surfaces, films and coatings. There are many other admirable optical techniques such as holography, speckle, heterodyne and moiré, to name but a few, which are widely used but only for limited applications and which do not appear to have as much potential as the broad band method. For a description of the other methods and their application see for example reference [14].

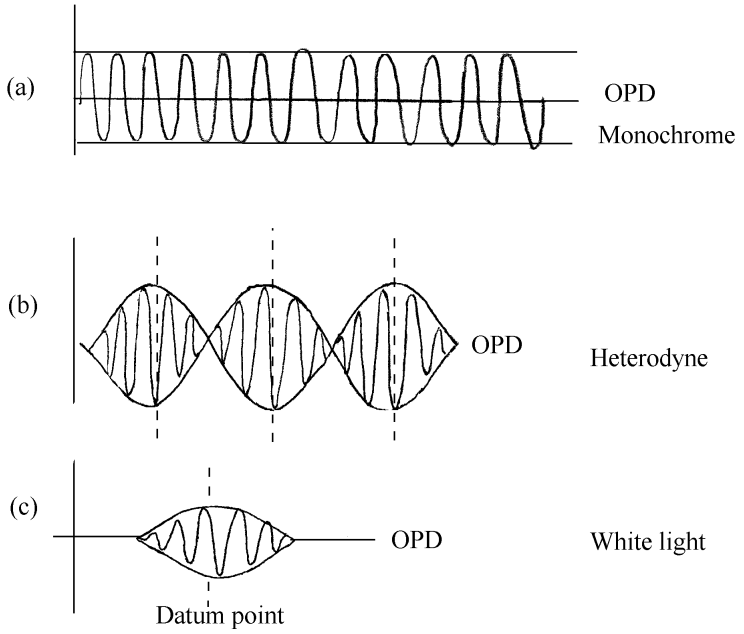


**Fig. 18** Fringe patterns as a function of bandwidth and measurement mode (OPD= Optical path differenced between the arms of the interferometer)

## *4.8 Scanning White Light Interferometer*

This type of instrument has grown in popularity due to the fact that it can be used as an absolute measure of length. A schematic view of an instrument is shown in Figure 19. It is an interference microscope in which the objective is an interferometer which has one or two arms of the interferometer in the line of the microscope tube thereby obeying Abbe's principle. In this form a Mirau interferometer is the objective. When the reference mirror situated above the semi-silvered mirror is the same distance as the specimen the optical path difference between the two is zero and the fringe contract is a maximum. If a monochromatic laser source is used the fringe contrast does not degenerate substantially as the specimen is moved away as seen in Figure 18 (a) but if a white light source is used as shown in Figure 19 then the fringe contrast becomes a function of the optical path difference as seen in Figure 18 (c). The function describing the decay is the coherence function (reciprocal bandwidth of the source) and the distance over which it decays to an arbitrarily small value say 1/e is called the coherence length. The important point is that the position of the maximum contrast acts as a reference from which any position of the specimen within the coherence length

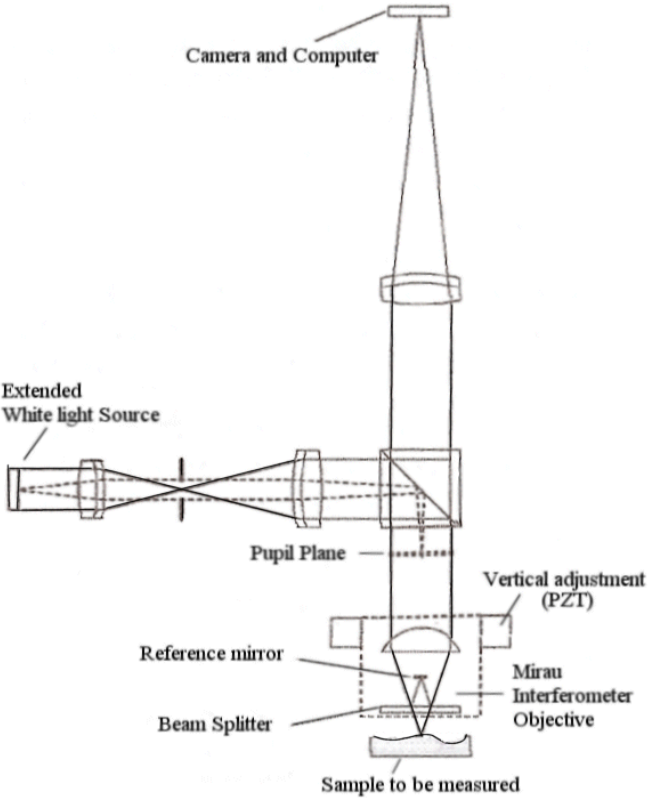


**Fig. 19** Schematic diagram of SWLI system

can be directly evaluated by the value of the fringe contrast at that point. Measurement of phase within each fringe can also be used with extra refinement but with a smaller range. The measurement is taken by moving the objective vertically while recording the intensity pattern at each pixel of the camera. With the wide band source this type of microscope is referred to as a Scanning White Light Interferometer (SWLI).

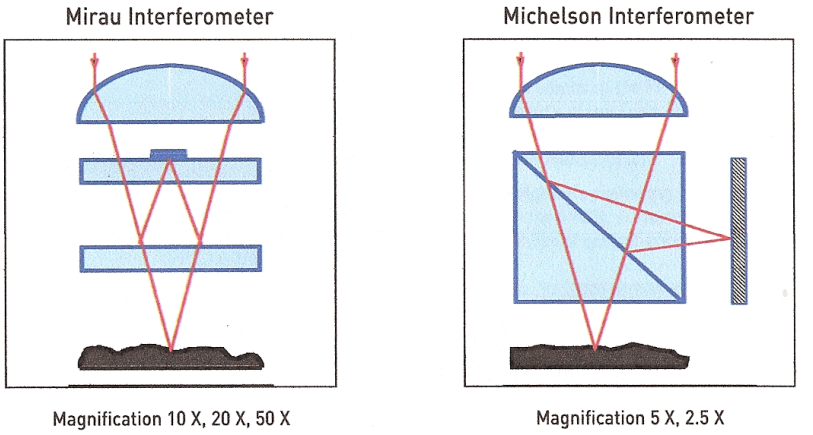


**Fig. 20** White light Scanning Interferometers (SWLI) (a) Mirau (b) Michelson Interferometer Objectives

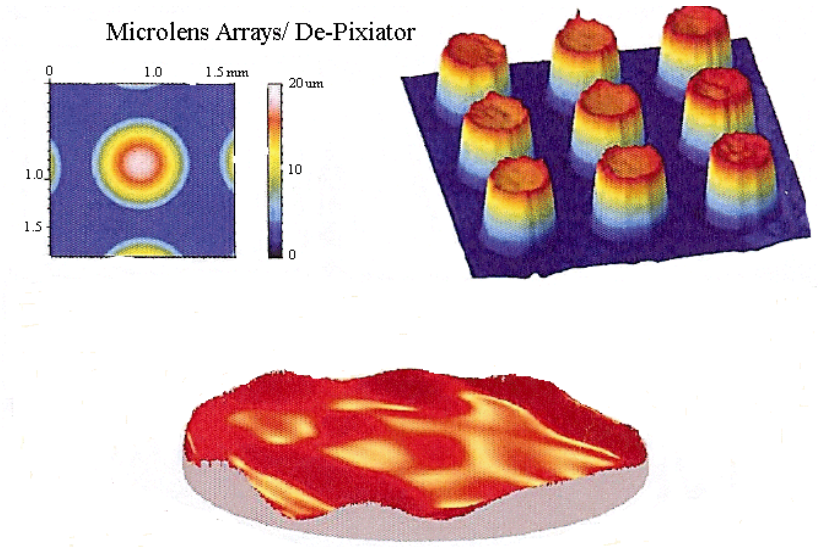


**Fig. 21** Shows the use of a scanning white light interferometer for microlens applications

Two forms of interferometry objective for use in the scanning white light interferometer are the Mirau type used for relatively small vertical range but high resolution and the Michelson interferometer used for the larger range. See Figure 20. Taken together there is the basis of a very useful instrument for covering small and large optical components when incorporating a wide range XY scan, as seen in Figure 22. The depixilated has been obtained with a mould measured with a white light interferometer.

## 5 Miniaturization

One requirement for modern metrology is to incorporate it into the manufacture so that the cycle time between checking the geometrical features and ordering the correction is minimized. Jiang has attempted to achieve this by means of a miniature interferometric system in which an optical probe is fixed to the machine tool such as a diamond turnig lathe and a novel scanner picks up the signal from the part (Figure 22). The innovation here is having two interferometers in parallel: both having a common path via a fibre optic cable from the processor to the probe thereby minimizing environmental effects. Scanning is achieved by means of phase grating and a tunable laser. The former is fixed in space within the probe such that the zero order diffraction impinges on a reference mirror and acts as the datum whereas the first order diffrection is focused onto the component under test. As the wavelength of the tunable laser is changed so the first order spot traverses the part thereby replacing the conventional stylus scan and so considerably increasing the speed with which the data is picked up. [15]

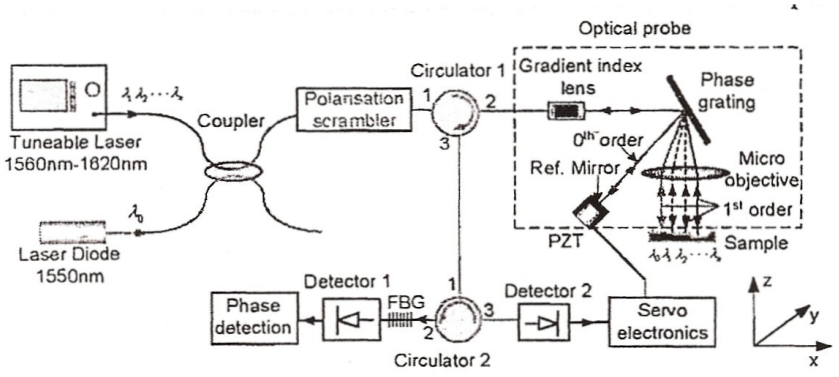


**Fig. 22** The increasing requirement for small versatile and robust instrumentation an example using wavelength division scanning via blazed grating [15]

This translation from laser wavelength to spatial position on the surface represent an intermediate step between the stylus or optical probe producing a high fidelity signal with a traversing unit, having a simple optical scan which is cheap and fast but delivers relatively crude information.

# 6 Software and Mathematical Enhancement

Perhaps one of the most significant advance in instrumention in recent years has been the use of software to improve not only the performance of instruments but also their control. There is no longer a willingness to spend many hours setting up and taking measurements as was the norm in the past. Nowadays there is a growing requirement to take mass measurements automatically and to evaluate the measurement statistics at the same time and if necessary take remedial action in the production cycle. There are a number of ways in which software can help to improve the performance of instruments. Some of these are:

a) Look up libraries for identifying specific features from within noisy signals
b) Neural networks for learning to deal with slightly different surfaces
c) Algorithms for:

    i. Robustness to identify and remove freaks
    ii. Stitching techniques to extend the lateral areal range of the instruments
    iii. Mathematical techniques for establishing references and for improving the signals to noise ratio

d) Simulations for pointing out new directions and to help to verify potential techniques

A few examples follow below.

## *6.1 Improved Resolution of Detail in Substrates*

The capability of the white light interferometer can be extended to some extent by analytical methods as reported by de Groot. [16] Semiconductor features such as transistor gates and line widths and etch depths of binary gratings are of the order of a few hundred nm down to tens of nm and can therefore be well below the Rayleigh criterion for resolution $61\lambda/NA$ so unresolved features of this kind cannot be measured directly as height objects in the usual way by interference microscopy. De Groot asserts that measurement of such depths and widths are possible once it is understood that features of this kind do affect 3D images and that once the nature of the interaction has been quantified then measuring an image can lead to an estimation of the size and geometry of the unresolved features.

As an example he considers a typical component shown in Figure 23:

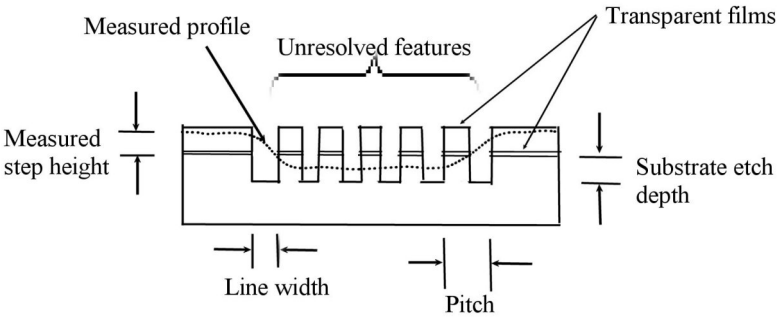


**Fig. 23** Sub-resolution measurement with white light interferometry

For example line widths and etch depths are of the order of a few hundred nm down to tens of nm and can therefore be well below the Rayleigh criterion for resolution 0.61λ/NA so unresolved features of this kind cannot be measured directly as height objects in the usual way by interference microscopy. De Groot asserts that measurement of such depths and widths are possible once it is understood that features of this kind do affect 3D images and that once the nature of the interaction has been quantified then measuring an image can lead to an estimation of the size and geometry of the unresolved features.

The apparatus consisted of a white light LED of mean wavelength 570nm as part of a white light interferometer with added polarizer: the linearly polarized light being an important factor because it increases sensitivity to specific geometric features for example depth of etches. A computer records intensity Interferograms for each pixel as a function of scan position so that height can be deduced. De Groot prefers to use the frequency domain analysis to implement the

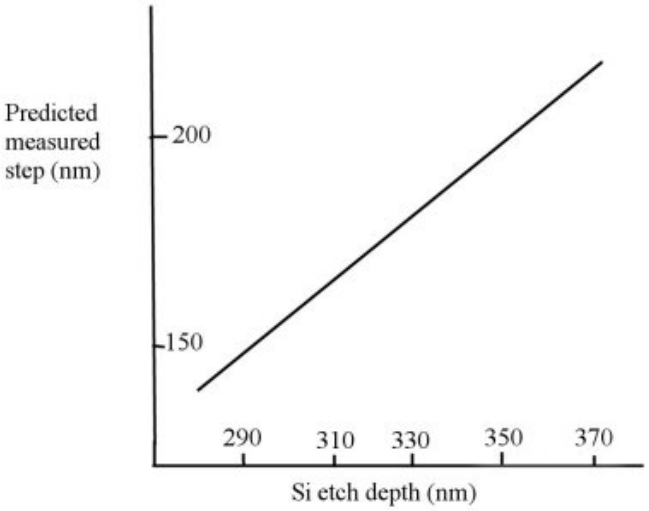


**Fig. 24** Rigorously coupled wave analysis (RCWA) (after [19])

'Rigorous Coupled Wave Analysis' (RCWA) method [17]. This is based on the work of Moharam et al [18] on binary gratings.

Figure 24 shows how the RCWA prediction of step height (ordinate axis) - which should be measured on the interferometer, actually relates to the unresolved etched line depth.

## 6.2 Thick and Thin Film Measurement

In the field of scanning white light interferometry it is well known that films of optical thickness in excess of the coherence length (reciprocal bandwidth) may be measured by taking advantage of the fact that such films exhibit interference maxima corresponding to each interface. However for thin films the interference maxima overlap and Mansfield has devised an ingenious scheme based on what he calls the 'Helical Complex Field' (HCF) which allows thin film thickness to be evaluated [20]. (See the CCI Taylor Hobson system.) This is an example of the use of field theory to help resolve difficult optical problems. Further work in this area suggests that the surface roughness at the interfaces may also be evaluated. This type of work is especially pertinent due to the fact that very thin films and coatings are becoming ever more important in nano technology.

## 6.3 Reference Fitting for Free Form Moulds

One of the biggest problems facing the new generation of optical parts particularly of the free form variety is the difficulty of measuring deviations from the usually

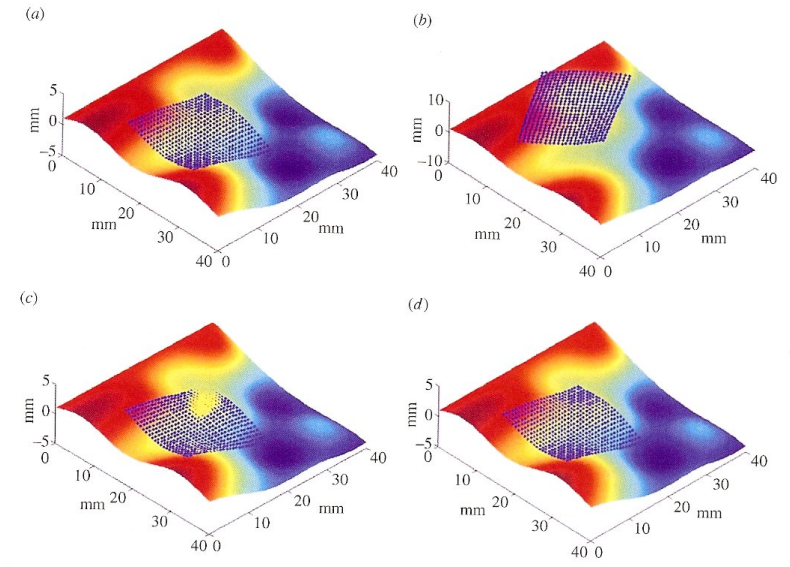


**Fig. 25** Free-form fitting (a) ideal position (b) transformed to new position (c) initial fitting result (d) final fitting result (after [21])

empirically determined accepted shape. This is because the equation of the shape is unknown and cannot therefore be operated on by a well defined linear procedure. It is not known, for example where the probe, here assumed to be of the stylus type, will make contact at any point. For this reason methods are being explored which are partially iterative in nature and which also make use of some useful properties of two dimensional splines e. g. NURBS [21]. Splines have the inherent property of minimizing the potential energy of the reference shape and so make a reasonably plausible reference from which to judge the manufactured part. An example is shown in Figure 25.

## 7 Other Issues

One factor which causes trouble now and more significantly in the future is when there is a mixture of geometries of different scales of size on any one component. This then requires nano as well as micro measurement such as is the case when it is required to look at molecular or atomic detail on a millimetre sized component or cases when all scales of size need to be examined. The NPL and PTB have endeavoured to solve this measurement problem by developing prototype instruments to cover the micro, nano and atomic ranges all with one instrument. An example is shown in Figure 26.

Yacoot and Koenders [22] have incorporated an X ray interferometer with an atomic force microscope (AFM) and an optical interferometer.

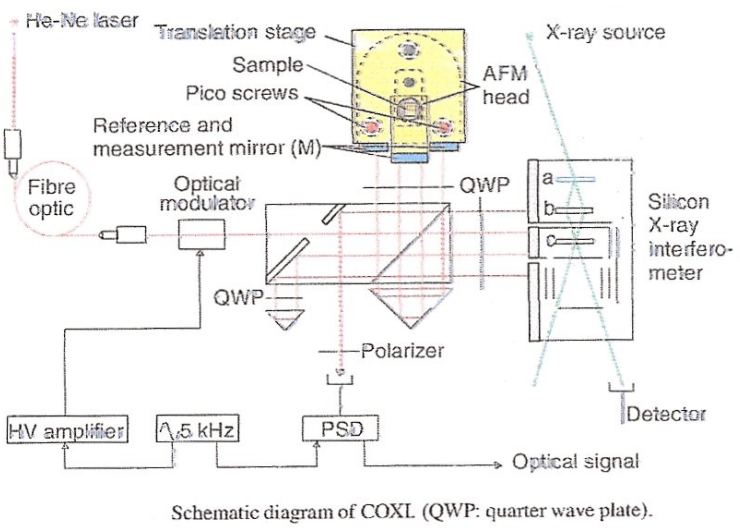


**Fig. 26** Combined SPM and x-ray and optical interferometers (After Yacoot and Koenders [22])

In operation both X ray and optical interferometers have servos that allow their interferometers to increment fringe by fringe or to be held at zero of the respective fringe. When both servos are used together any displacements of the X ray interferometer causes a corresponding displacement of the moving mirror of the optical interferometer. Consequently, this mirror can be moved in displacements equal to either a discrete number of optical fringes (158 nm since it has a double pass configuration) or a discrete number of X ray fringes of 0.192 nm which is the lattice spacing of the 220 plane of silicon. The problems associated with non linearity in the optical interferometer are avoided because any sub optical fringe displacements are using the X ray interferometer with the optical interferometer following in slave mode and always remaining locked on to a zero point crossing of an optical fringe.

Another practical case is where there is a mixture of large macro geometry, very fine surface finish, complicated shapes and extreme problems in tolerancing and assembly. The Webb telescope is an example of this situation. This telescope is intended to be a replacement for the Hubble space telescope due in about 2014 or thereabouts and has can be seen in Figure 27 the primary mirror is huge being 6.5 metre in diameter and being made up of 18 hexagonal sub-mirrors each of which will have to fit together precisely and have the correct roughness, shape and figure. The solution to this measurement problem is still being worked on but it illustrates one point of future metrology which is that more and more scales of size of features will be present on any one component and will have to be evaluated in parallel and in-situ.

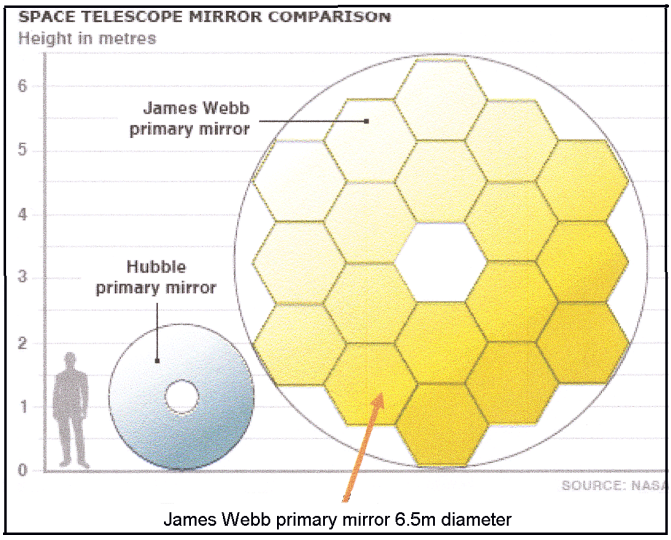


**Fig. 27** Webb Telescope – complex integrated optical system

Also, areal measurement of surfaces is proving to be invaluable for functional prediction well as for process control but there will be a need for advanced stitching techniques to cater for the large optical elements being visualized in the future and which are likely to be made up of multiple complex elements.

Figure 28 shows an unlikely but interesting attempt by Chen et al [23] to make use of any way of tapping into cheap but possibly effective technology. Basically the system consists of a mobile robot, an industrial control computer system, a machine vision positioning and navigation system linked to the Global Positioning Satellite system. The robot has four wheels two of which are castors and two are drive wheels which can be orientated to direct the path of the robot when on the surface. This has been developed in the first instance to polish very large free-form surfaces but could incorporate a metrology system. Irrespective of whether or not it is successful in helping the manufacturing process the use of inertial navigation for positioning is a case of metrology controlling the polishing and hence the function of large optical parts of the future. It seems that the thread between the past, the present and the future is assured.

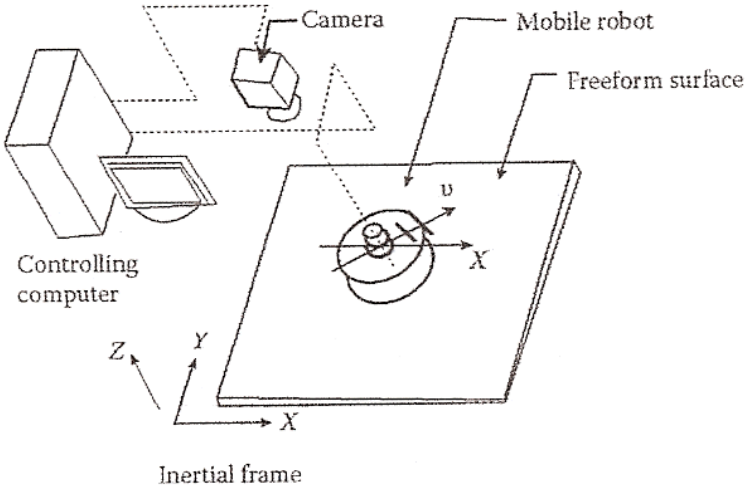


**Fig. 29** GPS guidance for help in manufacture and measuring large scale freeform optical parts

## 8 Conclusions

It has only been possible to consider a few aspects of the metrology and manufacture of optical parts. The first point is that there has been a move away from simple components such as spheres and planes to structured and freeform surfaces. At the same time there has been a move towards multiple miniature arrays of surfaces which present quite different measurement and manufacturing problems. Yet another swing has been towards components which have many factors of differing scales of size to be measured. These problems are stretching

the metrology community. However there has been progress in metrology instruments. The stylus method, which now has a very large dynamic range and high resolution, can routinely measure roughness, shape and curvature at very large surface angles.

Many optical, semiconductor and ceramic parts can be measured with non-contact methods but especially with white light interferometers. These continue to advance measurement technology. Thin multiple films will soon be measured for thickness as well as roughness at the interfaces.

Possibly the greatest potential is in the use of software and mathematical procedures for improving the performance of instruments as well as enabling fully automated measurements.

## References


[1] Scott, R.M.: Optical Manufacturing. In: Kingslake, R. (ed.) Applied Optics, vol. III, ch. 2. Academic Press, London (1965)

[2] Singer, C., Holmyard, E.J., Hall, A.R., Williams, T.I.: A History of Technology, vol. II, 336 p. Oxford University press, London (1956)

[3] Britain, A., Wolpert, S., Langford, L.M.: Engraving on Precious metals, ix p. NAG press, London (1958)

[4] Exodus. xxvii, 11

[5] Whitehouse, D.J.: Handbook of surface Metrology. Inst. of Physics publishing, Bristol and Philadelphia (1994)

[6] Whitehouse, D.J.: Surfaces and their measurement, Hermes Penton Science, vol. 7. Hermes Penton Science, London (2002); Tomlinson, P.: NPL research report, National Physical Laboratory, UK (1919)

[7] Schmalz, G.: Z. VDI 73, 144–161 (1929)

[8] Abbott, J., Firestone, A.: A new profilograph measures roughness of finely finished and ground surfaces. Autom. Ind., 204 (1933)

[9] Reason, R.E., Hopkins, Garrott: Rep. Rank Organisation (1944)

[10] Whitehouse, D.J.: Stylus Damage Protection Index. Proc. Inst. Mech. Eng. 214(pt. C), 975 (2000)

[11] Ogilvy, J.A.: Theory of wave scattering from random rough surfaces. Adam Hilger, Bristol (1991)

[12] Tiftikci, K.A.: Development and verification of a micro-mirror based high accuracy confocal microscope. Ph. D. Thesis Eindhoven University of Technology (2005)

[13] Whitehouse, D.J.: Handbook of surface and nano metrology, 2nd edn. Taylor & Francis, London (2010)

[14] Jiang, X., Whitehouse, D.J.: Miniaturized optical Measurement methods for Surface Nanometrology. Annals CIRP 55(1), 577–580 (2006)

[15] de Groot, P., de Lega, X.C., Leisener, J., Darwin, M.: Metrology of optically unresolved features using interferometric surface profiling and RCWA modelling. O.S.A. Optics Express 16(6), 3970 (2008)

[16] de Groot, P., Deck, L.: Surface profiling by analysis of white light interferograms in the spatial frequency domain. J. Mod. Opt. 42, 389–401 (1995)

[17] Moharam, M.G., Grann, E.B., Pommet, D.A.: Formulation for stable and efficient implementation of the rigorous coupled wave analysis of binary gratings. J. Opt. Soc. Am. 12, 1068–1076 (1995)

[18] Raymond, C.J.: Scatterometry for semiconductor metrology. In: Deibold, A.J. (ed.) Handbook of Silicon Semiconductor Metrology. Marcel Decker Inc., New York (2001)
[19] Mansfield, D.: The distorted Helix: thin film extraction from scanning white light interferometry. In: Proc. SPIE, vol. 2186 (2006)
[20] Zhang, X., Jiang, X., Scott, P.J.: A new free-form Surface Fitting Method for Precision Coordinate Metrology. In: 11th International Conference on the Metrology and Properties of Surfaces, Huddersfield UK, pp. 261–266 (2007); FIG 2, p. 264
[21] Yacoot, A., Koenders, L.: From nanometre to miilimetre: a feasibility study of the combination of scanning probe microscopy and a combined optical and x-ray interferometer. Meas. Sci. Technol. 14, N 59–N 63 (2003)
[22] Chen, G., et al.: Researching of a wheeled small polishing robot for large free form surfaces and its kinematics. In: ICFDM, Tianjin P.R. China (September 2008)

# Author Index